A novel genome-wide approach to identify *in vivo* targets of Notch signalling

Christina Morgenstern

University College London

and

Developmental Genetics Laboratory,

Cancer Research UK London Research Institute

Ph.D. Supervisor: Dr. David Ish-Horowicz, FRS

A thesis submitted for the degree of Doctor of Philosophy

University College London

June 2009

I, *Christina Morgenstern* confirm that the work presented in this thesis is my own. Where information has been derived from other sources, I confirm that this has been indicated in the thesis.

Abstract

The Notch signalling pathway regulates many developmental processes in metazoan embryos and adults such as cell proliferation, stem cell maintenance, cell fate specification and apoptosis. Despite the importance of this pathway, few targets have been identified, with the Hes (Hairy and Enhancer-of-split) protein family being the best-characterised group of downstream effectors.

I have established transgenic mice carrying Biotin Acceptor Peptide (BAP)-tagged versions of Notch1. The tagged protein is fully functional and is biotinylated after crossing to mice expressing the biotinylase from *E. coli*. Biotinylation was confirmed in a range of different tissues. However, streptavidin chromatin pull-down (bioChIP) experiments from these tissues showed no significant enrichment of known Notch1 target sequences. A possible explanation could be the indirect and transient nature of the interaction between Notch, its DNA binding partner CSL and the promoter of the target gene.

A transgenic mouse line expressing a BAP-tagged version of the transcription factor Hes7, a downstream effector of Notch signalling and key regulator of somitogenesis, was similarly generated. Although the tagged Hes7 protein is functional and gets biotinylated in cell culture assays, the transgenic mice exhibit a severe somite/skeletal phenotype indicating that the tagged allele is hypomorphic. A detailed analysis of the phenotype revealed differential axial requirements for Hes7.

Acknowledgements

I thank Cancer Research UK for the generous sponsorship of my Ph.D. and the many people who have supported me in the past four years.

I would first like to thank my wonderful husband, my parents and the rest of the family for their mentoring and encouragement: it would not have been possible without your support.

I am most grateful to my supervisor David Ish-Horowicz for his support and advice and allowing me the freedom to develop my scientific skills.

I thank my second and third supervisors, Julian Lewis and Nic Tapon, for their encouragement and valuable comments during our committee meetings.

I thank all past and present members of the Developmental Genetics Laboratory: Mark Wainwright, Sheena Pinchin, Michael Stauber, Chris Molenaar, Chetana Sachidanandan, Christian Dillon, Babis Rallis, Rhian Walther, Inbal Ringel, Emmanuel Vanrobays, Ravindra Prajapati, Barbara Jennings, Annalisa Vezzaro, Krzysztof Wicher, Rippei Hayashi and Ned Hoyle for providing a great environment to work in. I especially thank Michael Stauber for his continuous support in the lab, his suggestions and most importantly for his friendship.

I thank Holger Gerhardt for taking on the collaboration to identify Notch targets in the retina. Many thanks also to the members of the Vascular Biology lab, especially to Marta Busse, for introducing me to the mouse retina model system.

I thank Michael Stauber, Barbara Jennings, Claudia Linker, Mark Wainwright and Ned Hoyle for their helpful comments on this thesis.

I am grateful to Tim Zverev and Anthony Iglesias for taking care of my mice and setting up the crosses. I also thank Emma Murray, Clare Watkins and Scott Lighterness from the mouse facility at LIF and all other people from the Cancer Research UK core facilities for their support.

Finally, I thank my friends Tamara Grüner and Julia Eckl-Dorna for contributing to a wonderful time in London.

Table of contents

Table of figures

List of tables

CHAPTER 1: Introduction

1.1 Cell-cell signalling – A concept for communication

Development of a multicellular organism starts with a single cell, the fertilised egg. Subsequent cell proliferation and specification generate multiple cell types, and eventually functional tissues and organs (Alberts et al., 2007). One key question of developmental biology concerns the mechanism by which cellular diversity arises. Although each cell contains the same set of genes, the cellular function varies when different subsets of genes are expressed. This differentiation is achieved by regulated procedures involving complex communication networks between cells. Cells within the mitotically dividing embryo need to establish contacts with each other in order to ensure proper differentiation, morphogenesis and growth.

Cell-cell communication is an essential feature of all metazoan animals and is critical for the co-ordination of development, maintenance of tissue homeostasis and to fend off invaders that enter the system (Alberts et al., 2007). One form of cell-cell communication is mediated by signalling molecules. The signal-sending cell expresses a secreted or transmembrane ligand that binds its receptor on the surface of the signal-receiving cell. The signal is transmitted into the nucleus to mediate further responses.

Remarkably, there are relatively few signalling pathways directing cell fate decisions during the development of a multicellular organism: Wingless related (Wnt), Hedgehog (Hh), Transforming growth factor-β (TGF-β), receptor tyrosine kinase (RTK), Janus kinase (JAK)/signal transducer and activator of transcription (STAT), nuclear hormone pathways and the Notch signalling cascade (reviewed in Pires-daSilva and Sommer, 2003). These pathways are used many times during development in many different combinations and contexts, and provide highly flexible mechanisms by which distinct responses in different tissues and species are generated.

The various components of such signalling pathways can act through different modes and combinations thereof in order to generate a variety of outcomes. Five mechanisms to fine-tune cell signalling have been described. Firstly, in different tissues the same receptor can function through various intracellular transducers, e.g., in *Caenorhabditis elegans* lethal-23 (LET-23) RTK signalling is transduced through RAS/mitogen-activated protein kinase (MAPK) in the vulva (Aroian and Sternberg,

1991) whereas it is transduced through inositol-1,4,5-triphosphate in the germline (Clandinin et al., 1998).

Second, the strength of receptor-ligand interaction can also contribute to determine tissue specificity. Within the Wnt signalling cascade, the affinity of the receptor for its ligand can lead to the activation of different intracellular pathways. For example, the *Drosophila* Frizzled2 (Fz2) receptor has a tenfold higher affinity for Wingless (Wg) than its structurally related Frizzled (Fz) receptor. Interaction of Fz2 with Wg results in activation of the transcription factor Tcf, whereas interaction of Fz with Wg results in cytoskeletal remodelling (Rulifson et al., 2000).

A third mode of tuning communication responses is the integration of several signalling pathways at the level of target genes. The enhancer of the *Drosophila even-skipped* (*eve*) gene depends on activation by Wnt, TGF-β and RTK signalling (Halfon et al., 2000). Thereby, mutation of any of these sites within the enhancer abolishes *eve* expression.

Fourth, when exposed to the same signals, cells can respond differently due to the expression of tissue-specific target genes. For example, specification of the vulva in *C. elegans* is achieved through RTK-RAS-MAPK signalling and activation of the transcription factor lineage-defective-31 (LIN-31) in vulval precursor cells but not in other tissues (Tan et al., 1998).

Lastly, compartmentalisation of the signal through the formation of specific protein complexes can confer signalling specificity. For example, the Glycogen synthase kinase-3 (GSK-3) mediates Wnt signalling when complexed with the cytoplasmic protein complex adenomatous polyposis coli (APC)-axin. However, in an unbound state, GSK-3 responds to RTK signalling and regulates glycogen metabolism (Cohen and Frame, 2001).

Once the information from the signal-sending cell has been transduced to the nucleus a response is triggered, often by the activation of transcription factors. This transcriptional switch can be controlled in three different ways: in ‘type I’ transcriptional switching, the transcription factor responding to the signal functions as both repressor in the absence of the signal and activator of transcription upon ligand-induced signalling. Thus signalling can lead to a repressor becoming an activator. This is the case for Tcf/Lef during Wnt signalling, Gli/Ci (Cubitus interruptus) in Hh signalling and Suppressor of Hairless (Su(H)) in Notch signalling. In contrast, TGF-β

and RTK signalling pathways can achieve a transcriptional switch through separate repressor and activator proteins. In this type of transcriptional regulation repressors and activators can recognise the same (type II transcriptional switching) or distinct DNA binding sites (type III transcriptional switching) (reviewed in Pires-daSilva and Sommer, 2003).

In conclusion, cell-cell signalling pathways act in a non-linear and highly integrative way to confer reproducibility and flexibility during the development of metazoan organisms. Further robustness of the system is achieved through the assembly of positive and negative feedback loops promoting or limiting signalling, respectively (Freeman, 2000). The coordinated use and fine-regulation of different communication pathways, enable the development of a complex organism. This thesis focuses on one of these cell-cell communication pathways, the Notch signalling pathway, which is in the focus of subsequent chapters.

1.2 The Notch signalling pathway

The Notch signalling pathway is involved in regulating many cellular processes throughout development and renewal of adult tissue in metazoans. It functions in cell proliferation, maintenance of stem cells and their niche, cell fate specification and differentiation, and even in regulating cell survival, making it an extremely versatile pathway (reviewed in Artavanis-Tsakonas et al., 1999; Bray, 2006; Lai, 2004).

1.2.1 Key player and core principle of Notch induced signalling

Almost 90 years ago, the Notch gene in the fruit fly *Drosophila melanogaster* was discovered through the observation that heterozygosity results in notches at the wing margin (Mohr, 1919). It took 70 more years until the appearance of Notch protein as a receptor (Johansen et al., 1989) and its function in cell-cell signalling was revealed (Fehon et al., 1990). The early work was done using *Drosophila* as a model organism, but soon it became apparent that Notch also has important roles in vertebrate development and that domains within the receptor are highly conserved throughout the animal kingdom (Coffman et al., 1990; Del Amo et al., 1992; Ellisen et al., 1991; Kidd et al., 1986; Stifani et al., 1992; Weinmaster et al., 1991; Wharton et al., 1985).

Mutations in this evolutionary highly conserved cascade have fascinated researchers around the world ever since. One of the first phenotypes described, resulting

from loss-of-function mutations of Notch pathway components, is the neurogenic phenotype, where cells switch their fate from epidermal to neuronal (Artavanis-Tsakonas et al., 1999; Poulson, 1937). Furthermore, loss-of-function mutations of pathway components can lead to inherited genetic diseases such as spondylocostal dysostosis (SCD), Alagille syndrome and cerebral autosomal dominant arteriopathy with subcortical infarcts and leukoencephalopathy (CADASIL) (Gridley, 2003). On the other hand, activating mutations of Notch signalling cause T cell acute lymphatic leukaemia (T-ALL) (Demarest et al., 2008; Jundt et al., 2008; Weng et al., 2004). During tumorigenesis Notch not only acts as an oncogene as seen within the haematopoietic compartment but also functions as tumour suppressor in the skin (reviewed in Radtke and Raj, 2003).

In mammals there are four Notch receptors (Notch1-4). Other organisms can have fewer, like *C. elegans* with two (LIN-12 and GLP-1) and one in *D. melanogaster* (Notch) (Artavanis-Tsakonas et al., 1995). The Notch receptor is a trans-membrane protein with an extracellular domain encompassing 29-36 epidermal growth factor (EGF)-like and three cysteine-rich Notch/Lin-12 repeats (LNR). It is present on the cell surface as heterodimer following a furin cleavage in the Golgi apparatus at position S1 (Logeat et al., 1998) (Figure 1.1A). Pathway activation is mediated by ligand binding through EGF repeats 11 and 12 (Rebay et al., 1991). The Notch intracellular domain (NICD) consists of a RBP-jκ-associated molecule (RAM) domain, seven tandem ankyrin repeats (Zweifel and Barrick, 2001a; Zweifel and Barrick, 2001b), a glutamine-rich domain (opa), and a C-terminal PEST (rich in proline, glutamate, serine, threonine) sequence as well as nuclear localisation signals (Wharton et al., 1985) (Figure 1.1A).

There are two classes of Notch ligands, Delta-like (Dll) and Jagged (Delta and Serrate in *Drosophila*) depending on the absence or presence of a cysteine rich domain (Kiyota and Kinoshita, 2002). All Notch ligands are characterised by a N-terminal DSL (Delta, Serrate and LAG-2) domain that is essential for interactions with the Notch receptor. The extracellular domain consists, like in the Notch receptor, of EGF repeats (Figure 1.1A). In mammals there are five different Notch ligands, Delta-like 1, 3 and 4, and Jagged 1 and 2 (D'Souza et al., 2008).

All of the Notch receptors and ligands are required during embryonic development and the loss of one, cannot be compensated for by the other members. Generation of transgenic mice lacking either *Notch1, Notch2, Delta-like 1* or *Jagged1*

results in an embryonic lethal phenotype (Gale et al., 2004; Hrabe de Angelis et al., 1997; Shimizu et al., 1999; Swiatek et al., 1994; Xue et al., 1999) suggesting that each member exerts specific effects during metazoan development.

Binding of the receptor to its ligand on the neighbouring cell initiates the Notch signalling cascade. Subsequently, two proteolytic cleavages release the intracellular part of the Notch receptor (NICD), which translocates into the nucleus and activates transcription of targets through CSL (named after CBF1, Su(H) and LAG-1, the mammalian, *D. melanogaster* and *C. elegans* orthologues) (Figure 1.1). Although some organisms encode several different receptors and ligands there is usually only a single CSL nuclear effector. This protein is highly conserved between different species, for example up to 84% identity between *D. melanogaster* and humans (Kovall, 2007; Kovall and Hendrickson, 2004). CSL is not only involved in Notch target gene activation but also in repression of Notch targets in the absence of NICD (Pursglove and Mackay, 2005) mediating a 'type I' transcriptional switch of Notch pathway regulation.

In summary, the Notch pathway follows a linear principle: binding of the receptor to the ligand on the adjacent cell leads to a downstream response with various outputs ranging from developmental contexts to tumorigenesis (Figure 1.1B). In the following paragraphs, I will describe the different modes of regulating the Notch message at the level of receptor and ligand maturation to the assembly of an active transcriptional switch.

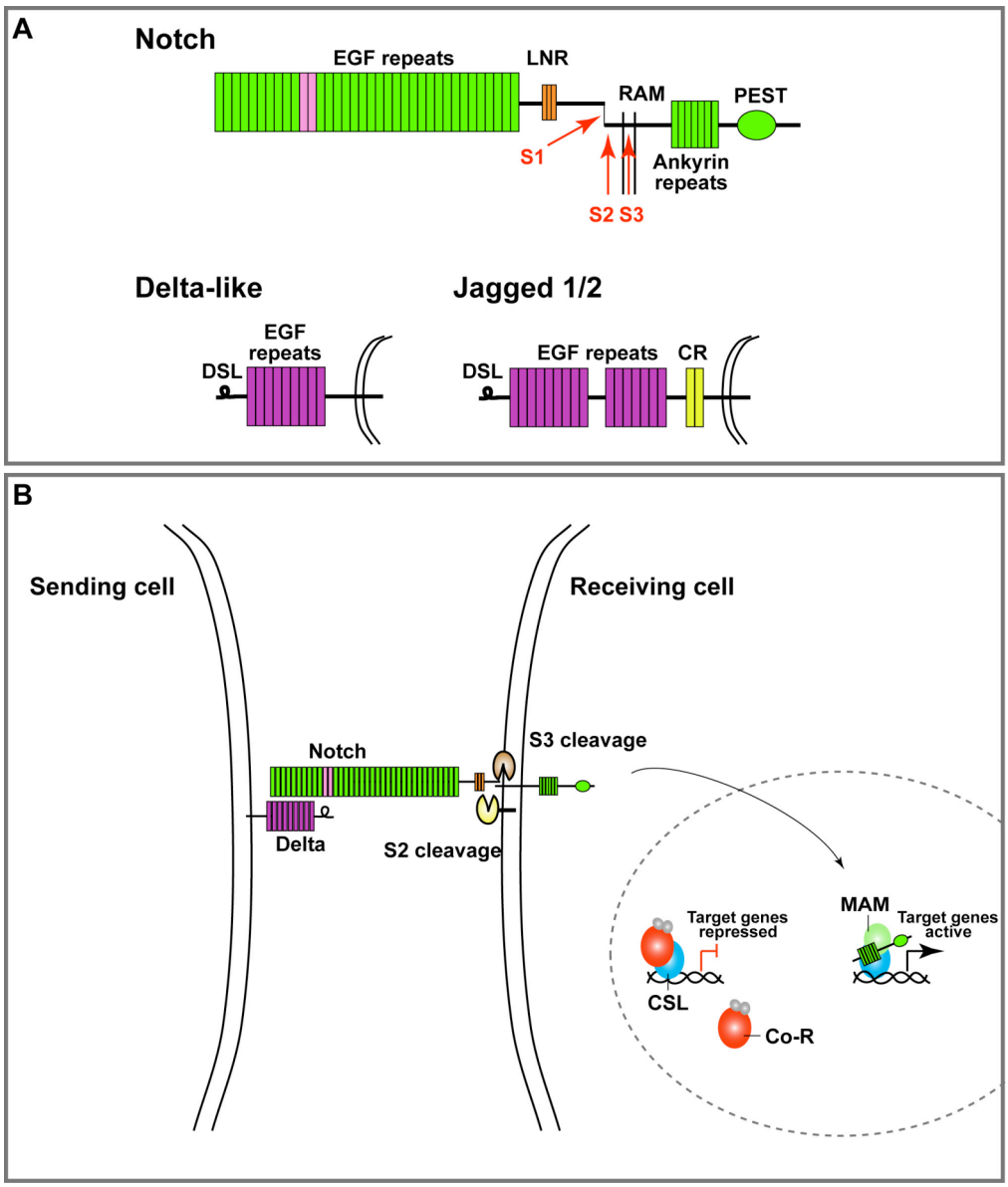

Figure 1.1 The core principle of the Notch signalling pathway. (A) Schematic structure of the Notch receptor (top) and its ligands Delta-like and Jagged. The extracellular domain of the receptor consists of 29-36 EGF repeats and 2 LNRs. EGF repeats 11 and 12 are essential for ligand binding (pink rectangles). The NICD consists of a N-terminal RAM domain, 7 ankyrin repeats and a PEST sequence. Red arrows indicate cleavage positions for receptor maturation. Furin-like convertase cleaves receptor at S1 in the Golgi apparatus. Ligands are transmembrane proteins containing a DSL motif and various EGF repeats. Ligands of the Jagged family additionally include a cysteine-rich domain (CR; yellow rectangles). (B) Interaction of the Delta ligand (purple) on the signal-sending cell with the Notch receptor (green) on the signal-receiving cell initiates two proteolytic cleavages of the receptor. The metalloprotease ADAM10 or TACE (yellow) catalyses the cleavage at S2. The remaining substrate is cleaved at S3 by the γ-secretase complex (brown) and results in the release of NICD. NICD translocates into the nucleus, where it interacts with the DNA-binding factor CSL (blue). This triggers the release of the co-repressor complex (Co-R; red and grey) and recruitment of the co-activator Mastermind (MAM; lime green) and other transcription factors.

The core of Notch signalling is the same in all Notch dependent processes but the fine-tuning of the pathway and ultimate effects on the cell differ. Post-translational modifications of ligands and receptors, as well as their trafficking and abundance on a cell have great impact on the duration of signalling and commitment to target genes, and thus regulate the outcome of pathway activation (reviewed in Bray, 2006). Here, I will give an outline of different modes of post-translational regulation, ranging from glycosylation, ubiquitylation and localisation, to modulate both Notch ligands and receptors.

1.2.1.1 Maturation of the Notch receptor

The first post-translational modification of the Notch receptor is the addition of *O*-fucose to serine or threonine residues to the EGF repeats of the extracellular domain (Panin et al., 2002). The process of *O*-fucosylation is catalysed by Protein *O*-fucosyltransferase, which is encoded by *Pofut1* in mammals and *Ofut1* in *Drosophila.* (Okajima and Irvine, 2002).

The corresponding *Drosophila* glycosyltransferase has been shown to be located in the endoplasmatic reticulum (Luo and Haltiwanger, 2005; Okajima et al., 2005). More strikingly, Ofut1 appears to work as a Notch chaperone that associates with folded EGF domains of Notch1 to keep it in shape for export (Okajima et al., 2005). Okajima et al. showed recently that the fucosyltransferase activity of Ofut1 is not essential for Notch signalling in *Drosophila*. They have generated a mutant version of the protein that lacks the fucosyltransferase activity but still possesses the chaperone function and concluded that this mutant of Ofut1 is sufficient to enable Notch signalling during embryonic neurogenesis as well as during wing disc development in *Drosophila* (Okajima et al., 2008).

Loss of function of *Ofut1/Pofut1* in *Drosophila* as well as in mammals leads to severe Notch pathway defects and embryonic lethality (Okajima and Irvine, 2002; Sasamura et al., 2003; Shi and Stanley, 2003). Moreover, a requirement for different Pofut1 levels during mammalian development was demonstrated using a hypomorphic *Pofut1* mutant. Schuster-Gossler et al. showed that early mouse development is highly sensitive to reduced levels of *Pofut1* resulting in defective somite patterning and thus axial skeleton development, whereas other processes such as neurogenesis and left-right patterning were not affected (Schuster-Gossler et al., 2009).

Once the receptor has been fucosylated on its EGF repeats it serves as a substrate for a glycosyltransferase, Fringe (Fng), which catalyses the transfer of N-acetylglucosamine (GlcNAc) onto *O*-fucose (Bruckner et al., 2000; Moloney et al., 2000). Fng is a secreted protein that resides in the Golgi apparatus and was first identified in *Drosophila* because of its role in modulating Notch signalling during wing development (Irvine and Wieschaus, 1994). Genetic studies in *Drosophila* led to the observation that Fng functions cell-autonomously to potentiate Delta-dependent Notch activation and to inhibit Serrate/Jagged-dependent Notch activation (Fleming et al., 1997; Klein and Arias, 1998; Panin et al., 1997). These opposing effects of Fng on ligand mediated Notch signalling lead to Notch activation in boundary cells along the dorsal-ventral compartment border of the wing (Irvine and Wieschaus, 1994). In contrast to the fly wing, the vertebrate homologue Lunatic Fringe (Lfng) negatively regulates Delta-dependent Notch signalling in the presomitic mesoderm of vertebrate embryos (Dale et al., 2003).

In mammals there are three Fringe paralogues, *Lunatic Fringe, Manic Fringe* and *Radical Fringe* (Johnston et al., 1997), whereas there is no *Fringe* in *C. elegans*. The most notable *Fringe* gene is *Lfng*, which plays an important role in the process of vertebrate somitogenesis (section 1.3). The loss of function of *Lfng* shows severe defects in somitogenesis in mammals (Dunwoodie, 2009; Sparrow et al., 2006) affects female meiosis (Hahn et al., 2005) and male fertility (Hahn et al., 2009) as well as T-cell development in mice (Visan et al., 2006).

Taken together, the extracellular domain of the Notch receptor can be modified with different sugar residues, such as *O*-fucose, *O*-glucose and complex *N*-glycans, which are proposed to modulate the level of Notch signalling (Stanley, 2007). In particular the conserved *O*-fucose site at EGF repeat 12 within the Notch receptor has been shown to contribute to decreased Notch-ligand interaction when mutated in flies (Lei et al., 2003) and mice (Ge et al., 2008). Thus, disruption of glycosylation or inactivation of enzymes performing the modification reactions leads to Notch signalling defects in *Drosophila* (Haines and Irvine, 2003), zebrafish (Appel et al., 2003) and mammals (Lu and Stanley, 2006). Glycosylation therefore provides an important level by which Notch signalling can be modified and allows fine-tuning of the message.

1.2.1.2 Notch receptor trafficking and endosomal sorting – degradation and recycling

In order to allow directed activation of the signalling pathway, steady-state levels of the Notch receptor need to be controlled through mechanisms that involve degradation and recycling (Nichols et al., 2007). Several E3 ubiquitin ligases have been shown to be associated with Notch and to label the receptor for endocytic pathways (Lai, 2002b). The modification of Notch by the Itch/Nedd4/Suppressor of deltex (Su(dx)) family of HECT (homologous to E6-associated protein C-terminus) E3 ligases target the receptor for degradation (Qiu et al., 2000). The target and interaction motif for the ligase to attach the ubiquitin to the receptor is not the PEST domain but the ankyrin repeats in the N-terminal part (Qiu et al., 2000).

Another class of E3 ubiquitin ligases shown to interact with the ankyrin repeats within NICD is the RING (really interesting new gene) finger domain protein Deltex (Matsuno et al., 2002). Deltex can promote Notch signalling in a CSL-independent manner in the *Drosophila* wing through enhanced endocytosis of the receptor (Hori et al., 2004). These data show that Notch signalling from the same receptor can occur through activation in different membrane-bound compartments. The regulation of the amount of Notch receptor by ubiquitination and endocytosis provides a powerful mechanism to modulate pathway activity.

1.2.1.3 Modulation of DSL ligand activity

Differential and dynamic expression of Notch ligands, as well as post-transcriptional modifications during development contribute to determine the assignment of the signal-sending cell. DSL ligands like Notch receptors (section 1.2.1.1) can be modified by *O*- and *N*-linked glycans (Panin et al., 2002) although it is not clear yet whether these glycosylations have an impact on ligand activity. However, ubiquitination of DSL ligands regulates cell-surface expression and plays an important role in ligand signalling activity (reviewed in D'Souza et al., 2008). Multiple lysine residues in the intracellular domain of *Drosophila* Delta and Serrate ligands, as well as Dll1, Dll4, Jagged1 and Jagged2 have been shown to be target sites for E3 ligases. The RING-containing E3 ubiquitin ligases Neuralized (Neur) and Mind bomb (Mib) directly interact with the Notch ligands and further promote ligand activation through enhanced endocytosis (Chitnis, 2006; Le Borgne and Schweisguth, 2003).

Neur and Mib have been shown to ubiquitinate both Delta and Serrate and despite their structural differences show redundant functions (Le Borgne et al., 2005; Pitsouli and Delidakis, 2005). Genetic studies in mice indicate that loss of *Neur1* and *Neur2* as well as *Mib2* gene expression is dispensable for normal development. However, additional removal of *Mib1* leads to a Notch-like phenotype including embryonic lethality (Koo et al., 2005). While *Neur1* and *Neur2* are not required for neurogenesis in mice, *Mib1* knock-out mice show a severe neurogenic phenotype in the neural tube and the brain (Koo et al., 2005; Koo et al., 2007).

In contrast to the mouse phenotype, zebrafish mutants lacking Mind bomb1 *(mib1)* are severely compromised with somite, neural crest and vascular defects (Jiang et al., 2000; Koo et al., 2005; Lawson et al., 2001). These studies show that Mib1 is absolutely required during zebrafish development for ubiquitination of multiple ligands (Itoh et al., 2003).

Endocytosis of the ligand was shown to be accompanied by endocytosis of the Notch extracellular domain (trans-endocytosis) in *Drosophila* imaginal tissues, which leads to the dissociation of the receptor and probably induces cleavage at S2 (Parks et al., 2000). Altogether, ligand modulation by Neur and Mib regulates internalisation and trafficking events of the ligand and thus fine-regulates Notch signalling.

1.2.2 Regulated proteolysis triggers Notch pathway activation

The Notch receptor is synthesised as a ~300 kDa precursor that undergoes three distinct proteolytic cleavages resulting in the active transcriptional activator. The first cleavage occurs in the trans-Golgi network and results in a heterodimeric molecule of 120 kDa and 180 kDa joined through non-covalent interactions which is the main form detected on the cell surface (Blaumueller et al., 1997; Logeat et al., 1998). This constitutive processing is carried out by a furin-like convertase (S1 cleavage; Figure 1.1A) and occurs C-terminal to the RQRR sequence (amino acids 1651-1654) (Logeat et al., 1998).

There is evidence that the full-length Notch receptor is also present on the cell surface and can mediate ligand-induced signalling in a CSL-independent manner (Bush et al., 2001). In *Drosophila* the predominant form of Notch is the full-length version, which might not undergo S1 cleavage (Kidd and Lieber, 2002). Mutations in *furin1* do not lead to Notch signalling defects, however there is a second furin-like paralogue,

which might act redundantly. Although mammalian and *Drosophila* Notch proteins show great homology, the proteolytic processing as well as their appearance on the cell surface greatly differs (Kidd and Lieber, 2002).

Once the Notch receptor has reached the cell surface it stays in an inactive state until interaction with its ligand is initiated. Endocytosis of the ligand generates a pulling force, which frees the proteolytic cleavage site at S2 within the heterodimer domain of Notch (Gordon et al., 2007). Once the S2 site is accessible, a proteolytic cascade is initiated leading to Notch pathway activation (S2 cleavage; Figure 1.1A). The a disintegrin and metalloprotease ADAM10 (also known as Kuzbanian; Kuz) and the tumour-necrosis factor-α (TNF-α)- converting enzyme (TACE or ADAM17) have been implicated in the S2 cleavage (Brou et al., 2000; Jarriault and Greenwald, 2005; Mumm et al., 2000). It has been demonstrated that Kuz and TACE have individual functions to modulate Notch activation at the receptor level during development. Moreover, Kuz and TACE have the ability to promote ligand-independent Notch activation (Delwig and Rand, 2008).

The S2 cleavage generates a membrane-tethered carboxy-terminal fragment, which is recognised as a substrate for the transmembrane γ-secretase protease complex, which cleaves the receptor at the transmembrane site (reviewed in Fortini, 2002). The γ-secretase complex consists of presenilin, nicastrin and other putative components. Upon removal of presenilin (Donoviel et al., 1999; Guo et al., 1999; Shen et al., 1997; Struhl and Greenwald, 1999; Wong et al., 1997) and nicastrin (Hu et al., 2002; Kopan and Goate, 2002; Lopez-Schier and St Johnston, 2002) flies, mice and worms develop Notch-like phenotypes. The cleavage at the conserved valine residue (Val1744) releases Notch intracellular domain and initiates the signalling cascade (S3 cleavage; Figure 1.1A) (Schroeter et al., 1998).

1.2.3 Notch mediated transcriptional switch

Once freed from the plasma membrane, NICD travels into the nucleus and forms a ternary complex with the DNA binding factor CSL and the transcriptional coactivator Mastermind (Sel-8/Lag-3 in *C. elegans*) (Petcherski and Kimble, 2000a; Petcherski and Kimble, 2000b; Wu et al., 2000). Complex formation initiates the displacement of CSL-associated co-repressors, such as CtBP, SMRT, SHARP, CoREST, Sin3A, CIR, histone deacetylases and MeCP2 (Lai, 2002a; Stancheva et al., 2003) (Figure 1.2). The

formation of the ternary complex is a prerequisite for the recruitment of the additional transcription factors CBP/p300 and PCAF, which through direct interaction with NICD and Mastermind lead to acetylation of the chromatin (Fryer et al., 2002; Kurooka and Honjo, 2000; Wallberg et al., 2002).

So far, six crystal structures of the CSL-mediated transcriptional complex have been determined in *C. elegans*, human and mouse (Friedmann et al., 2008; Kovall and Hendrickson, 2004; Nam et al., 2006; Wilson and Kovall, 2006). CSL proteins consist of three conserved domains: N-terminal domain (NTD), β-trefoil domain (BTD) and C-terminal domain (CTD) whereby NTD and BTD recognise specific DNA sequences and establish contacts in the major and minor groove (Kovall and Hendrickson, 2004). *In vitro* oligonucleotide enrichment experiments have identified the sequence 5'-C/TGTGGGAA-3' as the target DNA sequence motif (Chung et al., 1994; Tun et al., 1994) which agrees with known *in vivo* binding sites albeit not all are located close to promoters (Nellesen et al., 1999).

For the interaction of NICD with CSL and Mastermind, the RAM as well as the ankyrin domains are required (Nam et al., 2003). Around 20 residues of the RAM domain interact with the BTD of CSL whereas the ankyrin repeats mediate complex stabilisation by binding to the N-terminal domain of Mastermind (Kovall, 2008). The C-terminal domain of Mastermind has been shown to be important for interaction with CBP/p300 and further transcriptional activation (Fryer et al., 2002). Deletions of the C-terminal part results in a dominant-negative phenotype *in vivo*, which allows the ternary complex to form but abolishes transcriptional activation (Wu et al., 2000).

Once the ternary complex has assembled it is already targeted for degradation. Nuclear transcription factors need to have a short half-life in order to respond to rapidly changing activity levels. Mastermind can initiate complex destruction by recruiting cyclin-dependent kinase-8 (CDK8), which directly phosphorylates NICD within its transactivation domain and C-terminal PEST domain, thereby targeting it for degradation through the ubiquitin ligase Fbw7/Sel10 (Fryer et al., 2004). NICD harbouring C-terminal deletions results in a gain-of-function allele and thus can lead to oncogenic transformation *in vivo* (Weng et al., 2004).

Once NICD is degraded, the complex dissociates and recruitment of corepressors is initiated by CSL. The CSL-corepressor-complex is further associated with the DNA

but in contrast to the activation complex only confers a low stability DNA-interaction with a fast exchange rate (Krejci and Bray, 2007) (Figure 1.2).

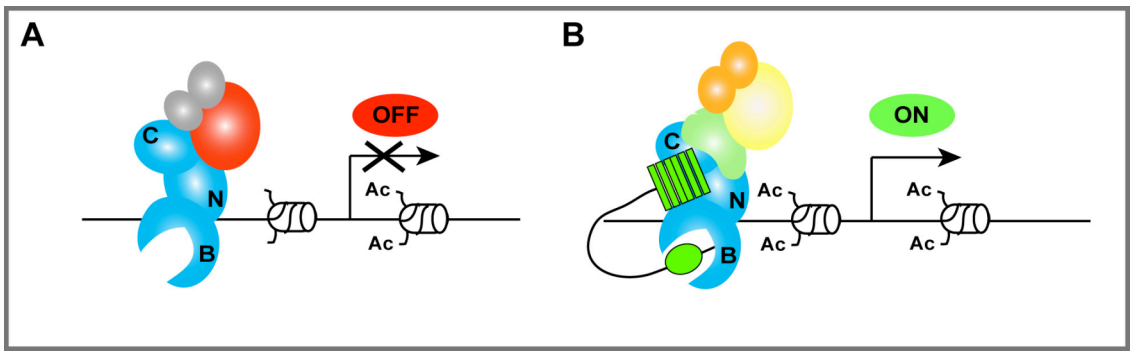

Figure 1.2 Formation of the Notch transactivation complex. (A) Repressor complex consisting of DNA-bound CSL (blue; B, BTD; N, NTD; C, CTD) and associated co-repressors (red and grey). (B) Formation of the Notch transactivation complex through binding of NICD (green) to CSL and recruitment of Mastermind (lime green) and co-activators (yellow and orange) leads to acetylation (Ac) of the chromatin and transcription of target genes.

1.2.4 Modes of Notch signalling

Several different modes of Notch signalling have been described during metazoan development and within self-renewing tissues. The most prominent role for Notch signalling is lateral inhibition. This mechanism is based on studies from *Drosophila* neurogenesis and *C. elegans* vulva development (Artavanis-Tsakonas et al., 1999). At the beginning, progenitors are similar and express equivalent amounts of Notch ligands. Through lateral inhibition, Notch signalling amplifies small differences within the cell population leading to two neighbouring cells being different.

Contrary to lateral inhibition, Notch is also able to exert lateral induction in the *Drosophila* wing margin (Bray, 1998; de Celis and Bray, 1997) and in some vertebrate cells. Thereby, Notch activation in one cell has a cooperative effect on its neighbouring cells leading to sharply defined gene expression boundaries (Lewis, 1998)

Notch can also function as a gate-keeper: for example, in the intestine where Notch keeps crypt progenitor cells in an undifferentiated state (Stanger et al., 2005). On the other hand, Notch is capable of inducing differentiation, as in the skin (Wilson and Radtke, 2006). Another mechanism includes binary cell fate decisions such as in the lymphoid system where Notch can specify the T cell lineage at the expense of the B cell

lineage, which arise from one single precursor (Radtke et al., 2004). Its function as an oncogene or tumour suppressor has further increased the interest in research of Notch signalling (Radtke and Raj, 2003).

1.2.5 Notch signalling targets

The assembly of the Notch transactivation complex mediates a transcriptional switch and leads to the activation of target genes. Although Notch plays an important role in numerous processes throughout metazoan development only relatively few direct target genes have been identified.

1.2.5.1 Basic helix-loop-helix (bHLH) family of Notch targets

The best characterised family of Notch targets is the Hes family in mammals, and the genes of the *Enhancer of Split (E(spl))* complex in *Drosophila* (referred to as Hes proteins) (reviewed in Artavanis-Tsakonas et al., 1999; Iso et al., 2003). Hes proteins are classified as bHLH-type transcriptional repressors and act by negatively regulating downstream target genes (Ishibashi et al., 1995; Ohtsuka et al., 1999). In the mammalian genome, seven members of the Hes family *(Hes1-7)* were characterised, however, mice do not have a *Hes4* gene. In *Drosophila,* the *E(spl)* complex comprises 11 genes which are activated in response to Notch signalling (Bailey and Posakony, 1995; Cooper et al., 2000; Lai et al., 2000; Lecourtois and Schweisguth, 1995) including seven members of the Hes family of bHLH transcriptional regulators (Jennings et al., 1994).

Hes factors contain three conserved domains, which confer transcriptional activity: bHLH, orange and WRPW tetrapeptide (tryptophan, argenine, proline, tryptophan) (Figure 1.3). The basic region mediates DNA binding whereas the HLH structure is responsible for dimerisation. In contrast to other bHLH factors, Hes proteins contain a distinctive proline residue in the centre of the basic region (Figure 1.3). Heterodimer partners are recruited and stabilised via binding to the orange domain (Dawson et al., 1995; Taelman et al., 2004). The C-terminal WRPW tetrapeptide is not only important for interaction with corepressors and thus transcriptional repression (Fisher et al., 1996) but also acts as poly-ubiquitination signal (Kang et al., 2005). Altogether, these domains are indispensable for the function of Hes proteins in transcriptional repression.

Two modes of repression have been described for Hes proteins: active and passive repression acting on conserved sequences in target promoters (Kageyama et al., 2007b). While most bHLH factors bind to the class A and B E-box consensus sequences (5'-CANNTG-3'), Hes proteins recognise class C sites (5'-CACG(C/A)G-3') or the N-box element in their target promoters (5'-CACNAG-3') (Akazawa et al., 1992; Ohsako et al., 1994; Sasai et al., 1992). However, most of these studies were done *in vitro* and it is not clear yet whether these sites are recognised *in vivo*. *Drosophila* E(spl) proteins were shown to bind to class B E-box sequences but the surrounding base pairs were more critical than the core E-box sequence (5-'CACGTG-3') (Jennings et al., 1999).

So far, nobody has systematically characterised the target sites of the vertebrate Hes proteins. During active repression, Hes proteins form homo- or heterodimers with Hey1 and bind to the N-box or class C site. This mechanism is dependent on the interaction of the WRPW domain with corepressors of the Transducine-like E(spl) (TLE) family, which are evolutionary conserved homologues of *Drosophila* Groucho. However, the modes by which Groucho mediates target gene repression are not fully understood yet. Groucho is able to bind to chromatin directly which subsequently is converted in a closed conformation thereby repressing transcription (Sekiya and Zaret, 2007). Groucho has also been shown to interact with histone deacetylases, which in turn inactivate the chromatin (reviewed in Jennings and Ish-Horowicz, 2008).

During passive repression, Hes proteins form heterodimers with other bHLH proteins. These complexes do not bind the DNA but rather (exhibit a dominant-negative effect on the E-box within the target promoter) neutralise those bHLH proteins and prevent their binding to E-boxes (reviewed in Kageyama et al., 2007b). This leads to sequestration of bHLH factors, which would normally form functional activating heterodimers binding to the E-box. bHLH proteins, other than Hes proteins, can also act as activators when bound in heterodimers and enhance expression of targets via the E-box (Johnson et al., 1992). *Drosophila* E(spl) proteins have additionally been shown to repress proneural target genes in a DNA-binding-independent mechanism through protein-protein interactions with proneural activators (Giagtzoglou et al., 2003). In conclusion, bHLH proteins can act as activators or repressors thereby leading to a concerted regulation of cell proliferation and differentiation in many organs (reviewed in Kageyama et al., 2007b).

In mammals, Hes genes are expressed in the central nervous system where they are implicated in maintaining the neural stem cell fate as well as in regulating boundary

formation. They are also involved in binary cell fate decisions mediating astrocyte versus neuronal cell fate specification (Kageyama et al., 2008). Stem cell maintenance and binary cell fate decision in the digestive organs is also regulated to some extend by Hes genes (reviewed in Kageyama et al., 2007b). Another function of Hes proteins involves the oscillator mechanism of *Hes1* and *Hes7* in the presomitic mesoderm (PSM) of the mouse embryo (section 1.3). *Hes1*, *Hes5* and *Hes7* are regulated by Notch signalling (Bessho et al., 2001a; Ohtsuka et al., 1999) whereas *Hes2*, *Hes4* and *Hes6* seem to act in a Notch-independent manner (Koyano-Nakagawa et al., 2000; Nishimura et al., 1998).

Another class of bHLH proteins has been classified as Notch target genes, the Hey/Hesr/HRT/CHF/gridlock/HERP family (hereafter referred to as HERP). HERP proteins are closely related to the Hes proteins but instead of the proline in the basic region, they carry a glycine residue (Figure 1.3). Moreover, HERP family members have a YRPW (tyrosine, arginine, proline, tryptophan) or related tetrapeptide signal instead of WRPW (Iso et al., 2001b). HERP proteins also have an additional conserved region TE(V/I)GAF (threonine, glutamic acid, valine/isoleucine, glycine, alanine, phenylalanine) C-terminal of the tetrapeptide that is absent in Hes proteins (Iso et al., 2003).

Notch activity is able to activate expression of *HERP1* and *Hes1* in a CSL-dependent manner in cultured cells, whereas *HERP2* shows a tissue-specific regulation through NICD when expressed in smooth muscle cells derived from the thoracic aorta (Iso et al., 2002; Iso et al., 2001a). Hes and HERP proteins can both repress transcription through formation of homodimers or heterodimers with each other. The mode of repression, however, differs between the two classes of bHLH factors: HERP proteins do not recruit TLE/Groucho but instead engage with the mSin3 complex, another major corepressor complex (Iso et al., 2001b).

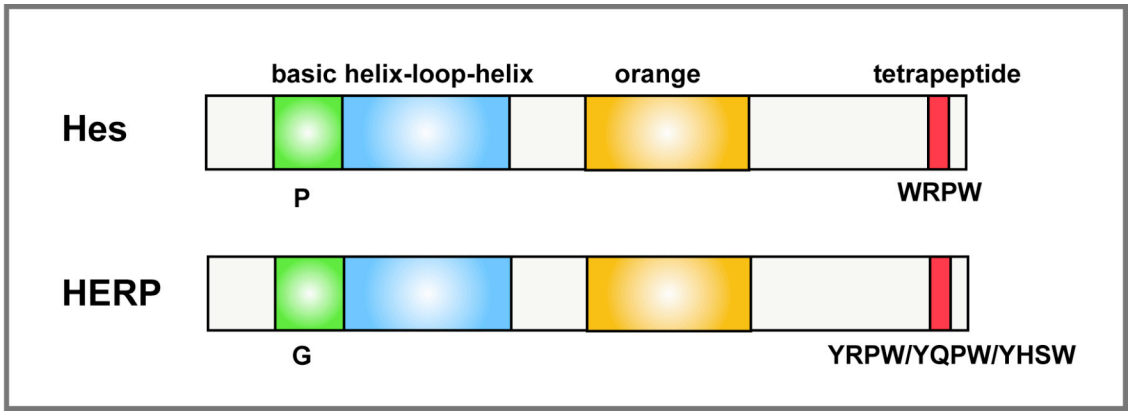

Figure 1.3 Domain structure of bHLH proteins Hes and HERP. Hes and HERP proteins are characterised by 4 distinct domains: basic domain (green, with class-defining residues P or G indicated); HLH domain (blue); orange domain (orange) and tetrapeptide motif at C-terminus (red).

1.2.5.2 Targets of Notch signalling after oncogenic transformation

All members of Notch have been implicated in cancer either acting as an oncogene or tumour suppressor (reviewed in Radtke and Raj, 2003). Initially, Notch1 was identified in human T cell acute lymphoblastic leukaemia (T-ALL), with activating mutations within the extracellular heterodimerization domain and/or the PEST region (Ellisen et al., 1991; Weng et al., 2004). Gene expression profiling and ChIP-chip (Chromatin immunoprecipitation combined with microarrays) analysis from T-ALL cell lines identified *c-Myc* as a transcriptional target of Notch1 (Palomero et al., 2006; Weng et al., 2006).

Similarly, the constitutive expression of NICD using a mouse mammary tumour virus leads to the development of lactation-dependent mammary tumours (Klinakis et al., 2006). ChIP analysis and electrophoretic mobility shift assay also revealed *c-Myc* as a Notch target gene during mammary tumourigenesis in mice and humans (Efstratiadis et al., 2007).

1.2.5.3 Targets of Notch signalling in other systems

Notch does not only cause T cell leukaemia when deregulated, but is also involved in normal T cell development (Hasserjian et al., 1996). Using cDNA Representational Difference Analysis (RDA) in murine thyoma cell lines Deftos et al. identified *Deltex*, *Meltrin β* (*ADAM* family metalloprotease), *Pre-Tα* (a component of the Pre-TCR complex involved in thymocyte development), *Hes1*, and members of the

Ifi-200 gene family (involved in transcriptional regulation and cell cycle control) as Notch1 target genes in T cells (Deftos and Bevan, 2000).

Moreover, the cell cycle regulator of G1 to S-phase transition and proto-oncogene *cyclinD1* was shown to be a Notch transcriptional target in rat kidney epithelial (RKE) cells (Ronchini and Capobianco, 2001). Other genes have been reported as being Notch targets, including *Notch1* itself (Kimble and Simpson, 1997), *CDKN1A* (gene for cyclin-dependent kinase inhibitor 1A (p21, Cip1)) in primary keratinocytes (Rangarajan et al., 2001) and the bHLH protein E47 in the B-lymphocyte lineage albeit in a CSL-independent manner (Ordentlich et al., 1998). The *Nrarp (Notch regulated ankyrin repeat protein)* gene was first identified as Notch target gene in *Xenopus* embryos (Lamar et al., 2001) and recently as Notch effector within the developing mouse retina (Phng et al., 2009).

Many of the experiments that were carried out to identify Notch targets, do not distinguish between a direct and an indirect response to Notch signalling. This can lead to the identification of genes that are not direct targets but are activated as a secondary effect.

A genome-wide study to identify Notch signalling targets in the *Drosophila* DmD8 muscle progenitor cell line using temporally controlled pathway activation and subsequent ChIP array analysis revealed several novel target genes (Krejci et al., 2009). *In vivo* validation confirmed an involvement of these targets in the maintenance of adult muscle progenitors and cell morphogenesis. There is also a considerable overlap between targets from the muscle specific cell line with targets from blood-related Kc cells. Notably, direct target genes were in most cases part of signal transduction pathways, such as the RTK (EGFR), Notch, TGF-β and Wnt pathways. This implies that the Notch signalling pathway has the ability to modulate other signalling pathways. Moreover, identified targets were from both categories, positive and negative regulators, suggesting a differential activation mechanism through Notch, depending on the context (Krejci et al., 2009).

The most difficult part in addressing novel Notch signalling targets to my mind is the establishment of a controllable system, which allows temporally regulated pathway activation in order to identify direct target genes. Krejci et al. have been successful in creating a tissue culture system that upon addition of ethylenediaminetetraacetic acid (EDTA) leads to cleavage of the Notch receptor and subsequent pathway activation

(Krejci and Bray, 2007). In their study, targets of Notch were identified 30 minutes after pathway activation using ChIP directed against CSL combined with a genome-wide array approach (Krejci et al., 2009). Previous studies have relied on long-term effects of blocking or increasing pathway activity in cultured cells. The challenge so far has been the realisation of a similar system in an animal model.

1.3 Vertebrate somitogenesis

One well-studied role of the Notch pathway in metazoan development is during the establishment of the repeated pattern of the vertebrate body axis. Epithelial blocks of mesoderm, called somites, are generated sequentially during embryogenesis and serve as precursors for vertebrae, ribs and attached skeletal muscles (Tam, 1986). They form one after another from the anterior part of the unsegmented presomitic mesoderm (PSM), which is located at the posterior tail end in vertebrate embryos (Figure 1.4). The periodicity by which somites are laid down is characteristic for each species, ranging from 30 min in the zebrafish, 90 min in the chicken and 120 min in the mouse, to 4-5 h in human embryonic development (reviewed in Dequeant and Pourquie, 2008). Pairs of somites are generated in a head-to-tail fashion and the number is regulated within each species, from 30 pairs in zebrafish, to several hundred in snakes (Gomez et al., 2008).

Strikingly, the period of the formation of one pair of somites matches the period of dynamic or oscillatory gene expression in the PSM. It has thus been proposed that the process of somitogenesis underlies the function of a "segmentation clock", which generates an oscillatory signal and leads to somite formation. This oscillator mechanism is joined by opposing fibroblast growth factor (Fgf)/Wnt and Retinoic acid gradients, which position the determination front. When cells reach this front, which is characterised by a signalling threshold, they become defined to the future segment. An initial model of the segmentation process was proposed by Cooke and Zeeman and was termed the "clock and wavefront model" (Cooke and Zeeman, 1976) (Figure 1.5).

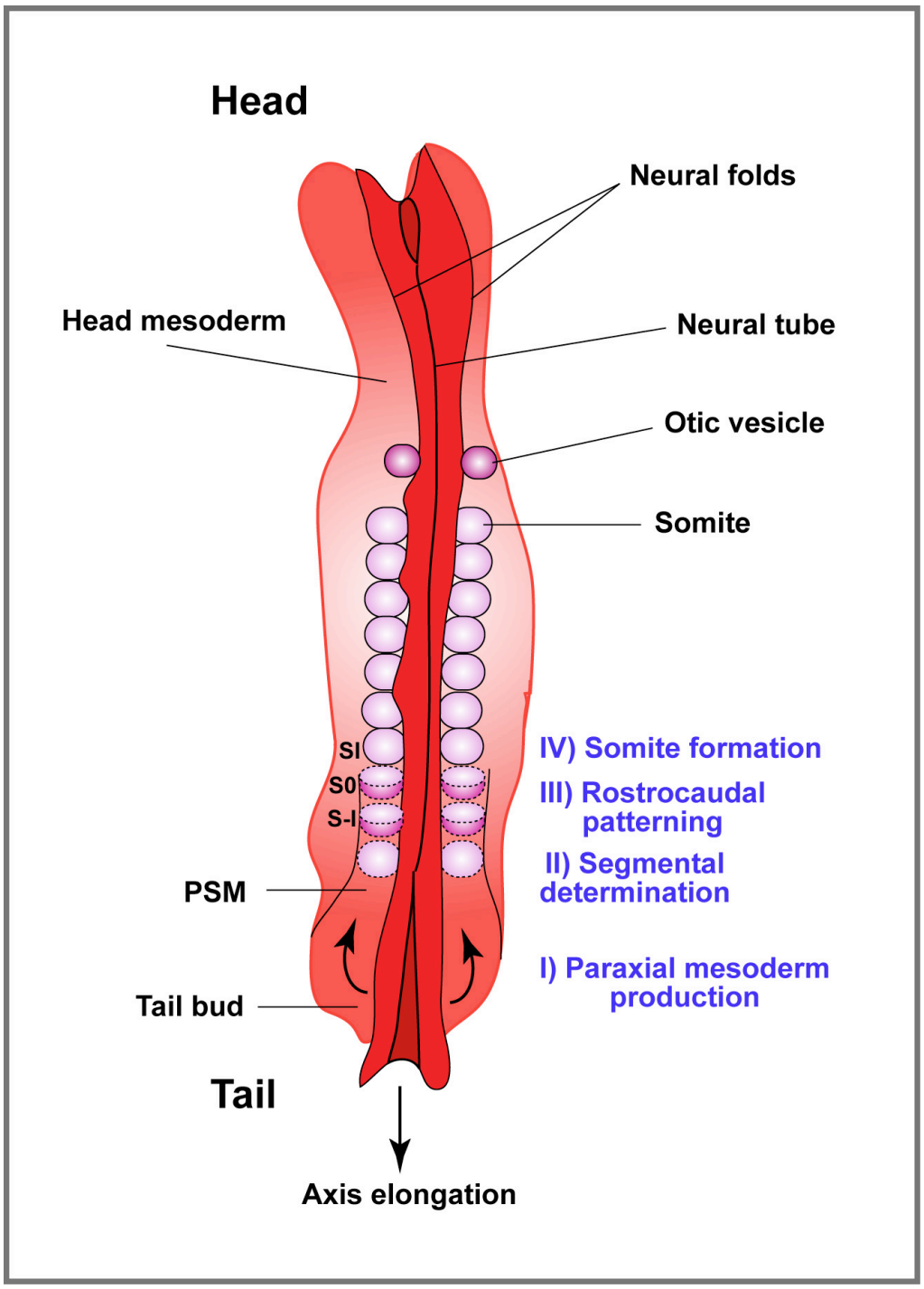

Figure 1.4 Segmentation of the vertebrate embryo (adapted from Dequeant and Pourquie, 2008). Dorsal view of an early human embryo demonstrating vertebrate segmentation: I) paraxial mesoderm production from the progenitor pool within the tail bud (bent arrows show movement of paraxial mesoderm cells into the presomitic mesoderm (PSM)), II) segmental determination, III) rostrocaudal patterning of presumptive somites and IV) somite formation. Anterior-most somites will be part of the occipital bone whereas subsequent somites give rise to the vertebrae. Numbering of prospective somites in the PSM in negative roman numerals according to (Pourquie and Tam, 2001). Newly-formed somites are labelled with increasing roman numerals according to Ordahl (1993). Straight arrow indicates direction of axial elongation.

The first oscillatory gene was identified in chicken, *c-hairy1*, a homologue of *Drosophila hairy* (Palmeirim et al., 1997). More recently, a genome-wide approach has uncovered approximately 30 genes with oscillatory transcription at a periodicity similar to somitogenesis in the PSM of mouse embryos (Dequeant et al., 2006). These genes were known targets of the Notch and Fgf signalling pathways on the one hand and the Wnt pathway on the other hand. All genes belonging to the Notch and Fgf pathways were found to oscillate in phase, but out of phase with genes of the Wnt pathway. However, the nature of the actual pacemaker, which drives oscillation of these genes and thus somite formation, still remains elusive. In the following paragraphs, I will discuss possible roles of the three cycling pathways, Notch, Wnt and Fgf in the segmentation clock.

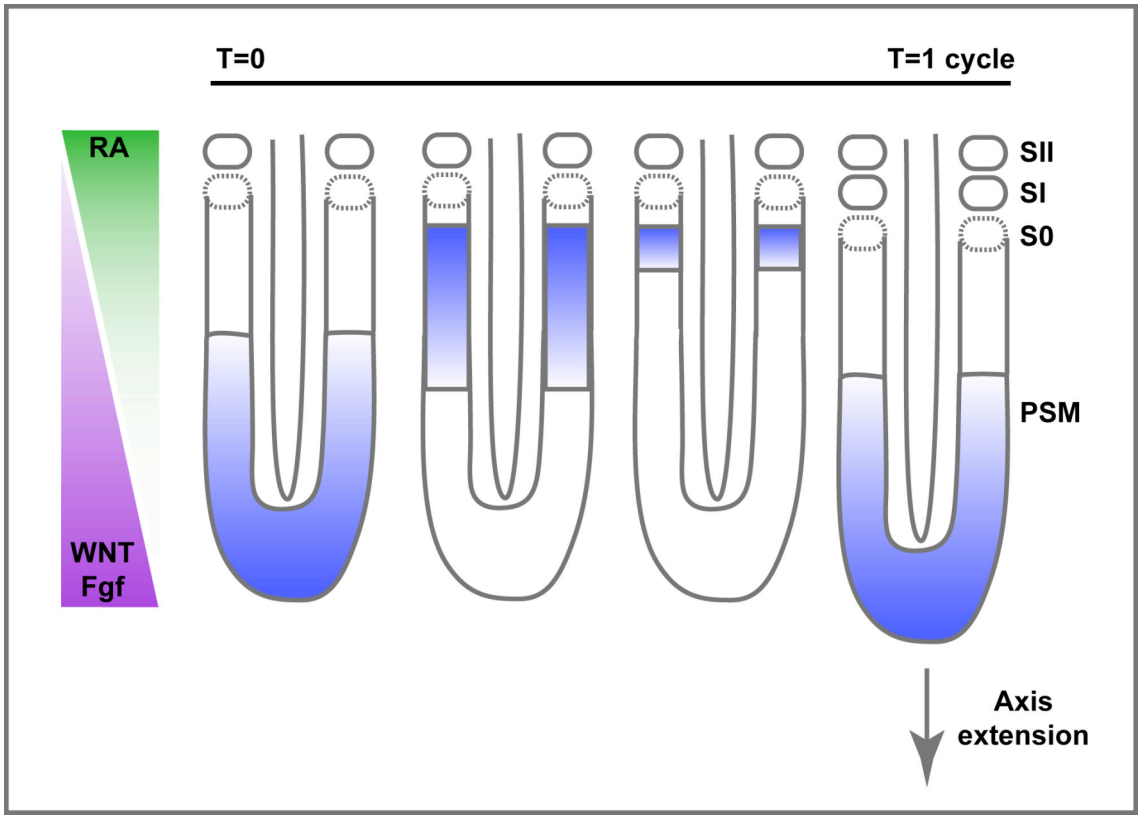

Figure 1.5 A model for somitogenesis: The clock and wavefront model. Sections of the posterior part of the vertebrate embryo are shown, including the presomitic mesoderm (PSM) as well as presumptive (S0) and already formed somites (SI and SII). The yet unidentified nature of the segmentation clock drives a wave of cyclic gene expression (blue) in the PSM whereas opposing retinoic acid (RA; green) and Wnt (purple)/Fgf gradients set the determination front. One cycle of the segmentation clock (T=1) leads to the formation of a new pair of somites and thereby promotes axis extension (arrow).

1.3.1 Role of Notch signalling during vertebrate somitogenesis

The anterior-posterior segmented body pattern is a hallmark not only of vertebrates but also of arthropods and annelids (Damen, 2007). A common genetic network defining the origin of segmentation is still debated. Segmentation in *Drosophila* has been demonstrated to depend on a hierarchical cascade of transcription factors and does not involve Notch signalling (Ingham, 1988; Nusslein-Volhard and Wieschaus, 1980; Pankratz et al., 1990; St Johnston and Nusslein-Volhard, 1992). However, Notch/Delta signalling has been shown to be required for segmentation in the spider *Cupiennius salei*, which suggests an evolutionary conservation of the pathway in the generation of the reiterated body pattern (Stollewerk et al., 2003).

Oscillating gene expression within the PSM of the vertebrate embryo is driven by the segmentation clock, which sets the pace for the periodic formation of somites. In order to generate oscillations, downstream signalling targets need to feedback negatively on the system including a delay resulting from transcriptional and translational timings (Lewis, 2003). Targets of the Notch pathway have been shown to fulfil these criteria (Giudicelli et al., 2007; Henry et al., 2002; Holley et al., 2002; Oates and Ho, 2002; Ozbudak and Lewis, 2008).

The bHLH transcriptional repressor and direct Notch target gene *Hes7* can inhibit its own transcription and has therefore been suggested to be a good candidate to act at the core of the mouse segmentation clock (Bessho et al., 2001a). *Hes7* knock-out mice show a severe skeletal phenotype with no regular vertebrae or ribs, which almost always results in post-natal lethality (Bessho et al., 2001b). Moreover target gene oscillations, such as of *Lfng* or *Dusp4*, are arrested in *Hes7* mutants and expressed throughout the PSM (Bessho et al., 2001b; Niwa et al., 2007). Since Hes7 also represses its own expression, *Hes7* dynamics are abolished as well (Bessho et al., 2003; Bessho et al., 2001b).

Stabilisation of Hes7 protein also disrupts Notch oscillations and suggests that a short half-life of Hes7 is crucial for the segmentation clock (Hirata et al., 2004). However, upon blockage of Notch signalling through knock-out of CSL, *Hes7* oscillations are still observed in the posterior PSM (Niwa et al., 2007). This, along with the observation that Wnt oscillations are still present in the absence of *Hes7* (Hirata et al., 2004) implies, that the *Hes7* regulatory feedback loop might not act as the pacemaker. Furthermore, regulation of *Hes7* transcription is not only dependent on

Notch signalling but also on Fgf signalling, which initiates *Hes7* oscillations in the posterior PSM. Notch is responsible for the propagation of *Hes7* transcription in the anterior PSM (Niwa et al., 2007).

A second potential mechanism for a segmentation clock driven by Notch signalling involves a *Lfng* negative feedback loop regulating periodic Notch activation (Dale et al., 2003). *Lfng* is a target of Notch in both mouse and chicken and upon deletion in mouse or overexpression in chick embryos, the regulatory function impinging on Notch signalling is lost (Dale et al., 2003; Morimoto et al., 2005). Mutations in *Lfng* have always been associated with defects in vertebrate segmentation and *Lfng* knock-out mice are born with severe axial deformations (Evrard et al., 1998; Zhang and Gridley, 1998).

Lfng is characterised by a striking expression pattern, with oscillatory expression in the posterior PSM and anterior non-oscillatory stripe transcription, which have been related to distinct enhancer elements in the *Lfng* promoter (Cole et al., 2002; Morales et al., 2002). Recently, Shifley et al. have generated transgenic mice lacking the promoter block, which is responsible for oscillatory expression of *Lfng*, and thereby driving *Lfng* transcription only in the stripe domain (Shifley et al., 2008). These mice show a regionalised skeletal phenotype with severely disorganised anterior cervical, thoracic and lumbar vertebrae and ribs, whereas sacral and tail vertebrae are only minimally affected. This suggests a differential role of Notch signalling in the formation of the anterior and posterior body halves (Shifley et al., 2008).

Results from our lab's studies driving chicken *Lfng* (*cLfng*) stripe expression in a *Lfng* null background recapitulate the data from Shifley et al. to some extent and shows dose-dependent rescue of the tail vertebrae and somites (Stauber et al., submitted). The sacral and to some degree adjacent lumbar areas also form regular vertebrae and somites. This is consistent with *Lfng* knock-out mice which are able to form regular patterned sacral vertebrae suggesting that *Lfng* and thus modulated Notch signalling is not required for the formation of the sacrum (Stauber et al., submitted). In conclusion, both investigations propose a differential regulation of the segmentation clock during the establishment of the vertebrate length axis.

One argument against the *Lfng* feedback loop as master oscillator in the vertebrate segmentation clock is the observation that the Notch target gene *Hes7* continues to oscillate upon loss of *Lfng* (Niwa et al., 2007) or when *Lfng* is overexpressed in the

mouse (Serth et al., 2003). Our studies show that these oscillations are perturbed and superimposed on uniform *Hes7* expression, suggesting that *Lfng* null embryos do not experience dynamic *Hes7* expression (Stauber et al., submitted).

Constitutive activation of Notch signalling in the mouse PSM does not abolish somite border formation, although Notch target genes, such as *Hes7* and *Lfng,* are expressed constitutively (Feller et al., 2008). These transgenic mice still show oscillating expression of the Wnt target *Axin2* (Feller et al., 2008) placing Wnt signalling upstream of Notch signalling. Altogether, these studies argue against Notch signalling being the primary pacemaker of the segmentation clock.

A new model for the role of Notch within the segmentation clock comes from studies in zebrafish, where all known cyclic components are part of the Notch pathway (Holley, 2007). In this system, Notch is responsible for synchronising cell-autonomous oscillations of neighbouring PSM cells rather than setting the pace for dynamic transcription (Jiang et al., 2000). The observed delayed disruption of somite boundaries in zebrafish Notch mutants, as well as after blockage of the pathway (by the γ-secretase inhibitor DAPT), may be due to a loss of cell-to-cell coupling (reviewed in Ozbudak and Pourquie, 2008). It has also been shown that boundary formation and thus segmentation can recover after removal of the γ-secretase inhibitor DAPT (Ozbudak and Lewis, 2008; Riedel-Kruse et al., 2007). Thus, at least in the zebrafish, Notch signalling acts as a coupling device for synchronisation of oscillations within PSM cells rather than as a pacemaker.

1.3.2 Wnt pathway oscillations within the segmentation clock

In mouse embryos, in contrast to zebrafish, several components of the Wnt signalling pathway exhibit oscillatory expression, such as the targets *Axin2*, *dickkopf homolog 1* (*Dkk1*), *c-Myc* and *dapper homolog 1* (*Dact1*) (Dequeant et al., 2006). Evidence for a role of Wnt signalling during segmentation comes from the hypomorphic *Wnt3a* mutant *vestigial tail* (*vt*), which exhibits loss of Notch and Wnt oscillations (Aulehla et al., 2003). This observation places the Wnt pathway upstream of the Notch signalling pathway in the generation of the repeated somites (Nakaya et al., 2005; Satoh et al., 2006).

Activation of the Wnt pathway leads to stabilisation and accumulation of β-catenin, which in turn translocates to the nucleus and activates target genes (Barker,

2008). A dynamically activated β-catenin loop was suggested to exert pacemaker functions in mouse embryos (Aulehla et al., 2003). As predicted, conditional loss-off function of β-catenin in the PSM leads to a loss of Notch and Wnt oscillations (Dunty et al., 2008). However, in a constitutively expressed β-catenin background, Notch and Wnt target oscillations are still observed, arguing against a pacemaker function of Wnt within the segmentation clock (Aulehla et al., 2008; Dunty et al., 2008). These results suggest that Wnt signalling, like Notch signalling, is not at the core of the segmentation clock.

1.3.3 Oscillatory expression of Fgf targets during somitogenesis

The same microarray study that identified oscillating Notch and Wnt genes also uncovered a novel class of dynamic genes within the Fgf pathway (Dequeant et al., 2006). *Sprouty homologue 2* (*Spry2*), *dual specificity phosphatase 6* (*Dusp6*) and *Dusp4* (Niwa et al., 2007) as well as *snail homologue 1* (*Snai1*) (Dale et al., 2006) are targets and negative feedback inhibitors of the Fgf pathway and contribute to periodic Fgf signalling activity. This notion is also supported by periodic phosphorylation of extracellular signal-regulated kinase (ERK) mediated through Dusp4 or Dusp6, which establishes a negative feedback circuitry essential for oscillations (Chu et al., 1996; Li et al., 2007).

Fgf signalling was proposed to lie upstream of Wnt and Notch signalling within the mouse segmentation clock, because a conditional knock-out of the *Fgf receptor 1* (*Fgfr1*) ceases oscillations in Fgf, Wnt and Notch pathway components (Niwa et al., 2007; Wahl et al., 2007). When blocking Fgfr1 with a chemical inhibitor (SU5402), *Lfng* oscillations are abolished with one cycle of delay, suggesting that Fgf signalling regulates Notch signalling indirectly (Niwa et al., 2007). The loss of Fgf signalling and thus *Lfng* oscillations can be rescued by elevated Wnt signalling through constitutive expression of β-catenin (Aulehla et al., 2008). This leads to a restoration of Notch oscillations in the absence of Fgf signalling and indicates that Fgf cannot act as the central pacemaker of the segmentation machinery, either.

According to the evidence provided, neither Notch, nor Wnt nor Fgf signalling acts independently at the heart of the segmentation clock to control the periodic formation of somites. Either these oscillating signalling pathways act redundantly, or they represent the output of a yet unidentified pacemaker.

1.4 Aim of this thesis

The Notch signalling pathway is an essential part of the communication system that supports and governs metazoan development. Although the pathway seems to follow a linear principle, fine-tuning can occur at many steps, leading to diverse outputs within various tissues or at different times.

In this introduction, I have highlighted several aspects of the Notch signalling cascade: its participants and modulation thereof, as well as a few biological functions and mechanisms. However, there are numerous processes involving Notch, which are not mentioned here, perhaps more are still to be discovered. While we are beginning to understand how the signal is initiated, modified and transmitted we know little about the nature of target genes and how they respond to the Notch signal. For example, what makes a gene a Notch target in one tissue and developmental context but not in another? Several attempts have been made towards this direction, mainly within a tightly regulated tissue culture system (see sections 1.2.5.2 and 1.2.5.3).

This work describes a novel approach, making use of a mouse-model combined with high-throughput sequencing, to find Notch signalling targets at any given time during development and in any tissue. To achieve this goal I have chosen to make use of a knock-in approach to attach a high-affinity tag to the endogenous *Notch1* locus. This tag is biotinylatable and thus the biotinylated NICD protein and its *in vivo* binding partners can be purified using the biotin-avidin system.

The same strategy can also be applied to unravel the mechanics of the vertebrate segmentation clock. Up to now we do not have an idea of what drives the periodic formation of somites in vertebrate embryos. The Notch signalling pathway has been shown to play an important role during segmentation, with its targets *Lfng* and *Hes7* at the core of feedback loops capable of generating oscillations (section 1.3.1). Through purifying targets of Hes7 during mouse embryogenesis (using the same approach) I am aiming to identify novel components within the segmentation clock circuitry, which might contribute to setting the pace of somite formation.

I will describe the use of two different strategies to investigate the nature of Notch target genes *in vivo*: the first looks at targets of Notch itself and the second searches for targets of Hes7. In the case of the direct Notch approach, targets would be identifiable in virtually any tissue Notch is expressed in, whereas the Hes7 strategy specifically

aims to broaden our understanding on somitogenesis. In this thesis, I present the first *in vivo* analysis to examine the specific properties of Notch target genes in different developmental contexts in vertebrates.

CHAPTER 2: Establishing a novel technique to identify *in vivo* targets of Notch signalling

2.1 Introduction

Chromatin immunoprecipitation (ChIP) is a widely used method to identify DNA binding sites of transcription factors and to explore the dynamics of gene regulation. In recent years genome-wide approaches combining ChIP with microarrays (ChIP-chip) or high-throughput sequencing (ChIP-seq) have led to a new area in understanding global transcriptional networks (Robertson et al., 2007).

Conventional ChIP experiments are often limited by the availability and quality of antibodies against the protein of interest. In order to circumvent these limitations, several technologies have been developed which usually involve the fusion of a peptide to the protein of interest and the use of antibodies with high affinity to these so called "tags". To study protein-protein and protein-DNA interactions several tags are available such as the maltose binding protein, the Haemagglutinin (HA)-tag, the FLAG-tag, the Tandem Affinity Purification (TAP)-tag, the Histidine (His)-tag and the Biotin Acceptor Peptide (BAP)-tag (Rigaut et al., 1999; Terpe, 2003).

The BAP-tag is biotinylatable and biotin is then recognised by avidin/streptavidin (instead of an antibody). The biotin-avidin system stands out among the affinity-based purification methodologies because of the exceptionally high affinity of its bond. With a K_D of 10^{-13} to 10^{-15} M the dissociation constant is several orders lower than that of an antibody (average K_D of antibodies is between 10^{-7} – 10^{-11} (Larvor et al., 1994)). It represents one of the strongest non-covalent interactions, allowing for more stringent washing conditions in the purification step. Moreover, the BAP-tag comprises of only 14 amino acids and is therefore unlikely to affect folding of the tagged protein (Beckett et al., 1999; Schatz, 1993).

Biotin, also known as vitamin H or B7, is an essential coenzyme synthesized by plants, most bacteria and some fungi and is required for all forms of life (Chapman-Smith and Cronan, 1999). Specific biotin-ligases (or biotinylases), of which most organisms have only one paralogue, add biotin to the epsilon amino group of the lysine residue within the acceptor sequence (Chapman-Smith and Cronan, 1999).

BirA from *Escherichia coli* is the best-studied biotinylase and has *in vivo* only a single target, the biotin carboxyl carrier protein subunit of the acetyl-CoA carboxylase. BirA is a 35.3 kDa multifunctional protein that not only catalyses biotinylation but also acts as the transcriptional repressor that regulates biotin biosynthesis in *E. coli* (Cronan, 1989). The biotinylation reaction is very specific and biotin-dependent carboxylases are the only known substrates *in vivo* (Barker and Campbell, 1981; Choi-Rhee et al., 2004).

In eukaryotes, biotin serves as a covalently bound coenzyme for acetyl-CoA carboxylase, pyruvate carboxylase, propionyl-CoA carboxylase and 3-methylcrotonyl-CoA carboxylase (Zempleni, 2005). These enzymes use biotin as a cofactor and mobile carboxyl carrier in processes like gluconeogenesis, lipogenesis, amino acid degradation and energy transduction (Samols et al., 1988).

Because of the advantages pointed out above, I decided to use the BAP/biotin-avidin system in transgenic mice to find novel targets of Notch signalling *in vivo*. This approach has been used before successfully in tissue culture cells to identify novel protein complex partners of the haematopoietic transcription factor GATA-1 (de Boer et al., 2003; Hamlett et al., 2008; Rodriguez et al., 2005). So far, there have been no records on the use of this method *in vivo*. My project describes the establishment of the BAP/biotin-avidin technique for the first time in a mouse model.

This chapter describes the step-wise set-up of the BAP/biotin-avidin system from cell culture assays to establishing the transgenic mouse lines. After first validating the BAP-tagged proteins in cell culture, I generated transgenic mice, which express BAP-tagged Notch1 and Hes7, respectively (see 1.2 for an introduction on the Notch signalling pathway). Biotinylation is achieved through inter-crosses of the BAP-tagged mice with mice expressing the BirA biotinylase from *E. coli* (Driegen et al., 2005).

2.2 Results

This chapter is divided into three parts: The first describes experiments in cell culture, including tests for functionality of tagged proteins and biotinylation of the fused BAP-tag. The second and the third part deal with the generation and the phenotypic analysis of knock-in mice carrying biotinylated alleles of *Notch1* or *Hes7*, respectively.

2.2.1 Validation of BAP-tagged Hes7 and Notch1 intracellular domain (NICD) in cell culture

2.2.1.1 Construction of BAP-tagged alleles of *Hes7* and *Notch1 intracellular domain* (*NICD)* for expression in tissue culture cells

I have generated BAP-tagged cell culture constructs of cDNAs from *Hes7 (Hes7^{BAP})* and *NICD (NICD^{BAP})* in order to test functionality of the proteins as well as biotinylation in cell culture based assays. The Hes7 tagging approach will be described first, followed by the NICD strategy.

Since I had no information on previous tagging approaches for Hes7, I decided to construct N- and C-terminally tagged Hes7^{BAP} fusion proteins, trying to avoid functionally important sequence motifs. In the N-terminal fusion, the BAP sequence (Figure 2.1A) (Beckett et al., 1999) was inserted at the translation start site of *Hes7* cDNA. The BAP peptide sequence is preceded by the dipeptide MA - methionine and alanine -, which ensures efficient translation of the protein. For the C-terminally BAP-tagged Hes7, I inserted the 14-mer tag 12 amino acids upstream of the conserved tetrapeptide motif (tryptophan, arginine, proline, tryptophan; WRPW) that is essential for TLE/Groucho mediated repression (Buscarlet and Stifani, 2007). I expected, that placing the BAP-tag further upstream should not interfere with this action.

To generate a *NICD^{BAP}* expression vector, I attached the 14-mer BAP-tag (Figure 2.1A) via a di-glycine linker to the C-terminal end. For the cell culture experiments, I chose to BAP-tag and express only the constitutively active form of Notch1 (NICD), which does not need to undergo maturation. However, the knock-in mice will express the full length Notch1 receptor with the BAP-tag and after maturation NICD^{BAP} translocates into the nucleus and activates target genes. Previous tagging strategies of Notch1 with an enhanced green fluorescent protein (EGFP) suggest, that the C-terminus provides an acceptable position for the tag (Jack et al., 2001). Moreover, the BAP-tag has to be within the cleaved C-terminal NICD part, which goes to the nucleus upon activation of the pathway.

Briefly, the cloning involved the amplification of two parts, 5' and 3' (referred to as upper and lower, respectively), by PCR with primers containing parts of the BAP sequence. Subsequently these products were cloned into a TOPO expression vector for sequencing. Once the sequence was confirmed, the two parts were ligated via the

*Eco*RV restriction site, which was generated within the BAP sequence through introduction of a silent mutation. The BAP-tagged cDNAs were further excised from the TOPO vector backbone and introduced into a mammalian expression vector, which drives high level expression from the human cytomegalovirus (CMV) immediate-early promoter/enhancer (see Figure 2.1B for the cloning strategy; section 7.1.3 for a detailed description of the cloning).

Using this split-construct technique described above, I was able to introduce the BAP-tag into various positions of mouse *Hes7* and *NICD* cDNAs efficiently, resulting in the construction of *pCI-Hes7*$^{C\text{-}BAP}$, *pCI-Hes7*$^{N\text{-}BAP}$ and *pcDNA3.1*$^{+}$*-NICD*^{BAP} for expression in cultured cells.

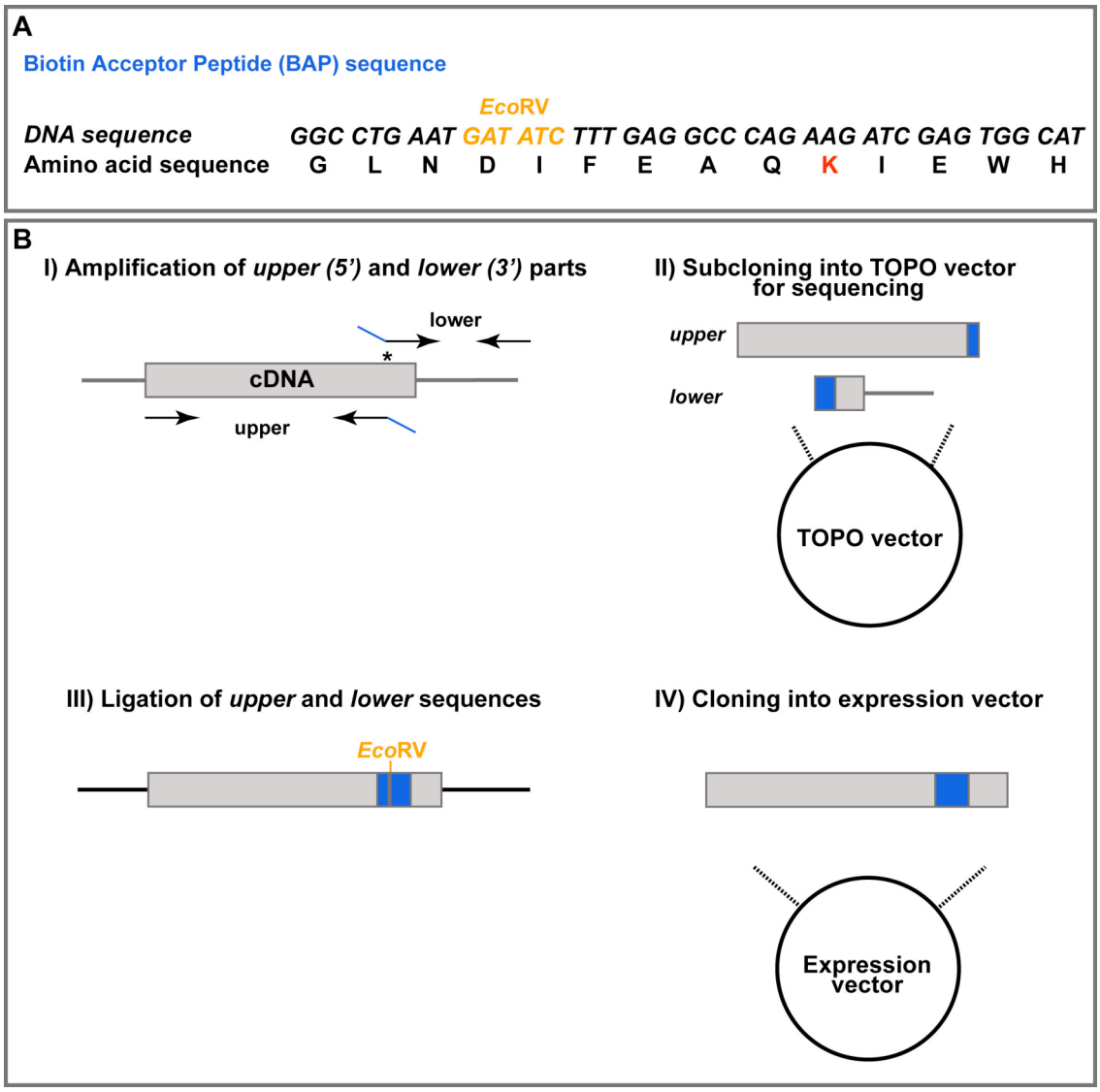

Figure 2.1 Cloning strategy to generate BAP-tagged *Hes7* and *NICD* cDNAs. (A) Nucleotide sequence of BAP-tag with highlighted position of the through silent mutation introduced *Eco*RV site (orange font). Specific lysine (K) residue for attachment of biotin is marked as red letter. (B) Outline of the cloning strategy to generate BAP-tagged cDNA. Asterisk indicates position for inserting BAP-tag (blue rectangle). The BAP sequence (blue line) is included in the upper reverse and lower forward primer sequences to generate upper and lower parts each harbouring a stretch of the BAP-tag. PCR products are subcloned individually into a TOPO cloning vector and subsequent *Eco*RV digest and ligation joins the BAP tag. The BAP-tagged cDNA is further cloned into a mammalian expression vector.

2.2.1.2 Validation of BAP-tagged proteins in a cell culture based assay

In order to check functionality of $Hes7^{N\text{-}BAP}$, $Hes7^{C\text{-}BAP}$ and $NICD^{BAP}$ proteins I performed luciferase reporter assays in tissue culture cells. Hes7 is a transcriptional repressor of the basic helix-loop-helix (bHLH) family and was previously shown to bind to a hexameric N-box sequence when expressed in cultured cells (Bessho et al., 2001a; Chen et al., 2005) For the $Hes7^{BAP}$ functionality test, the *firefly* luciferase is driven by the *β-actin* promoter, which contains six N-box repeats as binding sites for Hes7 (Ishibashi et al., 1994). Co-expression of this reporter with wildtype Hes7 in the mouse fibroblast cell line C3H10T½ leads to a 90% decrease in luciferase activity (Figure 2.2A; (Bessho et al., 2001a)). Similar results were obtained when expressing the $Hes7^{C\text{-}BAP}$ instead of wildtype Hes7 (Figure 2.2A). This suggests, that $Hes7^{C\text{-}BAP}$ is able to function as a repressor in cell-based assays and might exhibit full activity *in vivo*. In contrast, $Hes7^{N\text{-}BAP}$ is only able to reduce reporter activity by 40% (Figure 2.2A). These results show, that inserting the BAP-tag at the N-terminus of Hes7 impairs the function of Hes7, while inserting it 17 amino acids upstream of the C-terminus retains full repressor activity. Therefore, I chose to insert the BAP-tag at the C-terminal position within the *Hes7* locus to establish transgenic mice. In subsequent experiments, I refer to the $Hes7^{C\text{-}BAP}$ fusion as $Hes7^{BAP}$.

NICD is a transcriptional activator, which upon Notch pathway activation and subsequent proteolytic cleavage translocates into the nucleus and activates transcription of target genes (section 1.2.3). This is achieved through binding of NICD to CSL (CBF1 or RPB-jκ in vertebrates, Su(H) in *Drosophila*, Lag-1 in *Caenorhabditis elegans*; collectively referred to as CSL) thereby promoting the formation of a transactivation complex (Figure 1.2). CSL has been shown to recognise 5'-C/TGTGGGAA-3' as the target DNA sequence motif, which is present in Notch target gene promoters (Chung et al., 1994; Tun et al., 1994). To test, whether $NICD^{BAP}$ is functional as a transcriptional activator, I co-expressed it with a 509 bp *Hes1* promoter fragment driving *firefly* luciferase activity (Nishimura et al., 1998). The promoter fragment stretches from -758 bp to -249 bp and contains three CSL binding sites, which are bound by a complex of CSL and NICD and subsequently activate transcription (Nam et al., 2006; Wilson and Kovall, 2006). Upon co-expression of the wildtype NICD protein in C3H10T½ mouse fibroblasts the luciferase reporter shows 30-fold activation confirming *Hes1* as a Notch target gene (Figure 2.2B) (Nishimura et al.,

1998). $NICD^{BAP}$ is able to activate the reporter to the same extent, suggesting that the tagged protein retains its full function. In order to generate *in vivo* $Notch^{BAP}$ fusion protein the transgenic mice will carry the BAP-tag at this C-terminal position.

These results were obtained using the C3H10T½ mouse cell line. Other cell lines, such as NIH3T3 or L-cells did not replicate the data, suggesting that these results are cell-line specific (data not shown). Although the reporter assays in C3H10T½ cells indicate that $Hes7^{C\text{-}BAP}$ and $NICD^{BAP}$ are functional, it does not imply that this will also be the case *in vivo*. These experiments simply give a hint how the proteins might function *in vivo*.

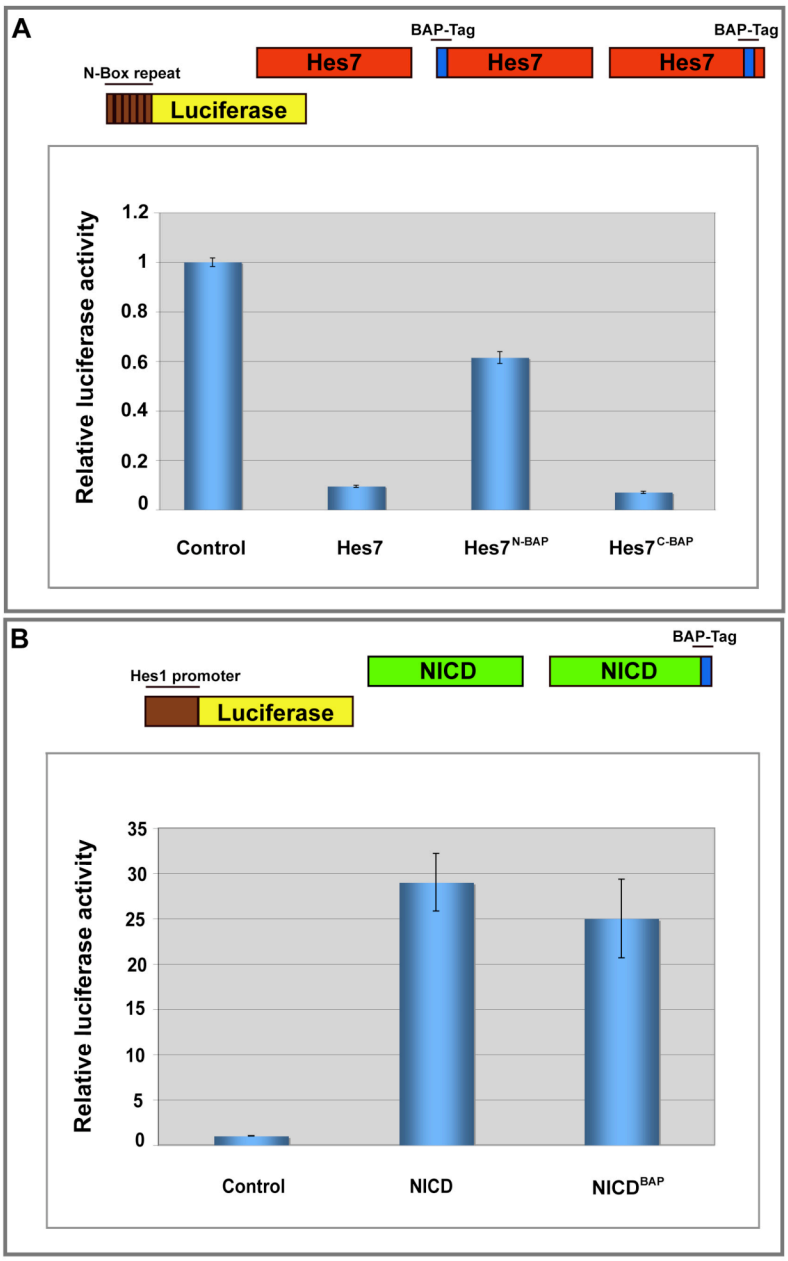

Figure 2.2 Luciferase reporter assay in C3H10T½ cells to validate Hes7^{BAP} (A) and NICD^{BAP} (B) fusion proteins. 100 ng of the *firefly* luciferase reporter, driven either by the *β-actin* promoter containing six N-box repeats (A) or a 509 bp *Hes1* promoter fragment (B) was co-transfected with 200 ng of *pCI* (Control), *pCI-Hes7*, *pCI-Hes7$^{N\text{-}BAP}$* (Hes7$^{N\text{-}BAP}$) or *pCI-Hes7$^{C\text{-}BAP}$* (Hes7$^{C\text{-}BAP}$) (A) and *pcDNA3.1^{+}* (Control), *pCDNA3.1^{+}-NICD* or *pcDNA3.1^{+}-NICD^{BAP}* (NICD^{BAP}), respectively (B). 4 ng of the *Renilla* luciferase were added to each well for reference reading. After 24 h of incubation the assay was analysed and relative luciferase activities (shown as mean ± standard deviation for three experiments) determined. Drawings above the diagrams show schematic outline of the constructs used. The binding site for Hes7 or NICD is indicated by a brown box upstream of the luciferase reporter (yellow). Hes7 and NICD proteins are drawn as red and green rectangles, respectively. The BAP-tag is shown as a blue box.

2.2.1.3 Biotinylation of BAP-tagged proteins in cell culture

After having shown that Hes7^{BAP} and NICD^{BAP} perform as well as the wildtype proteins in the luciferase reporter assays, I examined if the BAP-tag can be biotinylated efficiently in cells by the *E. coli* biotinylase BirA. Therefore I co-expressed equal amounts of either Hes7^{BAP} or NICD^{BAP} with BirA in the mouse fibroblast cell line C3H10T½. Using streptavidin coated magnetic beads, I was able to show that the biotinylated proteins Hes7^{BAP} and NICD^{BAP} can bind efficiently the streptavidin matrix (Figure 2.3).

In contrast, untagged Hes7 and NICD are not biotinylated and do not bind the streptavidin beads when co-expressed with the BirA biotinylase (Figure 2.3). I further tested if Hes7^{BAP} and NICD^{BAP} proteins can be biotinylated by endogenous biotinylases present in the cells. Expression of Hes7^{BAP} or NICD^{BAP} proteins in the absence of BirA did not lead to a signal on the western blot when developed with streptavidin and this suggests, that they are not biotinylated by endogenous biotinylases (Figure 2.3).

There are two prominent high-molecular weight bands, around 100 and 170 kD, that appear in each lane on the western blot in Figure 2.3 (asterisks). They represent endogenous biotinylated proteins, which mainly reside in the mitochondrial matrix and were identified as biotin-dependent carboxylases (Beckett, 2007). The presence of these carboxylases (pyruvate and propyonyl CoA carboxylases) was confirmed by protein identification through mass spectrometry (Figure 3.8C).

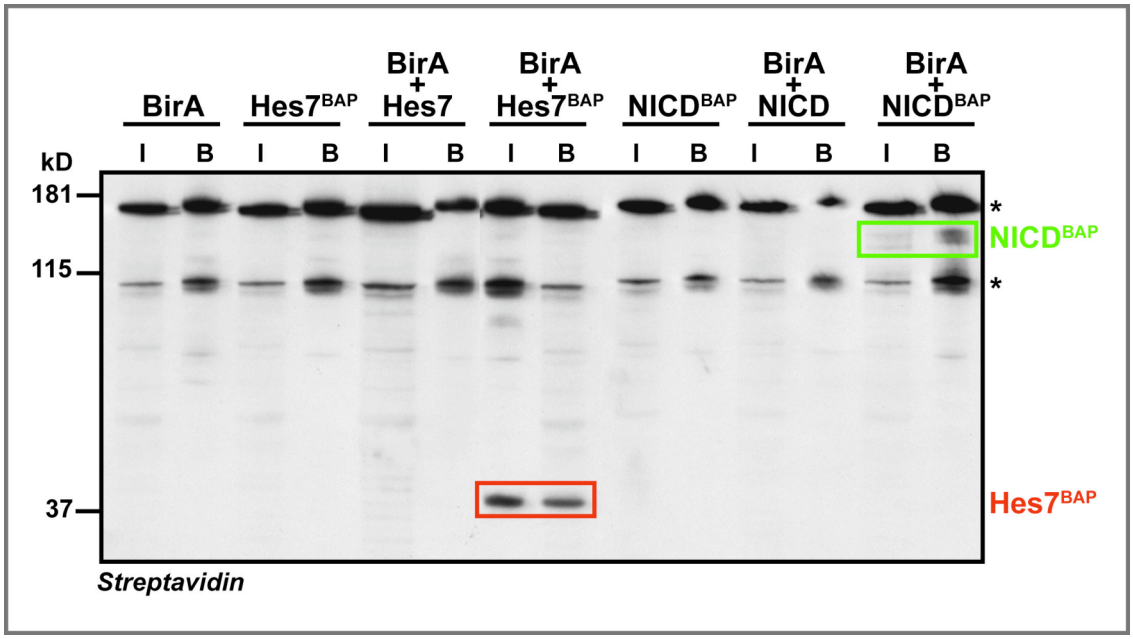

Figure 2.3 Hes7^{BAP} and NICD^{BAP} proteins are biotinylated upon co-expression of BirA in HeLa cells. HeLa cells were transfected with either *pCI-3xHA-BirA* (BirA), *pCI-Hes7^{BAP}* (Hes7^{BAP}) or *pcDNA3.1^{+}-NICD^{BAP}* (NICD^{BAP}) or BAP-tagged and untagged constructs together with equal amounts of *pCI-3xHA-BirA* (BirA). Crude nuclear extracts were prepared 24 h after transfection and 20 µg loaded onto 20 µl of blocked streptavidin beads for 1 h at 4 ºC. The beads were boiled at 95ºC for 5 minutes in 20 µl of loading buffer and samples run on a 4-12% Bis-Tris gel. Biotinylated proteins were detected with a streptavidin-probe (1:25,000). Red rectangle highlights biotinylated Hes7^{BAP} in input (I) fraction and after binding to streptavidin beads (B). Biotinylated NICD^{BAP} in I and B fractions are marked with a green box. Asterisks label endogenous biotinylated proteins.

2.2.2 Validation of Hes7^{BAP} and NICD^{BAP} *in vivo*

The BAP-tagging of Hes7 and NICD proved successful in that the proteins retain full functionality upon tagging, and biotinylation of the BAP-tag is specific in cell-based assays. However, before trying the system in the mouse, I asked the question if Hes7^{BAP} and NICD^{BAP} are functional in a different biological system such as the zebrafish *Danio rerio*. Overexpression of *Notch* in the zebrafish has previously been associated with a neurogenic phenotype leading to a massive decrease in neurons (Gray et al., 2001; Schier et al., 1996). Moreover, heat-shock mediated overexpression of *her7*, the zebrafish Hes7 orthologue and Notch target gene, has been shown to disrupt somitogenesis leading to irregularly spaced segments (Giudicelli et al., 2007). The

bHLH type repressors Her7 and Her1 were shown to act cooperatively to regulate the formation of somites in the zebrafish through autoregulatory feedback inhibition (Holley et al., 2002; Oates and Ho, 2002).

I prepared mRNA of *NICD*, *NICD*^{BAP}, *Hes7* and *Hes7*^{BAP} and injected each into two-cell stage fish embryos (section 7.2.2). In the case of the NICD and NICD^{BAP} *in vivo* functionality test, the embryos were fixed 15 hours after post fertilisation (hpf) and subsequently hybridised with an *islet1* probe, a marker for a subset of primary neurons (Inoue et al., 1994; Korzh et al., 1993). An excessive loss of neurons as described previously (Gray et al., 2001; Schier et al., 1996) was recapitulated upon injection with *NICD* or *NICD*^{BAP} mRNAs (Figure 2.4). This suggests that NICD^{BAP} still acts as a functional activator *in vivo* and is able to induce ectopic expression of Notch signalling in the zebrafish.

For the *Hes7* and *Hes7*^{BAP} mRNA injections, embryos were analysed 24 hpf in respect of a segmentation phenotype. However, upon injection of *Hes7* and *Hes7*^{BAP} mRNAs no obvious defects in the segmentation process were observed (not shown). Although both injection efficiency, as seen by co-expression of a fluorescent reporter, and mRNA quality were similar to the NICD injection experiment, the fish established regular somite patterns. The reason for this outcome is probably the fact that *Hes7* mRNA is degraded *in vivo* due to a lack of conservation between *her1* or *her7* and *Hes7*. Alternatively, Hes7 might not have a function within the zebrafish segmentation clock. From these experiments it is impossible to infer the affect of the BAP-tag on Hes7 in the zebrafish.

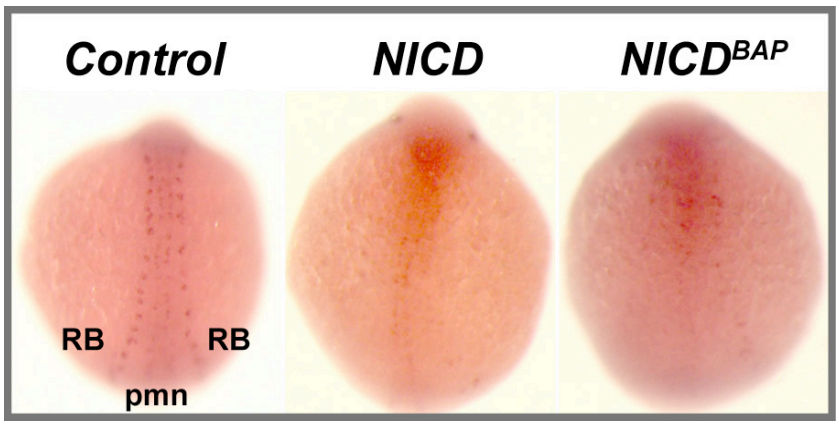

Figure 2.4 *Islet1 in situ* hybridisation of 15 hpf zebrafish embryos injected with either control (n=6), *NICD* (n=17) or *NICD*^{BAP} (n=13) mRNA. Dorsal views (anterior at the top) of 15 hpf zebrafish embryos hybridised with *islet1* probe. Primary motoneurons (pmn) normally form two rows in the median neural plate and Rohon Beard (RB) sensory neurons are visible at the lateral edges of the neural plate (control).

2.2.3 Establishing transgenic *Hes7*$^{BAP/BAP}$ and *Notch1*$^{BAP/BAP}$ mouse lines

2.2.3.1 Generation of *Hes7*^{BAP} and *Notch1*^{BAP} targeting constructs for homologous recombination in embryonic stem cells

The pre-experiments to validate BAP-tagged Hes7 and NICD in cell culture suggested that both proteins retain their function upon fusion with the BAP-tag. Moreover, *in vivo* experiments confirmed that NICD^{BAP} is still able to activate transcription in the zebrafish embryo. The functional analysis of the tagged proteins as well as the confirmation of biotinylation in cultured cells is an essential requirement before setting up an *in vivo* system.

The goal of my thesis is to find novel targets of Notch signalling *in vivo* using transgenic mouse lines that express either Hes7^{BAP} or Notch1^{BAP}. I used a knock-in strategy to integrate into sites of the open reading frame, tested above (section 2.2.1). The advantage of this method over the pro-nuclear injection technique (resulting in random integration) is, that - in homozygous knock-in mice - no endogenous, untagged protein would compete with the BAP-tagged proteins; and the use of the endogenous promoter leads to physiological levels of expression.

The targeting construct for homologous recombination comprises of two parts, the 5' and the 3' homologous regions (HR), which flank a *neomycin* resistance *(neo^{r})* cassette. I made use of the *pFloxR1-modified (pFloxR1-mod)* vector (Christine Laclef,

unpublished), which contains two multiple cloning sites for insertion of the HRs, and in between the *neo*^{r} gene with flanking *LoxP* sites for site-specific excision of *neo*^{r} (Figure 2.5).

Briefly, for the *Hes7*^{BAP} targeting construct, I PCR-amplified three parts, Hes7-BAP 5'-homology region *(Hes7*$^{BAP\ 5'HR}$*)*, Hes7-BAP 3'-homology region upper *(Hes7*$^{BAP\ 3'HR\ upper}$*)* and Hes7-BAP 3'-homology region lower parts *(Hes7*$^{BAP\ 3'HR\ lower}$*)*. The reason for having two stretches of the 3'HR was to facilitate the introduction of the BAP-tag through an *Eco*RV restriction site, which was created in the sequence as a silent mutation (Figure 2.1). I first tried a strategy using a 4 kb 5'HR and a 2.2 kb 3'HR, however I did not succeed to identify embryonic stem cell clones that had integrated the targeting construct after electroporation. Therefore, I cloned a new targeting construct with modified length of the HRs. I chose 1 kb for the 5'HR and 5.1 kb for the 3'HR (*pFloxR1-mod_Hes7*^{BAP} Figure 2.5; section 7.1.4). This strategy was successful and led to the identification of embryonic stem cells (ESC) that had integrated the *Hes7*^{BAP} targeting construct.

The targeting construct to insert the BAP-tag sequence into the *Notch1* locus was constructed similarly and consisted of a 3.3 kb 5'HR and a 2.5 kb 3'HR (*pFloxR1-mod_Notch1*^{BAP}, Figure 2.5B; section 7.1.4). Both constructs were further electroporated into ESCs by the Cancer Research UK Transgenics Facility in Clare Hall (section 7.3.1). The process of generating transgenic mice by homologous recombination involves the replacement of some parts of the gene with the targeting construct resulting in the recombined allele. The removal of the *neomycin* resistance cassette using Cre-specific excision at *LoxP* sites produces a floxed recombined allele harbouring one *LoxP* site (Figure 2.5).

2.2.3.2 Screening of embryonic stem cell clones (ESCC)

In order to find embryonic stem cells (ESC) that had integrated the targeting cassette, cells were selected for *neomycin* resistance (*neo*$^{+}$). Only 0.1 – 1% of integrations are correct for homologous recombination (Joyner, 1991; Templeton et al., 1997). In order to identify homologous recombinants, *neo*$^{+}$ ESCs were picked individually, placed into 96 well plates and grown to clones (section 7.3.1). Genomic DNA of these clones was prepared and analysed using PCR (section 7.3.4) and subsequently Southern blot analysis (section 7.3.5).

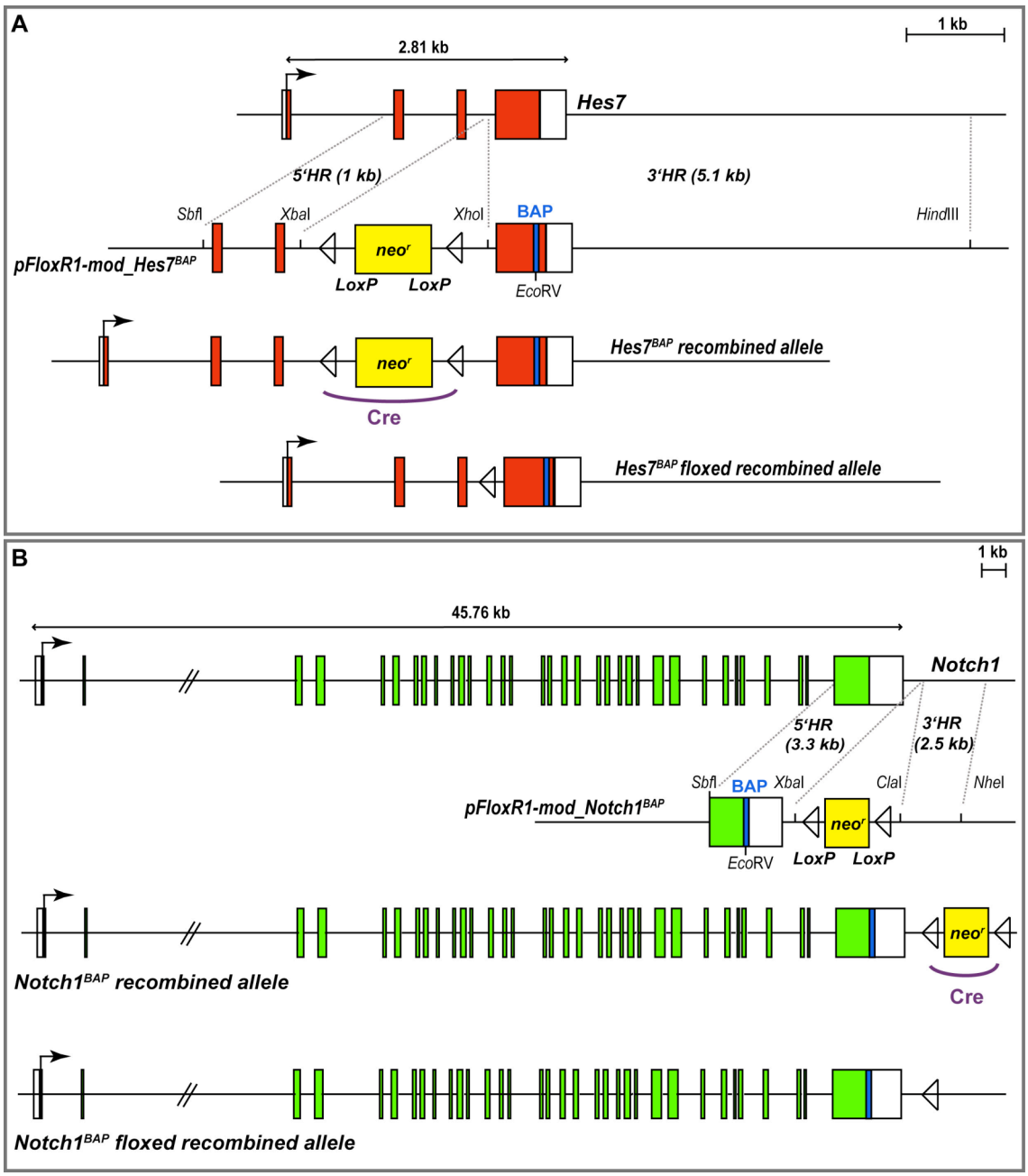

Figure 2.5 Targeting strategy for homologous recombination in embryonic stem cells to generate transgenic *Hes7*^{BAP} and *Notch1*^{BAP} mice. Strategy to replace parts of the endogenous *Hes7* (A) and *Notch1* (B) loci with a BAP-tagged version resulting in *Hes7*^{BAP} (A) and *Notch1*^{BAP} (B) recombined alleles. Targeting vectors contain a 5' and a 3'HR flanking a *neomycin* resistance cassette (*neo*^{r}, yellow box) and two *LoxP* sites (open rectangles) for site-specific excision. Homologous regions were inserted into the targeting vector *pFloxR1-mod* using the resctriction sites indicated. Subsequent expression of the Cre recombinase (purple) leads to excision of the *neo*^{r} cassette and results in *Hes7*^{BAP} (A, bottom) and *Notch1*^{BAP} floxed recombined alleles (B, bottom). The BAP-tag is shown in blue.

2.2.3.2.1 Polymerase chain reaction (PCR) screening of ESCC

In the first instance, the genomic DNA was screened by PCR (section 7.3.4), using primers in the BAP sequence or the *neo*^{r} cassette in combination with gene-specific primers outside the homology region covered by the targeting construct (Figure 2.6). These primer combinations amplify only the homologous recombinant alleles. At least two different primer pairs were used to confirm a positive clone (Table 7.10 for primer sequences) covering both 3' and 5' flanking regions for *Notch1*^{BAP} and only 5' flanking region for *Hes7*^{BAP} because of the long 5'HR.

Altogether, I screened 864 clones for *Hes7*^{BAP} homologous integration (including the first attempt) and 576 clones for *Notch1*^{BAP} homologous integration. For each targeting experiment two positive clones were found, which corresponds to 0.2% and 0.3% success rate, respectively (Table 2.1). This outcome lies within the expected frequency of 0.1 – 1% for homologous recombination in ES cells (Joyner, 1991; Templeton et al., 1997).

Construct	Number of screened ESCCs	Positive clones confirmed
pFloxR1-mod_Hes7^{BAP}	864	3C7, 4E7
pFloxR1-mod_Notch1^{BAP}	576	3E3, 6A12

Table 2.1 Statistics of PCR screening process.

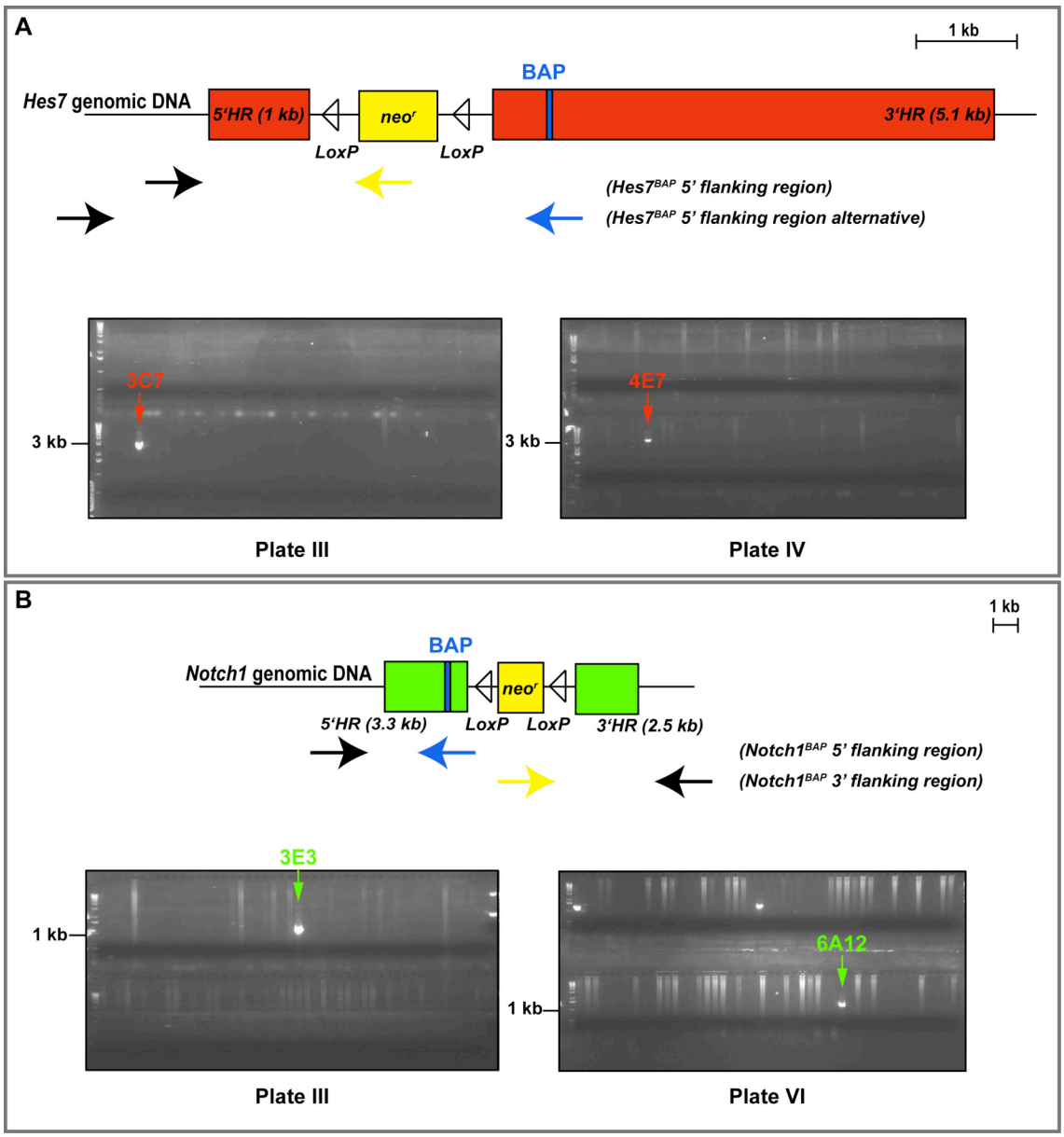

Figure 2.6 PCR screening strategy and results from *Hes7*^{BAP} (A) and *Notch1*^{BAP} (B) homologous recombination events. *Hes7*^{BAP} (A) and *Notch1*^{BAP} (B) recombined loci are shown with primer pairs in the BAP sequence (blue arrow) or the *neo*^{r} cassette (yellow arrow) combined with primers outside the homology region (black arrow). Primer combinations are named in brackets. Homology regions are shown as red *(Hes7*^{BAP}*)* or green *(Notch1*^{BAP}*)* rectangles. (A) PCR products of *Hes7*^{BAP} ESCCs in 96-well plates III and IV using one primer pair combination (*Hes7*^{BAP} *5' flanking region alternative*; 3013 bp) are separated on an agarose gel. Red arrows point to positive clones, 3C7 and 4E7. (B) Similarly, results from the PCR reaction (with primer combination *NICD*^{BAP} *5' flanking region*; 1364 bp) of embryonic stem cell clones in 96-well plates III and VI of *NICD*^{BAP} electroporated ESCCs reveal two positive clones. Green arrows show position of individual clones, 3E3 and 6A12 on the agarose gel.

2.2.3.3 Southern blot screening of PCR-positive ESCCs

Since the PCR screening procedure can lead to false positives due to over-amplification of the target sequences, mis-priming or contamination, additional Southern blot screening is indispensable to verify candidate clones. Southern blot analysis is a useful technique to identify specific DNA sequences, like the integrated targeting cassette, within a mixture of genomic DNA fragments (Southern, 1975). For that purpose, the genomic DNA needs to be digested with specific restriction enzymes that cut the locus at informative positions (e.g. in the resistance cassette as well as outside the homology region). This leads to distinct patterns of signals on the autoradiograph, which allows to distinguish between wildtype and homologous recombinant loci (section 7.3.5).

In order to analyse the four clones, *Hes7*^{BAP} 3C7 and 4E7 and *Notch1*^{BAP} 3E3 and 6A12, by Southern blotting I chose to use two different restriction digests in each case and further hybridisation with specific probes binding 5' and 3' of the targeting cassette within the genomic DNA (Figure 2.7). This strategy verifies if integration had occurred on both sides. The Southern blot analysis shows, that all four clones, *Hes7*^{BAP} 3C7 and 4E7 and *Notch1*^{BAP} 3E3 and 6A12, have the targeting construct integrated at the correct position (Figure 2.7).

Hes7^{BAP} clones 3C7 and 4E7 were digested either with *Eco*RI or with *Xho*I and *Kpn*I resulting in both cases in two signals on the autoradiograph (at 7.3 kb and 3.8 kb as well as at 14 kb and 7.7. kb; Figure 2.7A) confirming the integration of the targeting construct (Figure 2.7A). Genomic DNA from *Notch1*^{BAP} clones 3E3 and 6A12 was digested with either *Stu*I or *Eco*RV and *Xho*I resulting in 5.8 kb and 4.5 kb or 12.9 kb and 9.9 kb, respectively (Figure 2.7B). In each case the larger fragment represents the wildtype fragment, which can be separated from the smaller homologous recombinant fragment (WT and HR in Figure 2.7). Using the Southern blot strategy, integration of the targeting cassette by homologous recombination can be easily distinguished from non-homologous and tandem or multiple integration sites through the distinct fragmentation pattern.

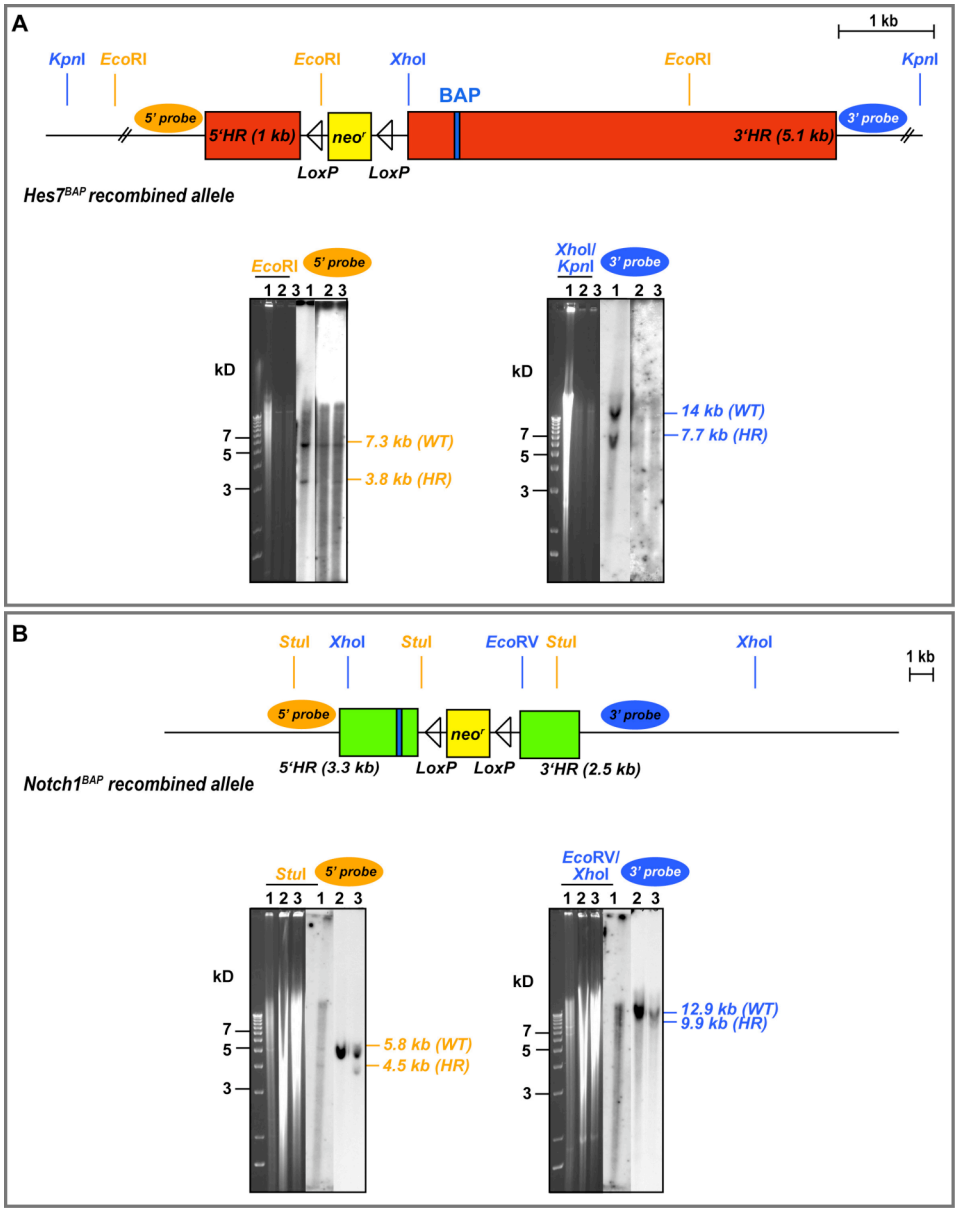

Figure 2.7 Southern blot screening strategy of *Hes7*$^{BAP/+}$ (A) and *Notch1*$^{BAP/+}$ (B) recombined loci. Two different restriction digests are used to test incorporation of the targeting cassette on both integration sides (orange and blue text). Homology regions are shown as red *(Hes7*^{BAP}*)* or green *(Notch1*^{BAP}*)* rectangles. Each Southern blot result shows the agarose gel of the digested genomic DNA (left) and an autoradiograph of the developed result (right). (A) *Eco*RI digest of *Hes7*^{BAP} clones 3C7 and 4E7 (1 and 3) and hybridisation with *Hes7*^{BAP} *5' probe* (orange oval) leads to a 7.3 kb wildype (WT) and a 3.8 kb homologous recombinant (HR) signal. Lane number 2 shows clone 4D6 (as a control), which is negative and only shows the WT fragment. The double digest with *Xho*I and *Kpn*I and subsequent hybridisation with *Hes7*^{BAP} *3' probe* (blue oval) indicates two fragments (14 kb and 7.7 kb) for the positive clones 3C7 and 4E7. (B) Clones 3E3 and 6A12 (1 and 3) have the targeting cassette integrated correctly as seen by hybridisation with *Notch1*^{BAP} *5' probe* (orange oval) and resulting signals at 5.8 kb (WT) and 4.5 kb (HR). Signals at 12.9 kb (WT) and 9.9 kb (HR) are the results for positive *Notch1*^{BAP} clones after hybridising the *Eco*RV/*Xho*I digested genomic DNA with *Notch1*^{BAP} *3' probe* (blue oval), whereas clone 5E8 (2) only shows the WT fragment on both Southern blots.

2.2.4 Establishing homozygous *Hes7*$^{BAP/BAP}$ and *Notch1*$^{BAP/BAP}$ mouse lines co-expressing BirA and phenotypic analysis

2.2.4.1 Mating strategy to obtain double homozygous *Hes7*$^{BAP/BAP}$;*Rosa26*$^{BirA/BirA}$ and *Notch1*$^{BAP/BAP}$;*Rosa26*$^{BirA/BirA}$ mice

The positive clones identified in the screening, *Hes7*^{BAP} 3C7 and 4E7 and *Notch1*^{BAP} 3E3 and 6A12, were injected into blastocyst stage embryos by the Cancer Research UK Transgenics Facility (section 7.3.6). These were implanted into foster mothers and the offspring tested for contribution by recombinant ESCs. C57Bl/6J blastocysts were obtained from the C57Bl/6J mouse line, which produce black/brown chimeras. A high level of coat colour contribution together with a bias to male chimera mice (as the ES cell line is male) was indicative of an ES clone that contributed to the germline. All four embryonic stem cell clones resulted in chimeric offspring with germline contribution as judged by the coat colour (Table 2.2). Chimeric mice were further back-crossed to wildtype C57Bl/6J mice to check for transgene transmission into the next generation. The integration of the BAP cassette into the *Hes7* and *Notch1* loci was confirmed by genotyping PCR from mouse ear biopsies (section 7.3.3). Each injected ESCC resulted in a mouse line (*Hes7*^{BAP} 4E7 and 3C7; *Notch1*^{BAP} 6A12 and 3E3), which showed transmission of the transgene into the next generation as determined by PCR screening of chimera offspring.

In order to remove the *neo*^{r} cassette, which has been shown to influence expression of adjacent genes (Muller, 1999), I crossed the transgenic mice to *PGK-Cre* mice, which ubiquitously express the Cre recombinase from the 3-phosphoglycerate kinase (PGK) promoter. *PGK* is a X-linked gene and therefore I used female *PGK-Cre* mice to remove the floxed gene from all progeny (Lallemand et al., 1998). The *PGK* promoter further drives transgene expression in all tissues, but the levels of expression vary between different cell types (McBurney et al., 1994). The Cre recombinase recognises the 34 bp *LoxP* sites flanking the *neo*^{r} cassette and catalyses site-specific recombination leading to the excision of the DNA between. Using genotyping PCR to detect the *neo*^{r} gene (Table 7.8), I was able to confirm the removal of the floxed *neo*^{r} in *Hes7*$^{BAP/+}$ and *Notch1*$^{BAP/+}$ transgenic mice leaving behind one *LoxP* site within the 3rd intron and another outside (3') of the 3' untranslated region (UTR).

To allow *in vivo* biotinylation, BAP-heterozygous mice *(BAP/+)* were mated to *BirA* homozygous males (kind gift of Dies Meijer, Erasmus Medical Center Rotterdam). These mice express the *E. coli* biotinylase from the *Rosa26* locus, which is ubiquitously expressed throughout development (Driegen et al., 2005). Double-heterozygous *BAP/+;BirA/+* offspring were inter-crossed to establish double-homozygous *BAP/BAP;BirA/BirA* mice. The primer pairs listed in Table 7.8 were used to genotype the pups of these breedings.

ESCC	Number of blastocysts	Number of mice born	Number of Chimeras	Contribution [%]	Males (contribution, %)
Hes7^{BAP} 4E7	11	5	3	70,70,80	3 (70,70,80)
Hes7^{BAP} 4E7	33	9	7	60,75,75,75	2 (75,75)
Hes7^{BAP} 3C7	26	6	2	70,80	2 (70,80)
Hes7^{BAP} 3C7	8	0	0	0	0
Notch1^{BAP} 6A12	13	4	2	85,65	1 (85)
Notch1^{BAP} 6A12	13	0	0	0	0
Notch1^{BAP} 3E3	13	0	0	0	0
Notch1^{BAP} 3E3	40	10	5	65,80,70,80, 50	2 (80, 50)

Table 2.2 Results from the injection of the homologous recombinant ES cell clones (ESC) *Hes7^{BAP}* 4E7 and 3C7 as well as *Notch1^{BAP}* 6A12 and 3E3 into blastocyst embryos and chimera production.

2.2.4.2 Phenotypic analysis of *Notch1$^{BAP/BAP}$;Rosa26$^{BirA/BirA}$* mutant mice

Since Notch signalling is an important key player during development of a mouse embryo e.g. during somitogenesis (section 1.3), I wanted to ask if Notch1^{BAP} retains full activity *in vivo*. Therefore, I chose to investigate the segmented pattern of *Notch1$^{BAP/BAP}$* embryos. Hybridisation of E9.5 homozygous *Notch1$^{BAP/BAP}$* embryos with *Uncx4.1*, a marker for the posterior somite half, did not show any obvious segmentation and compartmentalisation defects (Figure 2.8A). Regular *Uncx4.1* stripes were seen in the

homozygous mutant, which is indistinguishable from the pattern seen in wildtype and heterozygous littermates (Figure 2.8A). These experiments were done in the absence of BirA in order to exclude a possible interference of the biotinylase resulting in false negative results.

Although segmentation is not affected and *Notch1*$^{BAP/BAP}$ embryos appear normal, adult viability is reduced: only 27% (8/120) of expected *BAP/BAP* animals survived after weaning (Table 2.3). Examination of foetuses before birth (E17.5) however showed, that there was no discrepancy between the obtained number of *BAP/BAP* animals and the expected number (3/9; 133% of expected). The *BAP/BAP* foetuses do not seem to be compromised and have no obvious phenotype when compared to wildtype or heterozygous littermates (Figure 2.8A).

Initial viability issues of *Notch1*$^{BAP/BAP}$ animals were eradicated after crossing to *BirA* homozygous mice and subsequent breeding of *BAP/BirA* double heterozygous stock (Table 2.4). 60% of the expected number of double homozygous *Notch1*$^{BAP/BAP}$*;Rosa26*$^{BirA/BirA}$ mice were recovered (4/107) and further used for breeding and expanding the line. Both, male and female *BAP/BAP;BirA/BirA* mice are fertile and produced pregnancies (as judged by the copulation plug) in 76% of cases (16/21).

I next wanted to test if the Notch1^{BAP} protein is biotinylated in the *Notch1*$^{BAP/BAP}$*;Rosa26*$^{BirA/BirA}$ mice and therefore I performed western blot analysis of cell lysates from different mouse tissues using a streptavidin probe. I also chose to detect biotinylated Notch1^{BAP} within the developing retina at five days after birth (P5). The latter tissue provides more material for subsequent chromatin pull-downs. Upon co-expression of Notch1^{BAP} with BirA, I was able to confirm biotinylation of Notch1^{BAP} in both the PSM and the retina, which is seen as a ~150 kD signal on the western blot (Figure 2.8B). Extracts of tissues from *Rosa26*$^{BirA/BirA}$ mice were used as control and represent the biotinylated background binding (asterisks, Figure 2.8B). These data corroborate the cell culture validation experiments and show that Notch1^{BAP} is biotinylated *in vivo* by the BirA biotinylase in different tissues.

Notch1$^{BAP/BAP}$*;Rosa26*$^{BirA/BirA}$ mice do not show any phenotype and can be bred to expand the line for subsequent streptavidin chromatin pull-down experiments from tissues like the PSM or the retina in order to find novel targets of Notch signalling (section 3.2.5). Since Notch signalling is implicated in a variety of processes throughout

development of the embryo and the adult these animals can be used to address the question of Notch target genes in virtually any tissue that expresses *Notch1*.

Genotype	Survival rate past weaning
$Hes7^{BAP/+}$	26/41 (126%)
$Hes7^{BAP/BAP}$	2/41 (19%)
$Notch1^{BAP/+}$	67/120 (112%)
$Notch1^{BAP/BAP}$	8/120 (27%)

Table 2.3 Adult viability of the transgenic lines as determined through inter-crosses of heterozygous *BAP/+* animals. Survival rate past weaning: number of adults recovered / total number of offspring (% of expected).

Genotype	Survival rate past weaning
$Hes7^{BAP/BAP};Rosa26^{BirA/BirA}$	9/298 (48%)
$Hes7^{BAP/BAP};Rosa26^{BirA/+}$	7/298 (19%)
$Hes7^{BAP/BAP}$	3/298 (16%)
$Hes7^{BAP/+};Rosa26^{BirA/BirA}$	50/298 (134%)
$Hes7^{BAP/+};Rosa26^{BirA/+}$	101/298 (135%)
$Notch1^{BAP/BAP};Rosa26^{BirA/BirA}$	4/107 (60%)
$Notch1^{BAP/BAP};Rosa26^{BirA/+}$	6/107 (45%)
$Notch1^{BAP/BAP}$	1/107 (14%)
$Notch1^{BAP/+};Rosa26^{BirA/BirA}$	21/107 (157%)
$Notch1^{BAP/+};Rosa26^{BirA/+}$	25/107 (93%)

Table 2.4 Adult viability of the transgenic lines as determined through inter-crosses of double heterozygous *BAP/+;BirA/+* animals. Survival rate past weaning: number of adults recovered / total number of offspring (% of expected).

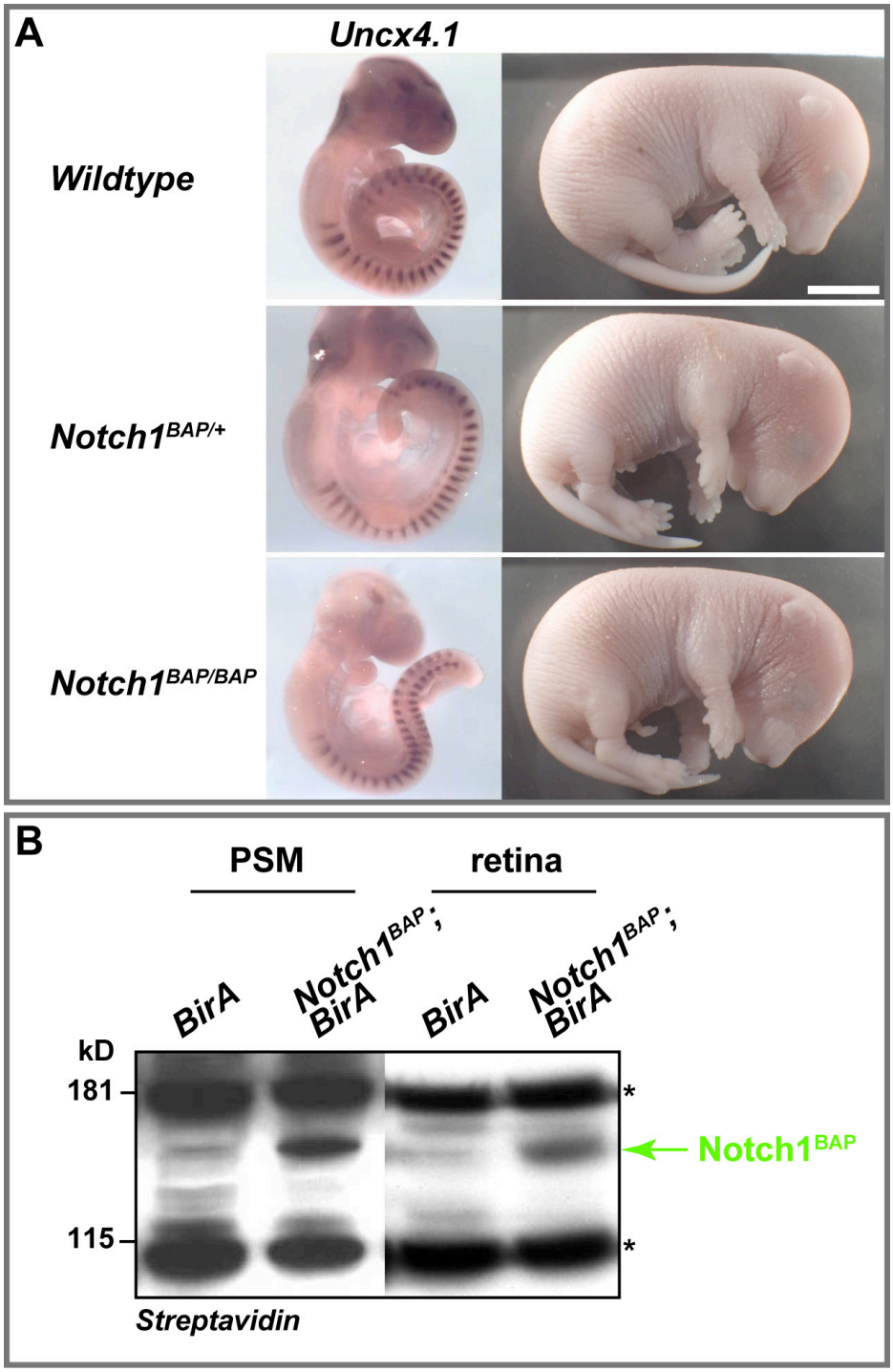

Figure 2.8 *Notch1*$^{BAP/BAP}$ mice are homozygous viable, show no obvious phenotype and Notch1^{BAP} can be biotinylated by BirA *in vivo*. (A) *Uncx4.1 in situ* hybridisation of wildtype, *Notch1*$^{BAP/+}$ and *Notch1*$^{BAP/BAP}$ E9.5 embryos show no differences in expression pattern (left). *Notch1*$^{BAP/BAP}$ E17.5 foetuses develop normally and are indistinguishable from their wildtype or heterozygous littermates. White rectangle represents 5 mm scale bar (B) Western blot analysis, using a streptavidin probe, (1:25,000) of presomitic mesoderm (PSM) extracts and P5 pup retina lysates of *Rosa26*$^{BirA/BirA}$ *(BirA)* and *Notch1*$^{BAP/BAP}$*;Rosa26*$^{BirA/BirA}$ *(Notch1*^{BAP}*;BirA)*. Green arrow points at biotinylated Notch1^{BAP}. Asterisks label endogenous biotinylated proteins.

2.2.4.3 Phenotypic analysis of *Hes7*$^{BAP/BAP}$;*Rosa26*$^{BirA/BirA}$ mutant mice

Introduction of the BAP-tag into the *Notch1* locus did not disrupt the function of Notch1. However, homozygous *Hes7*$^{BAP/BAP}$ mice on the other hand are severely compromised with axial truncations and fused vertebrae and ribs (Figure 2.9). Their adult viability is greatly reduced and only 19% of expected (2/41) animals survive past weaning (Table 2.3). Upon co-expression of the BirA biotinylase following *BAP/BirA* heterozygous inter-crosses 48% (9/298) of expected *Hes7*$^{BAP/BAP}$;*Rosa26*$^{BirA/BirA}$ adults were recovered (Table 2.4).

The survivor's tails are truncated by varying degrees and have several kinks (Figure 2.9). Vertebrae of the cervical and the thoracic areas are severely fused, whereas vertebrae of the sacrum form almost regularly (Table 2.5 and Figure 2.9B). The degree of severity also varies within the sacral and adjacent area and frequently, well-formed lumbar and tail vertebrae are observed (Table 2.5). Heterozygous littermates resemble wildtype although 2% show a kinked tail (Figure 2.9B). Both *Hes7*$^{BAP/BAP}$ lines that were established from 3C7 and 4E7 ESCCs show the same phenotype, suggesting that this is indeed due to integration of the BAP sequence into the *Hes7* locus.

Although *Hes7*$^{BAP/BAP}$;*Rosa26*$^{BirA/BirA}$ mice display a strong phenotype, they are viable (Table 2.4) and fertile (73% (19/26) of males produced a copulation plug and 28% (2/7) of plugged females had a litter). This allowed me to generate tissue for testing the biotinylation of Hes7^{BAP} *in vivo*. I collected embryos at E9.5 and subjected the lysate to western blot analysis using a streptavidin probe (Figure 2.10). No signal of Hes7^{BAP} was detected at ~37 kD as seen by probing with streptavidin (Figure 2.10). The fact that Hes7^{BAP} is not fully functional and apparently not biotinylated indicates that *Hes7*$^{BAP/BAP}$;*Rosa26*$^{BirA/BirA}$ mice can not be used in streptavidin chromatin pull-down assays (bioChIP) to identify novel targets of Hes7 during somitogenesis. Rather, these mice will be analysed in respect of their segmentation defect (chapter 4).

	BAP/+	***BAP/BAP***
Number of adult skeletons analysed	4	5
Length of whole vertebral column (mm)	147.5±2.8	74.4±12.5
Length of tail (mm)	87.25±4.8	32.4±10
Total number of regular lumbar vertebrae	6±0	1±1
Number of regular sacral vertebrae	4±0	3.2±1
Number of regular tail vertebrae	27±1.4	4±3.4
Number of ribs, left and right counted separately	13±0	9.8±0.8

Table 2.5 Comparison of *Hes7*$^{BAP/+}$ *(BAP/+)* and *Hes7*$^{BAP/BAP}$ *(BAP/BAP)* adult skeletons.

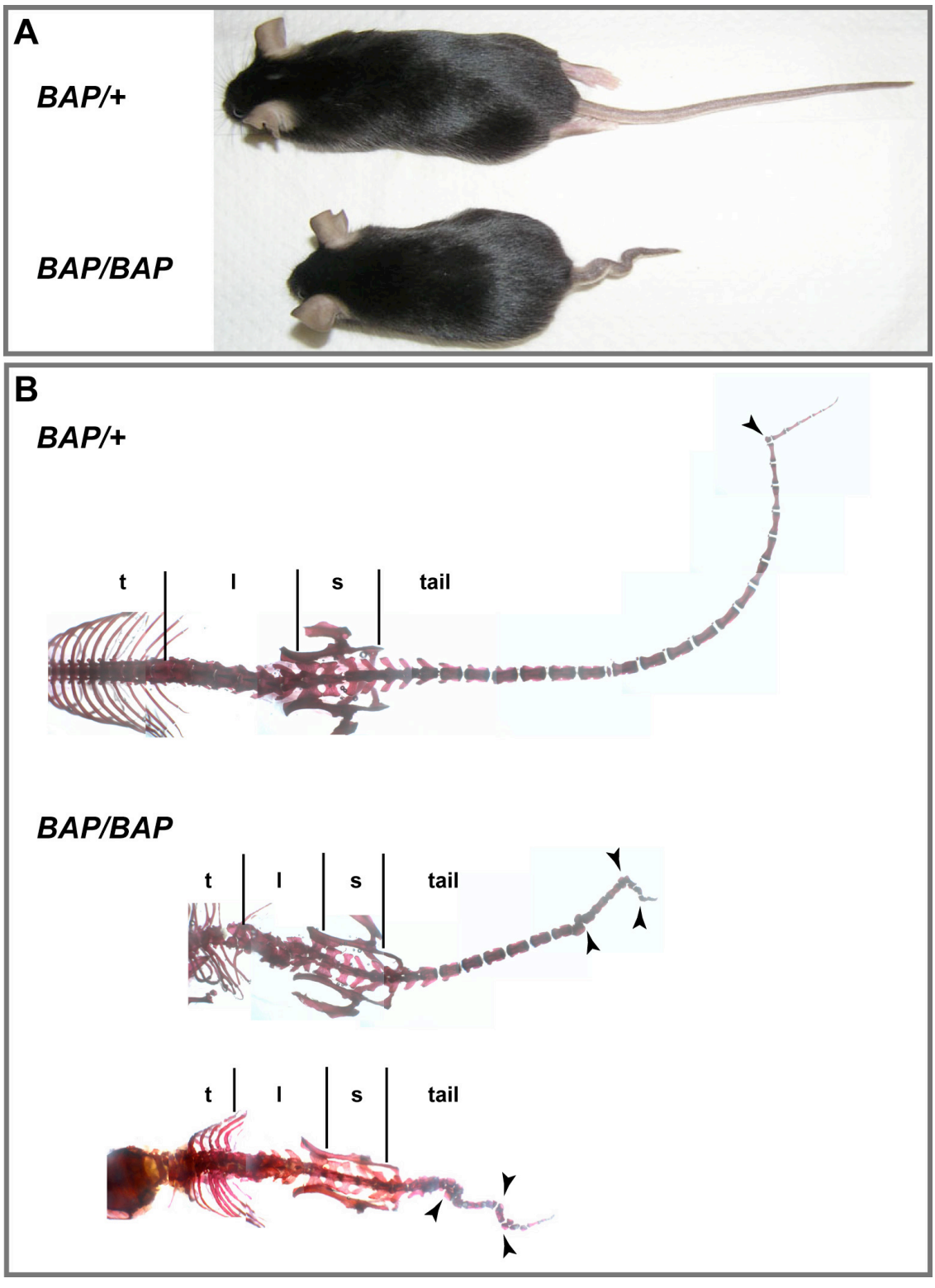

Figure 2.9 Phenotypes of *Hes7*$^{BAP/+}$ *(BAP/+)* and *Hes7*$^{BAP/BAP}$ *(BAP/BAP)* adults. (A) Comparison between *BAP/+* and *BAP/BAP* adult mice. (B) Skeleton preparations of *BAP/+* and *BAP/BAP* adult mice stained with alizarin red. Note variations in the severity of the *BAP/BAP* phenotype. Arrowheads point to kinks in the tail. t, thoracic vertebrae; l, lumbar vertebrae; s, sacral vertebrae; tail, tail vertebrae.

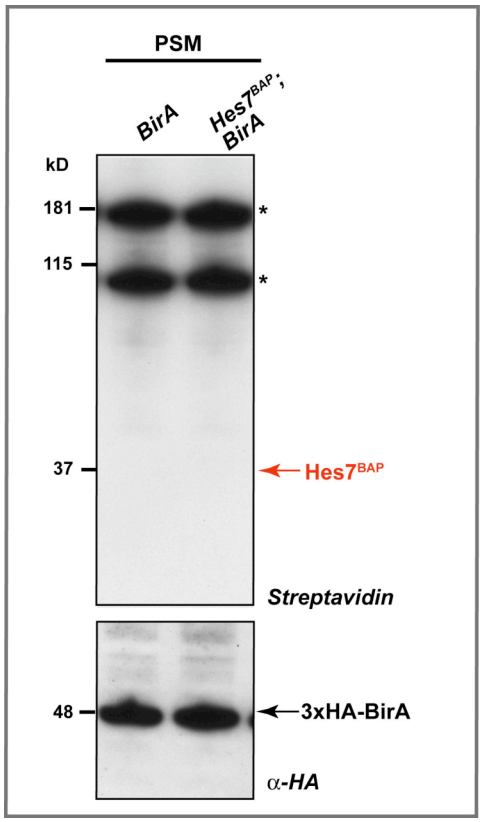

Figure 2.10 Western blot analysis of presomitic mesoderm tissue (PSM) from *Rosa26^{BirA} (BirA)* and *Hes7$^{BAP/BAP}$;Rosa26^{BirA} (Hes7^{BAP};BirA)* E9.5 embryos to detect biotinylated Hes7^{BAP}. *BirA* and *Hes7^{BAP};BirA* embryos were dissected and the posterior tail part isolated. Whole cell lysates were prepared and run on a 4-12% Bis-Tris gel. Detection of biotinylated proteins was done using a streptavidin-HRP probe (1:25,000) (top blot) for biotinylated Hes7^{BAP} or an anti-HA antibody (1:1,000) combined with a secondary anti-mouse-HRP (1:5,000) antibody to visualise HA-tagged BirA. Arrows point at detected protein signals. Asterisks label endogenous biotinylated proteins.

2.3 Discussion

This chapter describes the generation of BAP-tagged alleles of *Hes7* and *Notch1* for the identification of novel *in vivo* Notch signalling targets. Notch1^{BAP} is functional, and was used for streptavidin chromatin pull-down experiments (chapter 3), Hes7^{BAP} is not fully functional, and results in an interesting segmentation phenotype, which is analysed in chapter 4.

Cell culture experiments had predicted that Hes7^{BAP}, containing the BAP-tag 17 amino acids upstream of the C-terminus, could still repress target genes. But this is not the case *in vivo*, as seen in the hypomorph *Hes7*$^{BAP/BAP}$*;Rosa26*$^{BirA/BirA}$ strain. A possible explanation is that in the embryo *Hes7* expression is highly dynamic and only few molecules are synthesised and therefore the *in vivo* system is more fragile than in cultured cells. In contrast, in cell culture experiments Hes7^{BAP} protein was constitutively expressed at a very high rate, which repressed the reporter.

Expression of Hes7^{BAP} in a presomitic mesoderm (PSM) specific cell line, which is more similar to the *in vivo* situation than the fibroblast cell line, would have provided further evidence about Hes7^{BAP} functionality. So far, it is not possible to establish such a cell line and thus these experiments were not performed.

A further explanation for the loss of function *in vivo* might also be the fact that the BAP-tag disrupts binding of a necessary co-factor for repression. Hes proteins were shown to form hetero- or homodimers and down-regulation of target genes is achieved through recruitment of co-repressors (section 1.2.5.1). The BAP-tag could impair both, dimerisation and complex formation with co-repressors. However, I decided to insert the BAP-tag at a position, which has not been associated with an important binding site before.

I chose the BAP-tag because it has only 14 amino acids, which should minimise folding defects and has been used successfully before (de Boer et al., 2003; Hamlett et al., 2008; Rodriguez et al., 2005; Stachler et al., 2008). However, these studies use the BAP/biotin-avidin technique in cultured cells with inducible expression of the BAP-tagged transcription factor.

There are several possible explanations for why Hes7^{BAP} is not biotinylated *in vivo*. Firstly, Hes7 is a transcription factor, which mainly acts in the nucleus and

switches off transcription, while the BirA biotinylase resides in the cytoplasm. The short residence of Hes7^{BAP} in the cytoplasm during translation and further maturation might not be sufficient to biotinylate the protein. In future experiments one could attach a nuclear localisation signal (NLS) to the biotinylase in order to promote biotinylation within the nucleus, which is specifically important for nuclear transcription factors. In the case of Notch^{BAP} biotinylation, the BAP containing NICD moiety lies on the cytoplasmic side of the Notch1 receptor, which facilitates biotinylation through BirA.

Second, there is also a possibility that the BAP-tag in Hes7^{BAP} is not accessible for the biotinylase *in vivo* due to protein folding. Structural analysis of the purified protein would be needed to distinguish between these alternatives. However, if introduction of the BAP-tag would disrupt protein folding, I would not have seen biotinylation of Hes7^{BAP} in cultured cells. Finally, I cannot exclude that Hes7^{BAP} is not biotinylated because the abundance for this highly dynamic protein might lie below detection *in vivo*.

To conclude, Hes7^{BAP} protein function is greatly impaired but not completely abolished as *Hes7$^{BAP/BAP}$;Rosa26$^{BirA/BirA}$* mice differ from Hes7 knock-out *(Hes7$^{-/-}$)* mice, which are not viable and do not show any regular vertebrae (Bessho et al., 2001b).

I can still address novel Notch signalling targets using *Notch1$^{BAP/BAP}$;Rosa26$^{BirA/BirA}$* mice, which express functional and biotinylated Notch1^{BAP} (chapter 3). Given that Notch signalling is involved in numerous processes throughout development and disease these mice can be used to identify important downstream players and help understanding the complex functions of Notch.

CHAPTER 3: Testing various applications of the Notch1^{BAP}/biotin-avidin system in cultured cells and transgenic mouse tissues

3.1 Introduction

The Notch signalling pathway is an evolutionary conserved mechanism that controls cell fate decisions through local cell interactions in metazoan development and disease (reviewed in Artavanis-Tsakonas et al., 1999) (chapter 1). Today, we have a considerable understanding of what triggers the activation of the cascade and leads to the formation of the transactivation complex in the nucleus (Kovall, 2008). However, the question of how different target genes are activated by Notch in different cell types and time frames remain less clear. To date, only a few direct targets of Notch activity have been characterized (section 1.2.5) but even in those cases, it is not fully understood what makes a gene a target in specific cells.

With the help of genome-wide studies, like chromatin immunoprecipitation combined with high throughput sequencing (ChIP-seq), the number of target genes can eventually increase. Limitations in this procedure have been the quality of antibodies directed against the Notch1 intracellular domain (NICD), the extremely low abundance of this transcription factor in the nucleus and the fact that NICD does not bind the DNA itself but via CSL (named after CBF1, Su(H) and LAG-1, for the mammalian, *D. melanogaster* and *C. elegans* orthologues).

The BAP/biotin-avidin system, as outlined in chapter 2, provides an opportunity to circumvent these problems. First, through attachment of the BAP-tag epitope to NICD the antibody problem can be resolved. Further biotinylation of the BAP-tagged protein and the tight and specific binding by avidin (or its bacterial counterpart streptavidin) has an almost 10^3 - 10^6 times greater affinity than the interaction of epitopes with their antibodies. Once the biotin-avidin complex has formed, it remains stable even under very stringent washing conditions (Ford et al., 1991). This extremely high affinity of avidin for biotin should allow purifying low levels of biotinylated NICD from a restricted number of cells and efficient crosslinking can minimise the probability that the NICD/CSL/chromatin transactivation complex dissociates.

Streptavidin chromatin pull-downs or so called bioChIP (chromatin immunoprecipitation of biotinylated protein and their binding partners via streptavidin) experiments from different tissues together with high-throughput sequencing may lead to a better understanding of Notch signalling targets and their activation. The utility of the BAP-tag and streptavidin binding in chromatin immunoprecipitation assays has been used before and provided evidence that it can be used successfully in ChIP and ChIP-chip assays to identify genome-wide transcriptional targets (Kim et al., 2008; Kolodziej et al., 2009; van Werven and Timmers, 2006; Viens et al., 2004).

The BAP/biotin-avidin system seems to provide an alternative opportunity to address the question of Notch signalling targets *in vivo* in the developing and adult mouse. Here, I present a novel approach towards the identification of Notch target genes *in vivo* by bioChIP using the generated transgenic $Notch1^{BAP/BAP};Rosa26^{BirA/BirA}$ (chapter 2) mouse line.

3.2 Results

This chapter documents the different steps to optimise the streptavidin chromatin pull-down assays from cultured cells (that have been transduced with $NICD^{BAP}$ and BirA) and *Notch1*$^{BAP/BAP}$;*Rosa26*$^{BirA/BirA}$ mouse tissues. First, I established a bioChIP protocol using a well-studied transcription factor promoter system (section 3.2.1). Once I had the technique optimised I went on to perform Notch bioChIP experiments from stable cell lines expressing biotinylated $NICD^{BAP}$ (section 3.2.2) in order to test various parameters before performing the experiment on the mouse tissue (section 3.2.5). Additionally, I generated stable cell lines expressing a biotinylated and inducible $NICD^{BAP}$ to identify the "Notch targetome" upon oncogenic transformation (section 3.2.2). After I tested the system in cell culture I tried to identify Notch target genes from transgenic *Notch1*$^{BAP/BAP}$;*Rosa26*$^{BirA/BirA}$ mouse PSM and retina tissues (section 3.2.5). Although I was not successful in confirming known Notch target genes by quantitative PCR (qPCR) after bioChIP, I decided to perform high-throughput sequencing from bioChIP samples. Finally, I analysed protein-binding partners of $NICD^{BAP}$ after streptavidin protein purification and mass spectrometry from embryonic nuclear lysates, which is another application of the BAP/biotin-avidin system (section 3.2.7).

3.2.1 Establishing a bioChIP protocol using the well-studied binding of the transcription factor GATA-1 to the *Erythroid Kruppel-like Factor (EKLF)* gene promoter

Several different protocols for the bioChIP have been published previously using different versions of the BAP-tag (Kim et al., 2008; Kolodziej et al., 2009; van Werven and Timmers, 2006; Viens et al., 2004). First, I had to establish a ChIP protocol, which works for my tagged protein and with the instruments (e.g. type of sonicator) at my disposal. Several parameters had to be tested beforehand and were optimised accordingly. These parameters included the determination of the correct amount of starting material as well as the conditions for formaldehyde fixation (duration and quality of formaldehyde), the sonication timing and elution conditions during the bioChIP procedure.

A suitable system to establish a bioChIP protocol is the well-studied binding of the transcription factor GATA-1 to the *EKLF* promoter, which has already been used in bioChIP experiments before (Kolodziej et al., 2009). The haematopoietic transcription factor GATA-1 is a key regulator of the differentiation of the erythroid, megakaryocytic, eosinophilic and mast cell lineages and acts as both repressor and activator of transcription depending on its co-factors and the binding of other transcription factors (Lowry and Mackay, 2006). Previous studies using the high-affinity binding of the biotinylated GATA-1^{BAP} to streptavidin beads have identified a number of such GATA-1 co-factors (Hamlett et al., 2008; Rodriguez et al., 2005).

In order to test the bioChIP experimental procedure I performed streptavidin chromatin pull-downs from the established MEL cell line, which express an inducible *GATA-1^{BAP}* and the BirA biotinylase from *E. coli* (kind gift from John Strouboulis and Frank Grosveld, Erasmus Medical Center Rotterdam) (de Boer et al., 2003) (Figure 3.1A). As read-out for the bioChIP I examined known GATA-1 binding sites in the *EKLF* promoter by quantitative PCR (qPCR) (Merika and Orkin, 1995) (Figure 3.1C).

Briefly, after induction of GATA-1^{BAP}, cells were fixed with formaldehyde and chromatin was fragmented by sonication (section 7.6.1.1). The average length of chromatin should be between 300 and 500 bp and was confirmed on an agarose gel (Figure 3.1B). In order to check the influence of the amount of starting material, I used either 10 x 10^6 or 1 x 10^6 cells per bioChIP experiment. The fragmented chromatin was mixed with streptavidin-coated beads and washed according to the commercially available ChIP protocol (section 7.6.1.1). GATA-1^{BAP} bound DNA fragments were eluted (by reversing the crosslinks) and purified. Enrichment of GATA-1^{BAP} target DNA sequences was assayed by qPCR using primer pairs binding next to known GATA-1 binding sites (*"enhancer"* and *"basic promoter"*, Figure 3.1C and Table 7.18) and a primer pair binding in a region that lacks GATA-1 binding sites as a negative control (*"negative"*, Figure 3.1C and Table 7.18).

The results from the qPCR run of the bioChIP from MEL [BirA] and MEL [GATA-1^{BAP}; BirA] were normalised to an internal *necdin* control (Kolodziej et al., 2009) and plotted onto a graph showing the relative enrichment of the different *EKLF* promoter fragments (Figure 3.1D). bioChIP experiments with cells that express GATA-1^{BAP} and BirA show 35-40 fold enrichment of the positive *EKLF* promoter sites (*EKLF basic promoter* and *EKLF enhancer*, Figure 3.1D) but not of the *EKLF negative* site.

bioChIP with control cells that express BirA but not GATA-1^{BAP} does not result in enrichment of any of the positive *EKLF* promoter sites (*EKLF basic promoter* and *EKLF enhancer*; Figure 3.1D). These findings are consistent with previous bioChIP results (Kolodziej et al., 2009) and demonstrate that the parameters chosen (section 7.6.1.1) can indeed lead to the purification of target DNA fragments.

By contrast to the above results with 10 x 10^6 cells starting material, bioChIP on 10 times less cells did not work: it resulted in high variations in the cycle threshold (ct) values beyond cycle 30 of the qPCR and in an apparent enrichment of promoter sequences from the control cells that express only BirA (not shown).

Using a well-characterised bioChIP system, I was able to reproduce previous results indicating that - in principle - the bioChIP is working and should also be applicable in the case of the biotinylated Notch1^{BAP} in cultured cells and mouse tissues.

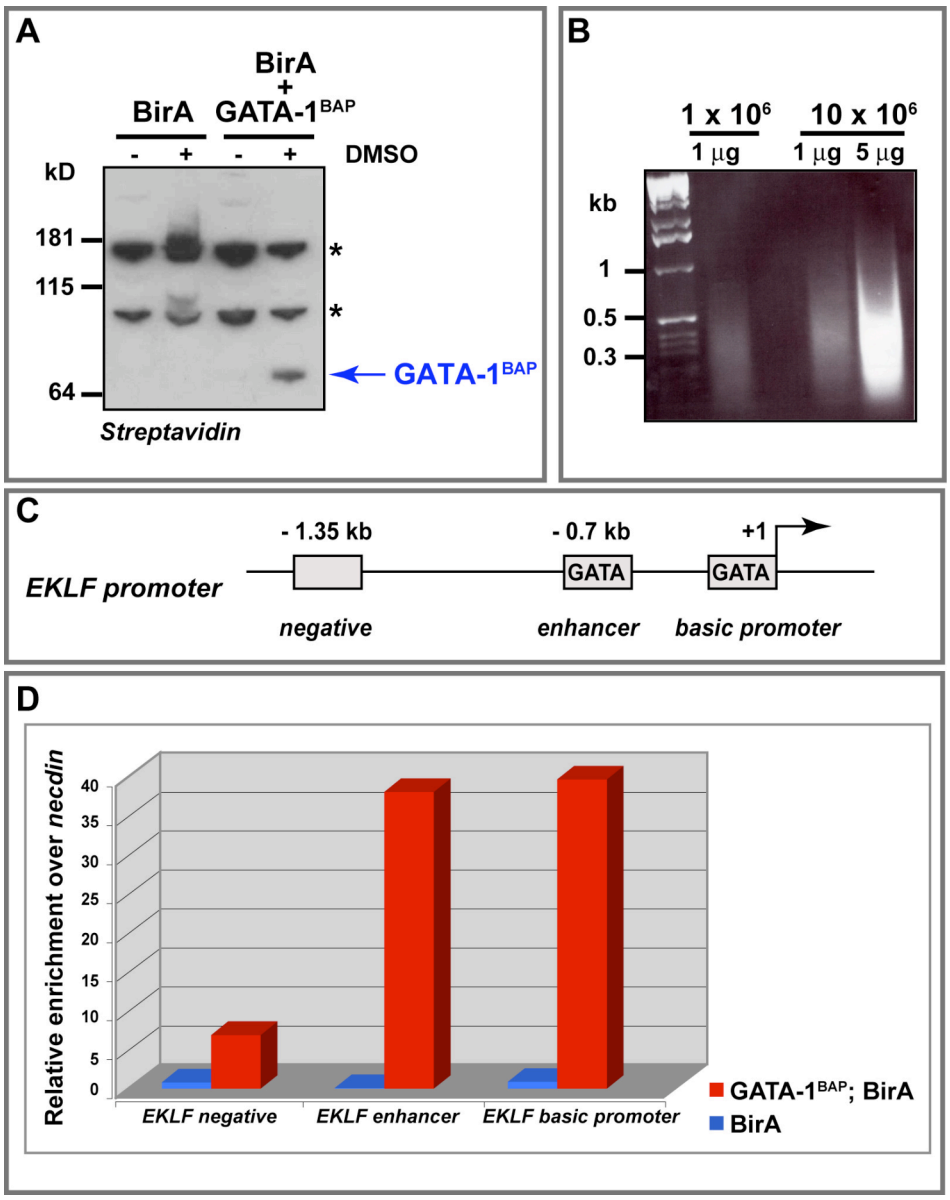

Figure 3.1 Enrichment of *EKLF basic promoter* and *enhancer* sites after bioChIP from MEL [GATA-1^{BAP}; BirA] cells. (A) Inducible *GATA-1^{BAP}* expression in MEL cells. MEL cells expressing BirA alone or BirA and GATA-1^{BAP} were cultivated in DMEM supplemented with 10% FCS at 37ºC for 4 days in the absence (-) or presence (+) of 2% DMSO. Western blot analysis of crude nuclear lysates probed with streptavidin-HRP (1:25,000) shows biotinylated GATA-1^{BAP} after DMSO induction in double stable MEL cells (~50 kD; blue arrow). Asterisks label signals from endogenous biotinylated proteins. (B) 1% agarose gel of sonicated chromatin from 1 x 10^6 and 10 x 10^6 MEL cells. 1 and 5 µg (second sample only) of chromatin was loaded. (C) *EKLF* promoter architecture showing GATA-1 binding sites (*basic promoter* and *enhancer*) and GATA-1 *negative* site used for analysis of GATA-1 bioChIP experiments. Arrow, start of transcription. (D) qPCR results of GATA-1 bioChIP from 10 x10^6 MEL [BirA] (blue columns) and [GATA-1^{BAP}; BirA] (red columns) cells. Each experiment shows relative enrichment of *EKLF negative*, *EKLF enhancer* and *EKLF basic promoter* sites (average of duplicates) over the internal control *necdin*.

3.2.2 Testing stable [NICD^{BAP}; BirA] cell lines for bioChIP

In order to optimise the NICD bioChIP in cultured cells I established stable cell lines expressing NICD^{BAP} and BirA. I made use of a retroviral gene delivery and expression system to control copy number and expression of the *BirA* and *NICD^{BAP}* constructs in different cell lines (sections 7.1.5 and 7.4.3). I chose to use the human breast epithelial cell line MCF10A because overexpression of NICD in that system was shown to lead to an oncogenic transformation (Imatani and Callahan, 2000; Robbins et al., 1992; Stylianou et al., 2006). NICD bioChIP experiments from stable MCF10A cell lines expressing biotinylated NICD^{BAP} before and after over-activation of Notch signalling could provide an insight into the mechanisms by which Notch governs tumourigenesis.

In order to have a temporally regulated induction of Notch activity, I constructed a hormone inducible *NICD^{BAP}* retroviral vector based on the estrogen receptor (ER) fusion strategy (Littlewood et al., 1995). Thereby, addition of the synthetic compound 4-Hydroxytamoxifen (4-OHT) should lead to activation of the ER-NICD^{BAP} fusion protein and in that way switches on Notch signalling. As control cells I established a mouse fibroblast C3H10T½ cell line stably expressing ER-NICD^{BAP} and BirA, which do not undergo oncogenic transformation upon over-expression of NICD.

After transduction of MCF10A and C3H10T½ cell lines with BirA and ER-NICD^{BAP} constructs I checked expression of biotinylated ER-NICD^{BAP} on a western blot. In both cell lines the biotinylated ER-fusion protein was detected at ~190 kD after probing whole cell lysates with streptavidin (Figure 3.2A, green arrow and box). In contrast, MCF10A and C3H10T½ cell lines, which were transduced only with the BirA containing virus, did not show a signal at this molecular weight (Figure 3.2A). However, the western blot from BirA cells detected endogenous biotinylated proteins at ~100 and ~170 kD, which were identified by mass spectrometry as the mitochondrial proteins pyruvate and propyonyl CoA carboxylases (Figure 3.8C). The detection of NICD^{BAP} on the western blot is consistent with previous results confirming the biotinylation of NICD^{BAP} in cell culture (Figure 2.3), which is a prerequisite for the bioChIP.

Next, I wanted to check if I could switch on the expression of the ER-NICD^{BAP} fusion by adding 4-OHT to the cells. An inducible system would have been helpful in

timing the activation of Notch signalling but is not an absolute requirement. The luciferase reporter assay described in chapter 2 was used as a read-out and to determine the strength of activation. In this case the luciferase is driven by a 509 bp *Hes1* promoter fragment containing three CSL transactivation sites (Ishibashi et al., 1995). The double stable cell lines C3H10T½ [ER-NICD^{BAP}; BirA] and MCF10A [ER-NICD^{BAP}; BirA] were transfected with the luciferase reporter construct and 24 hours later 4-OHT was added. After incubation of another 24 hours the cells were lysed and luciferase activity determined (section 7.4.4).

There was no obvious activation of the reporter upon addition of the 4-OHT and reflected great variation within different experiments suggesting that the ER-NICD^{BAP} might not be functional (Figure 3.2C). Therefore, I re-cloned *ER-NICD^{BAP}* cDNA into the *pcDNA3.1^{+}* expression vector and tested the construct in a transient reporter assay thereby comparing the activity of ER-NICD^{BAP} to NICD and NICD^{BAP} with and without 4-OHT.

The transient transfection assays showed that ER-NICD^{BAP} expression is activated upon transfection of the reporter even in the absence of the metabolite 4-OHT (Figure 3.2C and D) suggesting that the ER-system is leaky. Similarly, NICD and NICD^{BAP} are both able to activate the *Hes1* luciferase reporter (in the absence and presence of 4-OHT) in C3H10T½ and MCF10A transiently transfected cell lines (Figure 3.2D and E). The reduced level of induction is probably due to the fact, that in this case, cells were assayed 48 h after transfection whereas, in the initial experiment, I measured already after 12 - 24 h (compare Figure 3.2D and E with Figure 2.2B). In general, the activation in MCF10A cells does not seem to be as high as in C3H10T½ transfected cells (Figure 3.2D). Also, addition of 4-OHT seems to compromise the activation of NICD and NICD^{BAP} while ER-NICD^{BAP} expression remains constant.

This leakage of the ER-system (leading to the activation of ER-NICD^{BAP} even in the absence of 4-OHT) maybe due to the induction of the ER-domain by growth factors in the medium. Maybe using a more recent ER-domain (Kalaitzidis et al., 2004) would have circumvented this problem.

These results led me to abandon the inducible NICD system and I went on to establish MCF10A and C3H10T½ cell lines stably expressing NICD^{BAP} and BirA. Biotinylation of NICD^{BAP} was confirmed in both cell lines by western blot analysis with a streptavidin probe (Figure 3.2A). In this case, I chose a slightly longer NICD version

containing the S3 cleavage site (N1ΔE), which is recognised by the γ-secretase complex. Thus this leads to a constitutive active form of Notch, which is cleaved continuously. This strategy is advantageous because I could make use of a γ-secretase inhibitor (GSI) to block Notch signalling (at cleavage site S3) in these cells. This further provides an adjustable system for the bioChIP experiments in order to find Notch target genes by comparing GSI-treated and untreated cells.

In order to find a GSI that specifically blocks Notch signalling in my cells I treated C3H10T½ [$NICD^{BAP}$; BirA] stable cell lines with different compounds: DAPT (N-[N-(3,5-difluorophenacetyl)-L-alanyl]-S-phenylgly cine t-butyl ester, also called IX), X and XVII and performed western blot analysis of cell lysates with streptavidin or an α-NICD antibody. Only DAPT was able to block Notch signalling, leading to a stabilisation of the membrane-bound $N1\Delta E^{BAP}$ version (IX, Figure 3.2B).

In control treated cells (DMSO, Figure 3.2B) two fragments are visualised representing the longer $N1\Delta E^{BAP}$ protein and a shorter $NICD^{BAP}$ fragment, which results from constitutive cleavage in C3H10T½ [$NICD^{BAP}$; BirA] cells. Detection with an α-NICD antibody thus results only in the detection of the cleaved $NICD^{BAP}$ (Figure 3.2B, lower panel). A signal form the α-NICD antibody is absent in DAPT treated cells showing a successful blockage of S3 cleavage. These results show that $NICD^{BAP}$ is biotinylatable in the stable C3H10T½ and MCF10A cell lines and regulation of Notch activity is possible by blocking the processing of the extended $NICD^{BAP}$. In conclusion I generated two different stable cell line systems, which were used for bioChIP experiments in order to determine the optimal conditions.

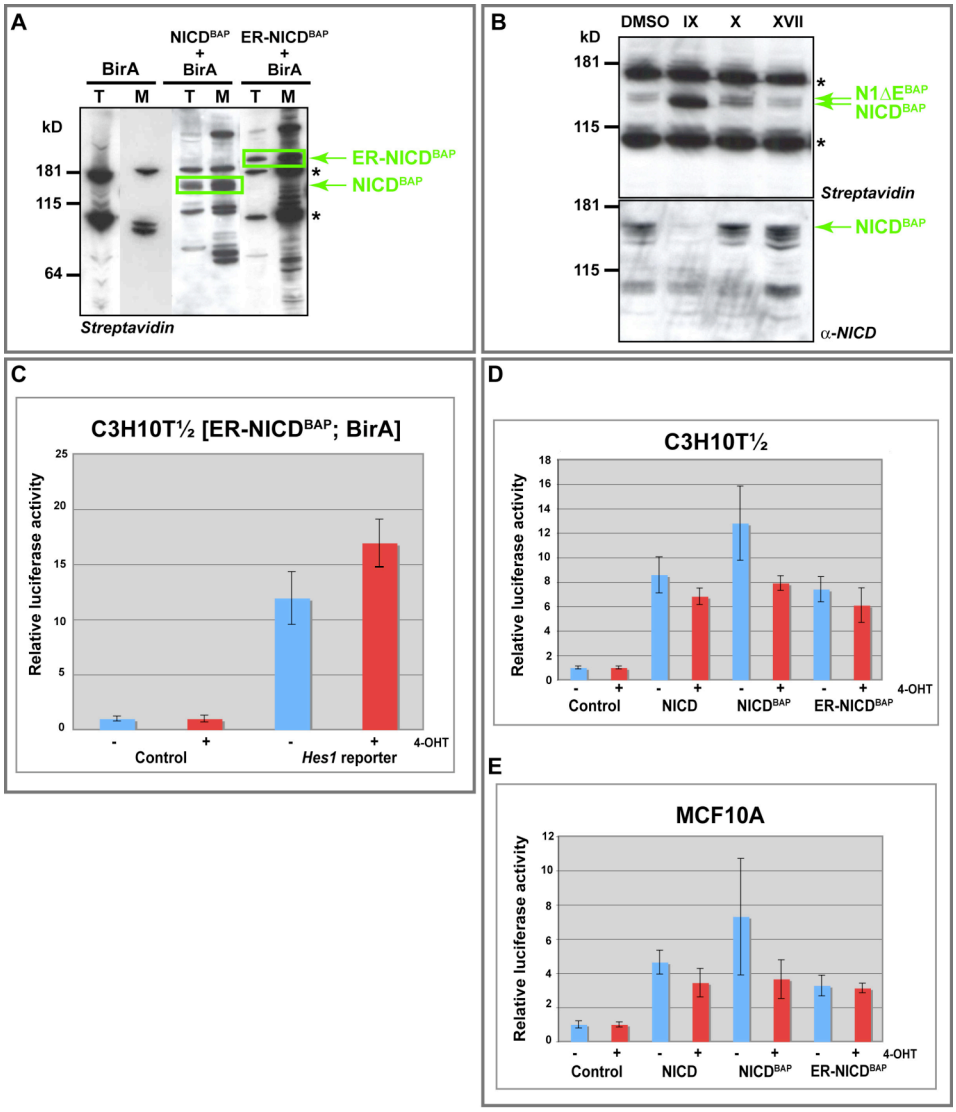

Figure 3.2 Evaluation of C3H10T½ and MCF10A stable cell lines expressing [BirA], [NICD^{BAP}; BirA] and [ER-NICD^{BAP}; BirA]. (A) Western blot of crude nuclear extracts from C3H10T½ and MCF10A cell lines stably expressing [BirA], [NICD^{BAP}; BirA] or [ER-NICD^{BAP}; BirA]. Detection of NICD^{BAP} and ER-NICD^{BAP} was done with a streptavidin-HRP probe (1:25,000) (green arrows). T, C3H10T½; M, MCF10A. (B) γ-secretase inhibitor experiment in C3H10T½ [NICD^{BAP}; BirA] cells detects two different Notch species: N1ΔE^{BAP} and NICD^{BAP}. Cells were incubated with the inhibitors DAPT (IX), X and XVII for 3 days at 37ºC/5% CO_2. Detection of cleaved Notch products was done by western blot analysis of cell lysates using a streptavidin (1:25,000) probe or an α-NICD antibody (1:1,000). Green arrows point at respective products. Asterisks label endogenous biotinylated proteins. (C, D, E) Luciferase reporter assay in C3H10T½ [ER-NICD^{BAP}; BirA] (C), C3H10T½ (D) and MCF10A (E) cell lines transiently transfected without (control) or with *Hes1*-reporter (C) or with the *Hes1*-reporter alone (control), NICD, NICD^{BAP} or ER- NICD^{BAP} (D, E). After 24 h of transfection, 4-OHT (+; 1 µM final concentration) or EtOH (-) was added and cells incubated for another 24 h at 37ºC/5% CO_2. Cells were lysed and the luciferase activity determined. Blue columns show luciferase activity of untreated cells and red columns represent reporter activation upon addition of 4-OHT.

3.2.3 Optimisation of NICD bioChIP experiments in established cell lines

Enriched promoter sequences after ChIP experiments are quantified using quantitative PCR (qPCR) assays and primers flanking potential transcription factor binding sites. It has been shown that the number and orientation of CSL binding sites determine the strength of activation by the Notch transactivation complex consisting of the DNA-bound CSL, NICD and the co-activator proteins of the Mastermind-like family (Nam et al., 2007; Ong et al., 2006). Head-to-head formation of two CSL sequences has been reported to constitute high affinity binding sites whereas tail-to-tail CSL sites correspond to low affinity binding in cell-based assays (Ong et al., 2006). Also the spacing between the individual CSL sites is crucial and promotes dimerisation of the Notch transactivation complex *in vitro* (Nam et al., 2007).

After validation of the cell lines C3H10T½ [$NICD^{BAP}$; BirA] and MCF10A [$NICD^{BAP}$; BirA], I performed bioChIP experiments to confirm activation of the *Hes1* promoter, a well-characterised Notch1 target, by the biotinylated $NICD^{BAP}$. In order to check for an enrichment of CSL-containing *Hes1* promoter sequences, I performed qPCR reactions with primers flanking the three CSL sites just upstream of the transcription start (Figure 3.3; section 7.6.1.1 and Table 7.19). The mouse and human *Hes1* promoters contain two CSL sequences in a head-to-head fashion, which are separated by 16 nucleotides and an additional low affinity binding site, all in close arrangement within 100 bp upstream of the transcription start (Figure 3.3A for MCF10A human and B for C3H10T½ mouse *Hes1* promoter arrangement).

The results from the bioChIP experiments from the stably transduced human and mouse cell lines indicated a slight enrichment (4-fold) of the CSL-containing *Hes1* promoter sequences close to the transcription start only in MCF10A [$NICD^{BAP}$; BirA] cells (Figure 3.3A). The distal CSL site, 5 kb upstream, was not pulled down in MCF10A [$NICD^{BAP}$; BirA] experiments (Figure 3.3A) demonstrating that this site might not bind the Notch transactivation complex as strongly or frequently as the proximal CSL close to the transcription start site during *hHes1* (*human Hes1*) target gene activation. The bioChIP from MCF10A [BirA] control cells did not enrich significantly any promoter sequences (blue columns, Figure 3.3A) indicating that the background binding is low.

By contrast to the human cell line, the results from the C3H10T½ [$NICD^{BAP}$; BirA] bioChIP did not show enrichment for CSL-containing promoter sequences (red columns, Figure 3.3B). The bioChIP from BirA-transduced C3H10T½ cells seemed to pull-down arbitrarily DNA sequences from any promoter (Figure 3.3B). The reason for these different outcomes could be the fact that the transgene has an effect on the human MCF10A cell line whereas Notch signalling is not active in C3H10T½ cells. Moreover, the timing of activation might be different in both cell lines. It has been documented that the transactivation complex does not always reside at the respective CSL sequences, and that its binding and dissociation from the DNA is highly dynamic (Krejci and Bray, 2007).

In summary, bioChIP experiments from MCF10A [$NICD^{BAP}$; BirA] cells produced an acceptable result, albeit with a weak enrichment (4-fold) of *hHes1* promoter sequences, whereas the analysis of the C3H10T½ [$NICD^{BAP}$; BirA] streptavidin chromatin pull-downs are not conclusive. Therefore, I continued my studies only with the MCF10A [$NICD^{BAP}$; BirA] cells.

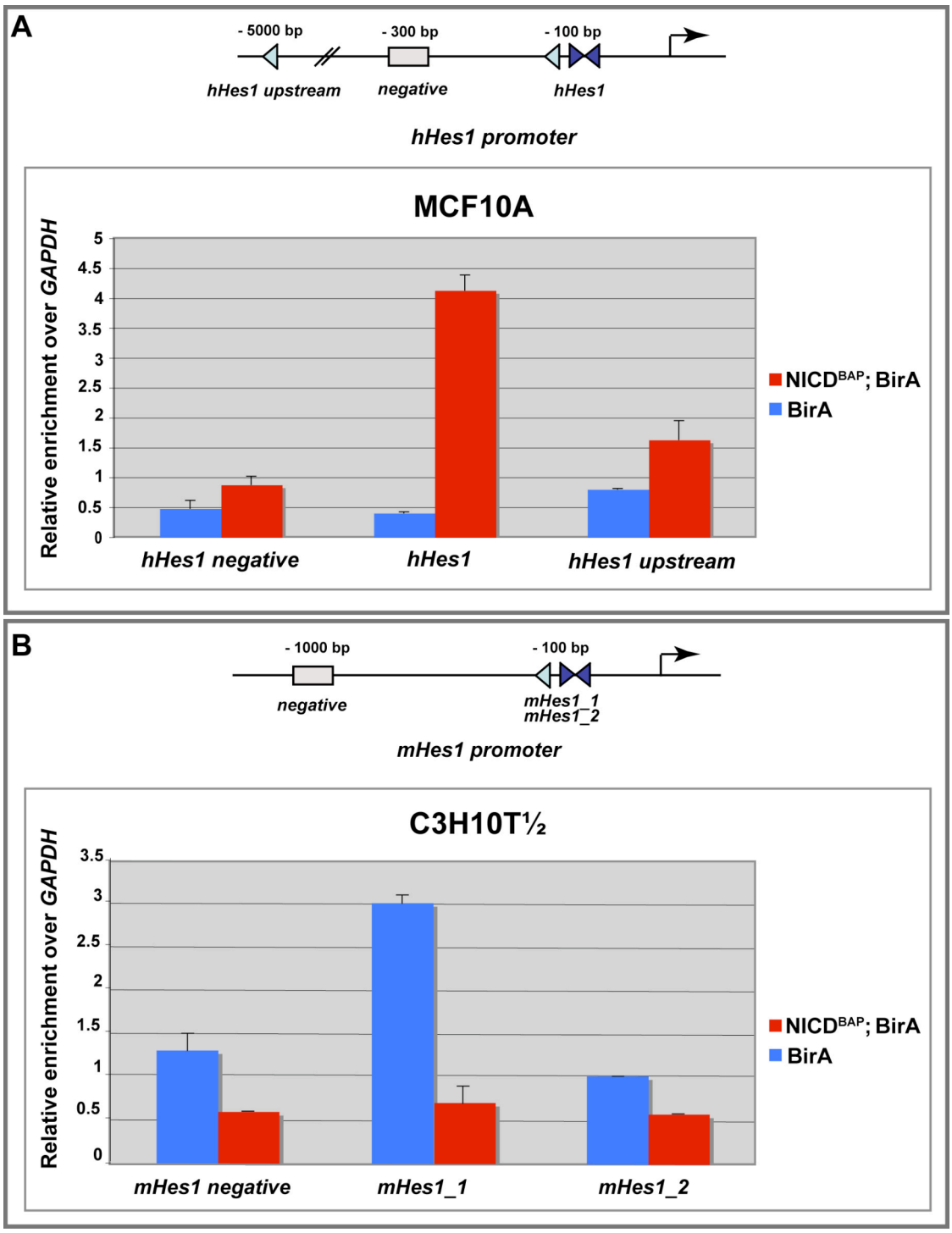

Figure 3.3 NICD bioChIP results from MCF10A [NICD^{BAP}; BirA] and C3H10T½ [NICD^{BAP}; BirA] cell lines. (A, B) qPCR results of NICD bioChIP experiments from MCF10A [NICD^{BAP}; BirA] and [BirA] (A) and C3H10T½ [NICD^{BAP}; BirA] and [BirA] (B) cell lines. Fold enrichment of [NICD^{BAP}; BirA] bioChIP (red columns) versus [BirA] experiments (blue columns) over *GAPDH* is shown. Arrangement of binding sites tested within the human *Hes1 (hHes1)* (A) and mouse *Hes1 (mHes1)* (B) promoters are indicated above the diagrams. Rectangles represent CSL binding sites and orientation. Colour of rectangles shows strength of binding: light blue, low affinity and dark blue, high affinity. Arrow, start of transcription.

My results were obtained using the commercially available protocol for recovering bound chromatin, which uses moderate washing conditions (section 7.6.1.1). In order to further optimise the bioChIP protocol, I tested more stringent washing conditions after chromatin binding from MCF10A [$NICD^{BAP}$; BirA] cells. Viens et al. found that washing with 2% SDS and subsequent high ionic strength buffer leads to a decreased background binding in bioChIP experiment (Viens et al., 2004). I applied these washing conditions to my bioChIP experiments in order to achieve a higher enrichment of *hHes1* promoter sequences in MCF10A [$NICD^{BAP}$; BirA] cells. Also, I tested another Notch target gene, *c-Myc*, which was shown to play a role in human acute T cell lymphoblastic leukaemia and lymphomas (T-ALL) and mammary tumorigenesis (Klinakis et al., 2006; Weng et al., 2006). The human *c-Myc* promoter contains one conserved CSL binding site located around the transcription start site (Figure 3.4).

The outcome of this bioChIP experiment showed that the increased stringency does not help to improve the previous results. In contrast, the qPCR data indicated an enrichment of *hHes1* promoter sequences even in the absence of the biotinylated $NICD^{BAP}$ (Figure 3.4). The activation of the human *c-Myc* promoter was not confirmed in this experiment either (Figure 3.4). A possible explanation of these results might be the high stringency in the washing step. Since NICD does not bind the DNA directly but through CSL the harsh washing could have led to the dissociation of the transactivation complex. This would show similar results for [$NICD^{BAP}$; BirA] and [BirA] cells (Figure 3.4).

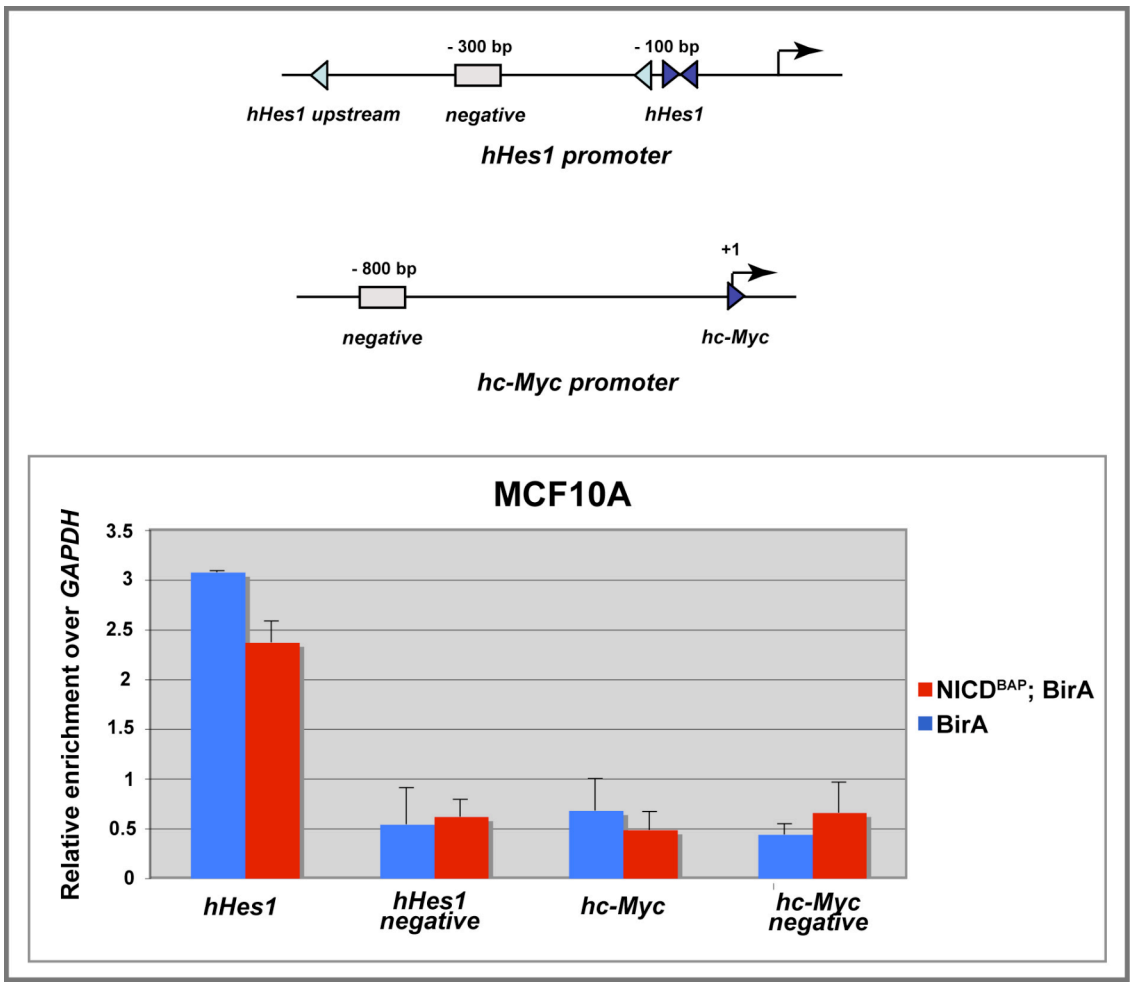

Figure 3.4 More stringent washing conditions do not improve bioChIP experiments from MCF10A [NICD^{BAP}; BirA] cells. qPCR results of bioChIP experiments from MCF10A [NICD^{BAP}; BirA] (red columns) and [BirA] (blue columns) stable cell lines. The relative enrichment of human *Hes1 (hHes1)* and human *c-Myc (hc-Myc)* promoter sequences is shown in relation to human *GAPDH*. The arrangement of CSL binding sites as well as the negative sites is indicated in the schematic *hHes1* and *hc-Myc* promoters above. Rectangles show position and orientation of CSL sites on the respective promoters. Colour of rectangles indicates strength of binding: light blue, low affinity and dark blue, high affinity. Arrow, start of transcription.

3.2.4 Visualisation of NICD^{BAP} in cultured cells and transgenic mouse embryos

An explanation for the lack of detection of NICD binding to the human *Hes1* promoter in subsequent experiments could also be due to a loss of NICD^{BAP} by the presumable stable cell lines. The NICD^{BAP} is expressed without antibiotic selection and the cells might lose the construct. To check this possibility, I performed immunofluoresence microscopy directed against the green fluorescent protein (GFP), which is expressed from the *NICD^{BAP}* di-cistronic message. Streptavidin coupled to a fluorophor should detect the biotinylated NICD^{BAP} in MCF10A [NICD^{BAP}; BirA] cells.

Using this approach I could show, that indeed most cells (~80%) of the double stable MCF10A [NICD^{BAP}; BirA] cell line had lost GFP expression and therefore NICD^{BAP} (Figure 3.5A, arrowheads). These results were further supported by western blot analysis of stable cell lines, which were cultured beyond 10 passages (not shown). The fact, that the double stable cell lines are unable to maintain a constant NICD^{BAP} expression (due to the lack of a resistance marker) explains the inconsistent results from the previous ChIP experiments. This suggests, that experiments with the MCF10A [NICD^{BAP}; BirA] cell line do not reproduce reliable results and therefore does not provide a suitable system to identify Notch signalling targets.

Another drawback of the BAP/biotin-avidin strategy became apparent in the immunofluorescence assay: the streptavidin probe did not pick up biotinylated NICD^{BAP} in MCF10A [NICD^{BAP}; BirA] cells but a structured network within the cell body, presumably the mitochondria (Figure 3.5A, red channel; compare to Figure 2 in (Millar et al., 2005)). The same pattern was visible when staining embryonic tail sections (Figure 3.5B) or retinas from transgenic *Notch1$^{BAP/BAP}$;Rosa26$^{BirA/BirA}$* and *Rosa26$^{BirA/BirA}$* and mice (Figure 3.5C and D). In contrast, sections from transgenic embryos probed with an α-NICD antibody resulted in a distinct expression pattern, which co-localised with the DNA-specific dye DAPI and confirmed a nuclear localisation of NICD^{BAP} (Figure 3.5B, arrowhead). Probing retinas from mice expressing only the biotinylase with streptavidin resulted in the same cytoplasmic pattern as detected in cells and tissues expressing biotinylated NICD^{BAP} (Figure 3.5D, green channel).

Additional evidence for an unspecific streptavidin binding comes from experiments demonstrating the localisation of biotinylated Hes7^{BAP} in cultured cells. An antibody raised against Hes7 was able to confirm nuclear localisation of Hes7^{BAP} whereas the streptavidin probe labelled cytoplasmic structures and was identical to the pattern seen in MCF10 [NICD^{BAP}; BirA] cells and transgenic animals (not shown). This suggests, that probing with streptavidin results in an unexpected high background. Therefore the BAP/biotin-avidin system cannot be used to determine the intracellular localisation of the biotinylated NICD^{BAP} protein by confocal microscopy. However, bioChIP experiments from transgenic *Notch1*$^{BAP/BAP}$*;Rosa26*$^{BirA/BirA}$ should not be affected by the mainly cytoplasmic noise because nuclear extracts are used for this kind of application.

In conclusion the experiments on the MCF10A [NICD^{BAP}; BirA] and C3H10T½ [NICD^{BAP}; BirA] cell lines suggest that these systems are not suitable to address the question of Notch signalling targets. First, the bioChIP procedure does not lead to reproducible results and thus is not robust enough to perform genome-wide studies. Possible reasons for this are the indirect binding of NICD to the DNA and the highly dynamic behaviour of the transactivation complex (Krejci and Bray, 2007). Second, I am not able to keep double stable cell lines due to the lack of selection for the NICD^{BAP}, which leads to a reduced expression of the biotinylated NICD^{BAP}.

Altogether, the optimisation of the bioChIP procedure on the stably transduced cell lines was useful in determining the formaldehyde fixation as well as sonication set-up and the application of different washing conditions. However, these data are erratic, do not show reproducible results and lead to a high variability between different cell lines. I therefore decided to stop working on these cell lines and instead continue with the *in vivo* bioChIP experiments from transgenic mouse tissue, where NICD^{BAP} is expressed from the endogenous *Notch1* promoter. The advantages of the *in vivo* system are that there is no untagged NICD present and the stable integration of the transgene in the knock-in mice.

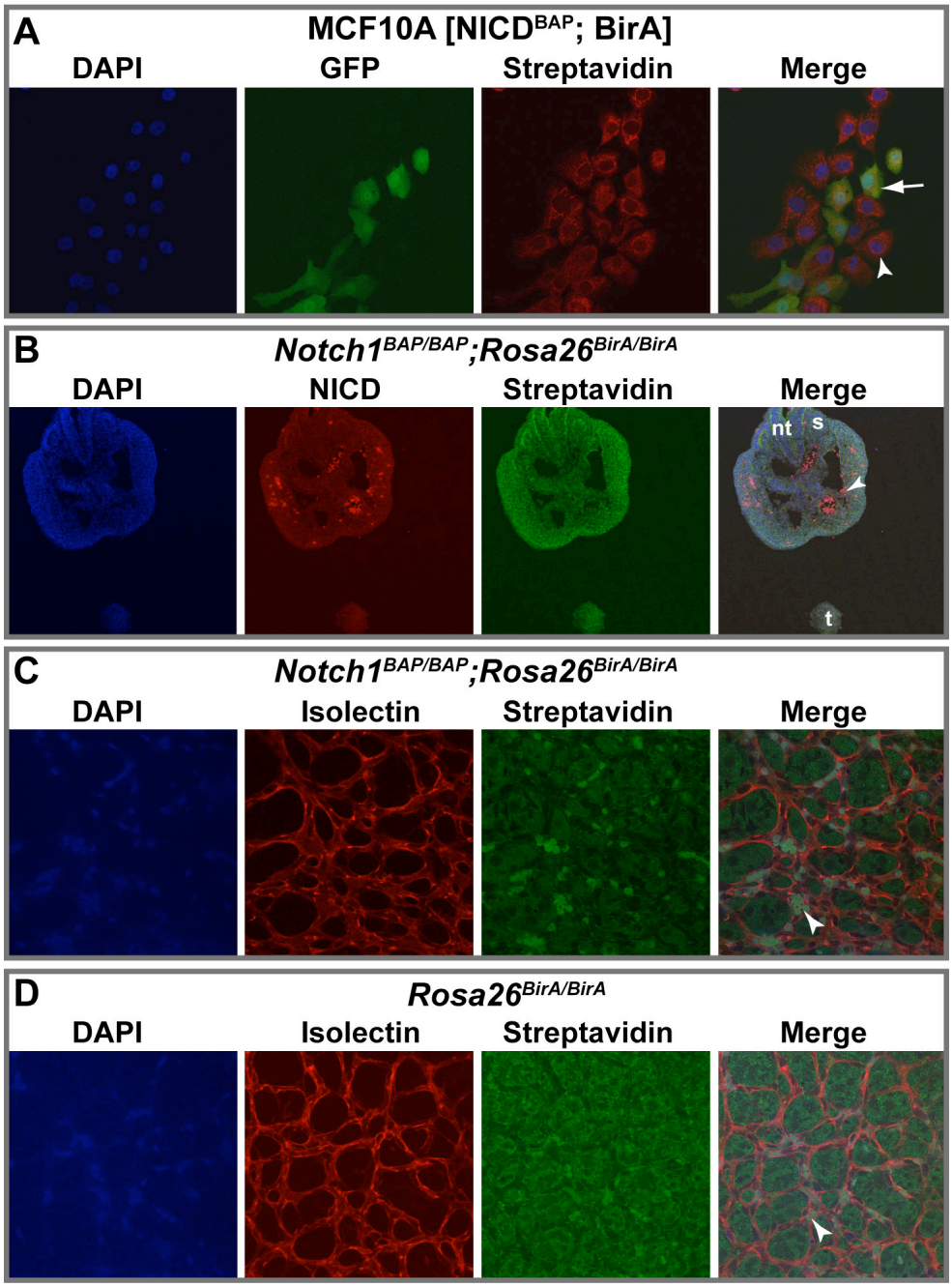

Figure 3.5 Application of the BAP/biotin-avidin system for intracellular localisation of the biotinylated NICD^{BAP} protein. (A) Immunostaining of MCF10A [NICD^{BAP}; BirA] cells with an α-GFP (1:100) antibody and streptavidin conjugated Alexa Fluor 594 (1:500). Nuclei were stained with DAPI. Arrowhead points at a cell without GFP expression. Arrow indicates cell with GFP and thus biotinylated NICD^{BAP} expression. (B) Immunostaining of transverse sections of *Notch1$^{BAP/BAP}$;Rosa26$^{BirA/BirA}$* embryonic tails with an α-NICD antibody (1:100) and streptavidin conjugated Alexa Fluor 488 (1:500). DNA was visualised with DAPI. Arrowhead points at nuclear NICD staining. s, somite; nt, neural tube; t, tip of the tail. (C, D) Immunostaining of P5 mouse retinas from *Notch1$^{BAP/BAP}$;Rosa26$^{BirA/BirA}$* (C) and *Rosa26$^{BirA/BirA}$* (D) transgenic mice with Isolectin coupled to Alexa Fluor 568 (1:500) to stain the blood vessels or streptavidin Alexa Fluor 488 (1:500) to visualise biotinylated NICD^{BAP}. DAPI was used to stain the DNA. Arrowheads point at auto-fluorescent erythrocytes.

3.2.5 Identifying Notch target genes from *Notch1$^{BAP/BAP}$;Rosa26$^{BirA/BirA}$* transgenic mice by bioChIP and high-throughput sequencing

I chose to investigate Notch activity by analysing binding to the *Hes1* promoter by bioChIP in cells of the developing mouse retina in the *Notch1$^{BAP/BAP}$;Rosa26$^{BirA/BirA}$* transgenic strain. It has been reported that inhibition of Notch signalling using γ-secretase inhibitors promotes vascular sprouting in the mouse retina (Hellstrom et al., 2007). In particular the number of tip cells, which lead each vessel sprout, increases. Conversely, the activation of Notch signalling causes a reduced tip cell fate (Hellstrom et al., 2007). In collaboration with Dr. Holger Gerhardt (Vascular Biology Laboratory, Cancer Research UK London Research Institute) I set out to identify Notch signalling targets that mediate the tip cell fate in the developing retinal vasculature. bioChIP experiments from retina tissue of *Notch1$^{BAP/BAP}$;Rosa26$^{BirA/BirA}$ (Notch1^{BAP};BirA)* and *Rosa26$^{BirA/BirA}$ (BirA)* mice, with or without γ-secretase inhibitor DAPT-treatment, are predicted to show a difference in the target gene pool. Novel candidate targets were analysed through high-throughput sequencing and their role in vessel sprouting investigated.

Briefly, *Notch1^{BAP};BirA* and *BirA* (control strain) five day old (P5) pups were injected subcutaneously with DAPT. In order to check if the DAPT treatment was efficient, I performed western blot analysis of skin tissue from injected *Notch1^{BAP};BirA* and *BirA* pups. A reduced level of NICD and NICD^{BAP} expression and hence the blockage of Notch signalling was confirmed (Figure 3.6A, middle blot). These results show that already after three hours a substantial decrease in NICD protein levels is observed (Figure 3.6A, middle blot). The duration of treatment seemed suitable for the bioChIP experiment because switching off target gene transcription occurs faster than protein degradation.

For the bioChIP experiment I harvested eyes and dissected retinas three hours after DAPT injection. From a pool of retinas I prepared chromatin and sheared it to an average length of 300 bp (Figure 3.6B). Following the streptavidin pull-down and washes, bound chromatin was eluted and analysed by qPCR in the first instance. bioChIP pre-experiments with transgenic mouse tissue (section 7.6.1.2) using qPCR to assay the outcome did not result in the purification of known Notch1 target sites in the promoter of *Hes1* or *Nrarp* (*Notch-regulated ankyrin repeat protein*, a previously

characterised Notch target gene in the retina, (Phng et al., 2009) (not shown). I hypothesised that these known targets might be obscured by a high amount of either other specifically or of unspecifically pulled-down DNA fragments. In order to thoroughly analyse my bioChIP results, I sequenced the entire eluate of the bioChIP experiment from transgenic retina tissue (Figure 3.6B).

Therefore, the bioChIP-enriched DNA was converted into a library suitable for high-throughput sequencing with Illumina Genome Analyzer. Subsequent steps involved the ligation of sequencing adapters to the DNA fragments, the amplification of the ChIP-seq library by PCR and gel purification of the DNA. Sequencing was done using the Illumina chemistry as described before (Bentley et al., 2008) and carried out at the Cancer Research UK Leeds Institute of Molecular Medicine.

Eight different samples, each comprising of an input (10% of starting material), a ChIP (purified chromatin) and two different treatment conditions (with and without DAPT; Table 7.20) were processed in the Illumina Genome Analyzer to yield 1Gbase of output reads. The sequencing process produces image files as raw format, which are processed to obtain nucleotide-base calls. The resulting 36 bp reads were subsequently aligned to the mouse genome using the standard Illumina pipeline.

However, due to an imbalance in forward and reverse sequence reads it was not possible to call “peaks” (of enriched loci) using *de facto* standard approaches. Several different analysis strategies were undertaken in order to align the sequence reads to the genome and to call peaks (section 7.6.1.3).

The Bio-Notch samples were subsequently corrected for the BirA background resulting in 4 experimental conditions: input neg, ChIP neg (without DAPT) and input pos, ChIP pos (with DAPT) and an enrichment of the ChIP sample over the Input calculated. The resulting peaks were mapped back onto the mouse genome and yielded a list of target genes for the two conditions (with and without DAPT). However, *Hes1* and *Nrarp*, two characterised target genes in the retina, were not called in the target list. The predicted outcome would have been to detect NICD at the *Hes1* and *Nrarp* promoters in the ChIP neg condition whereas NICD should be absent from these promoters in the DAPT treated condition.

These results mirror the NICD bioChIP experiments from cultured cells demonstrating a challenge in detecting NICD at known Notch target promoters. Most

likely the Notch transactivation complex exhibits a more dynamic behaviour than previously suggested. However, the list of identified target genes will be anlysed further and might contain interesting genes, which can be studied in vessel sprouting in the future.

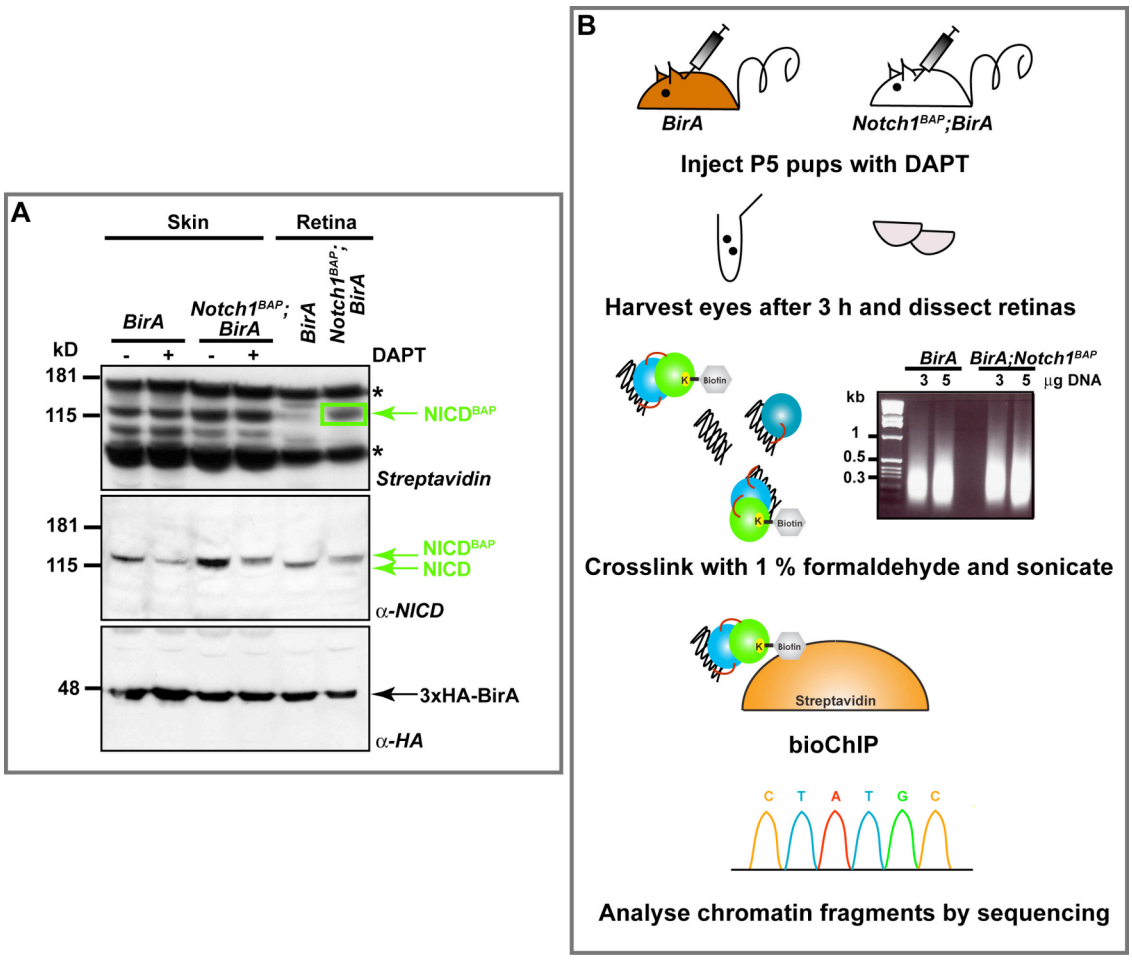

Figure 3.6 Strategy to identify novel *in vivo* targets of Notch signalling in the postnatal retina of *Notch1^{BAP};BirA* mice. (A) Wester blot of protein extracts from *Notch1^{BAP};BirA* and *BirA* skin and retina tissues were probed with streptavidin (1:25,000, top), α-NICD (1:1,000; middle) or α-HA antibodies (1:1,000) to detect biotinylated NICD^{BAP} (green arrow and rectangle), endogenous NICD (green arrow) or 3xHA-BirA (black arrow), respectively. Asterisks label signals from endogenous biotinylated proteins. (B) Schematic of NICD^{BAP} bioChIP procedure from DAPT treated or untreated P5 *BirA* and *Notch1^{BAP};BirA* retinas. Briefly, P5 pups were injected subcutaneously with DAPT or vehicle. After 3 h eyes were harvested and retinas dissected. Following the formaldehyde fixation, which generates protein-protein and protein-DNA crosslinks (red line), the chromatin was sonicated into fragments of defined lengths. 3 or 5 µg of DNA was loaded onto a 1% agarose gel to check average length. The crosslinked transactivation complex consistent of target bound CSL (blue) and NICD^{BAP} was purified through streptavdin binding (bioChIP). Bound material was eluted by reversing the crosslinks. Target genes were identified by Illumina sequencing.

3.2.6 Interaction of NICD with CSL in mouse embryos

So far, I could not show that the BAP/biotin-avidin system is working successfully in bioChIP assays to identify novel Notch target genes. One possibility might be the fact that NICD does not bind DNA directly but via CSL. Usually, ChIP (and bioChIP) experiments are designed to pull-down a transcription factor that directly binds its DNA target sites. A possible explanation for the failure in detection of known Notch signalling targets such as *Hes1* in bioChIP experiments could be the weak interaction between NICD and DNA-bound CSL leading to a dissociation of the transactivation complex during the bioChIP procedure.

In order to test a possible dissociation of NICD and CSL after crosslinking I performed streptavidin protein pull-down experiments from crosslinked embryonic *Notch1^{BAP};BirA* and *BirA* protein lysates to investigate CSL binding by western blot analysis (Figure 3.7). I failed to detect CSL in the bound fraction (Figure 3.7, S) of *Notch1^{BAP};BirA* embryos after binding to the streptavidin matrix whereas I clearly enriched for biotinylated NICD^{BAP} (Figure 3.7, green rectangle). CSL protein was only detected in the input (Figure 3.7, I) sample of *Notch1^{BAP};BirA* and *BirA* embryonic extracts.

This suggests, that the interaction between CSL and NICD^{BAP} despite formaldehyde crosslinking is lost during streptavidin purification or there might not have been an interaction in the first place. Proteins within the nucleus show a very dynamic behaviour (in protein-protein and protein-DNA interactions) because they need to respond quickly to cues transmitted by signalling cascades (reviewed in Misteli, 2001). Thus it is likely that NICD^{BAP} and CSL did not interact in my experiments or only transiently due to a highly dynamic environment. It has been shown previously that an interaction between NICD and CSL is confirmed only upon induction of Notch signalling (Krejci and Bray, 2007).

Another explanation for the observed lack of interaction between NICD^{BAP} and CSL in embryonic lysates could be that CSL dissociated during the washing step. Although, proteins were crosslinked this might not have been sufficient to maintain a link between NICD^{BAP} and CSL.

In conclusion these experiments are consistent with interactions between NICD and CSL being transient and does not allow me to identify novel targets of Notch

signalling through the approach of the bioChIP from my transgenic mice. Although target genes such as *Hes1* are expressed in embryonic and retina tissue my approach is greatly limited by temporally controlling Notch pathway activation. During normal signalling in the animal, Notch activity does not occur as concerted as in experiments by Krejcic et al., which profited from the ability to control the timing of activation precisely in their system (Krejci and Bray, 2007).

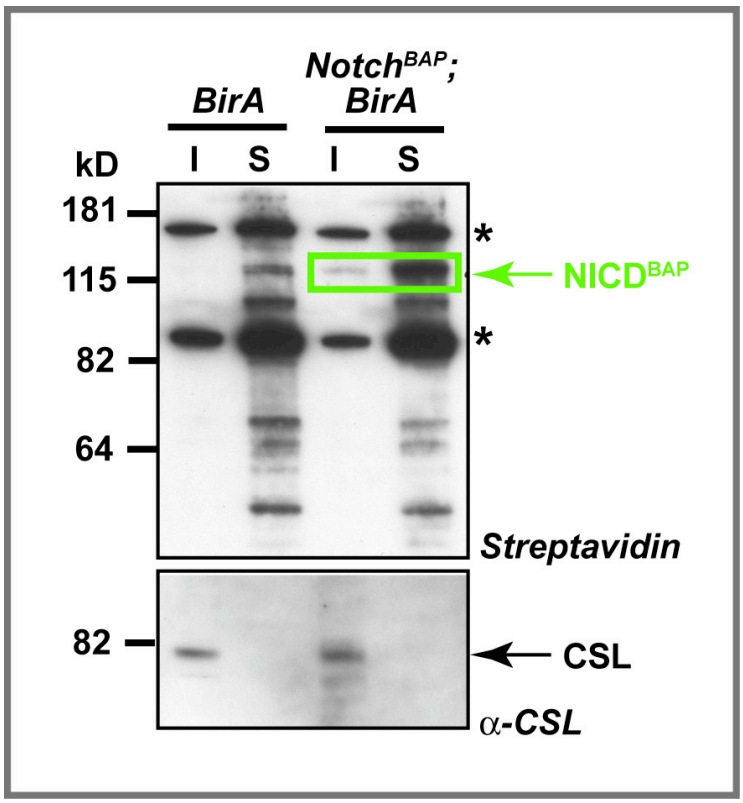

Figure 3.7 Streptavidin protein pull-down from *Notch1*^{BAP}*;BirA* E10.5 crosslinked embryos does not purify CSL, a direct protein partner of NICD. 500 µg of *BirA* and *Notch1*^{BAP}*;BirA* embryonic lysates were loaded onto streptavidin coated beads and incubated for 4 h at 4ºC. Beads were washed three times and bound material eluted by boiling in loading buffer. 20 µl eluate was run on a 4-12% Bis-Tris gel. 1% of the input fraction (I) was loaded next to the streptavidin pull-down sample (S). Western blot analysis with streptavidin-HRP probe (1:25,000; top) or an α-CSL antibody (1:1,000). Asterisks label signals from endogenous biotinylated proteins.

3.2.7 Identification of NICD protein binding partners *in vivo* via biotin-streptavidin binding

The BAP-biotin/avidin system has primarily been used for the identification of protein interaction partners (de Boer et al., 2003; Fernandez-Suarez et al., 2008; Furuyama and Henikoff, 2006; Grosveld et al., 2005; Hamlett et al., 2008; Rodriguez et al., 2005). Because of the direct binding, purification of such partners might be more robust than of chromatin. Identification of protein binding partners of NICD does not only help to further evaluate the bioChIP method, but it is also of biological interest.

For the activation of Notch target genes, the formation of a ternary complex consisting of NICD, the DNA-binding transcription factor CSL and the transcriptional co-activator Mastermind is obligatory (Kovall, 2008; Petcherski and Kimble, 2000b; Wu et al., 2000) (section 1.2.3). Recruitment of the general transcription factors CBP/p300 and PCAF is required for target gene activation and further factors are likely to be involved (Fryer et al., 2002; Kurooka and Honjo, 2000; Wallberg et al., 2002).

Are additional nuclear components involved *in vivo* for promotion or dissociation of the transactivation complex? In order to answer this question I performed streptavidin protein pull-down experiments (section 7.5.8) from transgenic embryos, which might lead to the identification of NICD binding partners. The protein profile after streptavidin pull-down of nuclear embryonic lysates from transgenic *Notch1^{BAP};BirA* embryos resulted in 11 proteins that were found in *Notch1^{BAP};BirA* but absent in *BirA* and wildtype (Figure 3.8A and Table 3.1). Prominent bands that were enriched after streptavidin binding, and consisted of several proteins, were isolated and analysed by mass spectrometry (see Figure 3.8A for annotation of the proteins analysed; section 7.5.9).

Pull-downs with epitope-tagged proteins normally lead to an enrichment of the tagged protein after purification compared to the input. Due to the extremely low concentration of the NICD protein I was not able to detect or to see an enrichment of NICD^{BAP} after purification on the stained gel (Figure 3.8A). However, on the western blot, which is a more sensitive method than protein identification by mass spectrometry I could visualise biotinylated NICD^{BAP} (Figure 3.8B, green arrow). This demonstrates, that the principle of the streptavidin purification is working in transgenic mouse tissues.

I chose to analyse the 30 bands, which highly enrich after streptavidin purification compared to the input fraction (Figure 3.8A, compare lane I to S for each genotype). Visual examination of the protein lanes from different genotypes suggested that there was no difference in the protein profile indicating a non-specific binding to the streptavidin matrix (Figure 3.8A). Mass spectrometry and further computational mapping of the peptides yielded 74 proteins most of which were identical in wildtype, *BirA* and *Notch1*^{BAP}*;BirA*. However, 11 "novel" proteins were identified in the *Notch1*^{BAP}*;BirA* lane only, likely Notch interaction partners pulled down with NICD^{BAP}, 9 of them came up in the analysis from fragment 30 (Table 3.1).

All of the 74 proteins identified were nuclear factors, mainly of the high abundant ribosomal protein family or proteins involved in the RNA metabolism (Figure 3.8D). None of the analysed proteins was directly related to the Notch pathway nor did I identify known binding partners such as CSL or Mastermind. The reason for this result might be that nuclear proteins arbitrarily bind the streptavidin beads and the background masks low abundance proteins, such as CSL.

Previous reports have indicated, that histones might be biotinylated as well (Camporeale et al., 2007; Camporeale et al., 2004; Chew et al., 2008; Kobza et al., 2005). In order to check this possibility, I used a 16% Tricine gel to separate the proteins after streptavidin pull-down for a better resolution in the low molecular weight range to detect the small histones. I identified histone cluster H1 in the protein pull-down from wildtype, *BirA* and *Notch1*^{BAP}*;BirA* embryonic tissues (Figure 3.8A; protein bands 1, 2, 3). However, biotinylation of histone H1 has not been shown in previous studies. Histone H1 fulfils a structural function within the chromatin and so far has not been reported to be involved in epigenetic modifications (Happel and Doenecke, 2009).

Since, histone cluster H1 was also purified with streptavidin from wildtype protein lysate, there might be a possibility, that histone H1 is naturally biotinylated. But, mass spectrometry and computational motif search did not reveal a site for biotinylation modification. This could be due to the mass spectrometry analysis technique, which was not sensitive enough for this kind of application. Further investigations towards a possible naturally occurring biotinylation of histone H1 were not pursued due to technical limitations.

Within the identified protein pool one protein with a possible biotinylation site was discovered (by computational motif search analysis): mCG3370, but the function

remains elusive (Mural et al., 2002). Since this protein was discovered in wildtype and transgenic embryonic lysates it can be excluded from the Notch target gene list.

In summary the streptavidin protein pull-down experiments from transgenic *BirA* and *Notch1*^{BAP}*;BirA* embryos were not satisfactory due to the high background binding, suggesting that this approach is not suitable to find novel NICD interacting proteins *in vivo*.

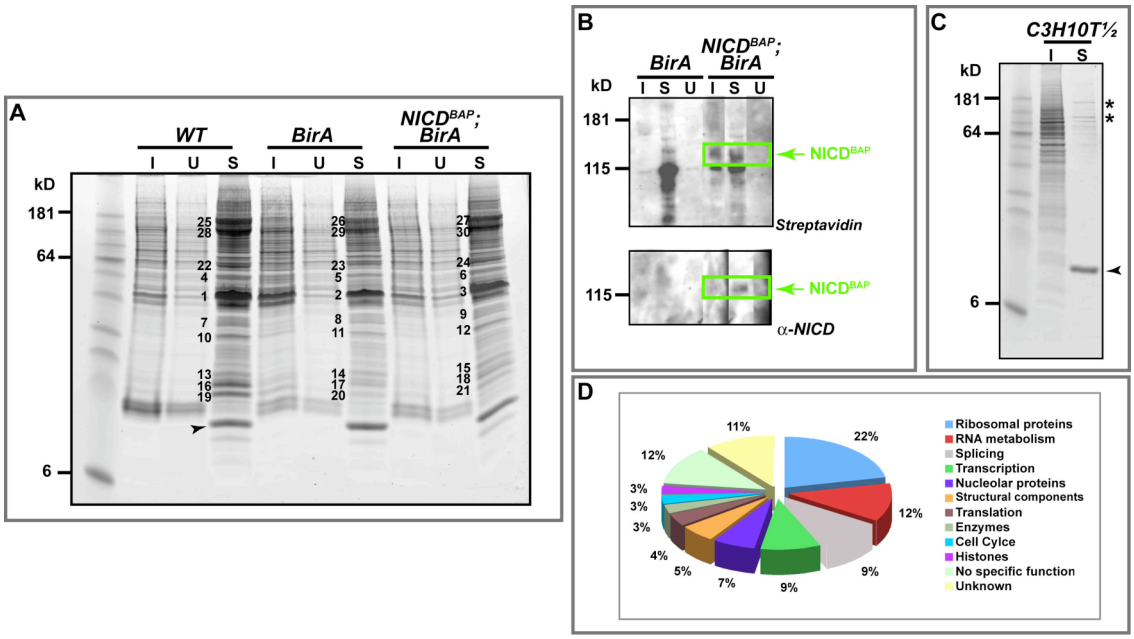

Figure 3.8 Application of the BAP/biotin-avidin system to identify novel protein binding partners of NICD in *Notch1^{BAP};BirA* embryos. (A) Streptavidin purification of biotinylated proteins from wildtype (WT), *BirA* and *Notch1^{BAP};BirA* embryonic lysates. 2 mg of nuclear extracts were bound to 40 µl of blocked streptavidin beads and incubated for 2 h at 4ºC. Beads were washed and subsequently eluted in 50 µl loading buffer by boiling. 20 µl was loaded onto a 16% Tricine gel. The gel was stained with Colloidal Blue and indicated products (1-30), consisting of several different proteins, cut out and analysed by mass spectrometry. I, input; U, unbound; S, streptavidin purification. Arrowhead points at streptavidin subunit (as identified in C). (B) Western blot to detect biotinylated Notch1^{BAP} from streptavidin pull-down of *BirA* and *Notch1^{BAP};BirA* embryonic extracts. Visualisation of the protein was done by streptavidin probe (1:25,000) or an α-NICD antibody (1:1,000). Green arrows point at detected biotinylated NICD^{BAP}. (C) Streptavidin protein purification from C3H10T½ cells identified endogenous biotinylated proteins as seen in western blots from whole and crude nuclear cell lysates (*) as well as the streptavidin precursor (arrowhead). (D) Classification of proteins from bands 1-30 (A) identified by mass spectrometry.

Protein identified	Sample number	Unique peptides	weight in kD
DEAH (Asp-Glu-Ala-His) box polypeptide 15 isoform 2 (NP_031865)	30	5	89
nucleolar complex associated 2 homolog (NP_067278)	30	4	86
tripartite motif protein 28 (EDL38082)	30	3	89
RNA binding motif protein 5 (NP_683732)	6	3	92
activating signal cointegrator 1 complex subunit 1 (NP_081213 XP_483908)	9	3	41
small nuclear ribonucleoprotein polypeptide A', isoform CRA_c (EDL07232)	30	3	25
tuftelin interacting protein 11 (NP_061253)	30	2	96
1810007M14Rik protein (AAH27145)	30	2	105
nucleolar RNA-associated protein beta (Nrap) (AAL74402)	30	2	129
similar to FtsJ homolog 3 isoform 2 (NP_079586)	30	2	96
RNA-binding protein 12B-B (RNA-binding motif protein 12B-B) (Q66JV4)	30	2	97

Table 3.1 Proteins identified in *Notch1*$^{BAP/BAP}$;*Rosa26*$^{BirA/BirA}$ embryonic nuclei. NCBI nucleotide accession numbers are given in brackets. Sample number indicates excised protein band from Figure 3.8A. Unique peptides identify the number of distinct peptides that were found by mass spectrometry and matched to a single protein.

3.3 Discussion

This chapter describes my endeavour to purify both Notch target chromatin and NICD-interacting proteins *in vivo* from transgenic *Notch1^{BAP};BirA* mice. However, my strategy did not prove successful. I was able to perform bioChIP experiments in a previously optimised system, the MEL [GATA-1^{BAP}; BirA] (de Boer et al., 2003) stable cell line, but NICD^{BAP} turned out not to be an applicable bait for bioChIP and streptavidin protein pull-down assays from cell lines or transgenic mouse tissue.

3.3.1 Testing the BAP/biotin-avidin system

Possible reasons why the GATA-1^{BAP} experiments worked while the NICD^{BAP} approach failed include: Firstly, identifying GATA-1 binding sites as well as protein complex partners was done within a cell culture system which allowed a timed activation (and overexpression) of the GATA-1 transcription factor. My attempts to create a controllable tissue culture system failed due to the constitutive activity of the supposedly hormone inducible ER-NICD^{BAP}.

Secondly, GATA-1 binds transcriptional targets directly and creates a stable complex on the DNA, whereas NICD target gene activation is complex and requires the additional adaptor protein CSL for physical interaction with the target DNA.

Lastly, The concentration of the biotinylated GATA-1^{BAP} protein lies orders above the one of NICD^{BAP} *in vivo* (Schroeter et al., 1998) which facilitates the purification of GATA-1^{BAP} associated proteins and chromatin.

Thus, the low level of NICD^{BAP} (Schroeter et al., 1998), the indirect DNA binding as well as the complex and transient interaction between NICD^{BAP} and its nuclear partners (Krejci and Bray, 2007) impede the application of the bioChIP procedure for identifying novel Notch signalling targets and protein binding partners.

Previous attempts to identify targets of NICD were limited to genomic arrays and comparative expression studies in tissue culture cells (Weng et al., 2006) as well as ChIP experiments directed against CSL in cultured *Drosophila* cells (Krejci et al., 2009) (section 1.2.5). Targeting CSL in search for novel Notch signalling targets could be a more promising approach because CSL binds DNA directly and can function as a readout for Notch signalling targets. However, one needs to consider the dynamic

behaviour of the different CSL complexes mediating repression and activation. It has been shown that a complex of CSL with its co-repressors resides on the target DNA only for a short time and is unstable (Krejci and Bray, 2007). Upon temporal activation of the Notch pathway, CSL forms a complex with NICD and co-activators, which leads to high stability DNA interaction in cultured *Drosophila* cells (Krejci et al., 2009; Krejci and Bray, 2007). Thus, in order to maximise target readout, a timely regulated Notch pathway activation can be of benefit (Krejci et al., 2009; Krejci and Bray, 2007).

Expressing biotinylated $NICD^{BAP}$ did not lead to the discovery of novel Notch targets. In the future, I would suggest testing a similar approach using *in vivo* biotinylated CSL because of the fact that CSL does bind DNA directly. Pre-experiments to investigate an appropriate position of the BAP-tag within CSL and confirmation of biotinylation would be crucial. Although experiments in tissue culture cells are useful, they do not always predict the *in vivo* behaviour as revealed by my transgenic $Hes7^{BAP/BAP}$ mice (chapter 4).

It has been reported, that histones are biotinylated in flies, mouse and human, which is mediated by the holocarboxylase synthetase (HCS) (Camporeale et al., 2006; Narang et al., 2004). In particular, biotinylation was shown for histone H2A (Chew et al., 2006) H3 (Kobza et al., 2005) H4 (Camporeale et al., 2004). Because of the high abundance of histones, I had to expect to pull-down these histones with my streptavidin beads. However, my attempt to identify biotinylated histones resulted only in the detection of the histone cluster H1 by mass spectrometry from both embryonic wildtype and transgenic tissues (Figure 3.8A protein bands 1,2,3 and D). Previous studies have not found histone 1 to be biotinylated nor to have a function in epigenetics but in chromatin structure (Happel and Doenecke, 2009). My results from the protein pull-down and further computational analysis of a possible biotin modification concluded that the histone 1 is probably not biotinylated and only represents background.

Altogether the BAP/biotin-avidin system is not appropriate to identify novel Notch DNA targets and protein binding partners *in vivo* or *ex vivo*. The complex nature of Notch target gene activation, as well as the extremely high background binding of naturally unbiotinylated proteins are the major drawbacks of this strategy.

3.3.2 Decoding the mouse retina "Notch targetome"

There is an increasing demand for the global mapping of transcription factors in order to gain insight into the complex gene regulatory network. However, transcription factors do not bind all targets in the genome, which contain their specific motif (Carroll et al., 2005; Rabinovich et al., 2008). Conversely, transcription factors can also bind non-canonical sequence motifs (Carroll et al., 2005; Cawley et al., 2004; Rabinovich et al., 2008) and motif patterns of a transcription factor can vary between different species (Borneman et al., 2007; Odom et al., 2007). ChIP-seq provides an opportunity to address these questions like in the context of Notch signalling in the retina.

I decided on ChIP-seq rather than ChIP-chip (hybridisation of the purified DNA pool to a tiling array) because of the greater resolution, higher sensitivity and specificity (reviewed in Schmidt et al., 2009). Moreover, ChIP-seq reactions require less input material than ChIP-chip (nanograms for ChIP-seq versus micrograms for ChIP-chip) and experiments can be done faster because they are not dependent on design and production of tiled microarrays. Another advantage of ChIP-seq is the possibility of detecting low-affinity transcription factor binding sites as well as mutations within binding sites.

However, ChIP-seq analysis data can be biased by different sources, which leads to the enrichment of non-specific genomic regions, like unspecific immunoprecipitation, imprecise mapping of sequence tags as well as bias resulting through PCR. Identified binding sites do not have to be real transcription factor targets: there is also a possibility that looping of the DNA as well as protein-protein interactions can lead to the identification of an enriched region. Furthermore with ChIP-seq experiments it is still not possible to distinguish between binding events within a whole cell population and an event in a single cell at a time. Technologies towards this goal still need to be established and optimised in order to perform single cell ChIP-seq and will be able to give answers about target activation in time (Jothi et al., 2008).

In contrast to the NICD approach, ChIP-chip and ChIP-seq experiments were performed successfully before with histones (Huebert et al., 2006; Negre et al., 2006; Robertson et al., 2008). However, core histones are the exception in the highly dynamic nuclear landscape and reside on the chromatin for several hours as compared to transcription factors which establish contact with their target sites for seconds (reviewed

in Misteli, 2001). This fact greatly facilitates ChIP approaches to map histones and modifications thereof on the chromatin.

Although I was not successful to identify the Notch targetome in the mouse retina using the NICD bioChIP-seq approach I have shown that Notch target gene activation might be more intricate and dynamic than previously thought.

CHAPTER 4: Characterisation of *Hes7*$^{BAP/BAP}$ mice reveal differential axial requirements for *Hes7* transcription

4.1 Introduction

The basic helix-loop-helix (bHLH) transcription factor Hes7 plays an important role during the formation of somites in the developing mouse embryo (Kageyama et al., 2007a; section 1.2.5.1). Both loss-of-function and persistent overexpression of *Hes7*, which normally has cyclic expression, leads to fused and irregular somites and thus severe malformation of vertebrae and ribs (Bessho et al., 2001b; Hirata et al., 2004). In order to find *in vivo* DNA targets of Hes7 during segmentation, I generated transgenic mice expressing an epitope-tagged version of Hes7 ($Hes7^{BAP}$) using a novel approach (chapter 2). However, tagging Hes7 itself caused an interesting segmentation phenotype, which differs from the *Hes7* null phenotype (Figure 4.1).

4.2 Results

This chapter deals with the analysis of the *Hes7*$^{BAP/BAP}$ (*BAP/BAP*) mice: first I characterise the skeletal phenotype in detail, and then I examine the expression of putative Hes7 target genes and other key factors of somitogenesis.

4.2.1 *BAP/BAP* mutant skeletons show a regionalised axial phenotype

In order to dissect the axial phenotype of *BAP/BAP* mice, I analysed skeletons of E18.5 foetuses and compared them to wildtype, heterozygous *Hes7*$^{BAP/+}$ (*BAP/+*) and *Hes7* knock-out specimens. In *Hes7*$^{-/-}$ mice most of the *Hes7* coding region was removed and instead, the *lacZ* gene was placed under the control of the endogenous promoter by homologous recombination in embryonic stem cells (Bessho et al., 2001b).

The wildtype skeleton consists of 7 cervical, 13 thoracic, 6 lumbar, 4 sacral and around 30 tail vertebrae (from head to tail) including 13 pairs of ribs which attach at the thoracic vertebrae (Tam, 1986) (not shown). *BAP/+* E18.5 skeletons are identical to wildtype skeletons in the number and size of vertebrae and will therefore be referred to as “control” in further experiments (Figure 4.1B; Table 4.1).

In contrast, *Hes7*$^{-/-}$ foetuses show a severely disorganised axial skeleton with a very short tail and no regular vertebrae or ribs (Figure 4.1D; Table 4.1) (Bessho et al., 2001b). The entire length of the vertebral column is significantly short with fused vertebral bodies and neural arches (Figure 4.1E; Table 4.1). The ribs are fused and the number of rib pairs is 7, instead of the normal 13 (Table 4.1).

Heterozygous *BAP/+* mutant mice are indistinguishable from wildtype mice, whereas *BAP/BAP* mice have severe segmentation defects in the cervical, thoracic and lumbar area with fused vertebrae and ribs, as well as truncated tails. Nevertheless, the *BAP/BAP* mutant phenotype is not as severe as that of *Hes7*$^{-/-}$ mice (Figure 4.1, compare C with E; Table 4.1). The number of ribs is reduced to 9 and left-right symmetry is disrupted (Table 4.1). Frequently ribs are fused and show ectopic branching.

Upon close examination of the skeleton, one area of well-segmented vertebrae stands out among the deformed structures: the sacral area, which connects to the pelvic girdle, is normal in *BAP/BAP* mice. *BAP/BAP* foetuses always form 4 regular sacral vertebrae and frequently 1-3 regular lumbar and 2-10 well-patterned tail vertebrae are seen (Figure 4.1C, E; Table 4.1). The differences in patterning of the skeleton in this intermediate area distinguish the *BAP/BAP* mutant from the *Hes7*$^{-/-}$ (Figure 4.1C-E; Table 4.1). These results indicate that in a homozygous state the *BAP* allele results in a hypomorphic phenotype due to reduced Hes7 function.

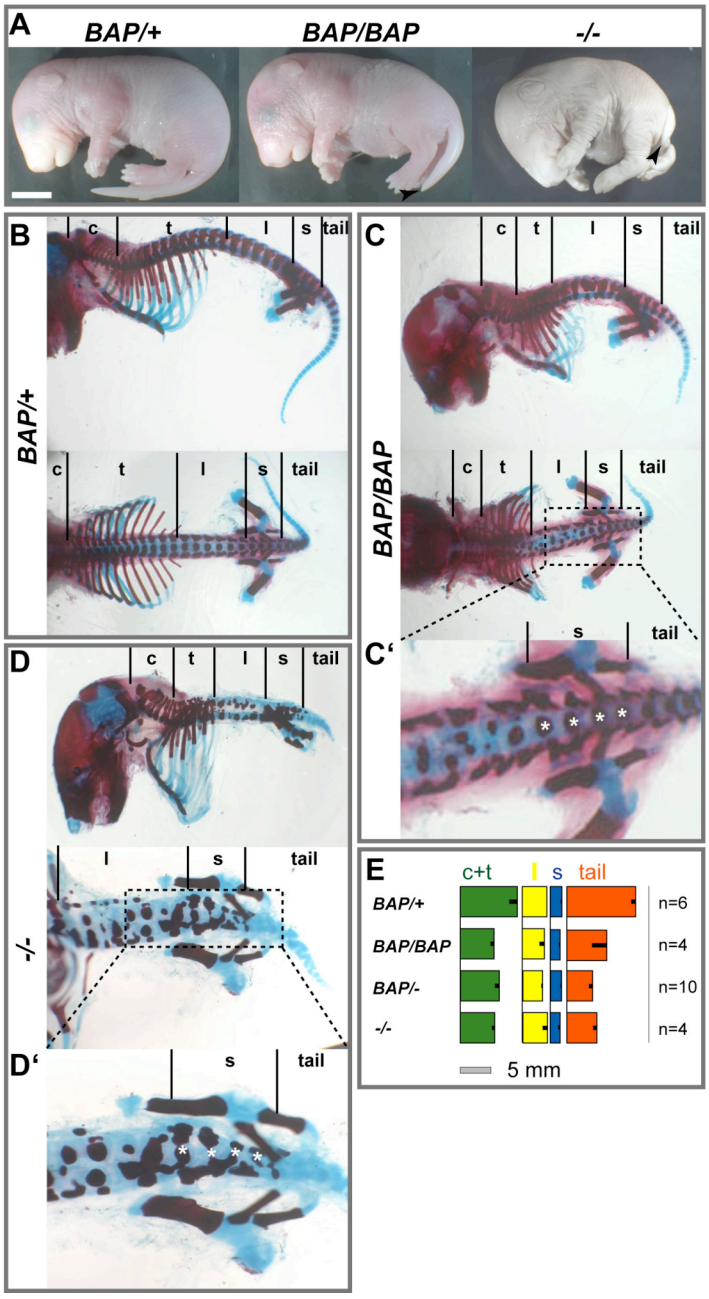

Figure 4.1 Analysis of *BAP/+*, *BAP/BAP* and *Hes7$^{-/-}$* *(-/-)* E18.5 foetuses. (A) *BAP/BAP* foetuses have shorter tails than *BAP/+* foetuses but considerably longer tails than -/-. Arrowheads point at the tip of the tail. White scale bar: 5 mm. (B-D) Lateral (top) and dorsal views of *BAP/+*, *BAP/BAP* and -/- E18.5 skeletal preparations. Bones are stained with alizarin red and cartilage with alcian blue. Compare the sacral (s) and adjacent lumbar (l) and tail (tail) areas between different skeleton preparations. C' and D' show magnifications of the sacral and surrounding area. Asterisks label vertebral bodies of the sacrum. (E) Average length of skeletal regions from *BAP/+*, *BAP/BAP*, *BAP/-* and -/- E18.5 foetuses (see Table 4.1). Boxes for each region are aligned to the left (anterior) end. Green box: c+t, cervical+thoracic vertebrae; yellow box: l, lumbar vertebrae; blue box: s, sacral vertebrae; orange box: tail vertebrae. Black bars indicate standard deviations.

	BAP/+	***BAP/BAP***	***-/-***	***BAP/-***
Number of E18.5 skeletons analysed	6	4	4	10
Length of whole vertebral column (mm)	27.5±1.6	20±1.9	16.3±0.5	16.5±1.2
Length of cervical plus thoracic region (mm)	9.3±1.3	5.5±0.6	5.6±0.8	6.3±0.7
Length of lumbar region (mm)	4±0	3.6±0.8	4.0±0.4	3.2±0.2
Length of sacral region (mm)	1.9±0.2	1.6±0.2	1.6±0.3	1.8±0.2
Length of tail (mm)	11.2±0.7	6.5±2.4	4.9±0.6	4.2±0.6
Total number of cervical vertebrae (normal and irregular)	7±0	4.75±0.5	4.6±0.9	5.6±0.5
Total number of regular lumbar vertebrae	6±0	2.3±0.9	0	0
Number of regular sacral vertebrae	4±0	3.8±0.5	0	0.4±0.7
Number of regular tail vertebrae	28±1	6.5±4.4	0	0
Number of ribs, left and right counted separately	13±0	9±0.9	7.3±0.7	5.2±0.4

Table 4.1 Comparison of *$Hes7^{BAP/+}$* *(BAP/+)*, *$Hes7^{BAP/BAP}$* *(BAP/BAP)*, *$Hes7^{-/-}$* *(-/-)* and *$Hes7^{BAP/-}$* *(BAP/-)* E18.5 foetal skeletons.

Most *$Hes7^{-/-}$* foetuses die within a few hours after birth, probably due to respiratory failure (Bessho et al., 2001b). However, one copy of wildtype *Hes7* fully restores viability and leaves only a mild kinked-tail phenotype in 43% of the adult population (Bessho et al., 2001b). Cell culture functional assays and phenotypic analysis of the *BAP/BAP* mutants suggest, that the *BAP* allele still has residual function, albeit less than wildtype *Hes7*. Therefore, I asked, is one copy of the *BAP* allele sufficient to rescue the null-phenotype?

Mice containing one BAP allele and one knock-out allele (*BAP/-*) die at birth (probably due to respiratory failure because of the malformed ribcage) and are

indistinguishable from *Hes7*$^{-/-}$ mice (compare Figure 4.1A and D with Figure 4.2A and C). They show a severely disorganised skeleton and do not form any regular vertebrae or ribs (Figure 4.2C and C'). The tail length is significantly reduced and resembles *Hes7*$^{-/-}$ tails (Figure 4.1E; Table 4.1). These results show, that one copy of the *Hes7*^{BAP} allele does not rescue the *Hes7* knock-out phenotype (compare Figure 4.1D with Figure 4.2C; Table 4.1). This further supports the hypothesis that, the *BAP* allele is a strong hypomorph allele because a weaker allele would be able to rescue the phenotype.

In summary, this part of the results confirms a requirement for one functional copy of *Hes7* during regular segmentation. The introduction of the BAP-tag sequence into the *Hes7* locus has disrupted some of the protein function. In a heterozygous state this partial loss-of-function can be compensated by the wildtype allele, which can still produce a fully functional Hes7 repressor. However, the residual function of Hes7^{BAP} is not sufficient to rescue the phenotype of a heterozygous *BAP/-* mutant. *BAP/BAP* mutant mice on the other hand survive and do not show an as severe axial phenotype as *Hes7*$^{-/-}$ or *BAP/-* mice. These results show that although Hes7^{BAP} has lost most of its function, it is still sufficient for survival and to form some regular vertebrae, if two copies are present (Table 4.1).

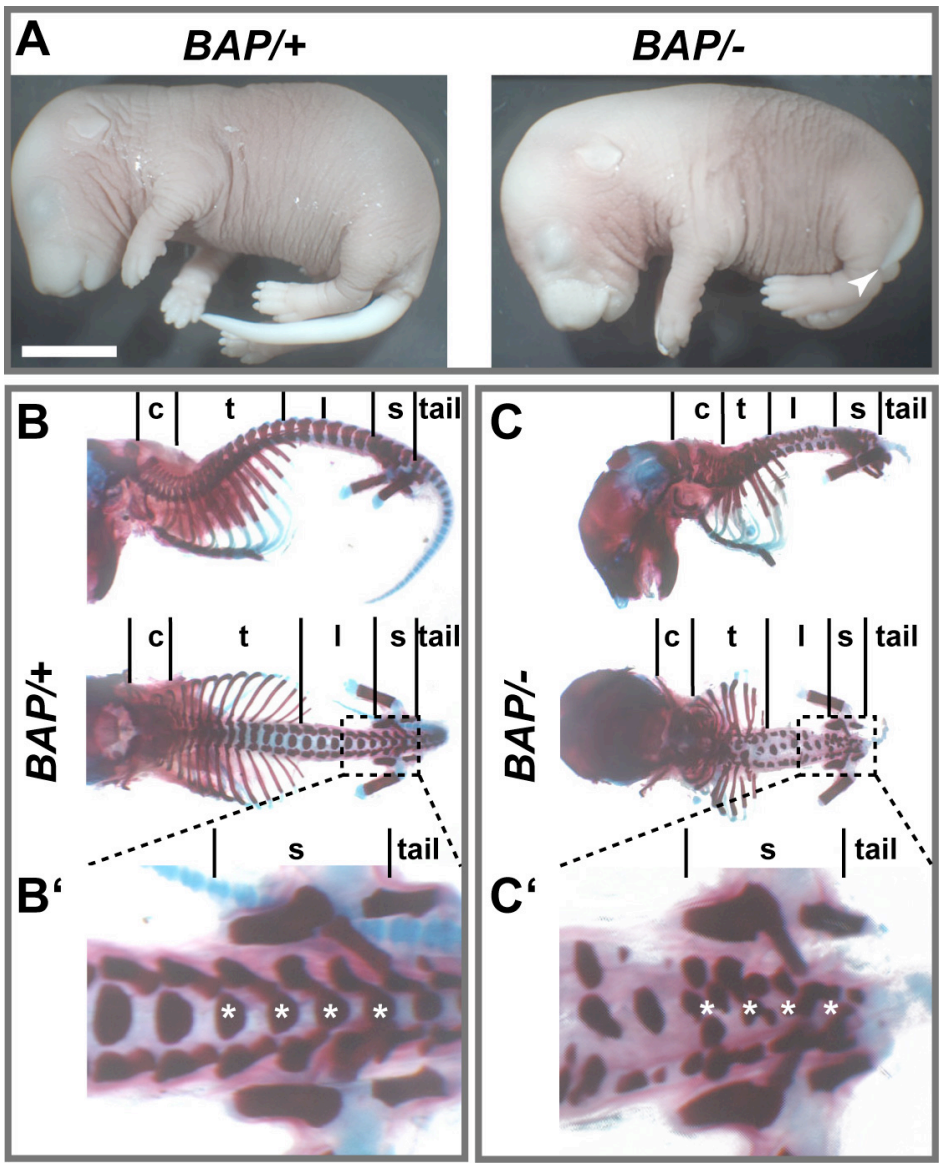

Figure 4.2 Genetic analysis of the *Hes7^{BAP}* allele in *BAP/+* and *BAP/-* E18.5 foetuses. (A) *BAP/+* and *BAP/-* E18.5 foetuses. Arrowhead points to the tip of the tail. White scale bar: 5 mm. (B–C') lateral (top) and dorsal views of heterozygous *BAP/+* (B) and heterozygous *BAP/-* (C) E18.5 foetal skeletons stained with alizarin red (bone) and alcian blue (cartilage). Magnifications of the sacral area are shown in (B') and (C'). Asterisks label regular (B') and irregular (C') vertebrae bodies of the sacrum. c, cervical vertebrae; t, thoracic vertebrae; l, lumbar vertebrae; s, sacral vertebrae; tail, tail vertebrae.

4.2.2 Regionally disrupted somite organisation in *BAP/BAP* embryos

The rescue of the sacral and adjacent lumbar and tail vertebrae in *BAP/BAP* mice could be due to the restoration of anterior-posterior compartmentalisation that leads to boundary formation. To test this hypothesis, I visualised the posterior somite halves with *Uncx4.1 in situ* hybridisation (Mansouri et al., 1997) in *BAP/BAP* and *BAP/+* embryos.

Heterozygous *BAP/+* E11.5 embryos (~48 somite pairs formed) hybridised with the *Uncx4.1 in situ* probe display a regular and distinct stripe pattern along the length axis visualising the posterior somite compartments (Figure 4.3A). In E11.5 *BAP/BAP* embryos, segmentation and anterior-posterior compartmentalisation is greatly disrupted as seen by irregular *Uncx4.1* expression (Figure 4.3B, black line). However, some regular *Uncx4.1* stripes are formed around the hind limb bud and tail area (somites ~28 onwards), albeit less distinctly than in *BAP/+* embryos (Figure 4.3A and B, asterisks). The well-patterned somites are consistent with the mild sacral vertebral phenotype observed in *BAP/BAP* mutants. The *Uncx4.1* stripe domains get fuzzy and less regular towards the tail end (Figure 4.3B') mirroring abnormalities in somite size and compartmentalisation of mutant embryos (Figure 4.3B).

Younger *BAP/BAP* embryos, at E9.5, have 3-5 additional regular *Uncx4.1* stripes in the anterior segmented region, which form the occipital bone (Figure 4.3D' and E', asterisks). This is consistent with $Hes7^{-/-}$ mice, which also form some regular anterior somites (Bessho et al., 2001b). It has also been shown that in *Notch1* knock-out mice the initial somites are formed, albeit delayed, independently of Notch signalling (Conlon et al., 1995; Huppert et al., 2005).

In section 4.2.1 I showed, that segmentation is affected in *BAP/BAP* mice, with severely fused vertebrae and ribs along the length axis except in the sacral and to some degree in the adjacent lumbar and tail areas. The *Uncx4.1 in situ* hybridisation results point out, that the adult skeletal phenotype is reflected by patterns of gene expression in newly formed somites, indicating that the defects arise early and are due to irregular somitogenesis. Hes7 is an important player in the formation of new somites, and disrupting its auto-inhibition loop, as in the case of the *BAP/BAP* mice, appears to have an influence on the segmentation clock.

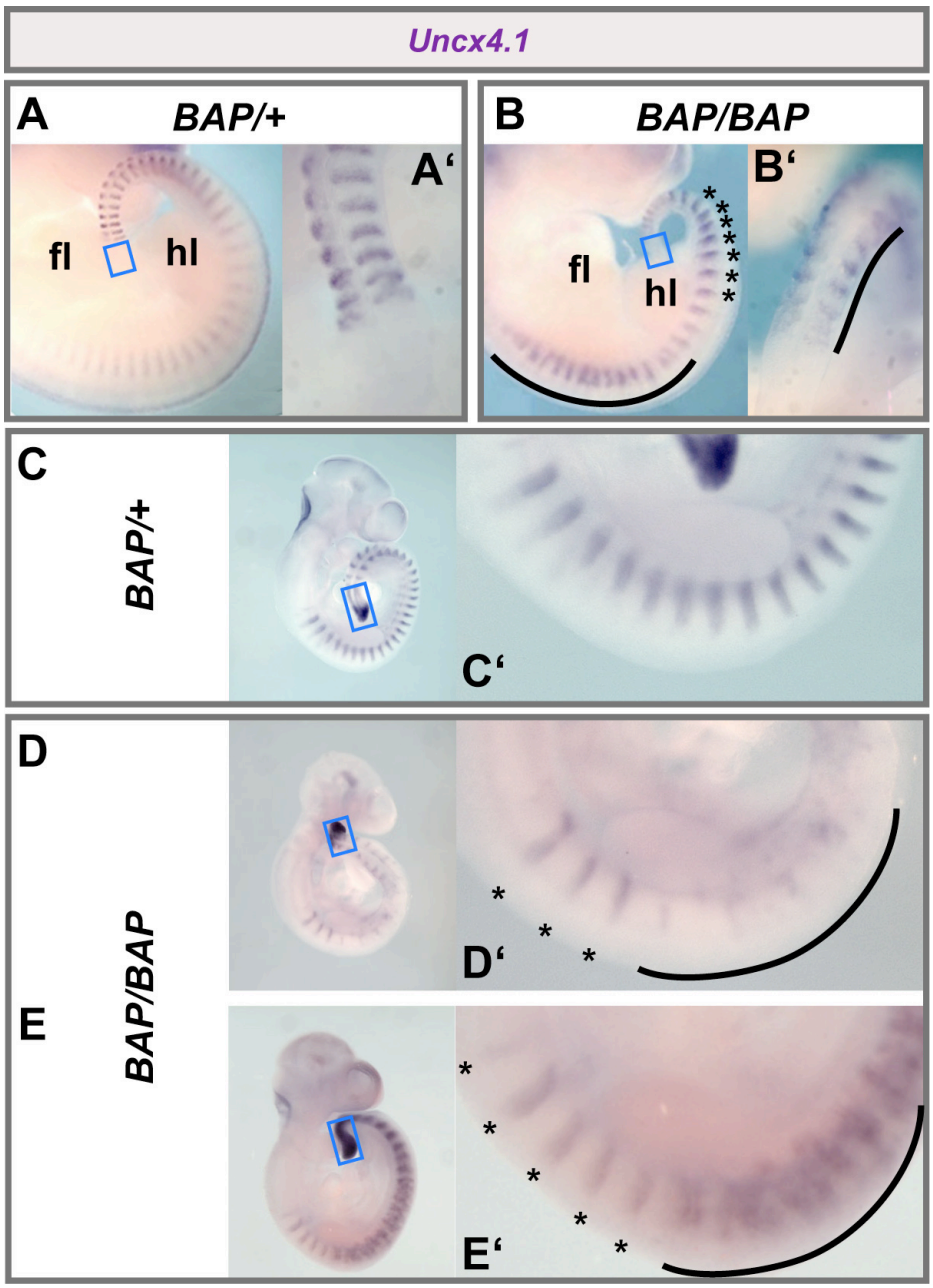

Figure 4.3 *Uncx4.1 in situ* hybridisation detects irregular somite compartmentalisation in *BAP/BAP* E11.5 and E9.5 embryos. (A, B) Lateral views of *BAP/+* (A, n=9) and *BAP/BAP* (B, n=9) E11.5 embryos hybridised with an *Uncx4.1* riboprobe. (A', B') show magnifications of the tail end region (anterior at the top). The black line marks irregular *Uncx4.1* pattern, whereas asterisks indicate regular somites. fl, forelimb bud; hl, hindlimb bud. (C-E) E9.5 *BAP/+* (C, n=5) and *BAP/BAP* (D, E, n=7) embryos hybridised with *Uncx4.1* and *Hes7 in situ* probes (lateral view). (C', D', E') magnified views of the anterior-most *Uncx4.1* stripes. Blue box indicates PSM.

4.2.3 *Hes7* does not need to oscillate when the sacral area is formed

Oscillations of *Hes7*, generated through an auto-regulatory negative feedback loop, were shown to play an important role in the segmentation clock (Bessho et al., 2001b). The mRNA as well as protein levels oscillate in wildtype embryos, which generates a distinct expression pattern (Bessho et al., 2001b; Masamizu et al., 2006).

Hes7 oscillations are best revealed using an intron probe to detect the nascent transcript by *in situ* hybridisation (Hirata et al., 2004; Niwa et al., 2007) (Figure 4.4C). Heterozygous *BAP/+* E10.5 embryos show oscillations in *Hes7* mRNA and nascent transcript levels (Figure 4.4A and C), whereas *BAP/BAP* embryos fail to do so (Figure 4.4B and D). Instead, *Hes7* transcription occurs evenly throughout the presomitic mesoderm (Figure 4.4B, D).

Differences in mRNA levels (dynamic vs. constitutive expression) in E9.5 embryonic tails were quantified using quantitative reverse transcriptase PCR (qRT-PCR; section 7.3.10) and showed and eight-fold increase in $Hes7^{BAP}$ mRNA in *BAP/BAP* embryos compared to wildtype (Figure 4.4E). This recessive overexpression of the $Hes7^{BAP}$ mRNA is a consequence of the suggested failure in the $Hes7^{BAP}$ feedback loop.

Sacral segments form normally in *BAP/BAP* embryos, despite the non-oscillatory *Hes7* expression. On the other hand, formation of anterior cervical, thoracic and lumbar as well as posterior tail somites requires oscillating *Hes7*. This regionalised skeletal phenotype has been described before in mice expressing only the non-oscillatory stripe domain of *Lfng,* a modulator of Notch signalling (Shifley and Cole, 2008; Stauber et al., submitted). The anterior half of the axial skeleton appears to rely on the oscillating *Lfng* domain, whereas the tail region needs mainly the *Lfng* stripe domain. Segmentation in the intermediate sacral region requires neither domain. My findings for the *BAP/BAP* hypomorph mice and the results of the *Lfng* mutants imply that the segmentation machinery changes along the anterior-posterior axis (Figure 4.8).

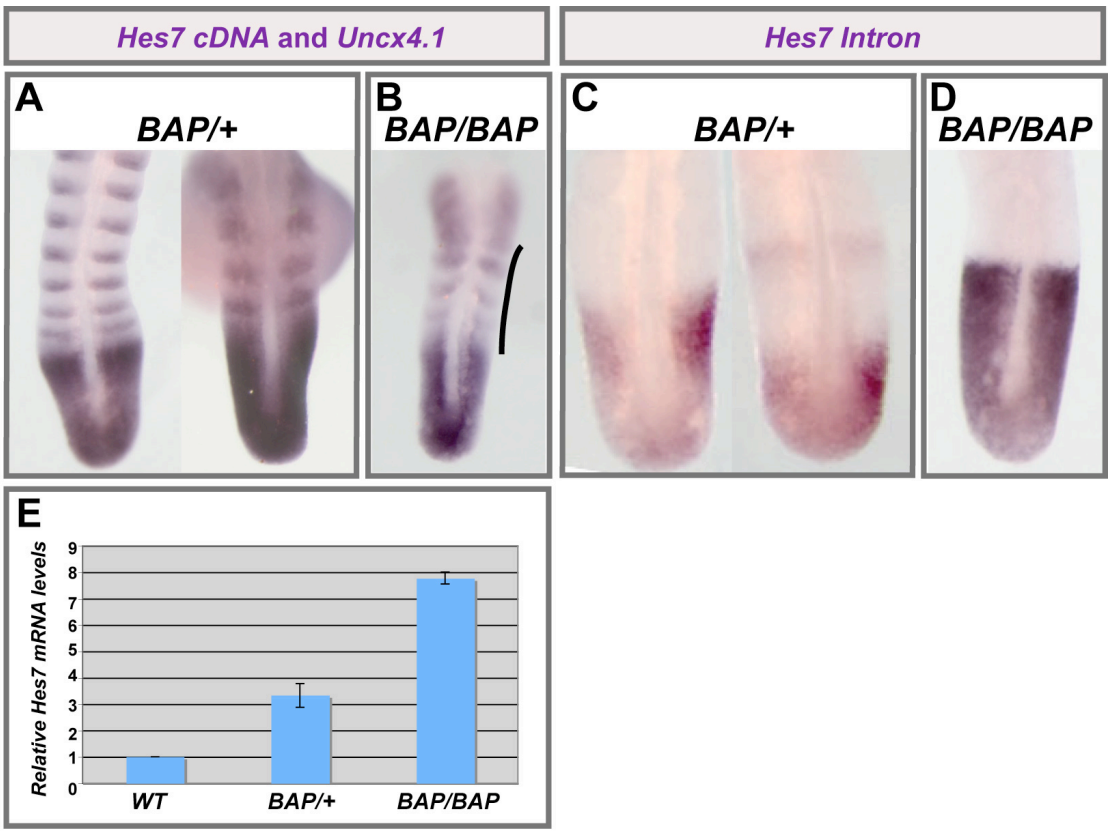

Figure 4.4 Recessive overexpression of *Hes7* mRNA in *BAP/BAP* E10.5 embryos. (A, B) *Hes7* mRNA levels in *BAP/+* (A, n=8) and *BAP/BAP* (B, n=9) embryos as visualised by cDNA *in situ* hybridisation. These embryos are additionally stained with *Uncx4.1*, which marks the posterior somite halves. Black line indicates irregular *Uncx4.1* pattern. (C, D) *Hes7* nascent transcript levels are detected using a *Hes7* intron probe for *in situ* hybridisation of *BAP/+* (C, n=8) and *BAP/BAP* (D, n=9) embryos. Ventral views of E10.5 tail ends. Anterior at the top. (E) Quantification of *Hes7* mRNA levels in wildtype (WT), *BAP/+* and *BAP/BAP* E9.5 embryonic tails using qRT-PCR. Error bars show standard deviation of 3 individual samples.

4.2.4 Altered gene expression of somitogenesis key factors in $Hes7^{BAP/BAP}$ mutants

Hes7 belongs to the bHLH type family of repressors and reduces target gene activity via binding to the target promoter (Bessho et al., 2001a; Kageyama et al., 2007b). A few Hes7 target genes have been described previously: They are mainly effectors of Notch signalling such as *Hes1*, *Lfng* and *Hes7* itself, as well as *Dusp4,* which is a component of the Fgf pathway (Bessho et al., 2003; Niwa et al., 2007).

Arrested *Hes7* oscillations, as seen in *BAP/BAP* embryos (Figure 4.4B, D) point to a non-functional feedback circuitry and further suggest that targets might not be repressed properly. This could lead to a loss of oscillations or an increase in mRNA levels of Hes7 target genes. I therefore examined expression of the known Hes7 targets, *Lfng* and *Dusp4*, by *in situ* hybridisation.

In *BAP/+* E10.5 embryos, the transcript levels for both *Lfng* and *Dusp4* are expressed dynamically (Figure 4.5A and C). *Lfng* is transcribed in a stationary stripe domain in the anterior PSM (adjacent to the boundary that is about to form between somitomeres S-I and S0) and within an additional oscillating domain in the posterior PSM (Cole et al., 2002; Morales et al., 2002) (Figure 4.5A). The Fgf signalling inhibitor *Dusp4* is also cyclically expressed in the PSM of *BAP/+* embryos albeit in a more diffuse pattern (Niwa et al., 2007) (Figure 4.5C).

In the PSM of *BAP/BAP* mutant embryos *Lfng* and *Dusp4* mRNA levels are constitutively up-regulated and staining is seen throughout the PSM (Figure 4.5B and D) These results are consistent with Hes7^{BAP} having a reduced repressor activity, and imply that Notch and Fgf signalling, as seen through *Lfng, Hes7* and *Dusp4* expression, are de-regulated in *BAP/BAP* mutants.

To further confirm a failure in Notch oscillations, I analysed the expression of another Notch target gene, *Nrarp*. *Nrarp* is expressed in a dynamic expression pattern, which resembles *Lfng* transcription, in the PSM of *BAP/+* embryos (Krebs et al., 2001) (Figure 4.5E). However, the oscillating transcription is abolished and *Nrarp* expression significantly reduced in *BAP/BAP* embryos corroborating a failure in Notch signalling (Figure 4.5F).

I also used an antibody to detect the Notch intracellular domain (NICD) in order to check if cyclic Notch activity is abolished in *BAP/BAP* mice. In heterozygous littermates, NICD is seen in two distinct phases in the anterior PSM: a single defined stripe domain and two rather indefinite domains (Figure 4.6A, black lines). However, in *BAP/BAP* embryos, only one phase was seen, reflecting the distinct stripe (compare Figure 4.6A and B). These results show that *Hes7* is at the core of Notch oscillations and that Hes7^{BAP} cannot maintain Notch oscillations, thereby leading to segmentation defects.

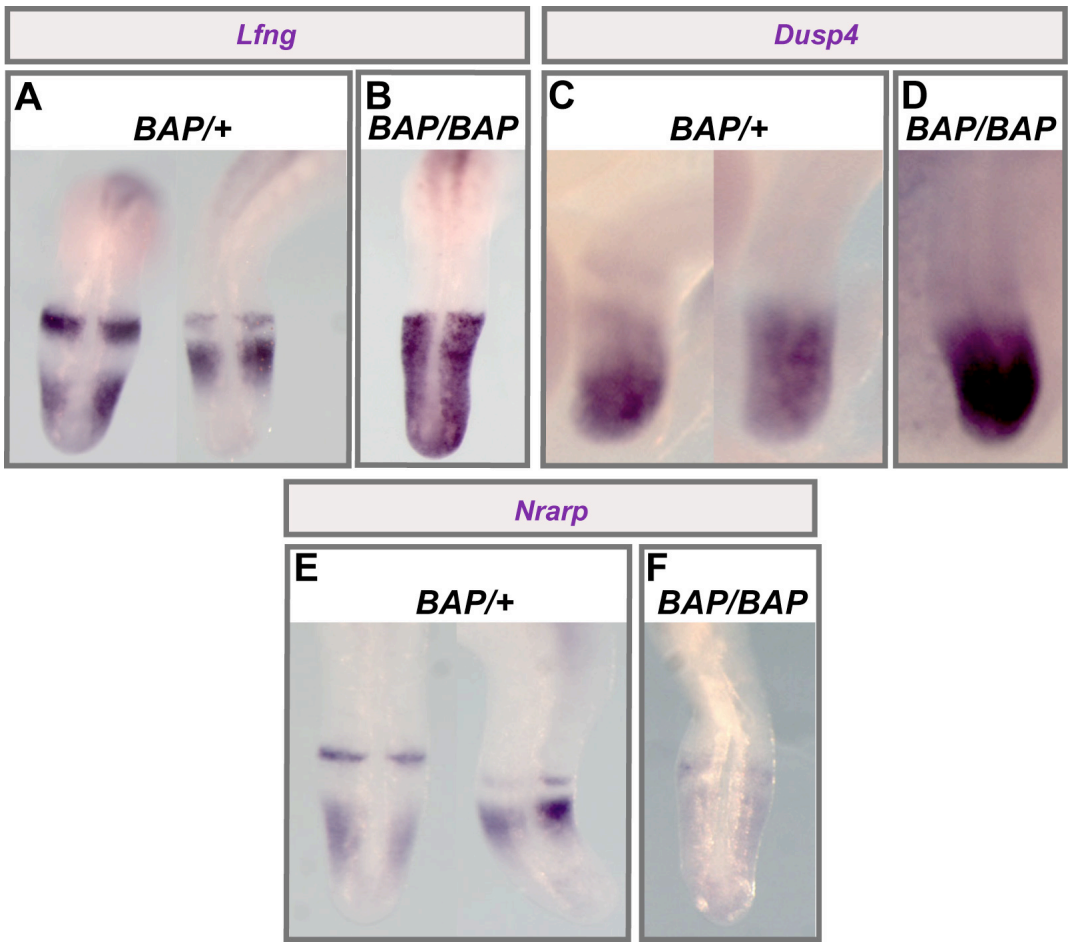

Figure 4.5 Deregulation of Notch and Fgf signalling targets in *BAP/BAP* E10.5 embryos. (A, B) *In situ* hybridisation to detect expression of cycling *Lfng* in *BAP/+* (A, n=11) and constitutive *Lfng* in *BAP/BAP* (B, n=7) E10.5 embryos. (C, D) Oscillating *Dusp4* transcription is seen in *BAP/+* (C, n=19) but not in *BAP/BAP* (D, n=7) E10.5 embryos. (E, F) Visualisation of *Nrarp* expression by *in situ* hybridisation of *BAP/+* (A, n=15) and *BAP/BAP* (B, n=7) E10. 5 embryos. Ventral (A, B, E, F) and lateral (C, D) views of embryonic tails. Anterior at the top.

It is believed that the segmentation clock is a complex interaction network comprising of different signalling pathways, such as the Notch, Wnt and Fgf pathways (Aulehla and Pourquie, 2008; Dequeant et al., 2006; Dequeant and Pourquie, 2008; Ozbudak and Pourquie, 2008). Notch and Fgf signalling targets are deregulated in *BAP/BAP* embryos. Next, I wanted to check if Wnt signalling is affected in *BAP/BAP* mutants and therefore examined *Axin2*, whose expression is dynamic in the PSM but oscillates in the opposite phase of Notch signalling components (Aulehla et al., 2003; Dequeant et al., 2006) (Figure 4.6C). No obvious differences are seen in *Axin2* target gene expression in E10.5 *BAP/BAP* embryos compared to *BAP/+* littermates, indicating that Wnt signalling is, as previously suggested, upstream of Notch signalling in the

segmentation machinery (Aulehla et al., 2003; Aulehla et al., 2008). The former described that both the *Hes7*$^{-/-}$, and the *Hes7*$^{118G/118G}$ mutant, (carrying a stabilised Hes7 protein through a lysine to arginine mutation at position 14), also show unchanged *Axin2* oscillations in the PSM (Hirata et al., 2004). This suggests that *Axin2* and *Hes7* oscillations can occur independently.

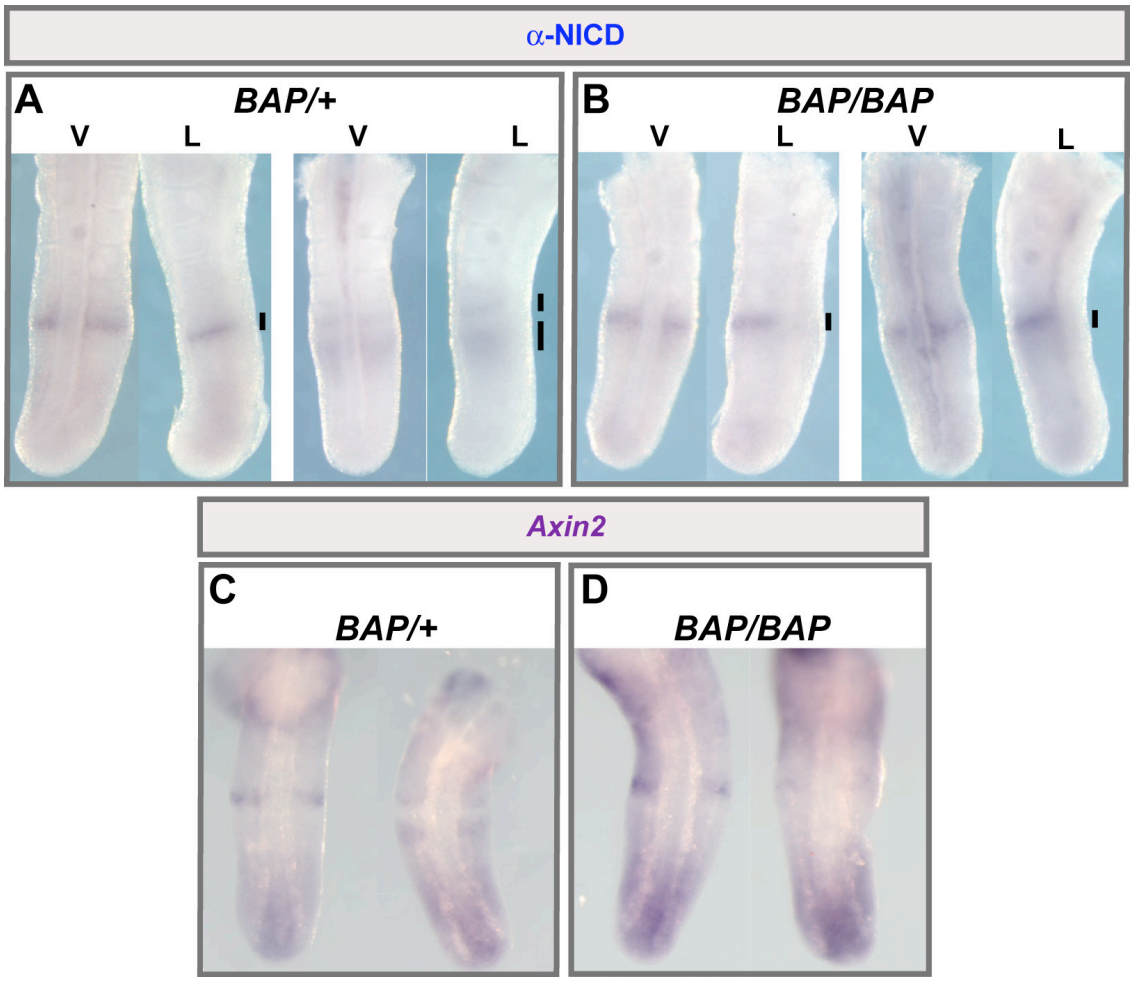

Figure 4.6 Notch signalling, but not Wnt signalling is affected in *BAP/BAP* embryos. (A, B) NICD antibody staining to detect Notch activity in *BAP/+* (E, n=8) and *BAP/BAP* (F, n=7) E10.5 embryos. Black bars indicate individual cyclic regions of Notch activity. v, ventral view; l, lateral view. (E, F) *Axin2* expression, as seen by *in situ* hybridisation of *BAP/+* (E, n=7) and *BAP/BAP* (F, n=11) E10.5 embryos. Ventral views of embryonic tails shown. Anterior at the top.

Arrested oscillations in Fgf and Notch signalling components (Figure 4.5B, D, F and Figure 4.6D) result in de-synchronisation of PSM cells. As a consequence, segmentation is impaired and leads to fused somites and therefore vertebrae and ribs.

I next wanted to examine somite border formation by *in situ* hybridisation with a *Mesp2* probe, which is expressed at the border of the next forming somite (Saga et al., 1997) (Figure 4.7B). *Mesp2* has been shown to be regulated by Notch signalling and to play an important role in the border formation between adjacent somites (Morimoto et al., 2005; Saga, 2007; Takahashi et al., 2000). In wildtype and *BAP/+* embryos, *Mesp2* is expressed in an anterior stripe next to the presumptive somite border (Figure 4.7A). Expression is greatly reduced, scattered and asymmetric in *BAP/BAP* mutant embryos demonstrating a failure in proper separation of the forming somites (Figure 4.7B). This is probably due to reduced cyclic Notch activity, leading to a deregulation of *Mesp2* expression and therefore border formation.

As somites are not compartmentalised correctly in *BAP/BAP* mutant embryos, I investigated if maturation of somites, such as skeletal muscle differentiation, is impaired as well. To address this, I hybridised *BAP/+* and *BAP/BAP* E10.5 embryos with a *MyoD* riboprobe to detect the myotome linage. *BAP/+* embryos show a regular *MyoD* expression pattern reflecting the regular *Uncx4.1* stripes (Figure 4.7C). Ectopic and fuzzy expression of this early myogenic marker is seen in the *BAP/BAP* mutant embryos mirroring the irregular *Uncx4.1* expression pattern (Figure 4.7D). These embryos were too young to visualise *MyoD* expression in the still undifferentiated and presumptive regular somites around somite ~28 onwards. Therefore I cannot conclude that *MyoD* expression would be regular in the sacral somite region. However, my results suggest that somite maturation is affected in *BAP/BAP* embryos due to a loss of somite compartmentalisation.

Altogether, *BAP/BAP* mice are able to survive to some extent but exhibit severe defects, mainly in the axial skeleton. However, muscle differentiation is compromised, and it is likely that the vascular network and the peripheral nervous system are affected since they initiate through inter-segmental regions during development (Figure 4.7D).

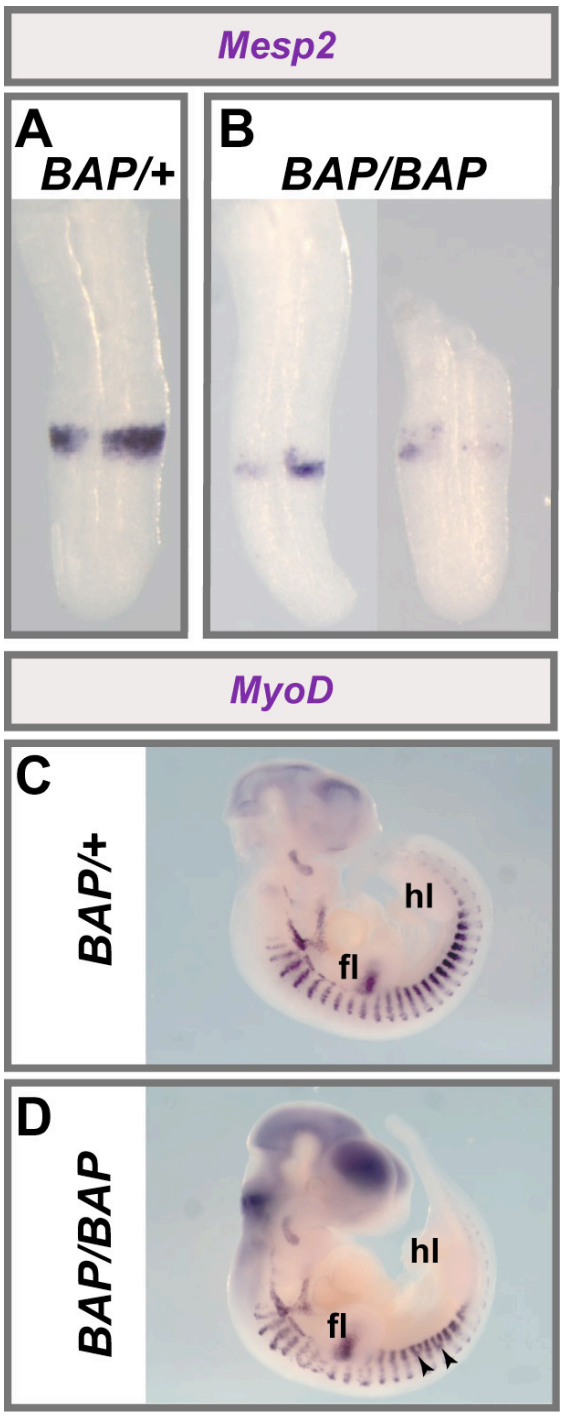

Figure 4.7 Somite segmentation and maturation defects in *BAP/BAP* embryos. (A, B) *Mesp2 in situ* hybridisation of *BAP/+* (A, n=4) and *BAP/BAP* (B, n=8) E10.5 embryos. Ventral views of embryonic tails shown. Anterior at the top. (C, D) Skeletal muscle differentiation as seen through *MyoD in situ* hybridisation in *BAP/+* (C, n=7) and *BAP/BAP* E10.5 embryos (D, n=4). Lateral view. fl, forelimb bud; hl, hind limb bud. Arrowheads point at ectopic initiation of *MyoD* expression.

4.3 Discussion

Here, I describe the phenotype of the *BAP/BAP* mouse strain which exhibits reduced Hes7 function through insertion of the BAP-tag. Although cell-based reporter assays predicted a fully functional repressor upon BAP-tagging this is clearly not the case *in vivo*. The reasons for a failure in the feedback-loop system remain unclear.

Most likely, BAP-tagging has reduced the function of Hes7^{BAP} leading to a failure in the auto-regulatory feedback loop and thus over-expression of the *Hes7* mRNA (Figure 4.4E). However, alternative explanations for the cause of the *BAP/BAP* phenotype include change of transcription timing and protein stability.

One possible explanation for the *BAP/BAP* phenotype might be a more stable *Hes7* mRNA due to longer transcription time. However, *in situ* hybridisation of heterozygous *BAP/+* embryos with a *Hes7* probe does not show an increase in transcript levels and excludes this hypothesis.

Since Hes7 has a short half-life of ~20 minutes, and lengthening the half-life leads to similar defects (Hirata et al., 2004), I hypothesised that Hes7^{BAP} might be more stable due to introduction of the tag. I tried to estimate the half-life of Hes7^{BAP} by transfecting tissue culture cells with the *Hes7^{BAP}* construct and subsequent blockage of translation with cycloheximide. However these experiments were not conclusive due to technical difficulties (data not shown).

The phenotype of *BAP/BAP* mutants suggests that there is a differential requirement for *Hes7* oscillations along the length axis. *Hes7* is required throughout segmentation (Bessho et al., 2001b) but it does not need to oscillate during the formation of the sacrum. My results define at least three phases of segmentation during the 5 days of mouse somitogenesis (Figure 4.8): phase A (somites 1-~30; E7.75-E10) and phase C (somites ~35-65; E10.5-E13.5) require oscillating *Hes7*, whereas the transition phase B (somites ~31-~34) is associated with constitutive *Hes7* activity. However, the region covered by phase B is not strictly limited to the 4 presumptive sacral vertebrae and can be extended anteriorly (1-3 regular lumbar vertebrae) or posteriorly (2-10 regular tail vertebrae) (Table 4.1).

Several other genes have been described, that when mutated or knocked-out, lead to a regional skeletal phenotype. As mentioned in section 4.2.3, *Lfng* mutants lacking the oscillating expression domain have a regularly patterned sacrum and the strength of

the stripe expression determines the tail length (Shifley et al., 2008; Stauber et al., submitted). Hemizygous animals (which have a duplicated stripe-enhancer B-block (Cole et al., 2002; Morales et al., 2002) of the *Lfng* promoter integrated; therefore referred to as *BBL* line) exactly resemble the *BAP/BAP* mutant phenotype (Stauber et al., submitted). However in a homozygous state, animals show a complete rescue of the tail.

Also, in the complete absence of $Lfng^{-/-}$, mice do form a well-patterned sacrum but the tails are short (Evrard et al., 1998; Stauber et al., submitted; Zhang and Gridley, 1998). Moreover, mice harbouring an in-frame insertion of *lacZ* in the *Lef1* gene form a severely disorganised skeleton with a regularly patterned sacral and anterior tail region (Galceran et al., 2004). These examples suggest that the architecture of the segmentation machinery changes along the length axis.

I can only hypothesise about what triggers and positions the different phases. In phase A, mesodermal cells ingress through the primitive streak whereas later (at around 30-somite stage) they are recruited from the tailbud (Wilson and Beddington, 1996). This change in cell movement coincides with the onset of phase B and could lead to a partial loss of synchronisation of PSM cells. At this point, the segmentation machinery might have to be modified to act against any de-synchronisation.

The reason for a regionally disorganised skeletal phenotype could be the differential regulation of mesoderm development along the length axis. *no tail*, *spadetail* and *tbx6* are zebrafish mutants that show a changing hierarchy of these T-box genes in the trunk versus tail (Griffin et al., 1998). A loss of function mutation of *α5-integrin* (Yang et al., 1993) also exhibits regionalised effects on somite formation for unknown reasons.

The *BAP/BAP* phenotype is probably a phenotype of reduced protein function. However, *BAP/BAP* mutants revealed the regional differences in the requirement for oscillating *Hes7*, which could not be seen before in wildtype or $Hes7^{-/-}$ animals (Bessho et al., 2001b). In wildtype embryos, oscillations in *Hes7* are seen from the onset of somitogenesis at ~E8.5 and persist until E12.5. The expression pattern of *Hes7* is characterised through three distinct phases (Bessho et al., 2001a; Bessho et al., 2001b; Kageyama et al., 2007a) and moves like a wave from the anterior to the posterior PSM.

Due to this overall dynamic behaviour it is not possible to detect differences in *Hes7* expression levels between the different phase transitions.

Together my results indicate that *Hes7* activity is required along the whole body axis for proper segmentation, but that *Hes7* oscillation is not essential during the formation of the sacrum and to some degree of adjacent lumbar and tail areas (Figure 4.8).

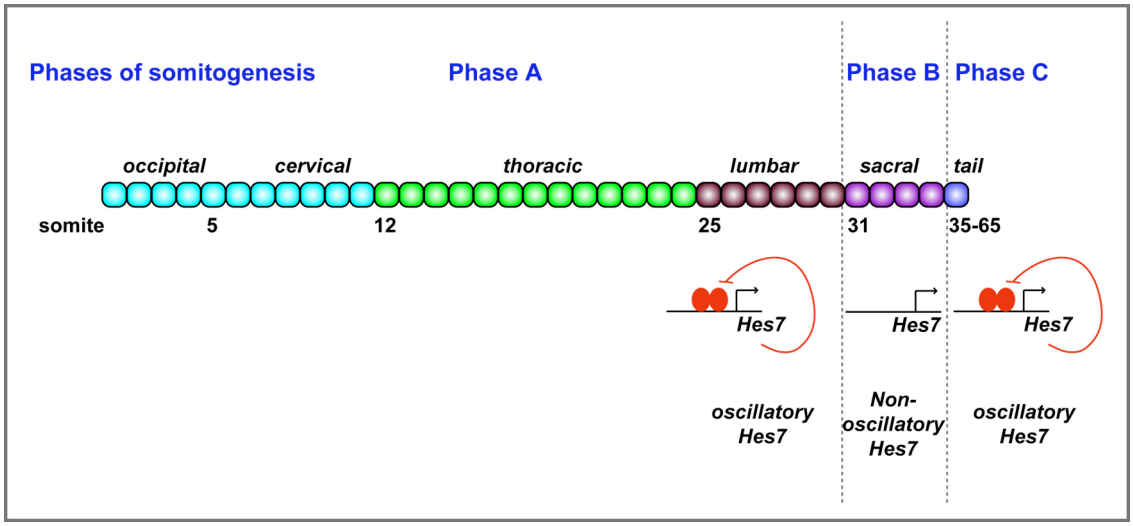

Figure 4.8 Model for differential axial requirements of oscillating *Hes7*. During phase A and C oscillating *Hes7* is required for the formation of somites 1- ~30 and somites 35-65, respectively. Phase B does not require oscillating *Hes7* for the generation of somites 31-35. The three Phases of somitogenesis are separated through a dashed line. Red ovals represent Hes7 protein, whereas red lines show the negative feedback loop. Coloured squares stand for occipital (turquoise), cervical (turquoise), thoracic (green), lumbar (brown), sacral (purple) and tail (blue) somites. Occipital somites will be part of the skull.

CHAPTER 5: Analysis of *Hes7* transcriptional regulation

5.1 Introduction

Mouse *Hes7* is expressed exclusively in the presomitic mesoderm (PSM), the caudal growth zone of the embryo that periodically generates somites (section 1.3). *Hes7* transcription oscillates with the same periodicity as the formation of somites (~2 h in mouse) and has been established as a key player within the segmentation clock (Bessho et al., 2003; Bessho et al., 2001a; Bessho et al., 2001b). Both homozygous disruption of the *Hes7* gene and non-oscillatory overexpression (by Hes7 protein stabilisation) causes aberrant somite formation and patterning, resulting in a severely disorganised and truncated axial skeleton (Bessho et al., 2001b; Hirata et al., 2004). The establishment of an autoinhibitory Hes7 feedback loop sustains oscillating gene expression, and this has been suggested – among other feedback circuits – to be the basic mechanism of the segmentation clock (Bessho et al., 2003).

The intricate regulation of oscillatory *Hes7* transcription, which may be at the core of the segmentation clock, led me to analyse the *Hes7* promoter using comparative studies of the promoter region and protein-DNA binding assays. Although Hes7 is able to bind both N-box and E-box sequences (via its basic domain) in cell-based reporter assays (Bessho et al., 2001a; Chen et al., 2005), it is not clear how the transcriptional feedback mechanism is regulated and what the nature of the target sequence *in vivo* is. In this chapter, I describe DNA binding studies such as Electrophoretic Mobility Shift Assay (EMSA) and DNaseI footprinting in order to unravel the exact binding site of Hes7 in the *Hes7* promoter.

5.2 Results

It was not possible to identify target binding sites of Hes7 by bioChIP from the established transgenic $Hes7^{BAP/BAP};Rosa26^{BirA/BirA}$ mouse line (section 2.2.4.3; chapter 4) due to the fact that $Hes7^{BAP}$ is not biotinylated *in vivo*. Thus, I made use of *in vitro* DNA-protein binding studies to unravel the Hes7 target motif.

5.2.1 Two separate blocks within 4.9 kb of the mouse *Hes7* promoter are conserved in higher mammals

In order to identify functionally important sites in the mouse *Hes7* promoter, which are likely to be evolutionarily conserved, I compared homologous *Hes7* promoters using the PIP Maker programme (Schwartz et al., 2000). *Hes7* promoter regions are fully sequenced in mouse, rat, human, cow, opossum, and zebrafish (*her1;* (Gajewski et al., 2003)), and sequenced with presumably minor gaps in macaque, dog, platypus, and frog.

Comparison of promoter sequences of *Hes7* homologues uncovers extended conservation between mouse and the other higher mammals spreading over 4.9 kb of the mouse *Hes7* promoter (including introns and the 3' flanking region) (Figure 5.1). These conserved upstream regions that are likely to harbour cis-regulatory elements, map to two areas separated by a gap: the proximal block (-3.0 kb – transcriptional start), that directly flanks the transcriptional start in all higher mammals, and the distal conserved block (-4.9 kb – -4.0 kb in mouse), which starts at different positions depending on the species (-4.9 kb in mouse, -4.7 kb in rat, -6.0 kb in macaque, -8.5 kb in cow, -9.1 kb in human) (Figure 5.1, yellow boxes). The expression pattern of *Hes7* is not known for most of the species compared (like dog). However, the similarities in the promoter region might be consistent with an oscillating transcription in higher mammals (most probably with different periodicities, e.g. 4-5 h in human, Sadler et al., 2000).

The conservation between *Hes7* of mouse or human and lower mammals/vertebrates is mainly restricted to exons, exon-intron boundaries and short interspersed nuclear elements (SINE) (Figure 5.1). Comparison of the mouse *Hes7* locus to more distantly related loci or non-homologous cycling genes revealed a lack of conservation within the promoter regions (mouse *Hes5*, chick *hairy1* and *hairy2;* not shown; sequence of chick *hairy1* and *2* promoters, Michael Stauber, unpublished) or a lack of overall similarity and thus of alignment (zebrafish *her1*/*her7*, mouse *Hes1*, mouse *Hey2*, mouse *Lfng*, mouse *Per1*; not shown).

Therefore, the high level of conservation of the *Hes7* promoter within higher mammals and the lack of conservation compared to lower vertebrates does not allow identification of other distinct and, potentially, functionally relevant elements.

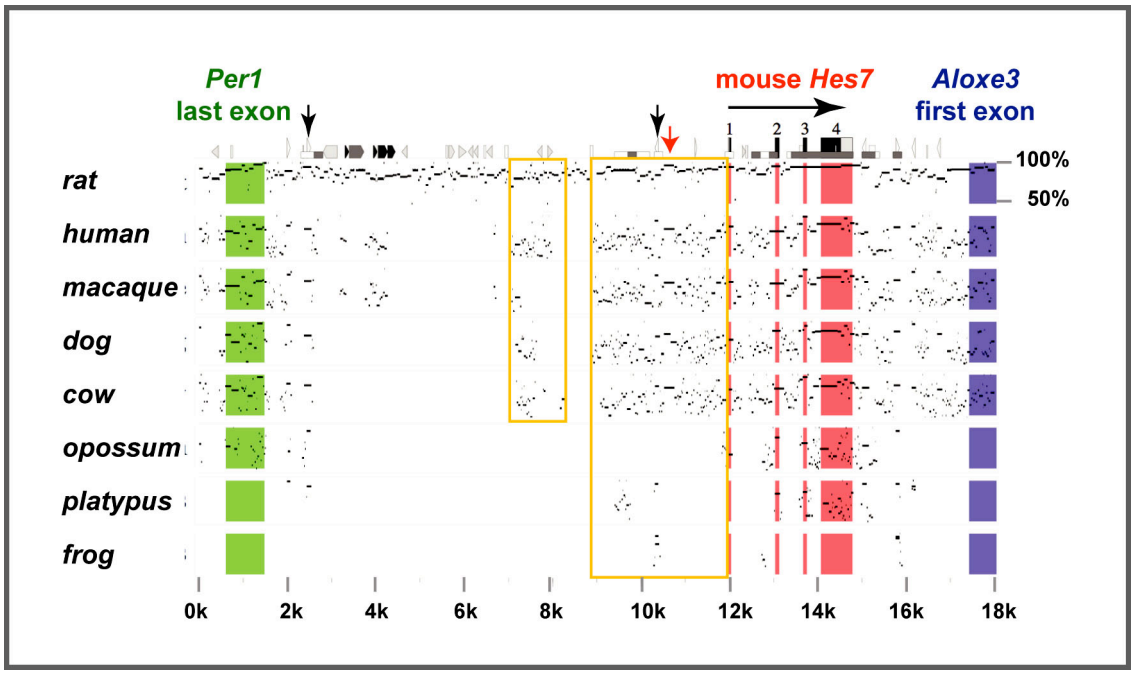

Figure 5.1 Sequence conservation of *Hes7* promoter regions. Percent identity plot of the mouse *Hes7* locus (also including the last *Per1* exon (green) and the first *Aloxe3* exon (blue); *Hes7* exons underlain in red) compared to homologues of higher mammals (rat, human, macaque, dog, cow), lower mammals (opossum, platypus), and the lower vertebrate *Xenopus* (frog). Analysed promoter fragments include 20 kb upstream of the first *Hes7* exon and 4 kb downstream of the last *Hes7* exon. Triangles on upper line indicate SINE positions (two well conserved ones are indicated by black arrows; for meaning of other symbols see pipmaker.bx.psu.edu/pipmaker/pip-instr.html). Red arrow points at a particularly long stretch of conserved genomic DNA. Distal and proximal conserved blocks are boxed in yellow.

5.2.2 Identification of Hes7 binding sites in the *Hes7* promoter

A crucial step in generating *Hes7* oscillations and maintaining the segmentation clock is repression of *Hes7* transcription by Hes7 protein (possibly as a dimer with a paralogous Hes or other bHLH protein (reviewed in Kageyama et al., 2007b). In order to examine Hes7 autoinhibition, I checked the *Hes7* promoter for Hes7 binding sites by EMSA (section 7.6.2).

In a binding assay, I tested 18 partially overlapping ~300 bp fragments covering 4.7 kb of the *Hes7* promoter (Figure 5.2A) with a truncated Hes7 protein that contained the basic helix-loop-helix (bHLH) domain. It was not possible to use the full-length Hes7 protein due to extensive degradation of the protein after glutathione-S-transferase (GST)-tag purification. Therefore, I tried to purify shorter versions of the protein, which still contain the DNA-binding domain. Using GST pull-down assays, I was able to purify a Hes7 protein, which lacks aminoacids 84-226 (hereafter referred to as $Hes7^{bHLH}$; Figure 5.4A; section 7.5.1).

Two fragments (F1, F10; Figure 5.2A) were efficiently shifted in the EMSA experiment when incubated with the $Hes7^{bHLH}$ protein (Figure 5.3A, red boxes). One of them (F1) showed an additional stronger shift of the fragment, indicating more than one occupied binding site (Figure 5.3A, red asterisks). Two more fragments were shifted with medium efficiency (F6, F7; Figure 5.3A). All shifted fragments lie within the 3.0 kb "core promoter" (Figure 5.2A), which was previously shown to be sufficient for generating oscillations (Chetana Sachidanandan, unpublished).

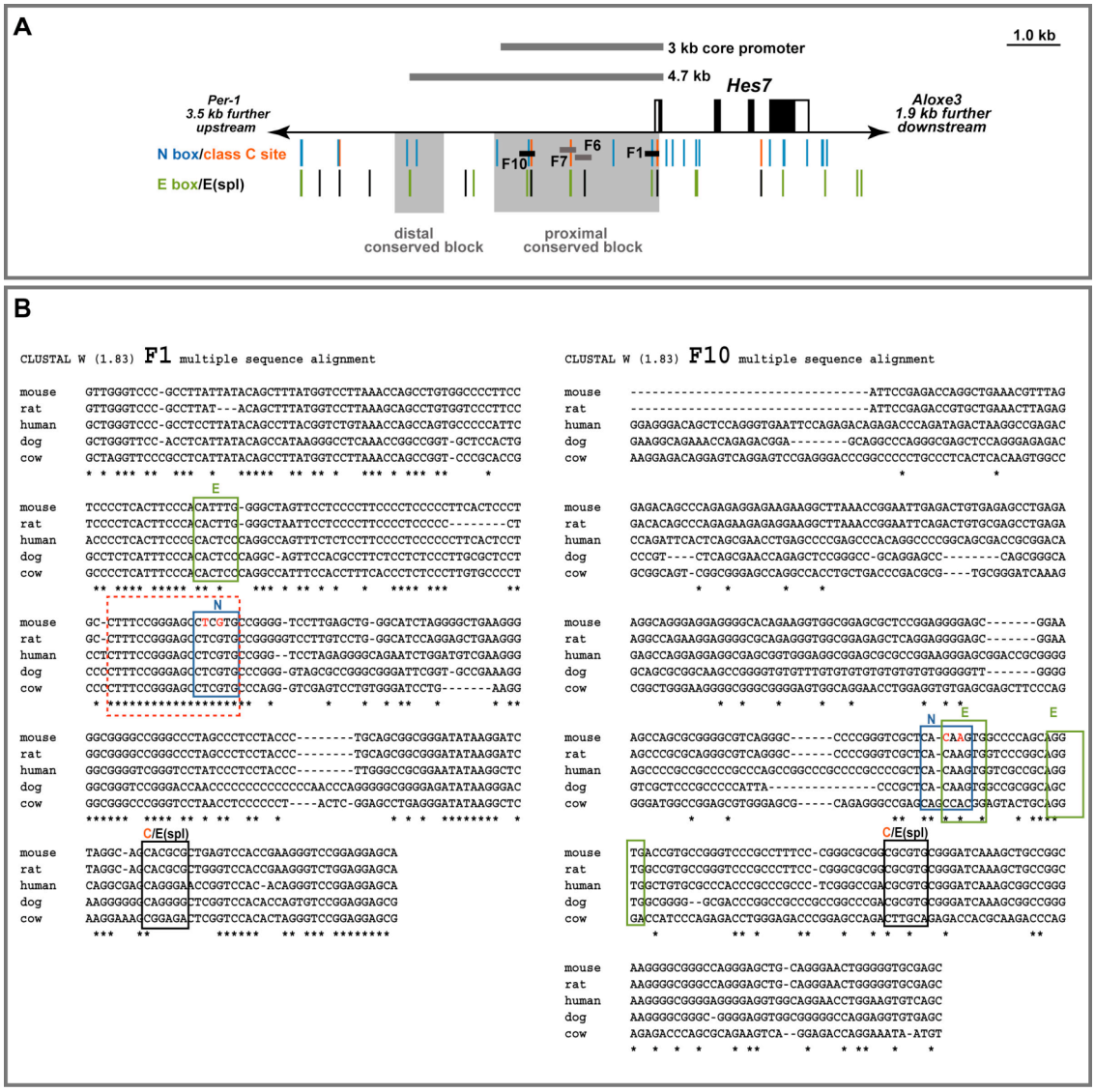

Figure 5.2 Predicted Hes7 repressor binding sites in the *Hes7* promoter. (A) *Hes7* exons are shown as boxes; ORF filled in black. Position of the promoter fragment (4.7 kb) analysed in EMSA is shown as a grey bar above the locus as is the 3 kb core promoter. N-boxes/class C binding sites were predicted according to the consensus sites (see main text); due to degenerate consensus some of these binding sites are identical to sites in the E-boxes/E(spl) row. Positions of fragments F1, F6, F7, and F10 used for Hes7 EMSA are shown in the N-box/class C site line. Distal and proximal conserved blocks are shaded in grey. (B) F1 and F10 sequences aligned to their homologues in higher mammals. Putative Hes7 binding sites (N-box/class C site, E-box/E(spl) are boxed. Position of nucleotide mutations within N-boxes of F1 and F10 for EMSA are shown in red letters. A red box with dashed lines highlights Hes7 footprint in F1. Asterisks label positions with identical bases in all species compared.

Fragments F1 and F10 contain one N-box (CACNAG) each (Figure 5.2A and B). Additionally, F1 and F10 contain class C sites (CACG(C/A)G) and E-boxes (CANNTG) (Figure 5.2A and B). Hes7 has been shown to bind N-boxes and class C sites more strongly than E-boxes *in vitro* (Bessho et al., 2001a; Chen et al., 2005; Kageyama et al., 2007b).

Next, I analysed whether the N-box, contained in each fragment, is the recognised Hes7 binding site. I mutated the N-boxes of F1 and F10 (marked with red letters in Figure 5.2B; F1: CTCGTG to 1. CACGTG or 2. CTCTTG; F10: CACAAG to 1. CATAAG or 2. CACATG). The mutation 1 in the N-box of F1 retains the simple shift, while mutation 2 disrupts the simple shift, yet retaining the additional shift (Figure 5.3B). Thus surprisingly, these close mutations (separated by only 1 bp) appear to disrupt different sets of Hes7 protein bound to its promoter, one generating the simple shift (possibly by binding by of a single Hes7 dimer), the other generating the additional shift (probably by binding of two or more Hes7 dimers).

Neither mutations of F10 (F10: CACAAG to 1. CATAAG or 2. CACATG) affected the bandshift (Figure 5.3B). I conclude that Hes7 is not binding the N-box of F10, but probably to the class C sites or an E-box (Figure 5.3B).

To further dissect the F1 region of the *Hes7* promoter fragment and to analyse the differential shift obtained upon mutating the N-box, I generated a new fragment with both mutations. However, the exchange of both nucleotides within the N-box (resulting in a CACTTG sequence) did not abolish the observed shift. Strikingly, this new fragment containing both mutations, is now shifted to the lower position resembling the shift of the fragment containing only mutation 1 (compare F1-M1 to F1-M1+2 in Figure 5.3B). These data suggest that the mutation of position 1 (CACGTG) disrupts some of Hes7 binding, but does not abolish it completely, and that the 5th nucleotide within the N-box, does not seem to be implicated in the contact of Hes7 to its promoter.

I hypothesised that there might be another binding element within the F1 fragment, which still can bind Hes7 upon mutation of the N-box, producing the observed shift. In order to test this possibility, I performed an EMSA assay with ~30 bp oligonucleotides that span the *Hes7* F1 fragment. Only the oligonucleotide containing the N-box (gggagcCTCGTGccggggtccttgagctgg) showed a shift after incubation with the Hes7 protein (fragment 6; Figure 5.3C). This indicates that Hes7 might only bind the N-box in F1.

Next, I attempted to determine the exact binding sequence of Hes7 using DNaseI footprinting experiments with Hes7 protein on the F1 and F10 fragments (Figure 5.4). In these conditions, I found protection of the sequence ctttccgggagcCTCGTG in F1, which coincides with the conservation around the N-box (Figure 5.2B and Figure 5.4) and might represent the full binding site covered by one Hes7 dimer (or by two Hes7 dimers creating the additional shift in the EMSA). A second 28 bp footprint is found directly 5' to the E-box of F1; this might be a second, unexpected Hes7 binding site (which does not lead to an EMSA shift). In contrast, the DNaseI footprint analysis of F10 did not reveal a Hes7 binding site (Figure 5.4).

It turned out that fragments F6 and F7 (with partial shift in the EMSA; Figure 5.3A) contain at their overlapping site a 95 bp conserved DNA stretch (red arrow, Figure 5.1), which lies within the proximal conserved region, 2 kb upstream in the *Hes7* promoter. Since the EMSA shifted both fragments with medium efficiency it is probable that an additional Hes7 binding site is positioned at the overlap of F6 and F7 within the conserved DNA region.

Together, these results indicate that Hes7 binds at least to one site within the 3.0 kb *Hes7* core promoter. This site includes the previously suggested N-box, but seems to extend beyond the hexamer nucleotide sequence. Therefore, this region most likely plays an important role in the autoinhibition of *Hes7* transcription.

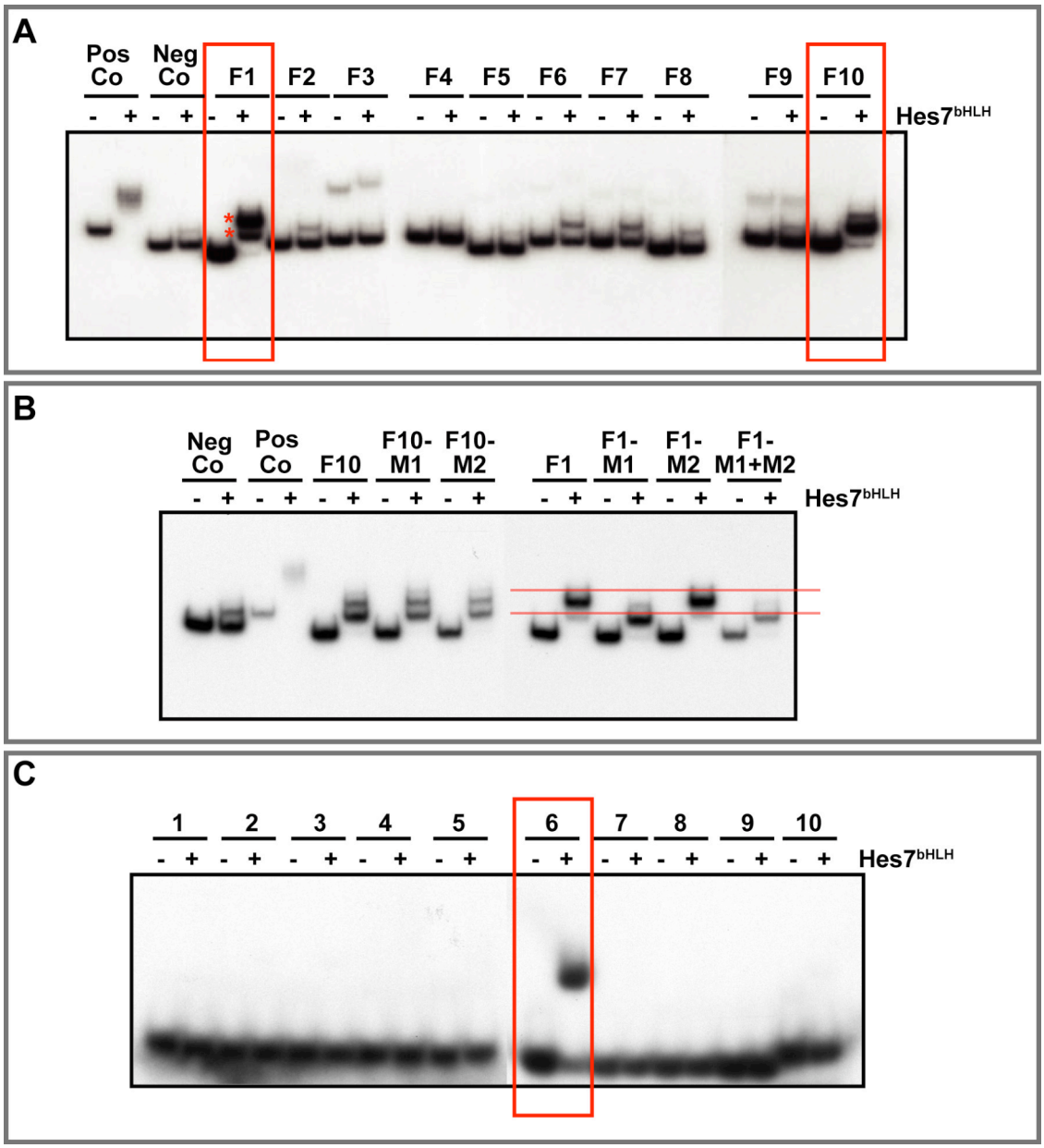

Figure 5.3 Identification of Hes7 binding sites in the *Hes7* promoter by EMSA. (A) Incubation of *Hes7* fragments F1-F10 with (+) or without (-) Hes7^{bHLH} protein. The two fragments with the strongest shifts, F1 and F10, are framed in red. For positions of F1, F6, F7, and F10 within the *Hes7* locus see Figure 5.2A. (B) EMSA of mutated F1 and F10 with Hes7^{bHLH} protein. Controls are the same as above. The differential shift is indicated with red lines. (D) EMSA of *Hes7* F1 30 bp oligonucleotides (Table 7.23) with Hes7^{bHLH} protein. A six N-box repeat and arbitrarily selected vector DNA served as positive (Pos Co) and negative (Neg Co), respectively. Shifted fragment is boxed in red.

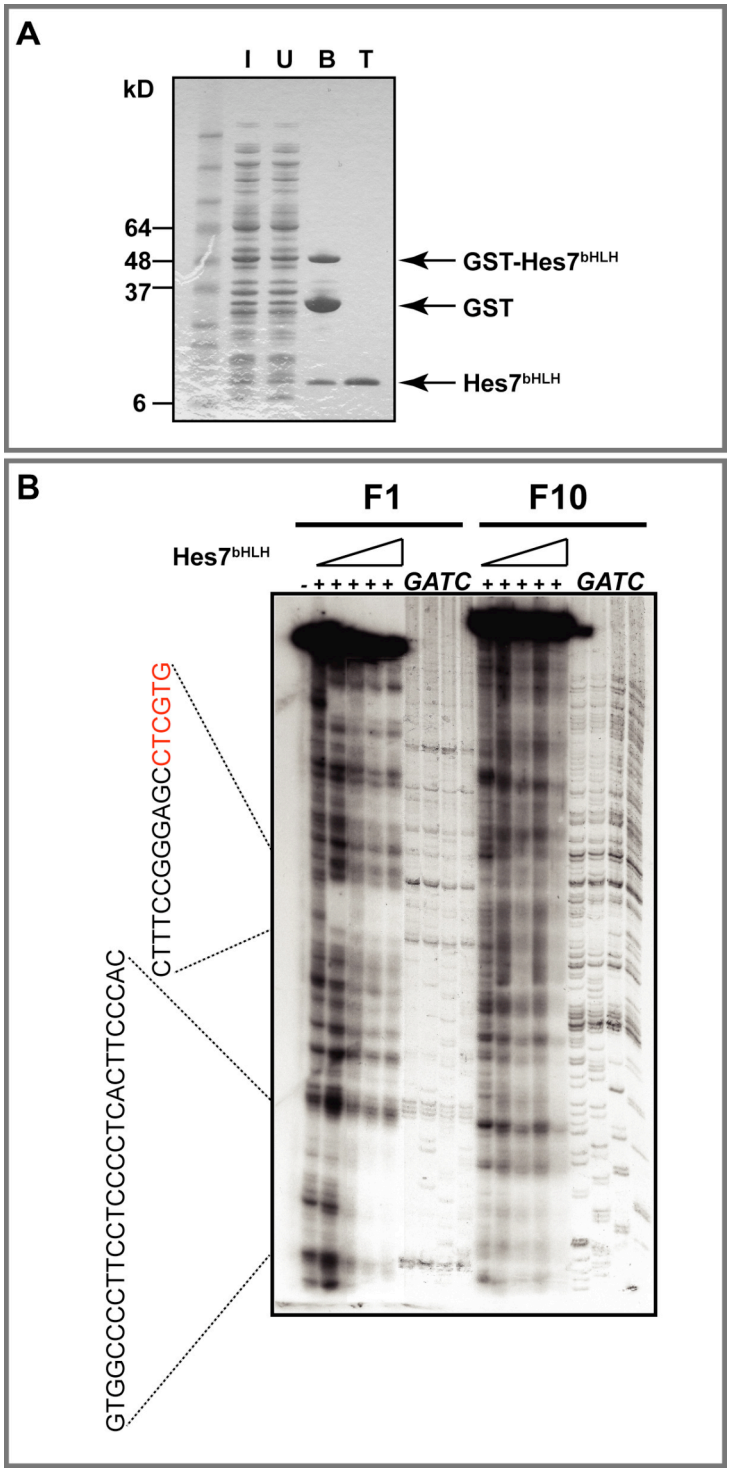

Figure 5.4 DNaseI footprinting analysis reveals two Hes7 binding sites on the *Hes7* promoter fragment F1. (A) GST-purification of Hes7^{bHLH} protein. Input (I), unbound (U), bound (B) and thrombin cleaved (T) protein fractions were loaded onto a 4-12% Bis-Tris gel. (B) Incubation of fragments F1 and F10 with increasing amounts (0/30/60/100/300 ng) of Hes7^{bHLH} protein in the absence (-) and presence (+) of DNaseI. Sequencing reactions of F1 and F10 (GATC) are aligned next to the footprinting experiments. Protected sequences are indicated on the left hand side. N-box sequence is marked in red letters.

5.3 Discussion

The *Hes7* promoter is peculiar in that its activity is limited to driving oscillating transcription in the PSM. It has been suggested that cyclic expression is due to the ability of Hes7 to bind and repress its own promoter (Bessho et al., 2003), thereby maintaining a negative feedback loop. The exact binding site sequence, as well as the regulation of the feedback inhibition, remains elusive.

In order to unravel the mechanics of *Hes7* oscillations, I have analysed the *Hes7* promoter first using computational tools. Comparison of homologous *Lfng* promoters of vertebrates has previously revealed three conserved regions in this promoter one of which drives its cyclic expression (Block A (Morales et al., 2002) or FCE1 (Cole et al., 2002)). The same strategy did not reveal distinct conserved elements of the *Hes7* promoter likely to mediate cyclic transcription due to a high conservation between higher mammals and a lack of conservation between lower vertebrates. Unlike *Lfng*, *Hes7* transcription does not exhibit an anterior PSM expression domain (Bessho et al., 2001a) suggesting a less complex array of *cis*-acting elements. The failure to identify distinct *cis*-regulatory features driving a dynamic *Hes7* feedback loop implies a more intricate regulation of *Hes7* oscillations.

Although we know that a 3 kb region of the *Hes7* promoter is sufficient to drive its oscillatory expression, and that a number of binding sequences (mediated by bHLH proteins) have been identified within this region, it is still not clear how Hes7 protein exerts the repressive action on its own promoter.

EMSA and DNaseI footprinting assays led me to identify a N-box element (-132 bp to -137bp) and surrounding nucleotides as a putative Hes7 binding site. In addition I uncovered a putative binding site ~2.4 kb upstream of the Hes7 transcription start site, however, I could not demonstrate an interaction with Hes7 protein by mutating the site or by DNaseI footprinting. This might be explained by the fact that such *in vitro* studies are highly susceptible to saturation with the protein. Increasing amounts of protein could lead to shifts of unspecific fragments and one has to be careful in setting the conditions. This possibility appears unlikely since careful titration experiments were performed to set the correct amount of protein to be used in these experiments. In order

to minimise unspecific effects, competition studies with unlabeled "cold" fragments or oligonucleotides could be performed.

Mutation of bases 3 and 5 of the core N-box sequence in F10 did not lead to an abolishment of the observed shift of fragment F10. This might be due to the fact, that this mutation did not hit important nucleotides responsible for this interaction. However, DNaseI footprinting did not reveal a Hes7 binding site within F10, suggesting that there might not be one.

Using EMSA and DNaseI footprinting tools, I confirmed that the N-box is a likely binding site for Hes7 on its own promoter. In addition, mutation of the N-box in F1 resulted in an unexpected outcome: a differential occupation of the N-box binding site was evident in the EMSA assays (Figure 5.3). In contrast to previous studies, which have used sets of oligonucelotides including N- or E-box binding motifs (Chen et al., 2005), I have analysed fragments for Hes7 binding covering 4.7 kb of the *Hes7* promoter.

Mutation of the N-box core sequence in F1 did not abolish the shift, but rather uncovered two different binding conformations. I suggest that Hes7 is able to multimerise *in vitro* and further occupies the N-box and surrounding sequences. This becomes clear through mutation 1 of the N-box in F1, which abolishes the supershift to the second position. Nevertheless, mutating both bases of the N-box in F1 still allows binding of Hes7 to the fragment. Either the chosen nucleotides are not responsible for establishing contact with Hes7, or that nucleotides around the N-box are more important for the binding.

Altogether, these experiments confirm previous studies indicating that the N-box is a putative Hes7 target sequence (Bessho et al., 2001a; Chen et al., 2005; Kageyama et al., 2007b). Furthermore, my results are consistent with previous observations showing that the murine bHLH proteins Hes1 (Ishibashi et al., 1993) and Hes5 (Akazawa et al., 1992; Sasai et al., 1992) are also able to bind to N-box sequences in DNaseI footprinting assays. In contrast, studies from *Drosophila* have identified the E-box as the target for E(spl) bHLH proteins *in vitro* and *in vivo*. In particular the nucleotides surrounding the core E-box have been demonstrated to be essential for establishing contact with the DNA sequence (Jennings et al., 1999). These findings are similar to my results demonstrating that nucleotides flanking the core N-box sequence are recognised in Hes7 binding and might have an important function.

It is not clear yet which nucleotides are recognised by Hes7 *in vivo*, and how the repressive feedback loop is maintained. Moreover, we do not have any evidence whether Hes7 acts as a homo- or heterodimer *in vivo*. The *in vitro* binding experiments performed here most likely lead to a multimerisation of the protein, but it is not possible to conclude if this is the case *in vivo*. Further studies are needed to investigate the nature of the target sequence *in vivo* and to unravel the autoregulatory feedback mechanism. Future experiments include tissue culture studies in order to test fragments F1 and F10 as well as mutated versions thereof in reporter assays for Hes7 binding. Once *ex vivo* studies have confirmed specific Hes7 binding sites, transgenic mice could be established harbouring mutations within the *Hes7* promoter to test the *in vivo* significance of the respective Hes7 binding sites.

CHAPTER 6: Concluding remarks

The Notch signalling pathway is a multifaceted cell communication pathway and has been demonstrated to be implicated in many different biological processes as diverse as generating the segmented vertebrate body pattern to causing oncogenic transformations (reviewed in Bray, 2006; section 1.2). It has been challenging to pin down common sets of Notch target genes within different cell or tissue systems and there is evidence that one target might not be a target in another context. Notch exerts multiple pleiotropic effects on cell proliferation, differentiation and survival but little is known about different targets of Notch isoforms.

It is important to unravel the nature of Notch targets not only to understand the Notch communication network but also to uncover novel targets during oncogenesis that can serve as putative therapeutic targets. Thus certain genes might be downstream Notch targets only in transformed tissues.

In this thesis, I describe a novel approach using the high affinity of the biotin-avidin system in chromatin immunoprecipitation (bioChIP) assays to identify novel targets of Notch1 signalling *in vivo* by means of two different strategies. The first strategy aimed at discovering specific DNA sequences, which are recognised by the Notch transactivation complex consisting of the Notch intracellular domain (NICD) and its nuclear effector CSL. This direct strategy should have allowed identification of Notch gene targets in any biological context in which Notch signalling is active. Futhermore, it would have been feasible to induce Notch-dependant tumours in the mouse and to search for novel targets after oncogenic transformation.

In contrast, the second approach made use of a previously characterised Notch target gene, *Hes7*, and aimed at identifying Notch targets in an indirect manner. This second system was limited to unravel the implications of the Notch pathway only within one model system: the vertebrate segmentation machinery.

6.1 Direct Notch signalling targets

In chapter 3 I describe several applications of the BAP/biotin-avidin system in cultured cells and from tissues of the established transgenic mice expressing biotinylated Notch1. Although, Notch1^{BAP} is biotinylated, I was not able to purify novel targets or protein interaction partners using streptavidin.

I was able to show that in principle the BAP/biotin-avidin system works in cultured cells by using a previously established cell line expressing the inducible biotinylated GATA-1^{BAP} transcription factor (section 3.2.1). However, several disadvantages of the approach to identify Notch1 signalling targets became apparent during my experiments: First, the high background binding resulting from biotinylated and non-biotinylated proteins has been a major drawback of the bioChIP experiments as well as for the streptavidin protein pull-down assays. Although the biotin-avidin interaction is able to withstand very stringent washing conditions I was not able to reduce the background. This is also an important fact when purifying dynamic and low-level proteins and targets thereof because the background binding does not allow detection of the protein of interest due to an unproportional ratio of background to bait protein.

Second, it can take a very long time to make knock-in mice which carry a biotinylated protein: In my case it took 2½ years to generate a targeting construct, screen for homologous recombinant embryonic stem cells and to establish the double homozygous mouse lines after multiple breeding steps. In contrast, the generation of an antibody for ChIP experiments can take 6-8 months for a monoclonal, less for a polyclonal antibody. Screening for a good antibody for a particular application additionally lasts several months and there is no guarantee that an antibody will work for ChIP if it can be successfully used for other applications e.g. western blot analysis. Usually, several different antibodies are tested for the use in ChIP experiments. In most cases, the affinity of an antibody for its epitope is sufficient for ChIP experiments.

Third, the indirect binding of NICD to its targets, the low physiological levels of NICD as well as the dynamic behaviour of the Notch transactivation complex made it difficult to optimise experimental conditions.

Possible alternative strategies to identify novel Notch target genes *in vivo* include ChIP analysis directed against CSL, which directly interacts with Notch target sites.

Additionally, a timed activation of the Notch signalling pathway potentiates the identification of direct Notch targets because CSL occupancy on target promoters is enhanced when NICD is available (Fryer et al., 2004; Krejci and Bray, 2007). In order to allow a specific activation of Notch and thus formation of the nuclear transactivation complex, one can make use of inducible systems like hormone receptor approach or a chemical-induced strategy (like EDTA, which worked in cultured *Drosophila* cells by calcium depletion induced Notch cleavage (Krejci and Bray, 2007; Rand et al., 2000)). Since it is not possible to establish a transgenic mouse line in the complete absence of Notch1, a tissue-specific Notch1 line could be generated where Notch1 is under the control of a tetracycline-inducible promoter. Thus upon addition of tetracycline, expression of Notch is induced in the specific tissue context and allows regulated Notch activation.

Similar experiments, using temporal Notch activation and ChIP-chip analysis, have already been conducted in *Drosophila* tissue culture cells and led to the identification of novel Notch targets, which were verified *in vivo* (Krejci et al., 2009). A comparable system needs to be established *in vivo*, in the mouse, to allow for a more regulated system, to detect target genes after an activation period. With the help of massive parallel sequencing of pulled-down chromatin (from ChIP with a CSL antibody), novel Notch target genes could be identified.

This approach, directed to find targets of CSL by ChIP, however, leads to uncover targets only of the CSL-dependent Notch signalling cascade. In contrast to previously suggested hypotheses, there might be CSL-dependent targets, which do not show increased levels of CSL binding after Notch activation. There is growing evidence that Notch can also signal through a CSL-independent manner in a non-canonical pathway. This view was supported for the first time by experiments from *Drosophila* which showed that a *Notch* knock-out exhibits a more severe phenotype than a *Su(H)* (CSL of *Drosophila*) knock-out fly (Rusconi and Corbin, 1998; Rusconi and Corbin, 1999; Zecchini et al., 1999) suggesting that Notch might be regulated independently of CSL (reviewed in Martinez Arias et al., 2002). In vertebrates, the evidence for a non-canonical Notch signalling is still unclear and so far has mostly been demonstrated in cultured cells (reviewed in Martinez Arias et al., 2002). Conversely, CSL can be activated in a Notch-independent manner in the socket cells of the mechanosensory

organ of *Drosophila* (Barolo et al., 2000) and thus would also show a bias in the identified target gene pool.

Another alternative strategy to find novel Notch targets could be the tagging of Notch with a different tag e.g. FLAG, HA or the TAP-tag and to use antibodies against the tag in ChIP experiments. However, it is unclear if this approach would work because the Notch transactivation complex most likely turns out to be unstable. Alternatively, antibodies against Notch itself could be raised and tested for their application in ChIP experiments. The ChIP approach combined with large scale sequencing still seems to be the best and directed approach to find novel nuclear Notch targets. Therefore the ChIP technique must be improved in order to detect NICD at physiological levels.

6.2 Indirect Notch signalling targets during vertebrate somitogenesis

The second approach to identify targets of Notch signalling in an indirect fashion via Hes7 signalling during vertebrate segmentation did not lead to novel nuclear targets either. Although Hes7^{BAP} was functional in *ex vivo* experiments, BAP-tagging resulted in a strongly hypomorphic allele *in vivo*. Moreover, biotinylation of Hes7^{BAP} could not be detected *in vivo* even though cell culture experiments showed successful biotinylation.

Several studies on identifying *Hes7* targets in the mouse presomitic mesoderm (PSM) have been conducted before this study: ChIP experiments using an antibody against Hes7 were performed and confirmed a predicted interaction (based on computational motif analysis) of Hes7 with the *Lfng*, *Hes1* and *Hes7* promoters (Bessho et al., 2003). Another approach used microarray analysis to compare *Hes7*$^{-/-}$ with *Hes7* transgenic mice (expressing *Hes7* persistently in the PSM) and found among others (15 genes >2.0-fold expression in *Hes7*$^{-/-}$ than *Hes7* transgenic mice) *Dusp4*, a negative regulator of Fgf signalling (Niwa et al., 2007). Althought the latter approach confirmed *Dusp4* as a direct Hes7 target gene, this strategy most likely can lead to false positives i.e. artefacts resulting from the overexpression.

To my mind, ChIP experiments combined with high-throughput sequencing, is the only way to identify real Hes7 targets in the PSM of mouse embryos. In order to achieve this goal either an alternative tagging approach needs to be carried out or a

high-quality antibody directed against Hes7 raised. The first option will be challenging in order to find and place a tag which does not disrupt Hes7 protein stability and integrity. The BAP-tag, although very small, appears not to provide a satisfactory solution due to the high-background binding during purification. Another challenge when purifying Hes7 is the fact that it is a dynamic protein with a fast turn-over rate and very low abundance in the PSM. Different ChIP conditions will need to be tested e.g. different antibodies (directed against Hes7 or the tag), amount of PSM material and washing conditions.

A ChIP-seq strategy would also allow to unravel the exact binding site of Hes7 in its target promoters. Previous studies including the one in this thesis (chapter 5) have used *in vitro* (Chen et al., 2005) (Figure 5.3 and Figure 5.4) and *ex vivo* (Bessho et al., 2001a) (Figure 2.2A) studies and showed binding of Hes7 to the N-box and E-box sequences with a stronger preference for the N-box. However, we are still far from understanding the Hes7 autoinhibitory feedback loop and further studies are needed to confirm that the N-box is indeed the recognised target site within the *Hes7* promoter *in vivo*.

6.2.1 Differential transcription of *Hes7*

The hypomorph $Hes7^{BAP}$ allele, however, led to the discovery of a differential regulation of *Hes7* transcription. Homozygous $Hes7^{BAP/BAP}$ embryos and adults show a disorganised skeletal phenotype albeit not as severe as in $Hes7^{-/-}$ mice with a rescue around the sacral and adjacent tail region (Figure 4.1). I have proposed a model for this differential transcription of *Hes7* whereby *Hes7* does not need to oscillate when the sacrum is formed but does show cyclic transcription during the establishment of the anterior cervical, thoracic and lumbar as well as posterior tail somites (Figure 4.8). My results are consistet with previous studies in transgenic mice lacking the cyclic expression domain of *Lfng* and have suggested that the architecture of the segmentation machinery changes during the establishment of the vertebrae precursors (Shifley et al., 2008; Stauber et al., submitted).

6.3 Final conclusion

Altogether, this thesis was aiming to contribute to the understanding of the target gene network that is regulated by Notch signalling *in vivo*. However, it turned out that the strategy chosen is not applicable for highly dynamic and low abundance proteins (such as Notch1 and Hes7) and that further information on the formation and dynamics of the Notch transactivation complex is needed in order to establish a suitable system.

The actual question of how cell diversity arises by the action of different cell communication networks still remains to be answered. Identifying Notch targets will only be a piece of the jigsaw puzzle. Target gene activation is not only limited to one single transcription factor but involves multiple transcription factors interacting with *cis*-regulatory sequences within the enhancer region. This suggests that there is a need for a complex transcription factor network, which determines the regulation of a certain gene and thus the cellular outcome.

CHAPTER 7: Materials and Methods

7.1 Molecular Biology

7.1.1 Polymerase Chain Reaction (PCR)

PCR reactions (Saiki et al., 1988) were carried out in 200 µl thin-walled 8 tube and flat cap strips (Thermo Scientific) or Thermo Fast 96 well plates (Thermo Scientific) using a Peltier (PTC-200, DNA Engine) thermal cycler. For cloning of expression constructs either *PfuTurbo* (Stratagene) or *TaKaRa LA Taq* (TaKaRa) polymerase was used. Genotyping PCR reactions were carried out with the *Taq* PCR Master Mix system (Qiagen). Reactions were performed in 50 µl with 10 µM of each primer (synthesised by Sigma-Aldrich), 20 mM dNTPs (deoxyribonucleotide triphosphates, Pharmacia Biotech), 2-10 ng of template DNA in 1 x polymerase buffer. The thermal cycling conditions were based on the basic settings listed in Table 7.1. The annealing temperature was adjusted to the melting temperatures of oligonucleotide primers and the extension time adjusted to the length of the product. PCR products were confirmed by electrophoresis in a 1% agarose gel (Ultra Pure, Invitrogen) with TAE (Tris-acetate, EDTA) running buffer.

	94ºC	3 minutes
	94ºC	30 seconds
40 cycles of	60ºC	30 seconds
	72ºC	1 minute/kb
	72ºC	10 minutes
	12ºC	forever

Table 7.1 Standard PCR thermal cycling conditions.

7.1.2 Ligation

Site-directed ligation was performed as previously described by Sambrook et al., 2001. Briefly, vector and insert DNA were digested from constructs using two different restriction enzymes (New England Biolabs) and their supplied buffers for at least 2 hours at 37ºC. Vector DNA was dephosphorylated with calf intestinal alkaline phosphatase (New England Biolabs) at 37ºC for 30 minutes. Both DNA fragments were purified through agarose gel electrophoresis and extracted from the gel matrix with the help of the QIAquick Gel Extraction Kit (Qiagen). Elution was into 50 µl of ultra pure water and ligations were done with T4 DNA Ligase (New England Biolabs) using a molar ratio of vector DNA to insert DNA of 1:3 in 20 µl. The reaction was incubated at 16ºC overnight and 2 µl used for subsequent transformation into chemically competent bacteria (section 7.1.7).

7.1.3 Cloning of BAP-tagged constructs for expression in cell culture

The cloning of the mouse *Hes7*^{BAP} constructs was done in three steps: The first step involved the PCR-amplification of two parts: *Hes7*$^{N\text{-}BAP\ upper}$ and *Hes7*$^{N\text{-}BAP\ lower}$ for the N-terminal fusion and *Hes7*$^{C\text{-}BAP\ upper}$ and *Hes7*$^{C\text{-}BAP\ lower}$ generating the C-terminal fusion, each harbouring a portion of the BAP-tag. An *Eco*RV restriction site was generated through introduction of a silent mutation so as to split the BAP sequence in two parts, which could then be easily reunited with blunt end ligation. Using this strategy greatly facilitated the introduction of the BAP-tag. Fusion of both sequences, *Hes7*$^{N\text{-}BAP\ upper}$ and *Hes7*$^{N\text{-}BAP\ lower}$ as well as *Hes7*$^{C\text{-}BAP\ upper}$ and *Hes7*$^{C\text{-}BAP\ lower}$ resulted in a correctly tagged *Hes7*$^{N\text{-}BAP}$ or *Hes7*$^{C\text{-}BAP}$, respectively. The primers were synthesised (Sigma-Aldrich) to include the BAP sequence and as template for the PCR reaction served the *pCI-Hes7* vector containing 790 bp of *Hes7* cDNA (Table 7.2, *Eco*RV sites in bold). The upper and lower parts were each subcloned into the *pCRII-TOPO* vector using the TOPO cloning strategy (Invitrogen) for sequencing with *M13 forward* and *M13 reverse* primers (Table 7.6). After verification of the DNA sequence the lower fragment was digested with *EcoR*V and *Xba*I for *Hes7*$^{C\text{-}BAP}$ or *EcoR*V for *Hes7*$^{N\text{-}BAP}$ from the *pCRII-TOPO* vector backbone, purified through agarose gel electrophoresis and ligated into *EcoR*V/*Xba*I or *EcoR*V digested *pCRII-TOPO-Hes7*$^{C\text{-}BAP\ upper}$ or *pCRII-TOPO-Hes7*$^{N\text{-}BAP\ upper}$ vector. The BAP-tagged *Hes7* cDNAs, *Hes7*$^{C\text{-}BAP}$ and *Hes7*$^{N\text{-}BAP}$, were digested with *Pst*I and *Xba*I and cloned into the similarly digested mammalian

expression vector *pCI* (Promega) to give *pCI-Hes7*$^{C\text{-}BAP}$ and *pCI-Hes7*$^{N\text{-}BAP}$ constructs for use in cell culture transfections (see Figure 2.1B for a schematic cloning strategy).

The construction of the mouse *NICD*^{BAP} expression vector was similar to the *Hes7*^{BAP} vectors. *NICD*$^{BAP\ upper}$ and *NICD*$^{BAP\ lower}$ parts were PCR-amplified from the *pcDNA3.1*$^{+}$*-NICD* template (Table 7.2) followed by subcloning into *pCR2.1-TOPO* vector (Invitrogen) and sequencing as previously (Table 7.6). In this case the lower part was introduced into *Eco*RV and *Xma*I restriction sites in *pcDNA3.1*$^{+}$ (Invitrogen). Following the digest of *pCR2.1-TOPO-NICD*$^{BAP\ upper}$ with *Eco*RV the upper part was isolated and cloned into *Eco*RV cut *pcDNA3.1*$^{+}$*-NICD*$^{BAP\ lower}$ to create a BAP-tagged *NICD* cDNA (Figure 2.1B).

Amplicon	Forward primer	Reverse primer
Hes7$^{N\text{-}BAP\ upper}$	5'- GCT GCA GAA GTT GGT CGT GAG G -3'	5'- **GAT ATC** ATT CAG GCC ACC AGC CAT TGC TCC TCC GGA ACC CTT CGG -3'
Hes7$^{N\text{-}BAP\ lower}$	5'- **GAT ATC** TTT GAG GCC CAG AAG ATC GAG TGG CAT GTC ACC CGG GAG CGA GCT GAG AAT AG -3'	5'- GAC TCT AGA GGT ACC ACG CGT G -3'
Hes7$^{C\text{-}BAP\ upper}$	5'- GCT GCA GAA GTT GGT CGT GAG G -3'	5'- **GAT ATC** ATT CAG GCC CCC GTC TTG TCT GTA AGG CGG TG -3'
Hes7$^{C\text{-}BAP\ lower}$	5'- **GAT ATC** TTT GAG GCC CAG AAG ATC GAG TGG CAT GCG CCC AAG GCC CCG TCA CTC C -3'	5'- GAC TCT AGA GGT ACC ACG CGT G -3'
NICD$^{BAP\ upper}$	5'- GCA TTG GGC GGC CGC G -3'	5'- **GAT ATC** ATT CAG GCC ACC TCC TTT AAA TGC CTC TGG AAT GTG G -3'
NICD$^{BAP\ lower}$	5'- **GAT ATC** TTT GAG GCC CAG AAG ATC GAG TGG CAT TAA ACA GAG ATG TGG GAT GCA G -3'	5'- GCT CCC GGG AGC TTT TTG C -3'

Table 7.2 PCR primer sequences to generate *Hes7*$^{N\text{-}BAP}$, *Hes7*$^{C\text{-}BAP}$ and *NICD*^{BAP} vectors for expression in cell culture. (*Eco*RV restriction sites shown in bold.)

For the BirA biotinylase, the cDNA sequence was taken from *pGEM-SD2-3xHA-BirA* (de Boer et al., 2003), which contains the biotinylase fused to three HA-tags. *3xHA-BirA* was cut with *Eco*RI from the *pGEM-SD2-3xHA-BirA* vector and subcloned into *Eco*RI digested *pCI* (Invitrogen), driving expression of *3xHA-BirA* from the human cytomegalovirus (CMV) immediate-early promoter.

7.1.4 Cloning of BAP-tagged constructs for homologous recombination in embryonic stem (ES) cells

For the $Hes7^{BAP}$ targeting construct, I PCR-amplified three parts, Hes7-BAP 5'-homology region $(Hes7^{BAP\ 5'HR})$, Hes7-BAP 3'-homology region upper $(Hes7^{BAP\ 3'HR\ upper})$ and Hes7-BAP 3'-homology region lower parts $(Hes7^{BAP\ 3'HR\ lower})$. The two parts for the 3'HR were amplified with TaKaRa LA Taq Polymerase as 1949 bp and 3202 bp pieces (using primers specified in Table 7.3 and genomic DNA from the mouse 129B6 strain as template), subcloned into *pCR2.1-TOPO* (Invitrogen) for sequencing (Table 7.6) and subsequently ligated using the *Eco*RV site.

The 1042 bp 5'HR was amplified with *Pfu* Turbo Polymerase using the primers listed in Table 7.3 and subcloned into the *pCRII-Zero-Blunt* vector (Invitrogen), for subsequent sequencing (Table 7.6). Both homology regions were cloned into *pFloxR1-modified*: The 5'HR was cloned into *Sbf*I/*Xba*I and the 3'HR into *Xho*I/*Hind*III (see Figure 2.5A for a schematic outline of the cloning strategy).

The targeting construct to insert the BAP-tag sequence into the *Notch1* locus was constructed similarly. The two homology regions were PCR-amplified as above: The 1320 bp and 2072 bp parts of the 5'HR were ligated via the *Eco*RV and insterted into *Sbf*I/*Xba*I in the targeting vector. The 2509 bp 3'HR was cloned into *pFloxR1-modified* using the *Cla*I/*Nhe*I sites in the multiple cloning site (see Figure 2.5B for the targeting strategy and Table 7.3 for primer sequences).

The targeting constructs *pFloxR1-mod_*$Hes7^{BAP}$ and *pFloxR1-mod_* $Notch1^{BAP}$ were linearised with *Sfi*I and subsequently purified by phenol-chloroform extraction. Briefly, 200 µl of phenol:chlorform:isoamylalcohol (25:24:1, Fluka) was added to 200 µl of the digested DNA and vortexed. After a 1 min spin at 16,000 x g the upper phase was transferred into a new tube and the extraction repeated. The DNA was precipitated with one tenth of the volume of 3 M sodiumacetate and 2.5 volumes of absolute ethanol

at -20ºC for several hours. The resulting pellet was washed twice with 70% ethanol, dissolved in 50 µl TE (10 mM Tris/HCl pH 7.5, 1 mM EDTA) buffer and adjusted to a final concentration of 1 µg/µl.

Fragment to be amplified by PCR	Forward primer	Reverse primer
Hes7$^{BAP\ 5'HR}$	5'- CCT GCA GGG AGT GAG AGG GAA ACG AAT GG -3'	5'- TCT AGA GAC ACG CGC GGG TGT TAT TAA CC -3'
Hes7$^{BAP\ 3'HR\ lower}$	5'- **GAT ATC** TTT GAG GCC CAG AAG ATC GAG TGG CAT GCG CCC AAG GCC CCG TCA CTC C -3'	5'- AAG CTT CCA CTG GTA GCA GGG AAA GTG G -3'
Hes7$^{BAP\ 3'HR\ upper}$	5'- CTC GAG TGT CTC TGT GTC TCC CTC ATT G -3'	5'- **GAT ATC** ATT CAG GCC CCC GTC TTG TCT GTA AGG CGG TG -3'
Notch1$^{BAP\ 3'HR}$	5'- ATC GAT AGA CCC CCT CAA AGA GTT GGG -3'	5'- GCT AGC TGC CTT AGA CGT ACA CAG TGC TG -3'
Notch1$^{BAP\ 5'HR\ lower}$	5'- **GAT ATC** TTT GAG GCC CAG AAG ATC GAG TGG CAT TAA ACA GAG ATG TGG GAT GCA G -3'	5'- TCT AGA TAA GCA GTC AAC AAG CAC AG -3'
Notch1$^{BAP\ 5'HR\ upper}$	5'- CCT GCA GGC TTT TGG ATG AGT ACA ACC TG -3'	5'- **GAT ATC** ATT CAG GCC ACC TCC TTT AAA TGC CTC TGG AAT GTG G -3'

Table 7.3 PCR primer sequences to construct *Hes7*^{BAP} and *Notch1*^{BAP} targeting vectors (*Eco*RV recognition sites are shown in bold).

7.1.5 Cloning of BAP-tagged constructs for viral gene transfer

For the generation of double stable cell lines, I chose to make use of the viral transduction system based on the Moloney Murine Leukaemia Virus (MMLV). To ensure expression of both the BirA biotinylase and either ER-NICD^{BAP} or N1ΔE^{BAP} two selection options must be in place. Therefore the 3xHA-tagged BirA was placed under neomycin selection and cloned via *Xho*I/*Not*I into the retroviral vector *pFBneo* (Stratagene).

N1ΔE^{BAP} cDNA was amplified from *pcDNA3.1^{+}-N1*ΔE^{BAP} by PCR using *PfuTurbo* DNA Polymerase and standard reaction conditions (section 7.1.1; Table 7.4) and further subcloned into *pCR-Blunt II-TOPO* for sequencing (section 7.1.8). Upon digestion with *Sal*I and *Eco*RI, the 2584 bp fragment of *N1ΔE^{BAP}* was introduced into similarly digested *pFB-IRES-GFP* (gift of Caetano Reis e Sousa, Cancer Research UK London Research Institute) to give the resulting *pFB-IRES-GFP-N1ΔE^{BAP}* retroviral expression vector. This allowed for selection of GFP positive cells and hence for cells that had integrated the *N1ΔE^{BAP}*.

To generate the *ER-NICD^{BAP}* fusion construct, I PCR-amplified a 969 bp stretch of the murine oestrogen receptor (ER) from the Δ*KS-βCat-ER* (obtained from Fiona Watt, Cancer Research UK Cambridge Research Institute) containing the restriction sites *Sal*I and *Bam*HI (Table 7.4). Similarly, 2094 bp containing *NICD^{BAP}* cDNA was amplified by PCR (section 7.1.1; Table 7.4). Both amplicons were subcloned into *pCR-Blunt II-TOPO* for sequencing (section 7.1.8). *pCR-Blunt II-TOPO-NICD^{BAP}* was further digested with *Bam*HI/*Eco*RI and inserted into *Eco*RI digested *pCR-Blunt II-TOPO-ER* to result in a functional tagged *ER-NICD^{BAP}* fusion construct. The *ER-NICD^{BAP}* fusion was released from the vector through *Sal*I/*Eco*RI digest and inserted into similar digested *pFB-IRES-GFP* construct.

Fragment to be amplified by PCR	Forward primer	Reverse primer
3xHA-BirA XhoI/NotI	5'- CTC GAG ATG GCC ACC TAT GAC GTC C -3'	5'- GCG GCC GCT TAT TTT TCT GCA CTA CGC AGG -3'
N1ΔE^{BAP} EcoRI /EcoRI	5'- GAA TTC GAC CAT GGA CTA CAA AGA CG -3'	5'- GAA TTC TTA ATG CCA CTC GAT CTT CTG G -3'
NICD^{BAP} BamHI /EcoRI	5'- GGA TCC CGC CGG CGC CAG -3'	5'- GAA TTC TTA ATG CCA CTC GAT CTT CTG G -3'
ER SalI/BamHI	5'- GTC GAC CGA AAT GAA ATG GGT GCT TCA G -3'	5'- GGA TCC GAT CGT GTT GGG GAA GCC -3'

Table 7.4 PCR primer sequences for cloning of BAP-tagged constructs for viral gene transfer.

7.1.6 Cloning of *Hes7* constructs for protein production

Three different lengths of Hes7 constructs were generated, namely Hes7^{ORF} (aminoacids 1-226) covering the full open reading frame, Hes7$^{N\text{-terminus}}$ (aminoacids 1-129) lacking the proline-rich and WRPW sequences and Hes7^{bHLH} (aminoacids 1-83) containing just the bHLH domain. Generating three different lengths of protein maximises the chances of producing a fully functional Hes7 protein. Constructs were amplified by PCR using *PfuTurbo* DNA Polymerase (section 7.1.1) and the primer sequences listed in Table 7.5. The forward and reverse primers included the restriction sites *Eco*RI and *Xho*I, respectively for further introduction in the final expression vector. Amplified fragments were subcloned into *pCR-Blunt II-TOPO* and verified by sequencing (section 7.1.8). Subsequent *EcoR*I/*Xho*I digest and ligation with similar digested *pGEX-4T-1* (Amersham Biosciences) yielded vectors for expression of glutathione S-transferase (GST) fusion constructs.

Constructs were transformed into chemically competent *E. coli BL21-CodonPlus (DE3)-RIL* cells (Stratagene) according to the manufacturers' guidelines for efficient high-level expression of heterologous proteins.

Fragment to be amplified by PCR	Forward primer	Reverse primer
Hes7^{ORF}	5'- CGG AAT TCA TGG TCA CCC GGG AGC GAG C -3'	5'- CCG CTC GAG TCA GGG CCA AGG TCT CCA AAA C -3'
Hes7$^{N\text{-}terminus}$	5'- CGG AAT TCA TGG TCA CCC GGG AGC GAG C -3'	5'- CCG CTC GAG TCA CGC TGG GAG CCC TGG ATC -3'
Hes7^{bHLH}	5'- CGG AAT TCA TGG TCA CCC GGG AGC GAG C -3'	5'- CCG CTC GAG TCA GCC TGG GGA CCG GGG AAC -3'

Table 7.5 PCR primer sequences to amplify *Hes7*^{ORF}, *Hes7*$^{N\text{-}terminus}$ and *Hes7*^{bHLH} constructs for Hes7 antibody production.

7.1.7 Transformation of competent bacteria and plasmid isolation

For propagation of the DNA constructs, One Shot chemically competent *Escherichia coli* (Invitrogen) cells were transformed according to the manufacturers' guidelines. Briefly, 2 μl of the TOPO (Invitrogen) cloning reaction was added to one vial of competent cells and incubated for 5-30 minutes on ice. Bacteria were heat-shocked for 30 seconds at 42ºC and immediately transferred to ice. After addition of 250 μl of S.O.C. (Super Optimal broth with Catabolite repression, Invitrogen) medium cells were regenerated through incubation at 37ºC shaking (200 rpm) for 1 hour. 10-50 μl of each transformation was spread onto selective plates and incubated at 37ºC overnight. Positive clones from the Zero Blunt TOPO cloning reactions were selected on Luria Bertani (LB) agar plates containing 25 μg/μl Zeocin (Invitrogen) whereas positive clones from the TOPO TA cloning reaction were selected with 100 μg/μl Ampicillin (Sigma-Aldrich) and 40 μl of 40 mg/ml X-gal (5'-Bromo-4-Chloro-3-Inodolyl-β-D-Galactoside, Sigma-Aldrich) for blue-white screening.

The next day colonies were picked and placed into 3 ml of LB broth containing the respective antibiotic and grown overnight at 37ºC and 200 rpm. Plasmids were isolated from bacterial pellets using the Qiagen liquid handling robot based on the Qiagen plasmid purification chemistry by the Cancer Research UK Equipment Park service.

After verification of the plasmid DNA by restriction digest of the miniprep DNA a larger quantity of plasmid DNA was prepared. For this purpose, the QIAfilter Maxi Plasmid Purification Kit was used (Qiagen) according to the manufacturers' guidelines.

7.1.8 Sequencing

Sequencing was performed using the BigDye Terminator v3.1 Cycle Sequencing Kit (Applied Biosystems). The PCR reactions were carried out on a Peltier (PTC-200, DNA Engine) thermal cycler using the conditions specified in Table 7.7. PCR reactions were purified with the DyeEx 2.0 Spin Kit (Qiagen) and dried in a speed vacuum. DNA sequencing was performed on an Applied Biosystems 3730 DNA Analyser by the Cancer Research UK Equipment Park facility.

Primer	Sequence
M13 forward	5'- CAG GAA ACA GCT ATG AC -3'
M13 reverse	5'- GTA AAA CGA CGG CCA G-3'

Table 7.6 Sequencing primers to verify TOPO cloning reactions.

	ramp to 96ºC at 2.5ºC/sec	
	96ºC	1 minute
24 cycles of	96ºC	10 seconds
	ramp to 50ºC at 1ºC/sec	
	50ºC	5 seconds
	ramp to 60ºC at 1ºC/sec	
	60ºC	4 minutes
	12ºC	forever

Table 7.7 Thermal cycler conditions for sequencing reactions.

7.2 Zebrafish

7.2.1 Zebrafish care

Zebrafish were raised according to standard procedures (Westerfield, 1993) at 28ºC on a 14- to 10-hour light-dark cycle.

7.2.2 Injection of mRNA into fish embryos

pCDNA3.1^{+}*-NICD*, *pCDNA3.1*$^{+}$*-NICD*^{BAP}, *pCI-Hes7* and *pCI*-Hes7^{BAP} as well as *pRSET-BtdTomato* were linearised with *Stu*I (NICD constructs), *Not*I (Hes7 constructs) or *EcoR*I (Tomato injection control). The purified linearised DNA was further extracted with phenol:cholorform:isoamylalcohol and precipitated with ethanol. Subsequently, DNA was transcribed with T7 RNA polymerase for 2-3 hours at 37ºC and RNA was recovered through phenol:cholorform:isoamylalcohol and ethanol precipitation. The quality of the RNA was verified on a 0.8% agarose gel in TBE (Tris-borate, EDTA) and the concentration determined using the NanoDrop spectrophotometer (Thermo Scientific). The injection mix contained approximately 1 μg of *NICD* or *Hes7* mRNA and 1 μg of control mRNA in injection buffer. The RNA was injected at concentrations of 50 μg/ml up to 1 mg/ml (i.e. from 25 pg to 500 pg RNA per cell) in 2-cell stage wildtype fish embryos in 1 x Ringer´s solution (115 mM NaCl, 5 mM KCl, 2 mM $CaCl_2$, 25 mM $NaHCO_3$, pH 7.3) containing 0.5% phenol red.

7.2.3 Whole-mount *in situ* hybridisation of fish embryos

Embryos injected with *NICD* or *NICD*^{BAP} mRNA were fixed in 4% paraformaldehyde (PFA) 15 hours after injection and hybridised with digoxigenin-labelled *islet1* RNA probe (Inoue et al., 1994). Briefly, embryos were dehydrated in a graded series of methanol (25%, 50%, 75%, 100%) for 10 minutes each. Embryos were stored in 100% methanol at -20ºC until needed and subsequently rehydrated in a graded series of methanol (75%, 50%, 25%) for 10 minutes each. This was followed by a wash in phosphate buffered saline including Tween-20 (PBST: 37 mM NaCl, 2.7 mM KCl, 10 mM sodium phosphate dibasic, 2 mM potassium phosphate monobasic pH 7.4, 0.1% Tween-20) for 10 minutes and incubation in pre-warmed hybridisation solution (50% formamide, 5x saline-sodium citrate (SSC) buffer: 0.75 M sodium chloride and 0.075 mM trisodium citrate pH 7.0, 50 μg/ml heparin, 500 μg/ml yeast tRNA, 0.1% Tween-

20, 0.0092 M citric acid) for 2 hours at 62ºC. Embryos were incubated with the probe in hybridisation solution overnight at 62ºC. The next day embryos were washed in 2xSSC/0.1% Trition-X-100 for 5 minutes and then for 30-40 minutes at 62ºC. After exchange of the solution embryos were washed in 0.2xSSC/0.1% Trition-X-100 for 30-40 minutes at 62ºC. Afterwards embryos were transferred into KTBT buffer (50 mM Tris/HCL pH 7.5, 150 mM NaCl, 10 mM KCl, 0.1% Triton-X-100) and incubated for 20 minutes at room temperature before blocking in 25% sheep serum in KTBT for 1 hour at room temperature. Embryos were further incubated with anti-digoxigenin antibody conjugated to alkaline phosphatase (Roche) 1:5,000 in KTBT including 25% sheep serum at 4ºC overnight. The next day, embryos were washed in KTBT three times for 30 minutes at room temperature before equilibration in AP buffer (100 mM Tris pH 9.5, 50 mM $MgCl_2$, 100 mM NaCl, 0.1% Triton-X-100) for 30 minutes at room temperature. The colour reaction was developed in the dark with Nitro-Blue Tetrazolium Chloride/5-Bromo-4-Chloro-3'-Indolyphosphate p-Toluidine salt (NBT/BCIP, Roche: 45 µl NBT [75 mg/ml in 70% dimethylformamide] + 35 µl BCIP [50 mg/ml in 100% dimethylformamide] in AP buffer. When the desired colouration was achieved, embryos were rinsed in KTBT and post-fixed in 4% PFA.

7.3 Transgenic mice

7.3.1 Electroporation of embryonic stem cells (ESC)

Electroporation of the targeting constructs *pFloxR1-mod_Hes7*^{BAP} and *pFloxR1-mod_ Notch1*^{BAP} was performed by the Cancer Research UK Transgenics facility in Clare Hall, London. The ES cells used were derived from 129 inbred mice and were maintained on primary embryonic fibroblast cells with the addition to the media of Leukaemia Inhibitory Factor (LIF), at 1000 units/ml, to prevent differentiation and to maintain pluripotence.

Constructs were electroporated into 5 x 10^6-10^7 ES cells. Selection was applied 24 hours after electroporation with the addition of 200 µg/ml Geneticin G418 sulphate (Gibco) in ES cell medium. After 8-10 days colonies were picked and placed into wells of a 96 well microtitre plate. These were further cultured and, when confluency was reached, half of the cells were frozen and half transferred to another 96 well plate and used for screening.

7.3.2 DNA extraction from mouse ear biopsies

Ear biopsies of transgenic mice were dissolved in 300 µl of lysis buffer (50 mM Tris pH 8.0, 5 mM EDTA pH 8.0, 100 mM NaCl, 0.5% SDS) containing 20 mg/ml Proteinase K (Roche) with constant rolling at 56ºC overnight. The next day, 120 µl of saturated sodium chloride solution was added. The solution was mixed and incubated on ice for 20 minutes. Precipitates were eliminated by centrifugation at 16,000 x g for 20 minutes and the supernatant transferred to a new tube. DNA was isolated by adding 600 µl of absolute ethanol and further centrifugation at 16,000 x g for 20 minutes. The pellets were washed with 300 µl of 70% ethanol and centrifugation at 16,000 x g for 20 minutes. Following the drying of the DNA it was dissolved in 100 µl of TE.

7.3.3 Genotyping of transgenic mice

For genotyping, 1 µl of the DNA solution prepared from ear biopsies (section 7.3.2) was used per PCR reaction together with 10 µM of each primer (Table 7.8) and the *Taq* PCR Master Mix (Qiagen). Thermo cycler conditions were as described in section 7.1.1.

Genotype	Forward primer	Reverse primer	Fragment size (bp)
Hes7$^{BAP/+}$	5'- TCT TTG AGG CCC AGA AGA TCG -3'	5'- AGA AAG CGA TTC AAA GGT TGT GG -3'	614 bp
Hes7$^{BAP/BAP}$	5'- CCC ATC CCA CTG CTC CTC TC -3'	5'- GGA TCC CTC TCC TGC CCT CT -3'	220 bp WT 262 bp Homo
Notch1$^{BAP/+}$	5'- GCA AGC TTG AAT GGC CAG -3'	5'- TTG AGG CCC AGA AGA TCG AGT G -3'	764 bp
Notch1$^{BAP/BAP}$	5'- CAG CTC CTC CCC GCA TTC C -3'	5'- TTG GTC GCC CCA GCA TCC -3'	194 bp WT 242 bp Homo
BirA/+	5'- GTT ACG ATG TGC CCG ACT ATG C -3'	5'- CGC CAT CAC GAT ACC GAT AAC C -3'	515 bp
BirA/BirA	5'- CTT GGA CTG GCT TGA CTC ATG G -3'	5'- CCA CTG GCT GGC TAA ACT CTG G -3'	799 bp WT or Het absent in Homo
neo^{r}	5'- GAC TGG GCA CAA CAG ACA ATC G -3'	5'- GCA ATA TCA CGG GTA GCC AAC G -3'	620 bp

Table 7.8 Primer sequences for genotyping of *Hes7*$^{BAP/BAP}$, *Notch1*$^{BAP/BAP}$ and *Rosa26*$^{BirA/BirA}$ mice. Abbreviations for genotypes are as follows: wildtype (WT), heterozygous (Het) or homozygous (Homo).

7.3.4 PCR Screening of embryonic stem cell clones (ESCCs)

ESCCs were picked by the Cancer Research UK Transgenics Facility in 96 well plates and subsequently lysed. DNA was precipitated by adding 50 µl of isopropanol to each well. The plates were incubated at room temperature for 30 minutes. Centrifugation at 1,500 x g for 10 minutes at room temperature generated a DNA pellet. The centrifugation step was repeated once to wash the pellet with 70% ethanol. The DNA was allowed to dry completely before dissolving in 100 µl TE. For PCR screening one primer was designed to bind in the targeting vector and the other to specifically recognise the flanking genomic region (Table 7.10). A master mix for all 96 reactions was prepared using 0.1 µl *TaKaRa LA Taq* DNA Polymerase, 4 µM of each oligonucleotide primer, 8 nM dNTPs and 5 µl of DNA from ESCC for each reaction. The plates were sealed and reactions performed on a Peltier (PTC-200, DNA Engine) thermo cycler using the programme specified in Table 7.9.

	94ºC	2 minutes
40 cycles of	94ºC	20 seconds
	60ºC	30 seconds
	72ºC	3 minutes
	72ºC	5 minutes
	12ºC	forever

Table 7.9 PCR programme for screening of electroporated ESCCs.

Region analysed	Forward primer	Reverse primer	Size of PCR product (bp)
Hes7^{BAP} 5' flanking region	5'- AAA GCG ACC CAA GGG ACT GG -3'	5'- TTG AAA ACC ACA CTG CTC GAT CC -3'	1166
Hes7^{BAP} 5' flanking region (alternative)	5'- TTG AAA ACC ACA CTG CTC GAT CC -3'	5'- TCC ATC CTT CTG AGA GGT CAT GC -3'	3013
Notch1^{BAP} 5' flanking region	5'- TTG AGG CCC AGA AGA TCG AGT G -3'	5'- CAG GAG CGT ATG CAC CAC GAT A -3'	1364
Notch1^{BAP} 3' flanking region	5'- GGG GCT CGA CTA GAG GAT CAG C -3'	5'- GAT GGT GAG ATT GAG GCC AAC C -3'	2845

Table 7.10 PCR screening primers to identify homologous recombinant ESCC.

7.3.5 Southern blot screening

7.3.5.1 Restriction enzyme digestion of mouse genomic DNA

Genomic DNA from ESCCs was precipitated by ethanol and centrifugation at 16,000 x g following a wash with 70% ethanol. The pellet was dissolved in 100 μl TE. 25 μl of the genomic DNA was digested with a suitable enzyme (Table 7.11) and the appropriate buffer as for plasmid DNA, except that the following components were added to the digestion mixture: 100 μg/ml bovine serum albumin (BSA, Sigma-Aldrich), 2.5 μg/ml RNaseA (Sigma-Aldrich) and 1 mM spermidine (Sigma-Aldrich). Digestions were allowed to proceed overnight at 37ºC with more enzyme added after 4 hours of incubation.

7.3.5.2 Preparation of Southern blot probes

Southern blot probes were amplified using *TaKaRa LA Taq DNA Polymerase* and primers specified in (Table 7.11). For cycling conditions and PCR set-up see section 7.1.1. The size of probe fragments was verified on an agarose gel after restriction digest. Labelling of DNA probes was performed using the Rediprime II Random Prime Labelling System (Amersham Biosciences) and ^{32}P-Nucleotides [α-^{32}P] dCTP Redivue Tips according to the manufacturers' instructions. Unincorporated nucleotides were removed using Micro Bio-Spin P-30 Tris chromatography columns (Bio-Rad).

Probe	Forward primer	Reverse primer	Restriction enzyme
Hes7^{BAP} *5'*	5'- TGA ACC ACC AAT GCA GAC AAG G -3'	5'- GGA TTC TAC TGG CTG GCT GTG G -3'	*Eco*RI
Hes7^{BAP} *3'*	5'- CTG CAG AGG CTT CGT GTG AGG -3'	5'- TCC AAT CAG GCT GCT CTC ACC -3'	*Xho*I/*Kpn*I
Notch1^{BAP} *5'*	5'- TCT GGC TTG GTC CAC CAC TAC C -3'	5'- GTC CAT GTG ATC CGT GAT GTC C -3'	*Stu*I
Notch1^{BAP} *3'*	5'- AAC AAA AAG GCC GAG GAC TGG -3'	5'- GCA GGA TCC TAG AGG CAG AAG C -3'	*Eco*RV/*Xho*I

Table 7.11 Primer sequences for the generation of Southern blot probes. Restriction enzymes to digest the genomic DNA are shown in the last column. For position of probes and restriction enzymes see Figure 2.7.

7.3.5.3 Southern blotting and hybridisation

Digested genomic DNA was separated on a 0.7% agarose gel in TBE using the Flowgen system for 10 hours and transferred on to Hybond-N^+ nylon transfer membrane (Amersham Biosciences). Blotting was performed as follows: A tray was filled with alkaline transfer buffer (400 mM NaOH) and a glass plate resting on an inverted plastic tub placed in the middle of the tray. Three pieces of 3 MM paper soaked in transfer buffer were then placed on the glass and their ends allowed to dip into the buffer, thereby acting as a wick. The agarose gel, which was pre-soaked in the transfer buffer for 20 minutes, was placed onto the 3 MM paper and the Hybond-N^+ nylon transfer membrane was placed on top of the gel. Air bubbles were removed by rolling with a pipette. Three more pieces of 3 MM paper, the same size as the gel, were placed on top of the membrane and Saran wrap was positioned around the edges of the blot apparatus to isolate the wick. A stack of tissues and then a glass plate were placed on top of the 3 MM paper. Finally a flask containing 500 ml of water was placed on top of the glass plate to weigh down the tissues. DNA blotting was allowed to proceed overnight. Once blotting was complete, the apparatus was carefully dismantled and the membrane washed in 2xSSC (300 mM sodium chloride, 30 mM sodium citrate) for 20 minutes at room temperature. The membrane was pre-hybridised with rotation for 2 hours at 65ºC in 20 ml Church buffer (200 mM sodium phosphate buffer pH7.2, 1 mM

EDTA, 1% BSA, 7% SDS, 15% formamide). The radio-labelled DNA probe was denatured by boiling for 2 minutes and placed on ice for 1 minute before being added directly to the pre-hybridisation buffer. Hybridisations were performed at 65ºC overnight.

Membranes were washed 3 times 30 minutes at 65ºC with Church wash buffer (40 mM sodium phosphate buffer pH7.2, 1 mM EDTA, 1% SDS). Once the majority of unbound probe had been washed away, the membrane was wrapped in Saran wrap and exposed to Kodak X-OMAT AR film at -80ºC.

7.3.6 Establishing transgenic mouse lines

Transgene constructs were injected into F1 x F1 (CBA x C57Bl/6J) mouse embryos, which were then implanted into pseudopregnant foster mothers. Transgenic founder lines were identified by screening DNA samples taken from these litters. Once a founder was identified, it was bred to establish whether the transgene could be transmitted and was capable of expression. Transgenic mice were kept in the C57Bl/6J background. C57Bl/6J also served as a wildtype control.

7.3.6.1 Chimera production

15-20 ES cells were microinjected into day 4 fertilised mouse embryos (blastocysts). Following injection, embryos were transferred into day 3 plugged pseudopregnant foster mice, which gave birth 18 days later. One week after birth the coat colour was determined which is a read-out for the success of germline contribution.

C57Bl/6J blastocysts produce black/brown chimeras. A high level of coat colour contribution together with a bias to male chimera mice (as the ES cell line is male) was indicative of an ES clone that contributed to the germline.

7.3.7 Skeleton preparation

Skeletons were prepared and stained with alcian blue/alizarin red S following standard procedures (Nagy et al., 2003). All photographs were taken with a Leica DC500 digital camera and Leica firecam version 1.7.1 software. Several photographs were assembled for adult skeletons.

7.3.8 Whole-mount *in situ* hybridization

Whole-mount *in situ* hybridisation was performed by a modification of the method used by (Henrique et al., 1995). Formaldehyde-fixed, proteinase K-treated embryos were pre-hybridised in hybridisation buffer (50% formamide; 1.3xSSC, pH 5.0, 5 mM EDTA, 0.2% Tween-20, 0.5% CHAPS, 50 µg/ml yeast RNA, 100 µg/ml heparin) at 70ºC for > 1h. Hybridisation with DIG-labelled RNA probes was performed in hybridisation buffer at 70ºC over night. Hybridised embryos were washed in hybridisation buffer at 70ºC for 1 h and in TBST (0.25 M Tris/HCl, pH7.5, 1.37 M NaCl, 27 mM KCl, 1% Tween-20) at room temperature for several hours, and subsequently incubated in TBST/10% heat-treated goat serum for > 1h and in alkaline-phosphatase coupled anti-DIG antibody (Roche; in TBST/10% goat serum) at 4ºC over night. After extensive washes in TBST, embryos were transferred to NTMT (100 mM NaCl, 100 mM Tris/HCl pH 9.5, 50 mM $MgCl_2$, 10% Tween-20) and the colour reaction performed with NBT/BCIP (Roche) at room temperature for several hours.

RNA probes were made from 0.7 kb *Hes7* ORF [subcloned from *pCl-Hes7* (Bessho et al., 2001a) into *pBluescriptII KS*, Stratagene], 1.2 kb mouse *Lfng* cDNA (IMAGE clone 408467), 0.7 kb *Uncx4.1* cDNA (Mansouri et al., 1997), 1.9 kb mouse *MyoD*, 1.2 kb *Dusp4* (Niwa et al., 2007), 2.8 kb *Axin2* (Aulehla et al., 2003) and 0.8 kb *Nrarp* (Phng et al., 2009). *Hes7* intron probe was synthesised from a 1 kb PCR product of the first intron cloned into *pCRII-TOPO* vector (Invitrogen) and used with the same hybridisation buffer as cDNA probes but at 65ºC instead of 70ºC. For generation of antisense riboprobes vectors were digested with an enzyme cutting 5' of the cDNA and further transcribed from the 3' end (Table 7.12).

Probe	Restriction digest	RNA polymerase
MyoD	*Bam*HI	T7
Uncx4.1	*Xho*I	T7
Dusp4	*Not*I	T7
Nrarp	*Sal*I	T7
Lfng	*Hind*III	T7
Hes7 intron	*Not*I	SP6
Hes7 cDNA	*Spe*I	T3
Mesp2	*Bam*HI	T7
Axin2	*Sal*I	T7

Table 7.12 Restriction digests and RNA polymerases used for transcription of riboprobes.

7.3.9 Whole-mount Notch intracellular domain (NICD) antibody staining

Whole-mount NICD antibody staining on E9.5 and E10.5 wildtype and transgenic *Hes7*$^{BAP/+}$ and *Hes7*$^{BAP/BAP}$ embryos was done as described by (Feller et al., 2008). Briefly, embryos were dissected in cold PBS, fixed in 50% DMSO in methanol for 5 minutes and subsequently washed 3 times for 10 minutes in NH_4Cl-PBS (50 mM NH_4Cl, 1xPBS). Following bleaching in 15% H_2O_2 in NH_4Cl-PBS for 35 minutes cells were transferred into TS-PBS (1% Triton-X-100, 10% FCS, 1xPBS) and washed 3 times for 10 minutes each. Incubation with the cleaved Notch1 (Valine 1744) antibody (Cell Signaling) diluted 1:100 in TS-PBS was performed overnight at 4ºC. The next day, embryos were washed 10 times 20 minutes in TS-PBS and incubated overnight at 4ºC with an anti-rabbit biotinylated antibody (BA1000, Vector) at a 1:100 dilution in TS-PBS. The following day, embryos were washed again 10 times for 20 minutes in TS-PBS but at 4ºC. Incubation with Streptavidin-HRP (NEN) 1:100 in TS-PBS was done overnight and washes as previously at 4ºC were carried out the next day. Detection was by incubation for 10 minutes in solution A (100 mM Tris pH7.5, 0.1% Triton-X-100, 224 nM 4-Chloro-1-Naphthol (Sigma-Aldrich)), 3 washes for 15 minutes in solution B (100 mM Tris pH7.5, 224 nM 4-Chloro-1-Naphthol), incubation for 15 minutes in solution C (40% ethanol, 2.8 mM 4-Chloro-1-Naphthol) and staining in

solution D (50% ethanol, 7.5% H_2O_2, 3.5 mM 4-Chloro-1-Naphthol). When judged complete, embryos were fixed in 2% PFA in 50% ethanol.

7.3.10 Quantitative reverse transcriptase PCR (qRT-PCR) from embryonic mouse tail tissue

E9.5 embryos of wildtype and transgenic *Hes7*$^{BAP/+}$ and *Hes7*$^{BAP/BAP}$ were harvested and the posterior tail dissected. Total RNA was isolated using the RNeasy Mini Handbook (Qiagen) and further treated with DNase (Invitrogen). qRT-PCR reactions were performed with the SuperScript III Platinum SYBR Green One-Step qRT-PCR Kit (Invitrogen) on a ABI 7500 Fast (Applied Biosystems) machine using primers listed in Table 7.13. *Hes7* mRNA levels were quantified relative to *GAPDH* mRNA expression.

mRNA	Forward primer	Reverse primer
GAPDH	5'- GGT GCT GAG TAT GTC GTG GA -3'	5'- GCG GAG ATG ATG ACC CTT T -3'
Hes7	5'- GGA GCG AGC TGA GAA TAG GG -3'	5'- CTT CTA GGC TGC GGT TGA TG -3'

Table 7.13 Primer sequences for quantification of *Hes7* mRNA levels in wildtype, *Hes7*$^{BAP/+}$ and *Hes7*$^{BAP/BAP}$ embryos by qRT-PCR.

7.4 Cell culture

7.4.1 Handling of cell lines

Cell lines were incubated in 37ºC incubators with 5% CO_2 using the appropriate medium conditions (Table 7.14). E4 (Cancer Research UK cell service equivalent to DMEM (Dulbecco's modification of Eagle's medium)) was used for murine cells supplemented with 10% foetal calf serum (FCS) whereas a combination of E4 and HAMS F12 was used for MCF10A cells. Cells were regularly split using trypsin/versene (Cancer Research UK cell services) to maintain a healthy population. Freezing of cells was done in full medium supplemented with 10% dimethyl sulfoxide (DMSO, Sigma-Aldrich).

Cell line	Species/ Morphology/ Type	Medium requirements	Source
C3H10T½	Mouse/ Fibroblasts/ Monolayer	E4 + 10% FCS	CR-UK Cell Services
MCF10A	Human/ Breast/ Monolayer	1:1 E4:HAMS F12 5% horse serum (Sigma-Aldrich), 10 μg/ml Insulin (Sigma-Aldrich), 5 μg/ml Hydrocortisone (Calbiochem), 20 ng/ml EGF (Calbiochem), 100 ng/ml Cholera Toxin (Quadratech)	CR-UK Cell Services
MEL [BirA] and [Bio-GATA-1]	Mouse/ Spleen/ Suspension	E4 + 10% FCS	Frank Grosveld, Erasmus Medical Center, Rotterdam
GP2-293	Human/ Kidney/ Monolayer (based on HEK-293 cell line)	E4 + 10% FCS	Pantropic Retroviral Expression system Kit (BD Biosciences)

Table 7.14 Cell lines used in this thesis.

7.4.2 Transfection

Transfection of cell lines was done with FuGENE 6 transfection reagent (Roche) according to the manufacturers' guidelines. The ratio of DNA to FuGENE 6 was 1:3.

7.4.3 Viral gene transfer

7.4.3.1 Preparation of virus-containing supernatants

3 x 10^6 GP2-293 cells were plated in full medium in a 10 cm dish the day before transfection. 5 μg of the plasmid encoding the vesicular stomatitis virus (VSV) G protein, which confers a polytrophic host range together with 5 μg of the retroviral construct and 30 μl FuGENE 6 transfection reagent were diluted in 500 μl E4 without antibiotics and serum. Viral supernatants were harvested 72 hours after transfection, filtered through a syringe driven filter unit (0.45 μm Millex HV syringe filter, Milipore) and used immediately for transduction or frozen in liquid nitrogen and stored at -80ºC.

7.4.3.2 Transduction of cell lines

In order to establish stable cell lines expressing biotinylated $NICD^{BAP}$, cells were first transduced with the biotinylase and selected for neomycin resistant clones. Positive clones (as verified by western blot analysis to detect HA-tagged BirA) were further transduced with viral particles containing $NICD^{BAP}$ and selected according to their GFP expression.

C3H10T½ and MCF10A cell lines were plated at 2 x 10^5 per well of a 6 well plate and incubated overnight at 37ºC and 5% CO_2. Virus containing the BirA biotinylase under neomycin selection was produced as described in 7.4.3.1 using the retroviral plasmids *pVSV-G* and *pFBneo-3xHA-BirA*. Cells were infected with the virus supernatant (titre ~10^8) by spin infection at 600 x g for 90 minutes at room temperature. Polybrene (Sigma-Aldrich) at a final concentration of 8 μg/ml was added to the infection mixture. After the centrifugation, cells were incubated for another 90 minutes at 37ºC and 5% CO_2. The medium was changed thereafter and the cells incubated for 3 days at 37ºC and 5% CO_2. To identify positive clones, which had integrated the biotinylase, cells were split 1:50 in 10 cm dishes and placed under Geneticin G418 sulphate (Gibco) selection. A final concentration of 1 mg/ml G418 was used to select for positive C3H10T½ [BirA] clones whereas 0.5 mg/ml of G418 was applied to identify stable MCF10A [BirA] clones. In each case 24 clones were picked and placed in separate wells. Cells were grown and further checked for expression of 3x-HA BirA by western blot analysis using an α-HA antibody (Roche).

Selected clones were further transduced with viral particles containing $NICD^{BAP}$ under GFP selection. Infection was performed as described above. However cells were sorted for GFP expression after 3 days of infection using Fluorescence-activated cell sorting (FACS).

7.4.3.3 Fluorescence-activated cell sorting (FACS)

For FACS sorting of infected live cells, cells were harvested by trypsinisation, washed once with E4 + 1% FCS and taken up in E4 + 1% FCS. Around 1 x 10^5 cells were sorted on a MoFlo (DakoCytomation, now BeckmanCoulter) cell sorter and plated in rich medium for expansion.

7.4.4 Luciferase reporter assay

C3H10T½ cells were plated at a density of 8 x 10^4 per well of a 24 tissue culture plate 24 hours before transfection. 100 ng of the firefly luciferase reporter was co-transfected with either 200 ng of *pCI* (Promega) or *pCDNA3.1*$^+$ (Invitrogen) as control or the respective construct containing untagged or BAP-tagged *Hes7* and *NICD* cDNAs. The reporter in the case of Hes7 is a synthetic *β-actin* promoter with a six N-box repeat (Ishibashi et al., 1994). To test for Notch1 activation, a 509 bp *Hes1* promoter fragment drives luciferase activity (Nishimura et al., 1998).

FuGENE 6 (Roche) was used as transfection reagent at a ratio of 1:3, DNA: FuGENE 6. 4 ng of the *Renilla* luciferase *pRL-TK* (Promega) in each sample served as a reference reading. After incubation for 24 hours at 37ºC and 5% CO_2 the assay was analysed using the Dual-Luciferase Reporter Assay System (Promega) according to the manufacturers' guidelines. *Firefly* and *Renilla* activities were read using the EnVision Multilabel Reader. The values of the reporter readings were normalised to the values of the *Renilla* reading. The resulting luciferase activity alone was taken 100%. Each experiment was done in triplicates and repeated at least three times.

7.4.5 Activation of ER-fusion proteins in cultured cells

4-Hydroxytamoxifen (Sigma-Aldrich) was added to the cell culture medium at a final concentration of 1 μM. Control cells were treated with ethanol (1:1000). Activation of the ER-fusion protein was tested after incubation at 37ºC and 5% CO_2 for 24 hours by luciferase reporter assay.

7.4.6 Immunofluorescence and confocal microscopy

For immunohistochemistry MCF10 cells stably expressing BirA and $NICD^{BAP}$ were cultured on chamber slides coated with Poly-D-Lysine (BD Biosciences). 24 hours after plating, the medium was aspirated and cells washed twice with PBS and fixed in 4% paraformaldeyhde (PFA) for 10 minutes at room temperature. Following two more washes with PBS, cells were treated with 0.1% Triton-X-100 in PBS for 5 minutes at room temperature. The first antibody was applied after another two washes with PBS and used at a concentration of 1:100 in TNB buffer (0.5% blocking reagent (Roche) in 0.1 M Tris/HCl pH 7.5, 0.15 M NaCl) for an overnight incubation. The next day, cells

were washed three x five minutes with 1xTBST (0.1 M Tris/HCl pH 7.5, 0.15 M NaCl, 0.1% Tween-20) and the secondary antibody applied at concentration of 1:500 for 3 hours at room temperature. This was followed by further washes in 1xTBST and dehydration through a series of alcohol. Cells were mounted in *SlowFade* Gold anti-fade reagent (Invitrogen).

For embryonic sections (15 μm thick) the first antibody was diluted 1:100 in immunostaining buffer (10% goat serum, 2% BSA, 0.1% Triton-X-100) and incubated overnight at 4ºC. Sections were rinsed with PBS containing 0.1% Triton-X-100 for 3 x 5 minutes at room temperature and further incubated for 3 hours at room temperature with the secondary antibody diluted 1:500 in the immunostaining buffer. Mounting of sections was as above.

Antibody staining on retinas was performed as follows: Eyes were harvested and put into 4% PFA for fixation for 2 hours at 4ºC. Retinas were dissected and blocked in Immunostaining buffer (PBS containing 0.5% Tween-20 and 1% BSA) for 2 hours at room temperature. Isolectin Alexa Fluor 568 and Streptavidin Alexa Fluor 488 (Invitrogen) directly coupled antibodies were applied 1:200 in the immunostaining buffer and left for 3 hours at room temperature. Washes and mounting were done as above.

For visualising of the nuclei, 4',6-diamidino-2-phenylindole (DAPI, Invitrogen) was added at a final concentration of 54.5 nM to the last wash and incubated for 5 minutes. Confocal imaging was performed on a Zeiss LSM 510 using a 40X water immersion lens. Digital images were processed and arranged using the Adobe Photoshop and Illustrator CS2 software.

Antibody	Company
Streptavidin Alexa Fluor 488	Invitrogen
Isolectin Alexa Fluor 568	Invitrogen
Cleaved Notch1 (Valine 1744)	Cell Signaling
Goat α-rabbit Alexa Fluor 568	Invitrogen

Table 7.15 Antibodies used for Immunohistochemistry.

7.5 Biochemistry

7.5.1 Glutathione-S-Transferase (GST) protein purification

Small scale GST-protein purification of GST-Hes7^{bHLH}, GST-Hes7$^{N\text{-terminus}}$ and GST-Hes7^{ORF} proteins from *E. coli BL21-CodonPlus (DE3)-RIL* cells showed that only the Hes7^{bHLH} protein could be isolated efficiently without being degraded. Large scale GST-protein purification from *E. coli BL21-CodonPlus (DE3)-RIL* [Hes7^{bHLH}] cells was prepared as follows: Cells were grown in 2 litres of LB medium containing 100 μg/ml Ampicillin until the culture reached an optical density at 600 nm (OD600) of 0.7. Induction of the GST-fusion was done by adding 0.1 mM Isopropyl β-D-1-thiogalactopyranoside (IPTG, Sigma-Aldrich) and further incubation at 18ºC overnight. Cells were harvested by centrifugation at 6,000 x g and 4ºC for 20 minutes. The pellets were washed once with 1xMTPBS (0.15 M NaCl, 0.16 M Na_2HPO_4, 4 mM NaH_2PO_4) including protease inhibitors (Complete EDTA free, Roche). Resuspended cells were aliquoted in 6 x 15 ml and sonicated twice for 1 minute with a Soniprep 150. Sonication was typically at 12-14 microns amplitude, as judged by a 'frying egg' noise. 0.2% of Igepal CA-630 (Sigma-Aldrich) was added and insoluble material removed by centrifugation at 12,000 x g for 10 minutes and 4ºC. Supernatants were pooled and mixed with 1 ml of 50% glutathione-Sepharose 4B beads (Pharmacia; 2 ml of 1:1 MTPBS slurry). The beads were prepared by pre-swelling and washing in MTPBS. The beads and supernatant were rolled for 30 minutes at 4ºC. To remove unbound material, the mixture was centrifuged at 500 x g for 5 minutes at 4ºC. The beads were further washed 6 times with MTPBS containing 0.1% β-Mercaptoethanol (Sigma-Aldrich) and spun as previously.

To cleave off the GST-tag 80 units of thrombin (Amersham Biosciences) were added to 920 μl of MTPBS and incubated with the beads for 2 hours at room temperature. Removal of the thrombin protease was done by incubation with 40 μl of Benzaminobenzamidine beads (Sigma-Aldrich) for 30 minutes at 4ºC. Beads were spun out and the supernatant removed and stored at -80ºC in 10% glycerol.

7.5.2 Protein gel electrophoresis

Proteins were separated and transferred using the NuPAGE system (Invitrogen) according to the manufacturers' instructions. NuPAGE Novex 4-12% Bis-Tris gels (Invitrogen) were used for most applications. For separation of small proteins Novex Tricine gels were run. Depending on the range of protein separation MOPS or MES running buffers (Invitrogen) were used for high molecular weight or low molecular weight proteins, respectively. Tricine gels were run in Tricine SDS running buffer (Invitrogen). For protein visualisation, gels were stained with Novex Colloidal Blue Staining Kit (Invitrogen).

Blotting of gels was performed as described in the manufacturers' manual. Proteins were blotted onto a Hybond-ECL membrane during the 90 minutes transfer in the supplied transfer buffer (Invitrogen).

7.5.3 Western blotting

Membranes were blocked for 1 hour at room temperature with 5% milk (Marvel) in PBS for standard western blot or with 5% BSA (Sigma-Aldrich) in TBS (10 mM Tris, 150 mM NaCl, pH 7.6) including 0.2% Tween-20 for detection of biotinylated proteins with streptavidin. Primary antibody incubation was performed for one hour at room temperature or overnight at 4ºC in blocking solution (Table 7.16). Following three washes for 5 minutes at room temperature in PBS including 0.1% Tween-20 for standard procedures or in TBS containing 0.5 M NaCl and 0.3% Triton-X-100 for biotinylated proteins the secondary antibody was applied. After incubation for 1 hour at room temperature, the membrane was washed as above and detection was carried out with the ECL Plus Western Blotting Detection System (GE Healthcare, formerly Amersham Biosciences) according to the manual. The membrane was exposed to the high performance chemiluminescence film Hyperfilm ECL (GE Healthcare) and the film further developed in the JPI Automatic X-ray Film Processor (Model JP-33).

Antibody	Source	Dilution	Company
Cleaved Notch1 (Valine 1744) antibody	Rabbit	1:1,000	Cell Signalling
Streptavidin-HRP		1:25,000	NEN
α-HA	Mouse	1:5,000	Roche
RBP-Jκ (H-50): sc-28713	Rabbit	1:1,000	Santa Cruz Biotechnology, INC
α-Hes7^{bHLH}	Rat	1:10,000	CR-UK Monoclonal Antibody Service
Goat α-Rat IgG Peroxidase Conjugate	Goat	1:10,000	Calbiochem
α-mouse IgG, Horseradish Peroxidase linked whole antibody	Sheep	1:10,000	Amersham Biosciences
Peroxidase-conjugated AffiniPure Goat α-Rabbit IgG (H+L)	Goat	1:10,000	Jackson ImmunoResearch Laboratories

Table 7.16 Antibodies used for western blotting.

7.5.4 Preparation of whole cell lysates

Whole cell lysates from cultured cells and mouse tissues were prepared using the Radio Immuno Precipitation Assay buffer (RIPA; 50 mM Tris/HCl pH 8, 150 mM NaCl, 1% Igepal CA-630, 0.5% sodium deoxycholate, 0.1% SDS, 2 mM EDTA). Briefly, cells were washed with ice-cold PBS and lysed in 1 ml RIPA per 10^7 cells/100 mm dish and further incubated under constant agitation for 30 minutes at 4ºC. Upon centrifugation at 16,000 x g at 4ºC the supernatant was removed and aliquoted. For storage protein lysates were quick-freezed in liquid nitrogen and kept at -80ºC.

Tissues of interest were dissected in ice-cold PBS and snap frozen in liquid nitrogen for further storage at -80ºC or immediate homogenisation. For a 5 mg piece of tissues 300 μl of RIPA buffer were added and the tissue homogenised. Constant agitation at 4ºC was maintained for 2 hours. After centrifugation at 16,000 x g at 4ºC the supernatant was transferred into a new tube and stored as above.

7.5.5 Crude nuclear extract preparation

Nuclear extracts from a small number of cells (up to 10^7) were prepared according to Andrews et al. (Andrews and Faller, 1991). Adherent cells were scraped in cold PBS on ice, pelleted by centrifugation for 30 seconds in an Eppendorf 4515D centrifuge and

resuspended in 1.5 ml cold PBS. Cells were pelleted for 10 seconds and resuspended in 400 µl cold Buffer A (10 mM HEPES-KOH pH 7.9 at 4ºC, 1.5 mM $MgCl_2$, 10 mM KCL, 0.5 mM dithiothreitol (DTT), 0.2 mM phenylmethanesulphonylfluoride (PMSF)) by flicking the tubes. The cells were allowed to swell on ice for 10 minutes and were then vortexed for 10 seconds. Samples were centrifuged for 10 seconds, the supernatant discarded and the pellet taken up in 1½ volumes of cold Buffer B (20 mM HEPES-KOH pH 7.9 at 4ºC, 25% glycerol, 420 mM NaCl, 1.5 mM $MgCl_2$, 0.2 mM EDTA, 0.5 mM dithiothreitol (DTT), 0.2 mM phenylmethanesulphonylfluoride (PMSF)). After incubation for 20 minutes on ice cellular debris is removed by centrifugation at 4ºC for 2 minutes. Protein lysates were stored as in section 7.5.4.

7.5.6 Protein concentration determination

The protein concentration was determined using either the Bio-Rad Protein Assay (Bio-Rad) or the RC DC Protein Assay (Bio-Rad) depending on the lysis buffer formulation and according to the manufacturers' guidelines.

7.5.7 Binding to streptavidin beads

Paramagnetic streptavidin beads (Dynabeads M-280, Dynal) were blocked by washing three times in TBS containing 200 ng/µl ovalbumin (Sigma-Aldrich). Binding was done in 1 x TBS/0.3% Igepal CA-630 at 4ºC for 1 h to overnight on a rotating wheel, followed by six washes in binding solution at room temperature. Bound material was eluted by boiling for 5 min in 2 x sample buffer (100 mM Tris/HCl pH 6.8, 4% SDS, 0.2% bromophenol blue, 20% glycerol, 200 mM β-Mercaptoethanol) and analyzed by western blotting (section 7.5.3).

7.5.8 Streptavidin protein pull-down from mouse embryos

Wildtype, $Rosa26^{BirA/BirA}$ and $Notch1^{BAP/BAP}$;$Rosa26^{BirA/BirA}$ E12.5 embryos were dissected in homogenisation buffer (0.25 M Sucrose, 10 mM HEPES-KOH pH 7.9, 25 mM KCl, 1 mM EDTA, 0.15 mM Spermine, 0.5 mM spermidine) and further homogenised using a B Dounce homogeniser (5 ml per g). The homogenate was filtered through a cell strainer and diluted 1:1 with homogenisation buffer. Following a centrifugation step at 800 x g at 4ºC for 10 minutes the pellet was resuspended in 10 ml homogenisation buffer and spun as above. The pellet was further taken up in 9 volumes

of sucrose cushion buffer (2.2 M sucrose, 10 mM HEPES-KOH pH 7.9, 25 mM KCl, 1 mM EDTA, 0.15 mM spermine, 0.5 mM spermidine) and put on ice for 20 minutes. Ultracentrifugation in a swinging-bucket rotor (Sw55Ti) for 2 hours at 4ºC and 141,000 x g resulted in a pellet of nuclei. The nuclei were lysed in an adequate volume of lysis buffer (10 mM HEPES-KOH pH 7.9, 100 mM KCl, 3 mM $MgCl_2$, 0.1 mM EDTA, 20% glycerol) and extracted by drop-wise addition of 3 M KCl until a final concentration of 400 mM was achieved. The samples were kept on ice for 20 minutes. Ultracentrifugation for 1 hour at 4ºC and 300,000 x g eliminated cellular debris. The supernatant corresponding to the nuclear extract was snap frozen in liquid nitrogen and stored at -80ºC. Protein concentration determination was performed as described in section 7.5.6.

For the streptavidin protein pull-down, 2 mg of nuclear extracts were mixed with 40 µl of blocked streptavidin M280 beads (Dynal). Blocking of beads was done for 1 hour at room temperature in 1ml of HENG buffer (10 mM HEPES-KOH, pH 9, 1.5 mM $MgCl_2$, 0.25 mM EDTA, 20% glycerol, 1 mM PMSF) including 200 ng/µl ovalbumin (Sigma-Aldrich). The beads were immobilized using a magnetic rack (Dynal MPC-S) and the blocking solution was removed. Nuclear extracts were diluted with HENG buffer to adjust to a final KCl concentration of 150 mM. Igepal CA-360 was added to a 0.3% final concentration. The nuclear extract was further mixed with the beads and incubated at 4ºC for 2 hours to overnight. Using the magnetic rack, the unbound fraction was discarded and the beads washed with HENG wash buffer (10 mM HEPES-KOH, pH 9, 250 mM KCl, 1.5 mM $MgCl_2$, 0.25 mM EDTA, 0.3% Igepal CA-360, 20% glycerol, 1 mM PMSF) as follows: 2 quick rinses followed by three washes, 10 minutes each at room temperature rotating. After the last wash, the beads were resuspended in 50 µl 2x sample buffer (100 mM Tris/HCl pH 6.8, 4% (w/v) SDS, 0.2% (w/v) bromophenol blue, 20% (w/v) glycerol, 200 mM β-Mercaptoethanol) and boiled at 95ºC for 5 minutes to elute proteins. Gel electrophoresis was done as described in 7.5.2.

7.5.9 Mass spectrometry

7.5.9.1 Sample preparation, digestion and extraction

Excised bands were diced, placed in 0.5 ml tubes (Bioquote) and de-stained in 200 µl 50% acetonitrile (CAN, Rathburn)/50% 10 mM triethylammonium bicarbonate (TEAB, Sigma-Aldrich) overnight. On removal of the de-stain solution the gel pieces

were swollen in 200 µl 10 mM TEAB for 10 minutes. This was removed and 200 µl ACN was used to dehydrate the gel pieces for 10 minutes. After removal of ACN the gel pieces were fully dehydrated in a SpeedVac (ThermoSavant) for 15 minutes. The gel pieces were reduced with 200 µl 10mM dithiothreitol (DTT, Sigma-Aldrich) in 10 mM TEAB for 45 minutes at 50˚C on a heating block. The DTT was removed and the gel pieces were alkylated with 200 µl 50 mM iodoacetamide (IAA) for 60 minutes at room temperature in darkness. This solution was removed and gel pieces were washed with 200 µl 10 mM TEAB. After its removal 200 µl ACN was added and subsequently dehydrated for 15 minutes in a SpeedVac, followed by a repetition of the washing. Porcine Trypsin (Promega) was re-suspended in 10 mM TEAB and a 10 µl aliquot containing 50 ng of trypsin was administered to the dehydrated gel pieces and left to re-swell on ice. After 20 minutes 30 µl of 10 mM TEAB was added and incubated for 16 hours at 37ºC. Digests were placed on dry ice for 5 minutes, allowed to thaw and the extract transferred to 0.2 ml PCR tubes (Bioquote). 30 µl of 10% ACN/5% formic acid (BDH) was added to gel pieces and placed in a sonicator (Jencons) for 15 minutes. The resulting extract was transferred to the PCR tubes. This was repeated once and the whole extract concentrated to dryness in a SpeedVac. Two separate 30 µl aliquots of HPLC Grade water (Rathburn) were administered to the extracts after each dry-down with all samples being stored dry at -20ºC until analysis.

7.5.9.2 NanoLC-MS/MS

The dried digest was reconstituted in 8 µl 1% formic acid and 2-6 µl (crudely determined by band intensity inspection) was analysed via electrospray on a QTOF 6510 mass spectrometer with Chip Cube™ source interface and 1200 series HPLC running MassHunter B.01.03 (Agilent Technologies). The samples were run with an automated acquisition method using an integrated 40 nl enrichment column, a 150 mm analytical column (both 300 Å C18 packing) and electrospray needle. The peptides were loaded onto the enrichment column at 3 µl/min in A buffer (0.1% formic acid) with a sample flush out factor of 5 µl and an injection flush volume of 10 µl. The enrichment column was then switched in-line with the analytical column that was equilibrated at 10% B buffer (80% acetonitirile/0.1% formic acid) and the following gradient was run at 300 nl/min:

Time	% B buffer
0	10
2	20
10	70
11	100
16	100
17	10

Table 7.17 Gradient for NanoLC-MS/MS.

MS data was acquired in the 290-2500 m/z (mass-to-charge) range at a scan rate of 6 spectra/second and MS/MS data was acquired in the 57-3000 m/z range at a scan rate of 4 spectra/second. The 3 highest peaks in an MS spectrum above 1000 counts were targeted for MS/MS with charge state preference being 3, 2, >3, unknown and the same m/z mass was actively excluded from fragmentation for 0.1 minutes. An internal reference mass of 299.294457 was introduced as per manufacturers' recommendations for calibration.

Data was exported as mzdata.xml within the MassHunter qualitative analysis software with no filters applied and searched against the NCBInr 20080210 database, on a Mascot in-house server version 2.2.04 (Matrix Science) using Mascot Daemon version 2.2.2 (Matrix Science). The search parameters were: peptide tolerances of 10 ppm and fragment tolerances of 0.05 Da with 1 missed cleavage and carboamidomethylation of cysteines as a fixed modification and oxidation of methionine, protein N-terminally acetylated, Gln>pyro-Glu as variable modifications. The Mascot generated search result files (*.dat) were loaded into Scaffold software 2.1 (Proteome Science). Peptide identifications were accepted if they could be established at greater than 20% probability as specified by the Peptide Prophet algorithm (Keller et al., 2002). Protein identifications were accepted if they could be established at greater than 99% probability and contained at least 2 identified peptides. Protein probabilities were assigned by the Protein Prophet algorithm (Nesvizhskii et al., 2003).

7.6 Protein-DNA interaction studies

7.6.1 bioChIP experiments

7.6.1.1 bioChIP from cultured cells

Chromatin immunoprecipitation (ChIP) from cultured cells was performed using the buffer formulations from the Upstate (now Milipore) ChIP Assay Kit. 10^7 cells were fixed by adding formaldehyde (Sigma-Aldrich) at a final concentration of 1% directly to the growth medium. Cells were incubated at 37ºC for 10 minutes. Crosslinking was stopped by adding 1/20 volume of 2.5 M glycine and further incubation at room temperature for 5 minutes. Next, cells were washed twice with cold PBS and scraped in 1 ml PBS. Cells were pelleted for 4 minutes at 4ºC and 400 x g and subsequently taken up in 5 volumes of lysis buffer (1% SDS, 10 mM EDTA, 50 mM Tris pH 8.1). Lysis was allowed to perform for 10 minutes on ice. Sonication of the chromatin was performed using the Bioruptor (diagenode) at setting 'H' for 10 times 30 seconds ON, 1 minute OFF. Samples are spun at 16,000 x g for 10 minutes at 4ºC and the chromatin aliquoted and stored at -80ºC. An aliquot was taken to confirm shearing of chromatin by agarose gel electrophoreses.

For the bioChIP, 20 µl of streptavidin M280 beads were blocked with 40 µl sonicated herring sperm DNA (Sigma-Aldrich) in 1 ml of ChIP dilution buffer (0.01% SDS, 1.1% Trition X-100, 1.2 mM EDTA, 16.7 mM Tris/HCl pH8.1, 167 mM NaCl) and rotated for 1 hour at room temperature. Before adding to the chromatin, beads were washed twice in ChIP dilution buffer. Chromatin was thawed at 4ºC on a rotating wheel and diluted with chromatin dilution buffer including protease inhibitors (Complete EDTA-free, Roche) to give a final volume of 1 ml. 20 µl of chromatin solution were taken and kept as Input fraction. Binding of chromatin to streptavidin beads was done overnight at 4ºC on a rotating wheel. The next day, beads were washed using the magnetic rack with 1 ml of each once: low salt immune complex wash buffer (0.1% SDS, 1% Triton X-100, 2 mM EDTA, 20 mM Tris HCl, pH 8.1, 150 mM NaCl), high salt immune complex wash buffer (0.1% SDS, 1% Triton X-100, 2 mM EDTA, 20 mM Tris HCl, pH 8.1, 500 mM NaCl), LiCl immune complex wash buffer (0.25 M LiCl, 1% Igepal CA-630, 1% deoxycholic acid (sodium salt), 1 mM EDTA, 10 mM Tris pH 8.1) and twice with 1 ml of TE. Elution was done by reversing the crosslinks in 500 µl of ChIP elution buffer (0.1% $NaHCO_3$, 1% SDS and 200 mM NaCl) and incubation at

65ºC for 6 hours. To 20 µl of input 480 µl of elution buffer was added and incubated as above. This was followed by proteinase K (Roche) treatment at 45ºC for 15 minutes and phenol/chloroform extraction. DNA was precipitated by adding 20 µg of glycogen, 50 µl of 3 M NaOAc pH 5.2 and 0.9 ml isopropanol and further incubation at -20ºC for 20 minutes. Samples were centrifuged at 16,000 x g and 4ºC for 15 minutes and washed with 70% ethanol. Finally, the DNA was resuspended in 200 µl of water.

For analysis of promoter sequences quantitative PCR was performed using the Platinum SYBR Green qPCR SuperMix-UDG with ROX (Invitrogen) chemistry including 4 µl of eluted DNA and 10 µM of each primer (Table 7.18 and Table 7.19). Reactions were run on the ABI 7900HT (Applied Biosystems) real time PCR machine and analysed using the SDS 1.9.1 software (Applied Biosystems). Enrichment of specific promoter sequences was calculated using the comparative C_T method (Litt et al., 2001). The formula $2^{Ct(IP)-Ct(Ref)}$ was used to calculate the enrichment of bound DNA over input.

Primer position	Forward primer	Reverse primer
EKLF enhancer	5'- CTG GCC CCC CTA CCT GAT -3'	5'- GGC TCC CTT TCA GGC ATT ATC -3'
EKLF basic promoter	5'- TAT CGC ACA CAC CCC TCC TT -3'	5'- CCC ACA TCT GAT TGG CTG TCT -3'
EKLF negative	5'- TGC TCC CCA CTA TGA TAA TGG A -3'	5'- GCC ACA ACC AAA GAA GAC ATT TT -3'
necdin	5'- GGT CCT GCT CTG ATC CGA AG -3'	5'- GGG TCG CTC AGG TCC TTA CTT -3'

Table 7.18 Primer sequences for amplification of *EKLF* (see Figure 3.1 for diagram of the *EKLF* promoter) and *necdin* promoter fragments.

Primer position	Forward primer	Reverse primer
mHes1_1	5'- TCC TCC CAT TGG CTG AAA GT -3'	5'- GCG AAC GGC TCG TGT GA -3'
mHes1_2	5'- GCC AGA CCT TGT GCC TAG C -3'	5'- TTC TTT CCC ACA GTA ACT TTC AGC -3'
mHes1 negative	5'- GGA CGG TAA GGG CAT GTT TA -3'	5'- TTC CCG CTC GAA CTC TGT AT -3'
mGAPDH	5'- GTG GGC ACT GTA CGG GTC TA -3'	5'- CAT CAC GTC CTC CAT CAT CC -3'
hHes1	5'- CCT CCC ATT GGC TGA AAG T -3'	5'- GGC CTC TAT ATA TAT CTG GGA CTG C -3'
hHes1 upstream	5'- GGC AGC TAC CAC GTC TCT G -3'	5'- GCC TGA GGA CTT GAA GCT TTT -3'
hHes1 negative	5'- CCA GAC CAT GTT CCC TGA AT -3'	5'- CTT AGT CGT GGG CTG GAG AG -3'
hGAPDH	5'- CTC TGC TCC TCC TGT TCG AC -3'	5'- TAG CCT CCC GGG TTT CTC -3'
hc-Myc	5'- CCC TGT GGA GAG CAC TCA TTT -3'	5'- CCC GCA GGA GCC TTG TAG -3'
hc-Myc negative	5'- CAG GGA GCA AAC AAA TCA TGT -3'	5'- ACT GTA TGT AAC CCG CAA ACG -3'

Table 7.19 Mouse (m) and human (h) qPCR primer sequences for validation of NICD bioChIP experiments from mouse C3H10T½ [NICD^{BAP}; BirA] and human MCF10A [NICD^{BAP}; BirA] cell lines.

7.6.1.2 bioChIP from retina tissue

5 day old (P5) mouse pups from *Rosa26*$^{BirA/BirA}$ and *Notch1*$^{BAP/BAP}$;*Rosa26*$^{BirA/BirA}$ strains were injected sub-cutaneously with 100 μg/g of γ-secretase inhibitor, N-[(3,5-Difluorophenyl)acetyl]-L-alanyl-2-phenyl]glycin e-1,1-dimethylethyl ester (DAPT; Calbiochem). After 3 hours pups were killed by decapitation, eyes harvested and retinas dissected in ice-cold PBS. Crosslinking of retinas was performed by adding 27 μl of 36.5% formaldehyde (Sigma-Aldrich) to 1 ml of PBS including protease inhibitors (Complete EDTA-free, Roche). Following the homogenisation of the retinas using a Dounce homogeniser, the samples were incubated for 10 minutes at room temperature with gentle agitation. 1/20 volume of 2.5 M glycine was added to stop the crosslinking and further incubation for 5 minutes at room temperature. Samples were centrifuged at

4ºC and 16,000 x g for 5 minutes, washed in ice-cold PBS plus protease inhibitors and spun again. Fixed retinas were snap frozen in liquid nitrogen and stored at -80ºC.

Chromatin preparation and bioChIP was carried out using a modified protocol for tissue ChIP from the Farnham Lab (http://www.genomecenter.ucdavis.edu/farnham/protocols/tissues.html). Pellet volume of pooled retinas (20-30) was measured and retinas subsequently lysed in 6 volumes of cell lysis buffer (5 mM PIPES pH 8.0, 85 mM KCl, 0.5% Igepal CA-630 and protease inhibitors added fresh) for 10 minutes on ice. The suspension was dounced with 5 strokes to aid nuclei release before centrifugation at 1,000 x g and 4ºC for 5 minutes. Nuclei were lysed in 5 volumes of nuclei lysis buffer (50 mM Tris/HCl pH 8.1, 10 mM EDTA, 1% SDS, protease inhibitors added fresh). Lysis was allowed to proceed for 20 minutes on ice. Samples were flash frozen in liquid nitrogen and thawed once. Sonication of chromatin was done using the Bioruptor (diagenode) at setting 'high (H)' for 10 cycles of 30 seconds ON and 1 minute OFF. After centrifugation at 16,000 x g and 4ºC for 15 minutes the supernatant corresponding to the chromatin solution was aliquoted and stored at -80ºC. An aliquot was used to check the quality of the chromatin.

For the bioChIP, streptavidin M-280 beads were blocked with 1 mg/ml BSA (Sigma-Aldrich) and 0.4 mg/ml single stranded herring sperm DNA (Sigma-Aldrich) in dialysis buffer (2 mM EDTA, 50 mM Tris/HCl pH 8.0) for 2 hours at 4ºC rotating. The beads were taken up in an equivalent volume of dialysis buffer and 1mM PMSF added. For each 200 µl aliquot of chromatin 800 µl of ChIP dilution buffer (0.01% SDS, 1.1% Triton X-100, 1.2 mM EDTA, 16.7 mM Tris/HCl pH 8.1, 167 mM NaCl) was added. 10% of input was taken from the chromatin solution and stored at -20ºC. 20 µl of blocked streptavidin beads were added to the chromatin and incubated overnight at 4ºC on a rotating wheel. Beads were further washed twice with dialysis buffer including 0.2% Sarkosyl and three times with IP wash buffer (100 mM Tris/HCL pH 8, 500 mM LiCl, 1% Igepal CA-630, 1% deoxycholic acid) at room temperature for 3 minutes each. Bound chromatin was eluted by adding 200 µl of elution buffer (50 mM $NaHCO_3$, 1% SDS) and NaCl to a final concentration of 0.5 M. Samples were incubated at 95ºC for 15 minutes. Input samples were processed as bioChIP samples apart from the fact that they were also treated with RNase and proteinase K. Purification of DNA was done using the QIAquick PCR Purification Kit (Qiagen) and elution in 50 µl of H_2O.

For high throughput sequencing, samples were sent to the Cancer Research UK Leeds Institute of Molecular Medicine and run on an Illumina GAII sequencer machine. Sample preparation and processing was done as described by the manufacturer. The data was analysed by the Cancer Research UK Bioinformatics and Biostatistics department.

Sample	Mouse strain	DAPT treatment [w or w/o]
Input_BirA neg	*Rosa26*$^{BirA/BirA}$	w/o
ChIP_BirA neg	*Rosa26*$^{BirA/BirA}$	w/o
Input_BirA pos	*Rosa26*$^{BirA/BirA}$	w
ChIP_BirA pos	*Rosa26*$^{BirA/BirA}$	w
Input_Bio-Notch neg	*Notch1*$^{BAP/BAP}$;*Rosa26*$^{BirA/BirA}$	w/o
ChIP_ Bio-Notch neg	*Notch1*$^{BAP/BAP}$;*Rosa26*$^{BirA/BirA}$	w/o
Input_ Bio-Notch pos	*Notch1*$^{BAP/BAP}$;*Rosa26*$^{BirA/BirA}$	w
ChIP_ Bio-Notch pos	*Notch1*$^{BAP/BAP}$;*Rosa26*$^{BirA/BirA}$	w

Table 7.20 Samples from Notch bioChIP experiment for sequencing. w, with; w/o, without.

7.6.1.3 Analysis of high-throughput sequencing

In order to call peaks of alignments Model-based Analysis of ChIP-Seq (MACS) was used (Zhang et al., 2008). However, this produced no peaks at a convincing false detection threshold. Examination of the data revealed that this was most likely due to an imbalance of forward and reverse strand alignments of reads, more specifically, although "reverse" alignments were being made, those regions displaying apparent peaks of forward alignments did not display corresponding peaks of reverse alignments, thus confounding the MACS algorithm.

In order to investigate the possible effects of nucleotide calling bias (Dohm et al., 2008), the R package Rolexa (Rougemont et al., 2008) was used to recall the sequences from the raw intensity files. Rolexa is specifically designed to combat the "A" bias, which has been observed on the Illumina platform. Once re-called, sequences were

aligned by Bowtie (Langmead et al., 2009) and peaks called by MACS. Unfortunately the forward alignment bias was still present resulting, once again, in a failure to detect peaks.

Standard approaches have failed to call peaks and therefore rather than using paired forward and reverse alignments to identify excess binding sites excess binding, whether forward or reverse, irrespective of pairing was considered. Using the Bioconductor (Gentleman et al., 2004) package "Short Reads" (http://bioconductor.org/packages/2.4/bioc/html/ShortRead.html) so called "pileups" were created of ELAND aligned reads; a pileup is simply a count of how many reads align across a particular nucleotide. Each aligned read (36bp) was adjusted to the full fragment length (300bp) taking into account directionality (forward alignments were extended 264 bp 3', reverses extended 264 bp 5' to correspond with the alignments reporting standards). Alignments were then filtered so that each 300 bp stretch of the genome was covered exactly by at most one forward and at most one reverse alignment. Finally, for each nucleotide, a count was made of how many alignments covered that nucleotide. This process was carried out for each experiment and, to control for "background", the results from the control (BirA) were subtracted from the Bio-Notch samples, and the results examined for peaks (resulting in four experimental conditions: Input neg and ChIP neg, w/o DAPT; Input pos and ChIP pos w DAPT).

Since many chromosomes displayed evidence of apparent PCR artefact spikes (Nix et al., 2008) (Chromosome 11 being a particularly good example), approximately half of the chromosomes needed to have the peak threshold adjusted to compensate for this skew. However, after these corrections in all four of the experimental conditions, most chromosomes had a threshold between 8 and 10 (that is, any nucleotide covered by more than 10 reads was deemed to be a peak.

Wiggle files (http://genome.ucsc.edu/goldenPath/help/wiggle.html) were produced to aid visualization on the UCSC genome browser (http://genome.ucsc.edu/cgi-bin/hgGateway) and those peaks, which covered a gene in the UCSC database were further annotated from the Ensembl (http://www.ensembl.org/index.html) database using biomaRt (http://bioconductor.org/packages/2.4/bioc/html/biomaRt.html).

All pileup analyses subsequent to the Solexa pipeline (i.e. post ELAND) were carried out with scripts written in R 2.8.1, using packages from Bioconductor 2.3

7.6.2 Electrophoretic Mobility Shift Assay (EMSA)

For *Hes7* promoter EMSA 18 fragments of 300 bp length covering 5 kb of the Hes7 promoter were amplified by PCR from the *pENTR-Hes7_5kp* template using *PfuTurbo* DNA polymerase (section 7.1.1 and Table 7.21). Purification of DNA fragments was performed through elution from a 1.2% agarose gel using QIAquick Gel Purification Kit (Qiagen). DNA was eluted in H_2O and the concentration determined by NanoDrop (Thermo Scientific) measurement. A 300 bp fragment containing the 6 N-box repeat from *pN6-luc* served as positive control whereas a 300 bp random vector sequence was chosen as negative control.

Fragments were labelled with T4 Polynucleotide Kinase (PNK; New England Bioloabs) and γ^{32}P-dATP (GE Healthcare) in kinase buffer (0.5 M Tris/HCL pH 7.9, 0.1 M $MgCl_2$, 50 mM DTT, 10 mM spermidine, 1 mM EDTA) for 37 minutes at 37ºC. The enzyme was inactivated by incubation at 68ºC for 15 minutes. For the binding reaction 3 fmol of the DNA fragment was mixed with 30 pmol of $Hes7^{bHLH}$ protein (section 7.5.1) and incubated in binding buffer (25 mM HEPES pH 7.5, 100 mM KCl, 20% glycerol, 0.1% Igepal CA-630, 10 μM $ZnSO_4$, 50 mM DTT) with 0.5 μg Poly [d(I-C)] (Roche), 0.18 M BSA for 30 minutes on ice. Reactions were run on a NuPAGE precast 6% DNA retardation gel at 100 V constant and 4ºC. The gel was dried on Whatman paper, sealed with Saran Wrap and exposed to KODAK BioMax MS Film for 1 hour at -80ºC.

Mutation of N-boxes was achieved through the QuikChange XL site directed mutagenesis Kit (Stratagene) according to the manufacturers' guidelines (Table 7.22).

Fragment	Forward primer	Reverse primer
1	5'- GCC TTA TTA TAC AGC TTT ATG G -3'	5'- TGC TCC TCC GGA CCC TTC -3'
2	5'- TGT GGG AAT TGA GTA GAA GAG ACA -3'	5'- GTA TAA TAA GGC GGG ACC CAA C -3'
3	5'- TGT AAA CGG AAA GGT ATC GCT TC -3'	5'- GCG CCG TTG TAT CTG TCT CTT C -3'
4	5'- GCC TTC TTG TCG TGT TAA ATT TCG -3'	5'- GCC GAG AAG CGA TAC CTT TCC -3'
5	5'- CAT TTG GCT GAA GTA GGG GAA GG -3'	5'- GGG CGA AGT GCC TGA GAA G -3'
6	5'- TTC TCA GAG GCA GAT CCA ATC C -3'	5'- CCC TCA GTA CAT CCC ACC TTC C -3'
7	5'- TGC GGA GTC AGA GAA TAA TTT TGG -3'	5'- GGA TTG GAT CTG CCT CTG AGA A -3'
8	5'- AAC TGG AAT GCC CAG GAC TGA A -3'	5'- CGG CTT GGA CGT TCC AAA ATT A -3'
9	5'- AGG GAG CTG CAG GGA ACT GG -3'	5'- GCA CCT TTT CCC CAT ATT CAG TCC -3'
10	5'- ATT CCG AGA CCA GGC TGA AAC -3'	5'- GCT CGC ACC CCC AGT TC -3'
11	5'- TTC TGC CTT CTT GGA TGT TTC C -3'	5'- TTC TCC TCT CTG GGC TGT CTC C -3'
12	5'- CTT ACA CCT GCC ATC CCC AAA T -3'	5'- CCA TTT TGA CGG GGA TGG T -3'
13	5'- GGA GAT GGA GGG TAT GAT GTT GG -3'	5'- GAA CCC GGA ACA GAG AAT TTG G -3'
14	5'- GGT GAA TCA GCC TTG CAC TTG A -3'	5'- ATA CCC TCC ATC TCC CGA CCA C -3'
15	5'- CCT GTC TCA GAA ATG GGT ACA ACG -3'	5'- GCA GAA GAA CTT CAA GTG CAA GG -3'
16	5'- ATT GGC TCT GGG CCA CTT C -3'	5'- ATC ATC ACA GTC ATC GTT GTA CCC -3'
17	5'- CCA GTT CAT TCA GCT GGT CTC C -3'	5'- ACG GAA GTG GCC CAG AGC -3'
18	5'- CAC CTC CCT AGA GGC CTA CAT G -3'	5'- CTT CTC AGG CCC TCC AGC -3'

Table 7.21 PCR primer sequences for amplification of *Hes7* promoter fragments for EMSA.

Fragment	Forward primer	Reverse primer
N-box1 Mut1	5'- CCG GGA GCC TCT TGC CGG GGT CCT TGA G -3'	5'- CTC AAG GAC CCC GGC AAG AGG CTC CCG G -3'
N-box1 Mut2	5'- CTT TCC GGG AGC CAC GTG CCG GGG TCC -3'	5'- GGA CCC CGG CAC GTG GCT CCC GGA AAG -3'
N-box1 Mut1+2	5'- CTT TCC GGG AGC CAC TTG CCG GGG TCC TTG AG -3'	5'- CTC AAG GAC CCC GGC AAG TGG CTC CCG GAA AG -3'
N-box10 Mut1	5'- GGG TCG CTCA TAA GTG GCC CCA GCA GG -3'	5'- CAC CTG CTG GGG CCA CAT GTG AGC GAC CC -3'
N-box10 Mut2	5'- GGG TCG CTC ACA TGT GGC CCC AGC AGG TG -3'	5'- CAC CTG CTG GGG CCA CAT GTG AGC GAC CC -3'

Table 7.22 Primer sequences to generate mutations in N-boxes of *Hes7* promoter fragments F1 and F10.

For EMSA of 30 bp oligonucleotides from fragment 1 (F1), HPLC purified oligonucleotides (Sigma-Aldrich; Table 7.23) were annealed in annealing buffer (10 mM Tris/HCl pH 7.5, 1 mM EDTA, 50 mM KCl) for 15 minutes at 99ºC and cooling to 4ºC at 0.1ºC/second. Labelling of oligonucleotide probes and binding to the Hes7^{bHLH} protein was done as above.

Oligo	Forward primer	Reverse primer
1	5'- GTT GGG TCC CGC CTT ATT ATA CAG CTT TAT -3'	5'- ATA AAG CTG TAT AAT AAG GCG GGA CCC AAC -3'
2	5'- TTA TGG TCC TTA AAC CAG CCT GTG GCC CCT -3'	5'- AGG GGC CAC AGG CTG GTT TAA GGA CCA TAA -3'
3	5'- CCC TTC CTC CCC TCA CTT CCC ACA TTT GGG -3'	5'- CCC AAA TGT GGG AAG TGA GGG GAG GAA GGG -3'
4	5'- TGG GGC TAG TTC CTC CCC TTC CCC TCC CCC -3'	5'- GGG GGA GGG GAA GGG GAG GAA CTA GCC CCA -3'
5	5'- TCC CCC TTC ACT CCC TGC CTT TCC GGG AGC -3'	5'- GCT CCC GGA AAG GCA GGG AGT GAA GGG GGA -3'
6	5'- GGG AGC CTC GTG CCG GGG TCC TTG AGC TGG -3'	5'- CCA GCT CAA GGA CCC CGG CAC GAG GCT CCC -3'
7	5'- CTG GGC ATC TAG GGG CTG AAG GGG GCG GGG -3'	5'- CCC CGC CCC CTT CAG CCC CTA GAT GCC CAG -3'
8	5'-GGG CCG GGC CCT AGC CCT CCT ACC CTG CAG-3'	5'- CTG CAG GGT AGG AGG GCT AGG GCC CGG CCC -3'
9	5'- CAG CGG CGG GAT ATA AGG ATC TAG GCA GCA -3'	5'- TGC TGC CTA GAT CCT TAT ATC CCG CCG CTG -3'
10	5'- GCA CGC GCT GAG TCC ACC GAA GGG TCC GGA GGA GCA -3'	5'- TGC TCC TCC GGA CCC TTC GGT GGA CTC AGC GCG TGC -3'

Table 7.23 Oligonucleotide sequences of *Hes7* promoter fragment F1 for EMSA.

7.6.3 DNaseI footprinting assay

7.6.3.1 Labelling of DNA fragments

Hes7 promoter fragments F1 (-269 bp - +1 bp) and F10 (-2611 bp - -2318 bp) were subcloned into *pCR-BluntII-TOPO* (Invitrogen) and 10 μg of each plasmid cut with *Hind*III (New England Biolabs) overnight. Digests were run on a 1% agarose gel and DNA purified by QIAquick gel extraction Kit (Qiagen). Probes were labelled by Klenow (New England Biolabs) fill-in with 50 μCi α-^{32}P dATP (GE Healthcare) and 50 μCi α-^{32}P dCTP for 30 minutes at room temperature. 1 μl of 10 mM dNTPs was added and the reaction incubated for another 15 minutes at room temperature. Unincorporated nucleotides were removed using Micro Bio-Spin P-30 Tris chromatography columns (Bio-Rad) according to the manufacturers' guidelines. The DNA was further precipitated with ethanol and digested with *Eco*RV (New England Biolabs). Probes were purified from a 6% non-denaturating polyacrylamide gel and Cerenkov counted in a scintillation counter. 10,000 cpm of each probe were used per DNaseI footprinting reaction.

7.6.3.2 DNaseI footprinting binding reaction

DNaseI footprinting reactions contained 30-300 ng of Hes7^{bHLH} (1-83 aminoacids), 10,000 cpm of 5' radiolabelled probe in DNaseI buffer (200 mM Tris/HCl pH7.5, 500 mM NaCl, 30 mM $MgCl_2$, 10 mM $CaCl_2$, 20 mM DTT, 10 μM $ZnCl_2$, 20% glycerol, 1 mg/ml BSA, protease inhibitors added fresh) with 2.5 ng Poly [d(I-C)] (Roche), 3 mM spermidine. After incubating at room temperature for 30 minutes, 0.25 units of DNaseI (Worthingtons) were added for 5 minutes on ice. Reactions were stopped with stop buffer (20 mM Tris HCl pH7.5, 50 mM EDTA, 2% SDS, 0.25 mg linear acrylamide, 0.2 mg proteinase K) at 50ºC for 1 hour. The DNA was precipitated with 10 μl of 1 M LiCl and 3 volumes 96% ethanol on dry ice for 30 minutes. After washing with 70% ethanol the DNA was pelleted and resuspended in 6 μl of formamide loading buffer (95% formamide, 20 mM EDTA, 0.01% (w/v) xylene cyanol, 0.01% (w/v) bromophenol blue) denaturated and run on a 6% denaturating gel (SequaGel system, National Diagnostics: 4.8 ml SequaGel concentrate, 1 ml 10xTBE, 14.2 ml SequaGel diluent, 30 μl 20% ammonium persulfate (Sigma-Aldrich) and 30 μl N,N,N',N'-Tetramethylethylenediamine (TEMED, Sigma-Aldrich). Samples were run at 16 mAmps in 0.5x TBE for 5 hours. Gels were transferred onto 3MM Whatman paper

and dried on a gel drier at 80ºC for 45 minutes. The footprint was visualised by overnight exposure to a KODAK BioMax MS film at -80ºC.

7.6.4 *Hes7* promoter comparison

Alignment of *Hes7* promoter sequences was done using the PipMaker programme according to the guidelines (pipmaker.bx.psu.edu/pipmaker/pip-instr.html; (Schwartz et al., 2000).

Accession numbers of sequences used are *Mus musculus* (mouse; ENSMUSG00000023781), *Rattus norvegicus* (rat; ENSRNOG00000007391), *Homo sapiens* (human; ENSG00000179111), *Macaca mulatta* (macaque; ENSMMUG00000019851), *Canis lupus familiaris* (dog; ENSCAFG00000016957), *Bos taurus* (cow; ENSBTAG00000012436), *Monodelphis domestica* (opossum; ENSMODG00000007704), *Ornithorhynchus anatinus* (platypus; ENSOANG00000022456), *Xenopus tropicalis* (frog; XB-GENE-876464).

CHAPTER 8: References

Akazawa, C., Sasai, Y., Nakanishi, S. and Kageyama, R. (1992). Molecular characterization of a rat negative regulator with a basic helix-loop-helix structure predominantly expressed in the developing nervous system. *J Biol Chem* **267**, 21879-85.

Andrews, N. C. and Faller, D. V. (1991). A rapid micropreparation technique for extraction of DNA-binding proteins from limiting numbers of mammalian cells. *Nucleic Acids Res* **19**, 2499.

Appel, B., Marasco, P., McClung, L. E. and Latimer, A. J. (2003). lunatic fringe regulates Delta-Notch induction of hypochord in zebrafish. *Dev Dyn* **228**, 281-6.

Aroian, R. V. and Sternberg, P. W. (1991). Multiple functions of let-23, a Caenorhabditis elegans receptor tyrosine kinase gene required for vulval induction. *Genetics* **128**, 251-67.

Artavanis-Tsakonas, S., Matsuno, K. and Fortini, M. E. (1995). Notch signaling. *Science* **268**, 225-32.

Artavanis-Tsakonas, S., Rand, M. D. and Lake, R. J. (1999). Notch signaling: cell fate control and signal integration in development. *Science* **284**, 770-6.

Aulehla, A. and Pourquie, O. (2008). Oscillating signaling pathways during embryonic development. *Curr Opin Cell Biol*.

Aulehla, A., Wehrle, C., Brand-Saberi, B., Kemler, R., Gossler, A., Kanzler, B. and Herrmann, B. G. (2003). Wnt3a plays a major role in the segmentation clock controlling somitogenesis. *Dev Cell* **4**, 395-406.

Aulehla, A., Wiegraebe, W., Baubet, V., Wahl, M. B., Deng, C., Taketo, M., Lewandoski, M. and Pourquie, O. (2008). A beta-catenin gradient links the clock and wavefront systems in mouse embryo segmentation. *Nat Cell Biol* **10**, 186-93.

Bailey, A. M. and Posakony, J. W. (1995). Suppressor of hairless directly activates transcription of enhancer of split complex genes in response to Notch receptor activity. *Genes Dev* **9**, 2609-22.

Barker, D. F. and Campbell, A. M. (1981). The birA gene of Escherichia coli encodes a biotin holoenzyme synthetase. *J Mol Biol* **146**, 451-67.

Barker, N. (2008). The canonical Wnt/beta-catenin signalling pathway. *Methods Mol Biol* **468**, 5-15.

Barolo, S., Walker, R. G., Polyanovsky, A. D., Freschi, G., Keil, T. and Posakony, J. W. (2000). A notch-independent activity of suppressor of hairless is required for normal mechanoreceptor physiology. *Cell* **103**, 957-69.

Beckett, D. (2007). Biotin sensing: universal influence of biotin status on transcription. *Annu Rev Genet* **41**, 443-64.

Beckett, D., Kovaleva, E. and Schatz, P. J. (1999). A minimal peptide substrate in biotin holoenzyme synthetase-catalyzed biotinylation. *Protein Sci* **8**, 921-9.

Bentley, D. R. Balasubramanian, S. Swerdlow, H. P. Smith, G. P. Milton, J. Brown, C. G. Hall, K. P. Evers, D. J. Barnes, C. L. Bignell, H. R. et al. (2008).

Accurate whole human genome sequencing using reversible terminator chemistry. *Nature* **456**, 53-9.

Bessho, Y., Hirata, H., Masamizu, Y. and Kageyama, R. (2003). Periodic repression by the bHLH factor Hes7 is an essential mechanism for the somite segmentation clock. *Genes Dev* **17**, 1451-6.

Bessho, Y., Miyoshi, G., Sakata, R. and Kageyama, R. (2001a). Hes7: a bHLH-type repressor gene regulated by Notch and expressed in the presomitic mesoderm. *Genes Cells* **6**, 175-85.

Bessho, Y., Sakata, R., Komatsu, S., Shiota, K., Yamada, S. and Kageyama, R. (2001b). Dynamic expression and essential functions of Hes7 in somite segmentation. *Genes Dev* **15**, 2642-7.

Blaumueller, C. M., Qi, H., Zagouras, P. and Artavanis-Tsakonas, S. (1997). Intracellular cleavage of Notch leads to a heterodimeric receptor on the plasma membrane. *Cell* **90**, 281-91.

Borneman, A. R., Gianoulis, T. A., Zhang, Z. D., Yu, H., Rozowsky, J., Seringhaus, M. R., Wang, L. Y., Gerstein, M. and Snyder, M. (2007). Divergence of transcription factor binding sites across related yeast species. *Science* **317**, 815-9.

Bray, S. (1998). Notch signalling in Drosophila: three ways to use a pathway. *Semin Cell Dev Biol* **9**, 591-7.

Bray, S. J. (2006). Notch signalling: a simple pathway becomes complex. *Nat Rev Mol Cell Biol* **7**, 678-89.

Brou, C., Logeat, F., Gupta, N., Bessia, C., LeBail, O., Doedens, J. R., Cumano, A., Roux, P., Black, R. A. and Israel, A. (2000). A novel proteolytic cleavage involved in Notch signaling: the role of the disintegrin-metalloprotease TACE. *Mol Cell* **5**, 207-16.

Bruckner, K., Perez, L., Clausen, H. and Cohen, S. (2000). Glycosyltransferase activity of Fringe modulates Notch-Delta interactions. *Nature* **406**, 411-5.

Buscarlet, M. and Stifani, S. (2007). The 'Marx' of Groucho on development and disease. *Trends Cell Biol* **17**, 353-61.

Bush, G., diSibio, G., Miyamoto, A., Denault, J. B., Leduc, R. and Weinmaster, G. (2001). Ligand-induced signaling in the absence of furin processing of Notch1. *Dev Biol* **229**, 494-502.

Camporeale, G., Giordano, E., Rendina, R., Zempleni, J. and Eissenberg, J. C. (2006). Drosophila melanogaster holocarboxylase synthetase is a chromosomal protein required for normal histone biotinylation, gene transcription patterns, lifespan, and heat tolerance. *J Nutr* **136**, 2735-42.

Camporeale, G., Oommen, A. M., Griffin, J. B., Sarath, G. and Zempleni, J. (2007). K12-biotinylated histone H4 marks heterochromatin in human lymphoblastoma cells. *J Nutr Biochem* **18**, 760-8.

Camporeale, G., Shubert, E. E., Sarath, G., Cerny, R. and Zempleni, J. (2004). K8 and K12 are biotinylated in human histone H4. *Eur J Biochem* **271**, 2257-63.

Carroll, J. S., Liu, X. S., Brodsky, A. S., Li, W., Meyer, C. A., Szary, A. J., Eeckhoute, J., Shao, W., Hestermann, E. V., Geistlinger, T. R. et al. (2005). Chromosome-wide mapping of estrogen receptor binding reveals long-range regulation requiring the forkhead protein FoxA1. *Cell* **122**, 33-43.

Cawley, S., Bekiranov, S., Ng, H. H., Kapranov, P., Sekinger, E. A., Kampa, D., Piccolboni, A., Sementchenko, V., Cheng, J., Williams, A. J. et al. (2004). Unbiased mapping of transcription factor binding sites along human chromosomes 21 and 22 points to widespread regulation of noncoding RNAs. *Cell* **116**, 499-509.

Chapman-Smith, A. and Cronan, J. E., Jr. (1999). The enzymatic biotinylation of proteins: a post-translational modification of exceptional specificity. *Trends Biochem Sci* **24**, 359-63.

Chen, J., Kang, L. and Zhang, N. (2005). Negative feedback loop formed by Lunatic fringe and Hes7 controls their oscillatory expression during somitogenesis. *Genesis* **43**, 196-204.

Chew, Y. C., Camporeale, G., Kothapalli, N., Sarath, G. and Zempleni, J. (2006). Lysine residues in N-terminal and C-terminal regions of human histone H2A are targets for biotinylation by biotinidase. *J Nutr Biochem* **17**, 225-33.

Chew, Y. C., West, J. T., Kratzer, S. J., Ilvarsonn, A. M., Eissenberg, J. C., Dave, B. J., Klinkebiel, D., Christman, J. K. and Zempleni, J. (2008). Biotinylation of Histones Represses Transposable Elements in Human and Mouse Cells and Cell Lines and in Drosophila melanogaster. *J Nutr* **138**, 2316-2322.

Chitnis, A. (2006). Why is delta endocytosis required for effective activation of notch? *Dev Dyn* **235**, 886-94.

Choi-Rhee, E., Schulman, H. and Cronan, J. E. (2004). Promiscuous protein biotinylation by Escherichia coli biotin protein ligase. *Protein Sci* **13**, 3043-50.

Chu, Y., Solski, P. A., Khosravi-Far, R., Der, C. J. and Kelly, K. (1996). The mitogen-activated protein kinase phosphatases PAC1, MKP-1, and MKP-2 have unique substrate specificities and reduced activity in vivo toward the ERK2 sevenmaker mutation. *J Biol Chem* **271**, 6497-501.

Chung, C. N., Hamaguchi, Y., Honjo, T. and Kawaichi, M. (1994). Site-directed mutagenesis study on DNA binding regions of the mouse homologue of Suppressor of Hairless, RBP-J kappa. *Nucleic Acids Res* **22**, 2938-44.

Clandinin, T. R., DeModena, J. A. and Sternberg, P. W. (1998). Inositol trisphosphate mediates a RAS-independent response to LET-23 receptor tyrosine kinase activation in C. elegans. *Cell* **92**, 523-33.

Coffman, C., Harris, W. and Kintner, C. (1990). Xotch, the Xenopus homolog of Drosophila notch. *Science* **249**, 1438-41.

Cohen, P. and Frame, S. (2001). The renaissance of GSK3. *Nat Rev Mol Cell Biol* **2**, 769-76.

Cole, S. E., Levorse, J. M., Tilghman, S. M. and Vogt, T. F. (2002). Clock regulatory elements control cyclic expression of Lunatic fringe during somitogenesis. *Dev Cell* **3**, 75-84.

Conlon, R. A., Reaume, A. G. and Rossant, J. (1995). Notch1 is required for the coordinate segmentation of somites. *Development* **121**, 1533-45.

Cooke, J. and Zeeman, E. C. (1976). A clock and wavefront model for control of the number of repeated structures during animal morphogenesis. *J Theor Biol* **58**, 455-76.

Cooper, M. T., Tyler, D. M., Furriols, M., Chalkiadaki, A., Delidakis, C. and Bray, S. (2000). Spatially restricted factors cooperate with notch in the regulation of Enhancer of split genes. *Dev Biol* **221**, 390-403.

Cronan, J. E., Jr. (1989). The E. coli bio operon: transcriptional repression by an essential protein modification enzyme. *Cell* **58**, 427-9.

D'Souza, B., Miyamoto, A. and Weinmaster, G. (2008). The many facets of Notch ligands. *Oncogene* **27**, 5148-67.

Dale, J. K., Malapert, P., Chal, J., Vilhais-Neto, G., Maroto, M., Johnson, T., Jayasinghe, S., Trainor, P., Herrmann, B. and Pourquie, O. (2006). Oscillations of the snail genes in the presomitic mesoderm coordinate segmental patterning and morphogenesis in vertebrate somitogenesis. *Dev Cell* **10**, 355-66.

Dale, J. K., Maroto, M., Dequeant, M. L., Malapert, P., McGrew, M. and Pourquie, O. (2003). Periodic notch inhibition by lunatic fringe underlies the chick segmentation clock. *Nature* **421**, 275-8.

Damen, W. G. (2007). Evolutionary conservation and divergence of the segmentation process in arthropods. *Dev Dyn* **236**, 1379-91.

Dawson, S. R., Turner, D. L., Weintraub, H. and Parkhurst, S. M. (1995). Specificity for the hairy/enhancer of split basic helix-loop-helix (bHLH) proteins maps outside the bHLH domain and suggests two separable modes of transcriptional repression. *Mol Cell Biol* **15**, 6923-31.

de Boer, E., Rodriguez, P., Bonte, E., Krijgsveld, J., Katsantoni, E., Heck, A., Grosveld, F. and Strouboulis, J. (2003). Efficient biotinylation and single-step purification of tagged transcription factors in mammalian cells and transgenic mice. *Proc Natl Acad Sci U S A* **100**, 7480-5.

de Celis, J. F. and Bray, S. (1997). Feed-back mechanisms affecting Notch activation at the dorsoventral boundary in the Drosophila wing. *Development* **124**, 3241-51.

Deftos, M. L. and Bevan, M. J. (2000). Notch signaling in T cell development. *Curr Opin Immunol* **12**, 166-72.

Del Amo, F. F., Smith, D. E., Swiatek, P. J., Gendron-Maguire, M., Greenspan, R. J., McMahon, A. P. and Gridley, T. (1992). Expression pattern of Motch, a mouse homolog of Drosophila Notch, suggests an important role in early postimplantation mouse development. *Development* **115**, 737-44.

Delwig, A. and Rand, M. D. (2008). Kuz and TACE can activate Notch independent of ligand. *Cell Mol Life Sci* **65**, 2232-43.

Demarest, R. M., Ratti, F. and Capobianco, A. J. (2008). It's T-ALL about Notch. *Oncogene* **27**, 5082-91.

Dequeant, M. L., Glynn, E., Gaudenz, K., Wahl, M., Chen, J., Mushegian, A. and Pourquie, O. (2006). A complex oscillating network of signaling genes underlies the mouse segmentation clock. *Science* **314**, 1595-8.

Dequeant, M. L. and Pourquie, O. (2008). Segmental patterning of the vertebrate embryonic axis. *Nat Rev Genet* **9**, 370-82.

Dohm, J. C., Lottaz, C., Borodina, T. and Himmelbauer, H. (2008). Substantial biases in ultra-short read data sets from high-throughput DNA sequencing. *Nucleic Acids Res* **36**, e105.

Donoviel, D. B., Hadjantonakis, A. K., Ikeda, M., Zheng, H., Hyslop, P. S. and Bernstein, A. (1999). Mice lacking both presenilin genes exhibit early embryonic patterning defects. *Genes Dev* **13**, 2801-10.

Driegen, S., Ferreira, R., van Zon, A., Strouboulis, J., Jaegle, M., Grosveld, F., Philipsen, S. and Meijer, D. (2005). A generic tool for biotinylation of tagged proteins in transgenic mice. *Transgenic Res* **14**, 477-82.

Dunty, W. C., Jr., Biris, K. K., Chalamalasetty, R. B., Taketo, M. M., Lewandoski, M. and Yamaguchi, T. P. (2008). Wnt3a/beta-catenin signaling controls posterior body development by coordinating mesoderm formation and segmentation. *Development* **135**, 85-94.

Dunwoodie, S. L. (2009). Mutation of the fucose-specific beta1,3 N-acetylglucosaminyltransferase LFNG results in abnormal formation of the spine. *Biochim Biophys Acta* **1792**, 100-11.

Efstratiadis, A., Szabolcs, M. and Klinakis, A. (2007). Notch, Myc and breast cancer. *Cell Cycle* **6**, 418-29.

Ellisen, L. W., Bird, J., West, D. C., Soreng, A. L., Reynolds, T. C., Smith, S. D. and Sklar, J. (1991). TAN-1, the human homolog of the Drosophila notch gene, is broken by chromosomal translocations in T lymphoblastic neoplasms. *Cell* **66**, 649-61.

Evrard, Y. A., Lun, Y., Aulehla, A., Gan, L. and Johnson, R. L. (1998). lunatic fringe is an essential mediator of somite segmentation and patterning. *Nature* **394**, 377-81.

Fehon, R. G., Kooh, P. J., Rebay, I., Regan, C. L., Xu, T., Muskavitch, M. A. and Artavanis-Tsakonas, S. (1990). Molecular interactions between the protein products of the neurogenic loci Notch and Delta, two EGF-homologous genes in Drosophila. *Cell* **61**, 523-34.

Feller, J., Schneider, A., Schuster-Gossler, K. and Gossler, A. (2008). Noncyclic Notch activity in the presomitic mesoderm demonstrates uncoupling of somite compartmentalization and boundary formation. *Genes Dev* **22**, 2166-71.

Fernandez-Suarez, M., Chen, T. S. and Ting, A. Y. (2008). Protein-protein interaction detection in vitro and in cells by proximity biotinylation. *J Am Chem Soc* **130**, 9251-3.

Fisher, A. L., Ohsako, S. and Caudy, M. (1996). The WRPW motif of the hairy-related basic helix-loop-helix repressor proteins acts as a 4-amino-acid transcription repression and protein-protein interaction domain. *Mol Cell Biol* **16**, 2670-7.

Fleming, R. J., Gu, Y. and Hukriede, N. A. (1997). Serrate-mediated activation of Notch is specifically blocked by the product of the gene fringe in the dorsal compartment of the Drosophila wing imaginal disc. *Development* **124**, 2973-81.

Ford, C. F., Suominen, I. and Glatz, C. E. (1991). Fusion tails for the recovery and purification of recombinant proteins. *Protein Expr Purif* **2**, 95-107.

Fortini, M. E. (2002). Gamma-secretase-mediated proteolysis in cell-surface-receptor signalling. *Nat Rev Mol Cell Biol* **3**, 673-84.

Freeman, M. (2000). Feedback control of intercellular signalling in development. *Nature* **408**, 313-9.

Friedmann, D. R., Wilson, J. J. and Kovall, R. A. (2008). RAM-induced allostery facilitates assembly of a notch pathway active transcription complex. *J Biol Chem* **283**, 14781-91.

Fryer, C. J., Lamar, E., Turbachova, I., Kintner, C. and Jones, K. A. (2002). Mastermind mediates chromatin-specific transcription and turnover of the Notch enhancer complex. *Genes Dev* **16**, 1397-411.

Fryer, C. J., White, J. B. and Jones, K. A. (2004). Mastermind recruits CycC:CDK8 to phosphorylate the Notch ICD and coordinate activation with turnover. *Mol Cell* **16**, 509-20.

Furuyama, T. and Henikoff, S. (2006). Biotin-tag affinity purification of a centromeric nucleosome assembly complex. *Cell Cycle* **5**, 1269-74.

Gajewski, M., Sieger, D., Alt, B., Leve, C., Hans, S., Wolff, C., Rohr, K. B. and Tautz, D. (2003). Anterior and posterior waves of cyclic her1 gene expression are differentially regulated in the presomitic mesoderm of zebrafish. *Development* **130**, 4269-78.

Galceran, J., Sustmann, C., Hsu, S. C., Folberth, S. and Grosschedl, R. (2004). LEF1-mediated regulation of Delta-like1 links Wnt and Notch signaling in somitogenesis. *Genes Dev* **18**, 2718-23.

Gale, N. W., Dominguez, M. G., Noguera, I., Pan, L., Hughes, V., Valenzuela, D. M., Murphy, A. J., Adams, N. C., Lin, H. C., Holash, J. et al. (2004). Haploinsufficiency of delta-like 4 ligand results in embryonic lethality due to major defects in arterial and vascular development. *Proc Natl Acad Sci U S A* **101**, 15949-54.

Ge, C., Liu, T., Hou, X. and Stanley, P. (2008). In vivo consequences of deleting EGF repeats 8-12 including the ligand binding domain of mouse Notch1. *BMC Dev Biol* **8**, 48.

Gentleman, R. C., Carey, V. J., Bates, D. M., Bolstad, B., Dettling, M., Dudoit, S., Ellis, B., Gautier, L., Ge, Y., Gentry, J. et al. (2004). Bioconductor: open software development for computational biology and bioinformatics. *Genome Biol* **5**, R80.

Giagtzoglou, N., Alifragis, P., Koumbanakis, K. A. and Delidakis, C. (2003). Two modes of recruitment of E(spl) repressors onto target genes. *Development* **130**, 259-70.

Giudicelli, F., Ozbudak, E. M., Wright, G. J. and Lewis, J. (2007). Setting the tempo in development: an investigation of the zebrafish somite clock mechanism. *PLoS Biol* **5**, e150.

Gomez, C., Ozbudak, E. M., Wunderlich, J., Baumann, D., Lewis, J. and Pourquie, O. (2008). Control of segment number in vertebrate embryos. *Nature* **454**, 335-9.

Gordon, W. R., Vardar-Ulu, D., Histen, G., Sanchez-Irizarry, C., Aster, J. C. and Blacklow, S. C. (2007). Structural basis for autoinhibition of Notch. *Nat Struct Mol Biol* **14**, 295-300.

Gray, M., Moens, C. B., Amacher, S. L., Eisen, J. S. and Beattie, C. E. (2001). Zebrafish deadly seven functions in neurogenesis. *Dev Biol* **237**, 306-23.

Gridley, T. (2003). Notch signaling and inherited disease syndromes. *Hum Mol Genet* **12 Spec No 1**, R9-13.

Griffin, K. J., Amacher, S. L., Kimmel, C. B. and Kimelman, D. (1998). Molecular identification of spadetail: regulation of zebrafish trunk and tail mesoderm formation by T-box genes. *Development* **125**, 3379-88.

Grosveld, F., Rodriguez, P., Meier, N., Krpic, S., Pourfarzad, F., Papadopoulos, P., Kolodziej, K., Patrinos, G. P., Hostert, A. and Strouboulis, J. (2005). Isolation and characterization of hematopoietic transcription factor complexes by in vivo biotinylation tagging and mass spectrometry. *Ann N Y Acad Sci* **1054**, 55-67.

Guo, Y., Livne-Bar, I., Zhou, L. and Boulianne, G. L. (1999). Drosophila presenilin is required for neuronal differentiation and affects notch subcellular localization and signaling. *J Neurosci* **19**, 8435-42.

Hahn, K. L., Beres, B., Rowton, M. J., Skinner, M. K., Chang, Y., Rawls, A. and Wilson-Rawls, J. (2009). A deficiency of lunatic fringe is associated with cystic dilation of the rete testis. *Reproduction* **137**, 79-93.

Hahn, K. L., Johnson, J., Beres, B. J., Howard, S. and Wilson-Rawls, J. (2005). Lunatic fringe null female mice are infertile due to defects in meiotic maturation. *Development* **132**, 817-28.

Haines, N. and Irvine, K. D. (2003). Glycosylation regulates Notch signalling. *Nat Rev Mol Cell Biol* **4**, 786-97.

Halfon, M. S., Carmena, A., Gisselbrecht, S., Sackerson, C. M., Jimenez, F., Baylies, M. K. and Michelson, A. M. (2000). Ras pathway specificity is determined by the integration of multiple signal-activated and tissue-restricted transcription factors. *Cell* **103**, 63-74.

Hamlett, I., Draper, J., Strouboulis, J., Iborra, F., Porcher, C. and Vyas, P. (2008). Characterization of megakaryocyte GATA1-interacting proteins: the corepressor ETO2 and GATA1 interact to regulate terminal megakaryocyte maturation. *Blood* **112**, 2738-49.

Happel, N. and Doenecke, D. (2009). Histone H1 and its isoforms: contribution to chromatin structure and function. *Gene* **431**, 1-12.

Hasserjian, R. P., Aster, J. C., Davi, F., Weinberg, D. S. and Sklar, J. (1996). Modulated expression of notch1 during thymocyte development. *Blood* **88**, 970-6.

Hellstrom, M., Phng, L. K., Hofmann, J. J., Wallgard, E., Coultas, L., Lindblom, P., Alva, J., Nilsson, A. K., Karlsson, L., Gaiano, N. et al. (2007). Dll4 signalling through Notch1 regulates formation of tip cells during angiogenesis. *Nature* **445**, 776-80.

Henrique, D., Adam, J., Myat, A., Chitnis, A., Lewis, J. and Ish-Horowicz, D. (1995). Expression of a Delta homologue in prospective neurons in the chick. *Nature* **375**, 787-90.

Henry, C. A., Urban, M. K., Dill, K. K., Merlie, J. P., Page, M. F., Kimmel, C. B. and Amacher, S. L. (2002). Two linked hairy/Enhancer of split-related zebrafish genes, her1 and her7, function together to refine alternating somite boundaries. *Development* **129**, 3693-704.

Hirata, H., Bessho, Y., Kokubu, H., Masamizu, Y., Yamada, S., Lewis, J. and Kageyama, R. (2004). Instability of Hes7 protein is crucial for the somite segmentation clock. *Nat Genet* **36**, 750-4.

Holley, S. A. (2007). The genetics and embryology of zebrafish metamerism. *Dev Dyn* **236**, 1422-49.

Holley, S. A., Julich, D., Rauch, G. J., Geisler, R. and Nusslein-Volhard, C. (2002). her1 and the notch pathway function within the oscillator mechanism that regulates zebrafish somitogenesis. *Development* **129**, 1175-83.

Hori, K., Fostier, M., Ito, M., Fuwa, T. J., Go, M. J., Okano, H., Baron, M. and Matsuno, K. (2004). Drosophila deltex mediates suppressor of Hairless-independent and late-endosomal activation of Notch signaling. *Development* **131**, 5527-37.

Hrabe de Angelis, M., McIntyre, J., 2nd and Gossler, A. (1997). Maintenance of somite borders in mice requires the Delta homologue DII1. *Nature* **386**, 717-21.

Hu, Y., Ye, Y. and Fortini, M. E. (2002). Nicastrin is required for gamma-secretase cleavage of the Drosophila Notch receptor. *Dev Cell* **2**, 69-78.

Huebert, D. J., Kamal, M., O'Donovan, A. and Bernstein, B. E. (2006). Genome-wide analysis of histone modifications by ChIP-on-chip. *Methods* **40**, 365-9.

Huppert, S. S., Ilagan, M. X., De Strooper, B. and Kopan, R. (2005). Analysis of Notch function in presomitic mesoderm suggests a gamma-secretase-independent role for presenilins in somite differentiation. *Dev Cell* **8**, 677-88.

Imatani, A. and Callahan, R. (2000). Identification of a novel NOTCH-4/INT-3 RNA species encoding an activated gene product in certain human tumor cell lines. *Oncogene* **19**, 223-31.

Ingham, P. W. (1988). The molecular genetics of embryonic pattern formation in Drosophila. *Nature* **335**, 25-34.

Inoue, A., Takahashi, M., Hatta, K., Hotta, Y. and Okamoto, H. (1994). Developmental regulation of islet-1 mRNA expression during neuronal differentiation in embryonic zebrafish. *Dev Dyn* **199**, 1-11.

Irvine, K. D. and Wieschaus, E. (1994). fringe, a Boundary-specific signaling molecule, mediates interactions between dorsal and ventral cells during Drosophila wing development. *Cell* **79**, 595-606.

Ishibashi, M., Ang, S. L., Shiota, K., Nakanishi, S., Kageyama, R. and Guillemot, F. (1995). Targeted disruption of mammalian hairy and Enhancer of split homolog-1 (HES-1) leads to up-regulation of neural helix-loop-helix factors, premature neurogenesis, and severe neural tube defects. *Genes Dev* **9**, 3136-48.

Ishibashi, M., Moriyoshi, K., Sasai, Y., Shiota, K., Nakanishi, S. and Kageyama, R. (1994). Persistent expression of helix-loop-helix factor HES-1 prevents mammalian neural differentiation in the central nervous system. *Embo J* **13**, 1799-805.

Ishibashi, M., Sasai, Y., Nakanishi, S. and Kageyama, R. (1993). Molecular characterization of HES-2, a mammalian helix-loop-helix factor structurally related to Drosophila hairy and Enhancer of split. *Eur J Biochem* **215**, 645-52.

Iso, T., Chung, G., Hamamori, Y. and Kedes, L. (2002). HERP1 is a cell type-specific primary target of Notch. *J Biol Chem* **277**, 6598-607.

Iso, T., Kedes, L. and Hamamori, Y. (2003). HES and HERP families: multiple effectors of the Notch signaling pathway. *J Cell Physiol* **194**, 237-55.

Iso, T., Sartorelli, V., Chung, G., Shichinohe, T., Kedes, L. and Hamamori, Y. (2001a). HERP, a new primary target of Notch regulated by ligand binding. *Mol Cell Biol* **21**, 6071-9.

Iso, T., Sartorelli, V., Poizat, C., Iezzi, S., Wu, H. Y., Chung, G., Kedes, L. and Hamamori, Y. (2001b). HERP, a novel heterodimer partner of HES/E(spl) in Notch signaling. *Mol Cell Biol* **21**, 6080-9.

Itoh, M., Kim, C. H., Palardy, G., Oda, T., Jiang, Y. J., Maust, D., Yeo, S. Y., Lorick, K., Wright, G. J., Ariza-McNaughton, L. et al. (2003). Mind bomb is a ubiquitin ligase that is essential for efficient activation of Notch signaling by Delta. *Dev Cell* **4**, 67-82.

Jack, C., Berezovska, O., Wolfe, M. S. and Hyman, B. T. (2001). Effect of PS1 deficiency and an APP gamma-secretase inhibitor on Notch1 signaling in primary mammalian neurons. *Brain Res Mol Brain Res* **87**, 166-74.

Jarriault, S. and Greenwald, I. (2005). Evidence for functional redundancy between C. elegans ADAM proteins SUP-17/Kuzbanian and ADM-4/TACE. *Dev Biol* **287**, 1-10.

Jennings, B., Preiss, A., Delidakis, C. and Bray, S. (1994). The Notch signalling pathway is required for Enhancer of split bHLH protein expression during neurogenesis in the Drosophila embryo. *Development* **120**, 3537-48.

Jennings, B. H. and Ish-Horowicz, D. (2008). The Groucho/TLE/Grg family of transcriptional co-repressors. *Genome Biol* **9**, 205.

Jennings, B. H., Tyler, D. M. and Bray, S. J. (1999). Target specificities of Drosophila enhancer of split basic helix-loop-helix proteins. *Mol Cell Biol* **19**, 4600-10.

Jiang, Y. J., Aerne, B. L., Smithers, L., Haddon, C., Ish-Horowicz, D. and Lewis, J. (2000). Notch signalling and the synchronization of the somite segmentation clock. *Nature* **408**, 475-9.

Johansen, K. M., Fehon, R. G. and Artavanis-Tsakonas, S. (1989). The notch gene product is a glycoprotein expressed on the cell surface of both epidermal and neuronal precursor cells during Drosophila development. *J Cell Biol* **109**, 2427-40.

Johnson, J. E., Zimmerman, K., Saito, T. and Anderson, D. J. (1992). Induction and repression of mammalian achaete-scute homologue (MASH) gene expression during neuronal differentiation of P19 embryonal carcinoma cells. *Development* **114**, 75-87.

Johnston, S. H., Rauskolb, C., Wilson, R., Prabhakaran, B., Irvine, K. D. and Vogt, T. F. (1997). A family of mammalian Fringe genes implicated in boundary determination and the Notch pathway. *Development* **124**, 2245-54.

Jothi, R., Cuddapah, S., Barski, A., Cui, K. and Zhao, K. (2008). Genome-wide identification of in vivo protein-DNA binding sites from ChIP-Seq data. *Nucleic Acids Res* **36**, 5221-31.

Joyner, A. L. (1991). Gene targeting and gene trap screens using embryonic stem cells: new approaches to mammalian development. *Bioessays* **13**, 649-56.

Jundt, F., Schwarzer, R. and Dorken, B. (2008). Notch signaling in leukemias and lymphomas. *Curr Mol Med* **8**, 51-9.

Kageyama, R., Masamizu, Y. and Niwa, Y. (2007a). Oscillator mechanism of notch pathway in the segmentation clock. *Dev Dyn*.

Kageyama, R., Ohtsuka, T. and Kobayashi, T. (2007b). The Hes gene family: repressors and oscillators that orchestrate embryogenesis. *Development* **134**, 1243-51.

Kageyama, R., Ohtsuka, T., Shimojo, H. and Imayoshi, I. (2008). Dynamic Notch signaling in neural progenitor cells and a revised view of lateral inhibition. *Nat Neurosci* **11**, 1247-51.

Kalaitzidis, D., Ok, J., Sulak, L., 2nd, Starczynowski, D. T. and Gilmore, T. D. (2004). Characterization of a human REL-estrogen receptor fusion protein with a reverse conditional transforming activity in chicken spleen cells. *Oncogene* **23**, 7580-7.

Kang, S. A., Seol, J. H. and Kim, J. (2005). The conserved WRPW motif of Hes6 mediates proteasomal degradation. *Biochem Biophys Res Commun* **332**, 33-6.

Keller, A., Nesvizhskii, A. I., Kolker, E. and Aebersold, R. (2002). Empirical statistical model to estimate the accuracy of peptide identifications made by MS/MS and database search. *Anal Chem* **74**, 5383-92.

Kidd, S., Kelley, M. R. and Young, M. W. (1986). Sequence of the notch locus of Drosophila melanogaster: relationship of the encoded protein to mammalian clotting and growth factors. *Mol Cell Biol* **6**, 3094-108.

Kidd, S. and Lieber, T. (2002). Furin cleavage is not a requirement for Drosophila Notch function. *Mech Dev* **115**, 41-51.

Kim, J., Chu, J., Shen, X., Wang, J. and Orkin, S. H. (2008). An extended transcriptional network for pluripotency of embryonic stem cells. *Cell* **132**, 1049-61.

Kimble, J. and Simpson, P. (1997). The LIN-12/Notch signaling pathway and its regulation. *Annu Rev Cell Dev Biol* **13**, 333-61.

Kiyota, T. and Kinoshita, T. (2002). Cysteine-rich region of X-Serrate-1 is required for activation of Notch signaling in Xenopus primary neurogenesis. *Int J Dev Biol* **46**, 1057-60.

Klein, T. and Arias, A. M. (1998). Interactions among Delta, Serrate and Fringe modulate Notch activity during Drosophila wing development. *Development* **125**, 2951-62.

Klinakis, A., Szabolcs, M., Politi, K., Kiaris, H., Artavanis-Tsakonas, S. and Efstratiadis, A. (2006). Myc is a Notch1 transcriptional target and a requisite for Notch1-induced mammary tumorigenesis in mice. *Proc Natl Acad Sci U S A* **103**, 9262-7.

Kobza, K., Camporeale, G., Rueckert, B., Kueh, A., Griffin, J. B., Sarath, G. and Zempleni, J. (2005). K4, K9 and K18 in human histone H3 are targets for biotinylation by biotinidase. *Febs J* **272**, 4249-59.

Kolodziej, K. E., Poufarzad, F., de Boer, E., Krpic, S., Grosveld, F. and Strouboulis, J. (2009). Optimal use of tandem biotin and V5 tags in ChIP assays. *BMC Mol Biol* **10**, 6.

Koo, B. K., Lim, H. S., Song, R., Yoon, M. J., Yoon, K. J., Moon, J. S., Kim, Y. W., Kwon, M. C., Yoo, K. W., Kong, M. P. et al. (2005). Mind bomb 1 is essential for generating functional Notch ligands to activate Notch. *Development* **132**, 3459-70.

Koo, B. K., Yoon, M. J., Yoon, K. J., Im, S. K., Kim, Y. Y., Kim, C. H., Suh, P. G., Jan, Y. N. and Kong, Y. Y. (2007). An obligatory role of mind bomb-1 in notch signaling of mammalian development. *PLoS ONE* **2**, e1221.

Kopan, R. and Goate, A. (2002). Aph-2/Nicastrin: an essential component of gamma-secretase and regulator of Notch signaling and Presenilin localization. *Neuron* **33**, 321-4.

Korzh, V., Edlund, T. and Thor, S. (1993). Zebrafish primary neurons initiate expression of the LIM homeodomain protein Isl-1 at the end of gastrulation. *Development* **118**, 417-25.

Kovall, R. A. (2007). Structures of CSL, Notch and Mastermind proteins: piecing together an active transcription complex. *Curr Opin Struct Biol* **17**, 117-27.

Kovall, R. A. (2008). More complicated than it looks: assembly of Notch pathway transcription complexes. *Oncogene* **27**, 5099-109.

Kovall, R. A. and Hendrickson, W. A. (2004). Crystal structure of the nuclear effector of Notch signaling, CSL, bound to DNA. *Embo J* **23**, 3441-51.

Koyano-Nakagawa, N., Kim, J., Anderson, D. and Kintner, C. (2000). Hes6 acts in a positive feedback loop with the neurogenins to promote neuronal differentiation. *Development* **127**, 4203-16.

Krebs, L. T., Deftos, M. L., Bevan, M. J. and Gridley, T. (2001). The Nrarp gene encodes an ankyrin-repeat protein that is transcriptionally regulated by the notch signaling pathway. *Dev Biol* **238**, 110-9.

Krejci, A., Bernard, F., Housden, B. E., Collins, S. and Bray, S. J. (2009). Direct response to Notch activation: signaling crosstalk and incoherent logic. *Sci Signal* **2**, ra1.

Krejci, A. and Bray, S. (2007). Notch activation stimulates transient and selective binding of Su(H)/CSL to target enhancers. *Genes Dev* **21**, 1322-7.

Kurooka, H. and Honjo, T. (2000). Functional interaction between the mouse notch1 intracellular region and histone acetyltransferases PCAF and GCN5. *J Biol Chem* **275**, 17211-20.

Lai, E. C. (2002a). Keeping a good pathway down: transcriptional repression of Notch pathway target genes by CSL proteins. *EMBO Rep* **3**, 840-5.

Lai, E. C. (2002b). Protein degradation: four E3s for the notch pathway. *Curr Biol* **12**, R74-8.

Lai, E. C. (2004). Notch signaling: control of cell communication and cell fate. *Development* **131**, 965-73.

Lai, E. C., Bodner, R. and Posakony, J. W. (2000). The enhancer of split complex of Drosophila includes four Notch-regulated members of the bearded gene family. *Development* **127**, 3441-55.

Lallemand, Y., Luria, V., Haffner-Krausz, R. and Lonai, P. (1998). Maternally expressed PGK-Cre transgene as a tool for early and uniform activation of the Cre site-specific recombinase. *Transgenic Res* **7**, 105-12.

Lamar, E., Deblandre, G., Wettstein, D., Gawantka, V., Pollet, N., Niehrs, C. and Kintner, C. (2001). Nrarp is a novel intracellular component of the Notch signaling pathway. *Genes Dev* **15**, 1885-99.

Langmead, B., Trapnell, C., Pop, M. and Salzberg, S. L. (2009). Ultrafast and memory-efficient alignment of short DNA sequences to the human genome. *Genome Biol* **10**, R25.

Larvor, M. P., Djavadi-Ohaniance, L., Nall, B. and Goldberg, M. E. (1994). Measurement of the dissociation rate constant of antigen/antibody complexes in solution by enzyme-linked immunosorbent assay. *J Immunol Methods* **170**, 167-75.

Lawson, N. D., Scheer, N., Pham, V. N., Kim, C. H., Chitnis, A. B., Campos-Ortega, J. A. and Weinstein, B. M. (2001). Notch signaling is required for arterial-venous differentiation during embryonic vascular development. *Development* **128**, 3675-83.

Le Borgne, R., Remaud, S., Hamel, S. and Schweisguth, F. (2005). Two distinct E3 ubiquitin ligases have complementary functions in the regulation of delta and serrate signaling in Drosophila. *PLoS Biol* **3**, e96.

Le Borgne, R. and Schweisguth, F. (2003). Notch signaling: endocytosis makes delta signal better. *Curr Biol* **13**, R273-5.

Lecourtois, M. and Schweisguth, F. (1995). The neurogenic suppressor of hairless DNA-binding protein mediates the transcriptional activation of the enhancer of split complex genes triggered by Notch signaling. *Genes Dev* **9**, 2598-608.

Lei, L., Xu, A., Panin, V. M. and Irvine, K. D. (2003). An O-fucose site in the ligand binding domain inhibits Notch activation. *Development* **130**, 6411-21.

Lewis, J. (1998). Notch signalling and the control of cell fate choices in vertebrates. *Semin Cell Dev Biol* **9**, 583-9.

Lewis, J. (2003). Autoinhibition with transcriptional delay: a simple mechanism for the zebrafish somitogenesis oscillator. *Curr Biol* **13**, 1398-408.

Li, C., Scott, D. A., Hatch, E., Tian, X. and Mansour, S. L. (2007). Dusp6 (Mkp3) is a negative feedback regulator of FGF-stimulated ERK signaling during mouse development. *Development* **134**, 167-76.

Litt, M. D., Simpson, M., Recillas-Targa, F., Prioleau, M. N. and Felsenfeld, G. (2001). Transitions in histone acetylation reveal boundaries of three separately regulated neighboring loci. *EMBO J* **20**, 2224-35.

Littlewood, T. D., Hancock, D. C., Danielian, P. S., Parker, M. G. and Evan, G. I. (1995). A modified oestrogen receptor ligand-binding domain as an improved switch for the regulation of heterologous proteins. *Nucleic Acids Res* **23**, 1686-90.

Logeat, F., Bessia, C., Brou, C., LeBail, O., Jarriault, S., Seidah, N. G. and Israel, A. (1998). The Notch1 receptor is cleaved constitutively by a furin-like convertase. *Proc Natl Acad Sci U S A* **95**, 8108-12.

Lopez-Schier, H. and St Johnston, D. (2002). Drosophila nicastrin is essential for the intramembranous cleavage of notch. *Dev Cell* **2**, 79-89.

Lowry, J. A. and Mackay, J. P. (2006). GATA-1: one protein, many partners. *Int J Biochem Cell Biol* **38**, 6-11.

Lu, L. and Stanley, P. (2006). Roles of O-fucose glycans in notch signaling revealed by mutant mice. *Methods Enzymol* **417**, 127-36.

Luo, Y. and Haltiwanger, R. S. (2005). O-fucosylation of notch occurs in the endoplasmic reticulum. *J Biol Chem* **280**, 11289-94.

Mansouri, A., Yokota, Y., Wehr, R., Copeland, N. G., Jenkins, N. A. and Gruss, P. (1997). Paired-related murine homeobox gene expressed in the developing sclerotome, kidney, and nervous system. *Dev Dyn* **210**, 53-65.

Martinez Arias, A., Zecchini, V. and Brennan, K. (2002). CSL-independent Notch signalling: a checkpoint in cell fate decisions during development? *Curr Opin Genet Dev* **12**, 524-33.

Masamizu, Y., Ohtsuka, T., Takashima, Y., Nagahara, H., Takenaka, Y., Yoshikawa, K., Okamura, H. and Kageyama, R. (2006). Real-time imaging of the somite segmentation clock: revelation of unstable oscillators in the individual presomitic mesoderm cells. *Proc Natl Acad Sci U S A* **103**, 1313-8.

Matsuno, K., Ito, M., Hori, K., Miyashita, F., Suzuki, S., Kishi, N., Artavanis-Tsakonas, S. and Okano, H. (2002). Involvement of a proline-rich motif and RING-H2 finger of Deltex in the regulation of Notch signaling. *Development* **129**, 1049-59.

McBurney, M. W., Staines, W. A., Boekelheide, K., Parry, D., Jardine, K. and Pickavance, L. (1994). Murine PGK-1 promoter drives widespread but not uniform expression in transgenic mice. *Dev Dyn* **200**, 278-93.

Merika, M. and Orkin, S. H. (1995). Functional synergy and physical interactions of the erythroid transcription factor GATA-1 with the Kruppel family proteins Sp1 and EKLF. *Mol Cell Biol* **15**, 2437-47.

Millar, J. K., James, R., Christie, S. and Porteous, D. J. (2005). Disrupted in schizophrenia 1 (DISC1): subcellular targeting and induction of ring mitochondria. *Mol Cell Neurosci* **30**, 477-84.

Misteli, T. (2001). Protein dynamics: implications for nuclear architecture and gene expression. *Science* **291**, 843-7.

Mohr, O. L. (1919). Character Changes Caused by Mutation of an Entire Region of a Chromosome in Drosophila. *Genetics* **4**, 275-82.

Moloney, D. J., Panin, V. M., Johnston, S. H., Chen, J., Shao, L., Wilson, R., Wang, Y., Stanley, P., Irvine, K. D., Haltiwanger, R. S. et al. (2000). Fringe is a glycosyltransferase that modifies Notch. *Nature* **406**, 369-75.

Morales, A. V., Yasuda, Y. and Ish-Horowicz, D. (2002). Periodic Lunatic fringe expression is controlled during segmentation by a cyclic transcriptional enhancer responsive to notch signaling. *Dev Cell* **3**, 63-74.

Morimoto, M., Takahashi, Y., Endo, M. and Saga, Y. (2005). The Mesp2 transcription factor establishes segmental borders by suppressing Notch activity. *Nature* **435**, 354-9.

Muller, U. (1999). Ten years of gene targeting: targeted mouse mutants, from vector design to phenotype analysis. *Mech Dev* **82**, 3-21.

Mumm, J. S., Schroeter, E. H., Saxena, M. T., Griesemer, A., Tian, X., Pan, D. J., Ray, W. J. and Kopan, R. (2000). A ligand-induced extracellular cleavage regulates gamma-secretase-like proteolytic activation of Notch1. *Mol Cell* **5**, 197-206.

Mural, R. J. Adams, M. D. Myers, E. W. Smith, H. O. Miklos, G. L. Wides, R. Halpern, A. Li, P. W. Sutton, G. G. Nadeau, J. et al. (2002). A comparison of whole-genome shotgun-derived mouse chromosome 16 and the human genome. *Science* **296**, 1661-71.

Nakaya, M. A., Biris, K., Tsukiyama, T., Jaime, S., Rawls, J. A. and Yamaguchi, T. P. (2005). Wnt3a links left-right determination with segmentation and anteroposterior axis elongation. *Development* **132**, 5425-36.

Nam, Y., Sliz, P., Pear, W. S., Aster, J. C. and Blacklow, S. C. (2007). Cooperative assembly of higher-order Notch complexes functions as a switch to induce transcription. *Proc Natl Acad Sci U S A* **104**, 2103-8.

Nam, Y., Sliz, P., Song, L., Aster, J. C. and Blacklow, S. C. (2006). Structural basis for cooperativity in recruitment of MAML coactivators to Notch transcription complexes. *Cell* **124**, 973-83.

Nam, Y., Weng, A. P., Aster, J. C. and Blacklow, S. C. (2003). Structural requirements for assembly of the CSL.intracellular Notch1.Mastermind-like 1 transcriptional activation complex. *J Biol Chem* **278**, 21232-9.

Narang, M. A., Dumas, R., Ayer, L. M. and Gravel, R. A. (2004). Reduced histone biotinylation in multiple carboxylase deficiency patients: a nuclear role for holocarboxylase synthetase. *Hum Mol Genet* **13**, 15-23.

Negre, N., Lavrov, S., Hennetin, J., Bellis, M. and Cavalli, G. (2006). Mapping the distribution of chromatin proteins by ChIP on chip. *Methods Enzymol* **410**, 316-41.

Nellesen, D. T., Lai, E. C. and Posakony, J. W. (1999). Discrete enhancer elements mediate selective responsiveness of enhancer of split complex genes to common transcriptional activators. *Dev Biol* **213**, 33-53.

Nesvizhskii, A. I., Keller, A., Kolker, E. and Aebersold, R. (2003). A statistical model for identifying proteins by tandem mass spectrometry. *Anal Chem* **75**, 4646-58.

Nichols, J. T., Miyamoto, A. and Weinmaster, G. (2007). Notch signaling--constantly on the move. *Traffic* **8**, 959-69.

Nishimura, M., Isaka, F., Ishibashi, M., Tomita, K., Tsuda, H., Nakanishi, S. and Kageyama, R. (1998). Structure, chromosomal locus, and promoter of mouse Hes2 gene, a homologue of Drosophila hairy and Enhancer of split. *Genomics* **49**, 69-75.

Niwa, Y., Masamizu, Y., Liu, T., Nakayama, R., Deng, C. X. and Kageyama, R. (2007). The initiation and propagation of Hes7 oscillation are cooperatively regulated by Fgf and notch signaling in the somite segmentation clock. *Dev Cell* **13**, 298-304.

Nix, D. A., Courdy, S. J. and Boucher, K. M. (2008). Empirical methods for controlling false positives and estimating confidence in ChIP-Seq peaks. *BMC Bioinformatics* **9**, 523.

Nusslein-Volhard, C. and Wieschaus, E. (1980). Mutations affecting segment number and polarity in Drosophila. *Nature* **287**, 795-801.

Oates, A. C. and Ho, R. K. (2002). Hairy/E(spl)-related (Her) genes are central components of the segmentation oscillator and display redundancy with the Delta/Notch signaling pathway in the formation of anterior segmental boundaries in the zebrafish. *Development* **129**, 2929-46.

Odom, D. T., Dowell, R. D., Jacobsen, E. S., Gordon, W., Danford, T. W., MacIsaac, K. D., Rolfe, P. A., Conboy, C. M., Gifford, D. K. and Fraenkel, E. (2007). Tissue-specific transcriptional regulation has diverged significantly between human and mouse. *Nat Genet* **39**, 730-2.

Ohsako, S., Hyer, J., Panganiban, G., Oliver, I. and Caudy, M. (1994). Hairy function as a DNA-binding helix-loop-helix repressor of Drosophila sensory organ formation. *Genes Dev* **8**, 2743-55.

Ohtsuka, T., Ishibashi, M., Gradwohl, G., Nakanishi, S., Guillemot, F. and Kageyama, R. (1999). Hes1 and Hes5 as notch effectors in mammalian neuronal differentiation. *Embo J* **18**, 2196-207.

Okajima, T. and Irvine, K. D. (2002). Regulation of notch signaling by o-linked fucose. *Cell* **111**, 893-904.

Okajima, T., Reddy, B., Matsuda, T. and Irvine, K. D. (2008). Contributions of chaperone and glycosyltransferase activities of O-fucosyltransferase 1 to Notch signaling. *BMC Biol* **6**, 1.

Okajima, T., Xu, A., Lei, L. and Irvine, K. D. (2005). Chaperone activity of protein O-fucosyltransferase 1 promotes notch receptor folding. *Science* **307**, 1599-603.

Ong, C. T., Cheng, H. T., Chang, L. W., Ohtsuka, T., Kageyama, R., Stormo, G. D. and Kopan, R. (2006). Target selectivity of vertebrate notch proteins. Collaboration between discrete domains and CSL-binding site architecture determines activation probability. *J Biol Chem* **281**, 5106-19.

Ordentlich, P., Lin, A., Shen, C. P., Blaumueller, C., Matsuno, K., Artavanis-Tsakonas, S. and Kadesch, T. (1998). Notch inhibition of E47 supports the existence of a novel signaling pathway. *Mol Cell Biol* **18**, 2230-9.

Ozbudak, E. M. and Lewis, J. (2008). Notch signalling synchronizes the zebrafish segmentation clock but is not needed to create somite boundaries. *PLoS Genet* **4**, e15.

Ozbudak, E. M. and Pourquie, O. (2008). The vertebrate segmentation clock: the tip of the iceberg. *Curr Opin Genet Dev* **18**, 317-23.

Palmeirim, I., Henrique, D., Ish-Horowicz, D. and Pourquie, O. (1997). Avian hairy gene expression identifies a molecular clock linked to vertebrate segmentation and somitogenesis. *Cell* **91**, 639-48.

Palomero, T., Lim, W. K., Odom, D. T., Sulis, M. L., Real, P. J., Margolin, A., Barnes, K. C., O'Neil, J., Neuberg, D., Weng, A. P. et al. (2006). NOTCH1 directly regulates c-MYC and activates a feed-forward-loop transcriptional network promoting leukemic cell growth. *Proc Natl Acad Sci U S A* **103**, 18261-6.

Panin, V. M., Papayannopoulos, V., Wilson, R. and Irvine, K. D. (1997). Fringe modulates Notch-ligand interactions. *Nature* **387**, 908-12.

Panin, V. M., Shao, L., Lei, L., Moloney, D. J., Irvine, K. D. and Haltiwanger, R. S. (2002). Notch ligands are substrates for protein O-fucosyltransferase-1 and Fringe. *J Biol Chem* **277**, 29945-52.

Pankratz, M. J., Seifert, E., Gerwin, N., Billi, B., Nauber, U. and Jackle, H. (1990). Gradients of Kruppel and knirps gene products direct pair-rule gene stripe patterning in the posterior region of the Drosophila embryo. *Cell* **61**, 309-17.

Parks, A. L., Klueg, K. M., Stout, J. R. and Muskavitch, M. A. (2000). Ligand endocytosis drives receptor dissociation and activation in the Notch pathway. *Development* **127**, 1373-85.

Petcherski, A. G. and Kimble, J. (2000a). LAG-3 is a putative transcriptional activator in the C. elegans Notch pathway. *Nature* **405**, 364-8.

Petcherski, A. G. and Kimble, J. (2000b). Mastermind is a putative activator for Notch. *Curr Biol* **10**, R471-3.

Phng, L. K., Potente, M., Leslie, J. D., Babbage, J., Nyqvist, D., Lobov, I., Ondr, J. K., Rao, S., Lang, R. A., Thurston, G. et al. (2009). Nrarp coordinates endothelial Notch and Wnt signaling to control vessel density in angiogenesis. *Dev Cell* **16**, 70-82.

Pires-daSilva, A. and Sommer, R. J. (2003). The evolution of signalling pathways in animal development. *Nat Rev Genet* **4**, 39-49.

Pitsouli, C. and Delidakis, C. (2005). The interplay between DSL proteins and ubiquitin ligases in Notch signaling. *Development* **132**, 4041-50.

Poulson, D. F. (1937). Chromosomal Deficiencies and the Embryonic Development of Drosophila Melanogaster. *Proc Natl Acad Sci U S A* **23**, 133-7.

Pourquie, O. and Tam, P. P. (2001). A nomenclature for prospective somites and phases of cyclic gene expression in the presomitic mesoderm. *Dev Cell* **1**, 619-20.

Pursglove, S. E. and Mackay, J. P. (2005). CSL: a notch above the rest. *Int J Biochem Cell Biol* **37**, 2472-7.

Qiu, L., Joazeiro, C., Fang, N., Wang, H. Y., Elly, C., Altman, Y., Fang, D., Hunter, T. and Liu, Y. C. (2000). Recognition and ubiquitination of Notch by Itch, a hect-type E3 ubiquitin ligase. *J Biol Chem* **275**, 35734-7.

Rabinovich, A., Jin, V. X., Rabinovich, R., Xu, X. and Farnham, P. J. (2008). E2F in vivo binding specificity: comparison of consensus versus nonconsensus binding sites. *Genome Res* **18**, 1763-77.

Radtke, F. and Raj, K. (2003). The role of Notch in tumorigenesis: oncogene or tumour suppressor? *Nat Rev Cancer* **3**, 756-67.

Radtke, F., Wilson, A. and MacDonald, H. R. (2004). Notch signaling in T- and B-cell development. *Curr Opin Immunol* **16**, 174-9.

Rand, M. D., Grimm, L. M., Artavanis-Tsakonas, S., Patriub, V., Blacklow, S. C., Sklar, J. and Aster, J. C. (2000). Calcium depletion dissociates and activates heterodimeric notch receptors. *Mol Cell Biol* **20**, 1825-35.

Rangarajan, A., Talora, C., Okuyama, R., Nicolas, M., Mammucari, C., Oh, H., Aster, J. C., Krishna, S., Metzger, D., Chambon, P. et al. (2001). Notch signaling is a direct determinant of keratinocyte growth arrest and entry into differentiation. *Embo J* **20**, 3427-36.

Rebay, I., Fleming, R. J., Fehon, R. G., Cherbas, L., Cherbas, P. and Artavanis-Tsakonas, S. (1991). Specific EGF repeats of Notch mediate interactions with Delta and Serrate: implications for Notch as a multifunctional receptor. *Cell* **67**, 687-99.

Riedel-Kruse, I. H., Muller, C. and Oates, A. C. (2007). Synchrony dynamics during initiation, failure, and rescue of the segmentation clock. *Science* **317**, 1911-5.

Rigaut, G., Shevchenko, A., Rutz, B., Wilm, M., Mann, M. and Seraphin, B. (1999). A generic protein purification method for protein complex characterization and proteome exploration. *Nat Biotechnol* **17**, 1030-2.

Robbins, J., Blondel, B. J., Gallahan, D. and Callahan, R. (1992). Mouse mammary tumor gene int-3: a member of the notch gene family transforms mammary epithelial cells. *J Virol* **66**, 2594-9.

Robertson, A. G., Bilenky, M., Tam, A., Zhao, Y., Zeng, T., Thiessen, N., Cezard, T., Fejes, A. P., Wederell, E. D., Cullum, R. et al. (2008). Genome-wide relationship between histone H3 lysine 4 mono- and tri-methylation and transcription factor binding. *Genome Res*.

Robertson, G., Hirst, M., Bainbridge, M., Bilenky, M., Zhao, Y., Zeng, T., Euskirchen, G., Bernier, B., Varhol, R., Delaney, A. et al. (2007). Genome-wide profiles of STAT1 DNA association using chromatin immunoprecipitation and massively parallel sequencing. *Nat Methods* **4**, 651-7.

Rodriguez, P., Bonte, E., Krijgsveld, J., Kolodziej, K. E., Guyot, B., Heck, A. J., Vyas, P., de Boer, E., Grosveld, F. and Strouboulis, J. (2005). GATA-1 forms distinct activating and repressive complexes in erythroid cells. *Embo J* **24**, 2354-66.

Ronchini, C. and Capobianco, A. J. (2001). Induction of cyclin D1 transcription and CDK2 activity by Notch(ic): implication for cell cycle disruption in transformation by Notch(ic). *Mol Cell Biol* **21**, 5925-34.

Rougemont, J., Amzallag, A., Iseli, C., Farinelli, L., Xenarios, I. and Naef, F. (2008). Probabilistic base calling of Solexa sequencing data. *BMC Bioinformatics* **9**, 431.

Rulifson, E. J., Wu, C. H. and Nusse, R. (2000). Pathway specificity by the bifunctional receptor frizzled is determined by affinity for wingless. *Mol Cell* **6**, 117-26.

Rusconi, J. C. and Corbin, V. (1998). Evidence for a novel Notch pathway required for muscle precursor selection in Drosophila. *Mech Dev* **79**, 39-50.

Rusconi, J. C. and Corbin, V. (1999). A widespread and early requirement for a novel Notch function during Drosophila embryogenesis. *Dev Biol* **215**, 388-98.

Saga, Y. (2007). Segmental border is defined by the key transcription factor Mesp2, by means of the suppression of Notch activity. *Dev Dyn* **236**, 1450-5.

Saga, Y., Hata, N., Koseki, H. and Taketo, M. M. (1997). Mesp2: a novel mouse gene expressed in the presegmented mesoderm and essential for segmentation initiation. *Genes Dev* **11**, 1827-39.

Saiki, R. K., Gelfand, D. H., Stoffel, S., Scharf, S. J., Higuchi, R., Horn, G. T., Mullis, K. B. and Erlich, H. A. (1988). Primer-directed enzymatic amplification of DNA with a thermostable DNA polymerase. *Science* **239**, 487-91.

Samols, D., Thornton, C. G., Murtif, V. L., Kumar, G. K., Haase, F. C. and Wood, H. G. (1988). Evolutionary conservation among biotin enzymes. *J Biol Chem* **263**, 6461-4.

Sasai, Y., Kageyama, R., Tagawa, Y., Shigemoto, R. and Nakanishi, S. (1992). Two mammalian helix-loop-helix factors structurally related to Drosophila hairy and Enhancer of split. *Genes Dev* **6**, 2620-34.

Sasamura, T., Sasaki, N., Miyashita, F., Nakao, S., Ishikawa, H. O., Ito, M., Kitagawa, M., Harigaya, K., Spana, E., Bilder, D. et al. (2003). neurotic, a novel maternal neurogenic gene, encodes an O-fucosyltransferase that is essential for Notch-Delta interactions. *Development* **130**, 4785-95.

Satoh, W., Gotoh, T., Tsunematsu, Y., Aizawa, S. and Shimono, A. (2006). Sfrp1 and Sfrp2 regulate anteroposterior axis elongation and somite segmentation during mouse embryogenesis. *Development* **133**, 989-99.

Schatz, P. J. (1993). Use of peptide libraries to map the substrate specificity of a peptide-modifying enzyme: a 13 residue consensus peptide specifies biotinylation in Escherichia coli. *Biotechnology (N Y)* **11**, 1138-43.

Schier, A. F., Neuhauss, S. C., Harvey, M., Malicki, J., Solnica-Krezel, L., Stainier, D. Y., Zwartkruis, F., Abdelilah, S., Stemple, D. L., Rangini, Z. et al. (1996). Mutations affecting the development of the embryonic zebrafish brain. *Development* **123**, 165-78.

Schmidt, D., Wilson, M. D., Spyrou, C., Brown, G. D., Hadfield, J. and Odom, D. T. (2009). ChIP-seq: Using high-throughput sequencing to discover protein-DNA interactions. *Methods*.

Schroeter, E. H., Kisslinger, J. A. and Kopan, R. (1998). Notch-1 signalling requires ligand-induced proteolytic release of intracellular domain. *Nature* **393**, 382-6.

Schuster-Gossler, K., Harris, B., Johnson, K. R., Serth, J. and Gossler, A. (2009). Notch signalling in the paraxial mesoderm is most sensitive to reduced Pofut1 levels during early mouse development. *BMC Dev Biol* **9**, 6.

Schwartz, S., Zhang, Z., Frazer, K. A., Smit, A., Riemer, C., Bouck, J., Gibbs, R., Hardison, R. and Miller, W. (2000). PipMaker--a web server for aligning two genomic DNA sequences. *Genome Res* **10**, 577-86.

Sekiya, T. and Zaret, K. S. (2007). Repression by Groucho/TLE/Grg proteins: genomic site recruitment generates compacted chromatin in vitro and impairs activator binding in vivo. *Mol Cell* **28**, 291-303.

Serth, K., Schuster-Gossler, K., Cordes, R. and Gossler, A. (2003). Transcriptional oscillation of lunatic fringe is essential for somitogenesis. *Genes Dev* **17**, 912-25.

Shen, J., Bronson, R. T., Chen, D. F., Xia, W., Selkoe, D. J. and Tonegawa, S. (1997). Skeletal and CNS defects in Presenilin-1-deficient mice. *Cell* **89**, 629-39.

Shi, S. and Stanley, P. (2003). Protein O-fucosyltransferase 1 is an essential component of Notch signaling pathways. *Proc Natl Acad Sci U S A* **100**, 5234-9.

Shifley, E. T. and Cole, S. E. (2008). Lunatic fringe protein processing by proprotein convertases may contribute to the short protein half-life in the segmentation clock. *Biochim Biophys Acta* **1783**, 2384-90.

Shifley, E. T., Vanhorn, K. M., Perez-Balaguer, A., Franklin, J. D., Weinstein, M. and Cole, S. E. (2008). Oscillatory lunatic fringe activity is crucial for segmentation of the anterior but not posterior skeleton. *Development* **135**, 899-908.

Shimizu, K., Chiba, S., Kumano, K., Hosoya, N., Takahashi, T., Kanda, Y., Hamada, Y., Yazaki, Y. and Hirai, H. (1999). Mouse jagged1 physically interacts with notch2 and other notch receptors. Assessment by quantitative methods. *J Biol Chem* **274**, 32961-9.

Southern, E. M. (1975). Detection of specific sequences among DNA fragments separated by gel electrophoresis. *J Mol Biol* **98**, 503-17.

Sparrow, D. B., Chapman, G., Wouters, M. A., Whittock, N. V., Ellard, S., Fatkin, D., Turnpenny, P. D., Kusumi, K., Sillence, D. and Dunwoodie, S. L. (2006). Mutation of the LUNATIC FRINGE gene in humans causes spondylocostal dysostosis with a severe vertebral phenotype. *Am J Hum Genet* **78**, 28-37.

St Johnston, D. and Nusslein-Volhard, C. (1992). The origin of pattern and polarity in the Drosophila embryo. *Cell* **68**, 201-19.

Stachler, M. D., Chen, I., Ting, A. Y. and Bartlett, J. S. (2008). Site-specific modification of AAV vector particles with biophysical probes and targeting ligands using biotin ligase. *Mol Ther* **16**, 1467-73.

Stancheva, I., Collins, A. L., Van den Veyver, I. B., Zoghbi, H. and Meehan, R. R. (2003). A mutant form of MeCP2 protein associated with human Rett syndrome cannot be displaced from methylated DNA by notch in Xenopus embryos. *Mol Cell* **12**, 425-35.

Stanger, B. Z., Datar, R., Murtaugh, L. C. and Melton, D. A. (2005). Direct regulation of intestinal fate by Notch. *Proc Natl Acad Sci U S A* **102**, 12443-8.

Stanley, P. (2007). Regulation of Notch signaling by glycosylation. *Curr Opin Struct Biol* **17**, 530-5.

Stauber, M., Sachidanandan, C., Morgenstern, C. and Ish-Horowicz, D. (2009). Differential axial requirements for Lunatic fringe and Hes7 transcription during mouse somitogenesis. Manuscript submitted.

Stifani, S., Blaumueller, C. M., Redhead, N. J., Hill, R. E. and Artavanis-Tsakonas, S. (1992). Human homologs of a Drosophila Enhancer of split gene product define a novel family of nuclear proteins. *Nat Genet* **2**, 119-27.

Stollewerk, A., Schoppmeier, M. and Damen, W. G. (2003). Involvement of Notch and Delta genes in spider segmentation. *Nature* **423**, 863-5.

Struhl, G. and Greenwald, I. (1999). Presenilin is required for activity and nuclear access of Notch in Drosophila. *Nature* **398**, 522-5.

Stylianou, S., Clarke, R. B. and Brennan, K. (2006). Aberrant activation of notch signaling in human breast cancer. *Cancer Res* **66**, 1517-25.

Swiatek, P. J., Lindsell, C. E., del Amo, F. F., Weinmaster, G. and Gridley, T. (1994). Notch1 is essential for postimplantation development in mice. *Genes Dev* **8**, 707-19.

Taelman, V., Van Wayenbergh, R., Solter, M., Pichon, B., Pieler, T., Christophe, D. and Bellefroid, E. J. (2004). Sequences downstream of the bHLH domain of the Xenopus hairy-related transcription factor-1 act as an extended dimerization domain that contributes to the selection of the partners. *Dev Biol* **276**, 47-63.

Takahashi, Y., Koizumi, K., Takagi, A., Kitajima, S., Inoue, T., Koseki, H. and Saga, Y. (2000). Mesp2 initiates somite segmentation through the Notch signalling pathway. *Nat Genet* **25**, 390-6.

Tam, P. P. (1986). A study of the pattern of prospective somites in the presomitic mesoderm of mouse embryos. *J Embryol Exp Morphol* **92**, 269-85.

Tan, P. B., Lackner, M. R. and Kim, S. K. (1998). MAP kinase signaling specificity mediated by the LIN-1 Ets/LIN-31 WH transcription factor complex during C. elegans vulval induction. *Cell* **93**, 569-80.

Templeton, N. S., Roberts, D. D. and Safer, B. (1997). Efficient gene targeting in mouse embryonic stem cells. *Gene Ther* **4**, 700-9.

Terpe, K. (2003). Overview of tag protein fusions: from molecular and biochemical fundamentals to commercial systems. *Appl Microbiol Biotechnol* **60**, 523-33.

Tun, T., Hamaguchi, Y., Matsunami, N., Furukawa, T., Honjo, T. and Kawaichi, M. (1994). Recognition sequence of a highly conserved DNA binding protein RBP-J kappa. *Nucleic Acids Res* **22**, 965-71.

van Werven, F. J. and Timmers, H. T. (2006). The use of biotin tagging in Saccharomyces cerevisiae improves the sensitivity of chromatin immunoprecipitation. *Nucleic Acids Res* **34**, e33.

Viens, A., Mechold, U., Lehrmann, H., Harel-Bellan, A. and Ogryzko, V. (2004). Use of protein biotinylation in vivo for chromatin immunoprecipitation. *Anal Biochem* **325**, 68-76.

Visan, I., Tan, J. B., Yuan, J. S., Harper, J. A., Koch, U. and Guidos, C. J. (2006). Regulation of T lymphopoiesis by Notch1 and Lunatic fringe-mediated competition for intrathymic niches. *Nat Immunol* **7**, 634-43.

Wahl, M. B., Deng, C., Lewandoski, M. and Pourquie, O. (2007). FGF signaling acts upstream of the NOTCH and WNT signaling pathways to control segmentation clock oscillations in mouse somitogenesis. *Development* **134**, 4033-41.

Wallberg, A. E., Pedersen, K., Lendahl, U. and Roeder, R. G. (2002). p300 and PCAF act cooperatively to mediate transcriptional activation from chromatin templates by notch intracellular domains in vitro. *Mol Cell Biol* **22**, 7812-9.

Weinmaster, G., Roberts, V. J. and Lemke, G. (1991). A homolog of Drosophila Notch expressed during mammalian development. *Development* **113**, 199-205.

Weng, A. P., Ferrando, A. A., Lee, W., Morris, J. P. t., Silverman, L. B., Sanchez-Irizarry, C., Blacklow, S. C., Look, A. T. and Aster, J. C. (2004). Activating mutations of NOTCH1 in human T cell acute lymphoblastic leukemia. *Science* **306**, 269-71.

Weng, A. P., Millholland, J. M., Yashiro-Ohtani, Y., Arcangeli, M. L., Lau, A., Wai, C., Del Bianco, C., Rodriguez, C. G., Sai, H., Tobias, J. et al. (2006). c-Myc is an important direct target of Notch1 in T-cell acute lymphoblastic leukemia/lymphoma. *Genes Dev* **20**, 2096-109.

Wharton, K. A., Johansen, K. M., Xu, T. and Artavanis-Tsakonas, S. (1985). Nucleotide sequence from the neurogenic locus notch implies a gene product that shares homology with proteins containing EGF-like repeats. *Cell* **43**, 567-81.

Wilson, A. and Radtke, F. (2006). Multiple functions of Notch signaling in self-renewing organs and cancer. *FEBS Lett* **580**, 2860-8.

Wilson, J. J. and Kovall, R. A. (2006). Crystal structure of the CSL-Notch-Mastermind ternary complex bound to DNA. *Cell* **124**, 985-96.

Wilson, V. and Beddington, R. S. (1996). Cell fate and morphogenetic movement in the late mouse primitive streak. *Mech Dev* **55**, 79-89.

Wong, P. C., Zheng, H., Chen, H., Becher, M. W., Sirinathsinghji, D. J., Trumbauer, M. E., Chen, H. Y., Price, D. L., Van der Ploeg, L. H. and Sisodia, S. S. (1997). Presenilin 1 is required for Notch1 and DII1 expression in the paraxial mesoderm. *Nature* **387**, 288-92.

Wu, L., Aster, J. C., Blacklow, S. C., Lake, R., Artavanis-Tsakonas, S. and Griffin, J. D. (2000). MAML1, a human homologue of Drosophila mastermind, is a transcriptional co-activator for NOTCH receptors. *Nat Genet* **26**, 484-9.

Xue, Y., Gao, X., Lindsell, C. E., Norton, C. R., Chang, B., Hicks, C., Gendron-Maguire, M., Rand, E. B., Weinmaster, G. and Gridley, T. (1999). Embryonic lethality and vascular defects in mice lacking the Notch ligand Jagged1. *Hum Mol Genet* **8**, 723-30.

Yang, J. T., Rayburn, H. and Hynes, R. O. (1993). Embryonic mesodermal defects in alpha 5 integrin-deficient mice. *Development* **119**, 1093-105.

Zecchini, V., Brennan, K. and Martinez-Arias, A. (1999). An activity of Notch regulates JNK signalling and affects dorsal closure in Drosophila. *Curr Biol* **9**, 460-9.

Zempleni, J. (2005). Uptake, localization, and noncarboxylase roles of biotin. *Annu Rev Nutr* **25**, 175-96.

Zhang, N. and Gridley, T. (1998). Defects in somite formation in lunatic fringe-deficient mice. *Nature* **394**, 374-7.

Zhang, Y., Liu, T., Meyer, C. A., Eeckhoute, J., Johnson, D. S., Bernstein, B. E., Nussbaum, C., Myers, R. M., Brown, M., Li, W. et al. (2008). Model-based Analysis of ChIP-Seq (MACS). *Genome Biol* **9**, R137.

Zweifel, M. E. and Barrick, D. (2001a). Studies of the ankyrin repeats of the Drosophila melanogaster Notch receptor. 1. Solution conformational and hydrodynamic properties. *Biochemistry* **40**, 14344-56.

Zweifel, M. E. and Barrick, D. (2001b). Studies of the ankyrin repeats of the Drosophila melanogaster Notch receptor. 2. Solution stability and cooperativity of unfolding. *Biochemistry* **40**, 14357-67.

Books

Alberts, B., Johnson, A., Lewis, J., Raff, M., Roberts, K., Walter, P. (2007) Molecular Biology of the Cell, Fifth Edition, Garland Science,

Nagy, A., Gertsenstein, M., Vintersten, K., Behringer, R. 2003 Manipulating the mouse embryo, A laboratory manual, Third Edition, Cold Spring Harbour Laboratory Press, Cold Spring Harbour, New York,

Ordahl, C.P. 1993 Myogenic lineages within the developing somite, In: M. Bernfield, Editor, Molecular Basis of Morphogenesis, John Wiley and Sons, New York

Sadler, T. W., Langman J. 2000, Langman's Medical Embryology, Lippincott Williams & Wilkins, Baltimore

Sambrook, J., Russel, D. W. 2001, Molecular Cloning A Laboratory Manual, Third Edition, Cold Spring Harbour Laboratory Press, Cold Spring Harbour, New York

Westerfield, M. 1993, The Zebrafish Book, Eugene, OR: University of Oregon